Dissertation
submitted to the
Combined Faculty of Natural Sciences and Mathematics
of the Ruperto Carola University Heidelberg, Germany
for the degree of
Doctor of Natural Sciences

Presented by

Master of Science David Eisel
born in: Mannheim-Neckarau
Oral examination: 07.12.2018

Reprogramming of M2-like macrophages by $CD4^+$ T cells, transcription factor knockdown and miRNA transfection

First examiner:	Prof. Dr. Viktor Umansky
Second examiner:	Prof. Dr. Stefan Eichmüller

Sworn Affidavit according to § 8 of the doctoral degree regulations of the Combined Faculty of Natural Sciences and Mathematics of the Heidelberg University

1. The thesis I have submitted entitled

   “Reprogramming of M2-like macrophages by $CD4^+$ T cells, transcription factor knockdown and miRNA transfection”

   is my own work.

2. I have only used the sources indicated and have not made unauthorized use of services of a third party. Where the work of others has been quoted or reproduced, the source is always given.
3. I have not yet presented this thesis or parts thereof to a university as part of an examination or degree.
4. I confirm that the declarations made above are correct.
5. I am aware of the importance of a sworn affidavit and the criminal prosecution in case of a false or incomplete affidavit
6. I affirm that the above is the absolute truth to the best of my knowledge and that I have not concealed anything.

Heidelberg, 30.08.2018

_____

David Eisel

Table of contents

Abstract

Macrophages are a subset of myeloid cells showing phenotypic and functional plasticity. Tumor cells secrete chemokines which attract macrophages resulting in their accumulation within the tumor microenvironment. Depending on the environmental signals they receive, these tumor associated macrophages (TAMs) can differentiate into M1-like or M2-like TAMs with different phenotype and function. M1-like TAMs produce proinflammatory cytokines and display tumoricidal activity, whereas M2-like TAMs have an immunosuppressive phenotype typically associated with enhanced tumor growth. At later stages of tumor development, the majority of TAMs resemble the M2-like phenotype, thereby contributing to the establishment of an immunosuppressive tumor microenvironment. As M2-like TAMs are generally associated with poor prognosis in most tumor entities, they are considered as a suitable target for cancer therapy. In this study, we reprogrammed M2-like macrophages by cognate interaction with $CD4^+$ T cells, transcription factor knockdown and miRNA transfection.

Within the first part of the thesis, we demonstrate by comprehensive gene and protein expression analyses as well as functional assays that M2-like (IL-4 treated) peritoneal exudate cells (PECs) can be repolarized *in vitro* into immunostimulatory M1-like macrophages through cognate interaction with $CD4^+$ T cells. Moreover, a MHC II (IA^b) deficient, ovalbumin (OVA) expressing B16F10 clone (M2KO/OVA) was established to investigate the effect of adoptively transferred OVA specific $CD4^+$ T cells on TAM polarization in a mouse model where MHC II restricted interaction between tumor cells and T cells is precluded. Adoptive transfer of $CD4^+$ T cells into M2KO/OVA tumor bearing mice resulted in a decreased expression of the M2-associated protein CD206 and an increased expression of M1-associated genes (*Il1b, Cd86, Cxcl10 and Nos2*) in TAMs freshly isolated from M2KO/OVA tumors, pointing towards reprogramming of M2-like TAMs. In the second part of the project we combined transcription factor (TF) binding information with RNA expression profiles of *in vitro* polarized PECs and identified five transcription factors (CTCF, E2F1, MYC, PPARγ and STAT6) involved in the induction and maintenance of the M2-like phenotype. siRNA mediated knockdown of these TFs in M2 polarized PECs induced the expression of M1-associated genes, whereas the expression of M2-associated genes was significantly reduced. In addition, the expression of proinflammatory cytokines (IL-1α, IL-6, MCP-1 and TNFα) was upregulated upon siRNA mediated TF knockdown, demonstrating a successful reprogramming of M2-like macrophages. In the third part of the project we were aiming at the identification of miRNAs involved in macrophage polarization. Therefore, we performed small RNA sequencing of *in vitro* polarized PECs, leading to the identification of 19 miRNAs which were differentially expressed between M1-like and M2-like macrophages. Based on their expression level and their expression fold changes, six miRNAs significantly upregulated in M1-like PECs were selected for subsequent validation. The expression analysis of M2-like and untreated PECs upon co-transfection of these miRNAs revealed enhanced expression levels of M1-associated genes and decreased expression levels of M2-associated genes, indicating a polarization towards the M1-like phenotype. Taken together, our results reveal new insights into the transcriptional, post-transcriptional and T cell mediated reprogramming of macrophages and might be useful for the identification of novel therapeutic targets to repolarize M2-like TAMs.

Zusammenfassung

Makrophagen sind myeloide Zellen, die eine große phänotypische und funktionale Plastizität aufweisen. Tumorzellen sekretieren Chemokine, die eine Akkumulation von Makrophagen im Tumormikromilieu induzieren können. In Abhängigkeit von den umgebenden Signalen können diese Tumor-assoziierten Makrophagen (TAMs) in M1 oder M2 Makrophagen mit unterschiedlichem Phänotyp differenzieren. M1 TAMs produzieren proinflammatorische Zytokine und haben eine tumorizide Aktivität, während M2 TAMs einen immunsupprimierenden Phänotyp aufweisen und mit verstärktem Tumorwachstum assoziiert sind. In späteren Tumorstadien weisen die meisten infiltrierten Makrophagen einen M2 Phänotyp auf und tragen dadurch zu der Etablierung eines immunsupprimierenden Tumormikromilieus bei. M2 polarisierte Makrophagen sind in den meisten Tumorentitäten mit einer schlechten Prognose assoziiert und stellen daher ein geeignetes Ziel für Krebstherapien dar. In dieser Arbeit konnten M2 Makrophagen durch die MHC II restringierte Interaktion mit $CD4^+$ T-Zellen, die Herabregulation von Transkriptionsfaktoren (TFs) oder durch die Transfektion von miRNAs zu M1 Makrophagen reprogrammiert werden.

Im ersten Teil der Arbeit wird anhand umfassender Genexpressionsanalysen und mithilfe funktionaler Testverfahren gezeigt, dass M2 polarisierte (IL-4 induziert) peritoneale Exsudatzellen (PECs) durch eine antigen-spezifische Interaktion mit $CD4^+$ T-Zellen *in vitro* in M1 Makrophagen repolarisiert werden können. Außerdem wurde ein IA^b defizienter, Ovalbumin (OVA) exprimierender B16F10 Klon etabliert (M2KO/OVA), um die Effekte von adoptiv transferierten $CD4^+$ T-Zellen auf TAMs unter Ausschluss einer direkten MHC II restringierten Interaktion zwischen Tumorzellen und T-Zellen *in vivo* untersuchen zu können. Der adoptive Transfer von $CD4^+$ T-Zellen in M2KO/OVA tumortragende Mäuse resultierte in einer verminderten Expression des M2-assoziierten Proteins CD206 und einer erhöhten Expression von M1-assoziierten Genen (*Il1b, Cd86, Cxcl10 and Nos2*) in frisch isolierten TAMs aus M2KO/OVA Tumoren. Im zweiten Teil der Arbeit wurden, auf Grundlage vorhergesagter TF Bindungsstellen und experimentell ermittelten RNA Expressionsprofilen von *in vitro* polarisierten PECs, fünf TFs identifiziert (CTCF, E2F1, MYC, PPARγ and STAT6), die für die Induktion und Aufrechterhaltung eines M2 Phänotyps von Bedeutung sind. Eine siRNA vermittelte Herunterregulation dieser TFs induzierte die Expression von M1-assoziierten Genen, wohingegen die Expression von M2-assoziierten Genen signifikant reduziert war. Zusätzlich war die Expression von proinflammatorischen Zytokinen (IL-1α, IL-6 and TNFα) nach siRNA Transfektion erhöht, wodurch die erfolgreiche Repolarisierung der M2 Makrophagen zusätzlich bestätigt werden konnte. Im dritten Teil des Projektes wurden basierend auf miRNA Sequenzierdaten von *in vitro* polarisierten PECs 19 miRNAs detektiert, die zwischen M1 und M2 polarisierten Makrophagen differentiell exprimiert waren. Basierend auf deren Expressionsstärke wurden sechs miRNAs mit hoher Expression in M1 Makrophagen für die weitere Validierung ausgewählt. Nach Ko-Transfektion aller sechs miRNAs in M2 PECs oder in unbehandelte PECs wurde eine erhöhte Expression von M1-assoziierten Genen und ein reduziertes Expressionsniveau von M2-assoziierten Genen detektiert, was auf eine Polarisation in Richtung des M1 Phänotyps hindeutet. Unsere Ergebnisse gewähren neue Einblicke in die transkriptionelle, post-transkriptionelle und durch T-Zellen vermittelte Umprogrammierung von Makrophagen und könnten für die Entwicklung neuer therapeutischer Ansätze zur Repolarisation von M2 TAMs nützlich sein.

List of Figures

List of Tables

Abbreviations

ACT	adoptive cell therapy
ADCC	antibody-dependent cellular cytotoxicity
AKT1	RAC-alpha serine/threonine-protein kinase
APC	antigen presenting cell
ARID1A	AT-rich interactive domain-containing protein 1A
B2M	β_2 microglobulin
BCG	bacillus Calmette-Guérin
BMMs	bone marrow-derived macrophages
BRAF	v-Raf murine sarcoma viral oncogene homolog B1
C/EBPβ	CCAAT/enhancer-binding protein beta
CAF	cancer-associated fibroblast
CAR	chimeric antigen receptor
Cas	CRISPR-associated
Cat. No.	catalog number
CCD	charge-coupled device
CCL	CC-chemokine ligand
CCR	C-C chemokine receptor
CD	cluster of differentiation
CDC	complement-dependent cytotoxicity
CDK	cyclin-dependent kinase
CDKN2A	cyclin-dependent kinase Inhibitor 2A
cDNA	complementary DNA
CI	confidence interval
CRISPR	clustered regularly interspaced short palindromic repeats
CTCF	CCCTC-binding factor
CTL	cytotoxic T lymphocyte
CTLA-4	cytotoxic T-lymphocyte-associated protein-4
CXCL	C-X-C motif chemokine
d	downstream
DCs	dendritic cells
ddH_2O	double-distilled water
dLNS	draining lymph nodes
DMSO	dimethyl sulfoxide
DNA	deoxyribonucleic acid
DUSP1	dual specificity protein phosphatase 1
E2F1	E2F transcription factor 1
EDTA	ethylenediaminetetraacetic acid
EGF	epidermal growth factor
EGFR	epidermal Growth Factor Receptor
ER	endoplasmic reticulum
ERK	extracellular signal-regulated kinase
FACS	fluorescence-activated cell sorting
FCS	fetal calf serum
FcγR	Fc-gamma receptor
FDA	Food and Drug Administration

FISH	fluorescence in situ hybridization
FoxP3	forkhead box P3
g	gravitational force
GITR	glucocorticoid-induced TNFR-related protein
GM-CSF	granulocyte macrophage colony-stimulating factor
Gy	gray
h	hours
H2R	histamine receptor type 2
HBSS	hanks' balanced salt solution
HER2/neu	human epidermal growth factor receptor 2
HLA	human leukocyte antigen
HPV	human papillomavirus
HRG	histidine-rich glycoprotein
HRP	horseradish peroxidase
i.p.	intraperitoneal
i.v.	intravenously
ICAM	intercellular adhesion molecule
ICP	infected cell protein
IDO	indoleamine 2,3-dioxygenase
IFNAR	IFN-α/β receptor
IFNGR	interferon-gamma receptor
IFNGR	IFN-γ receptor
IFNγ	interferon-gamma
IKK	IκB kinase
IL	interleukin
IL1RL1	interleukin 1 receptor-like 1
iNOS	inducible nitric oxide synthase
IRAK	IL-1 receptor associated kinase
IRF	interferon regulatory factor
ISGF-3	interferon-stimulated gene factor-3
JAK	janus kinase
KLF4	krüppel-like factor
KO	knockout
LFA	lymphocyte function-associated antigen
LMP	low molecular mass protein
LPS	lipopolysaccharide
M2KO	MHC II knockout
MACS	magnetic activated cell sorting
MAGE	melanoma-associated antigen
Mal	MyD88-adapter like
MAP	mitogen-activated protein
MART	melanoma antigen recognized by T cells
M-CSF	macrophage colony-stimulating factor
MDSC	myeloid-derived suppressor cells
MEK	mitogen-activated protein kinase kinase
MHC	major histocompatibility complex
MIC	MHC class I chain-related protein
min	minutes

miRNA	micro RNA
MMP	Matrix metalloproteinase
MyD88	myeloid differentiation primary response 88
nd or n.d.	not detected
NEMO	NF-kappa-B essential modulator
NFAT	nuclear factor of activated T-cells
NFKB1	NF-κB subunit p50
NFKBIZ	NF-κB inhibitor zeta
NF-κB	nuclear factor kappa-light-chain-enhancer of activated B cells
NK	natural killer
NKG2D	natural killer group 2D
NLR	NOD-like receptor
NOD	nucleotide-binding oligomerization domain
NRAS	neuroblastoma rat sarcoma
ns	not significant
NY-ESO	New York esophageal squamous cell carcinoma
ORR	overall response rate
OS	overall survival
OVA	Ovalbumin
OVA-F	native, full length OVA (secreted)
OVA-T	truncated OVA (not secreted)
PAGE	polyacrylamide gel electrophoresis
PAMP	pathogen-associated molecular pattern
PCR	polymerase chain reaction
PD-1	programmed cell death protein 1
PDCD4	programmed cell death protein-4
PD-L	programmed death-ligand
PECs	peritoneal exudate cells
PI3K	phosphatidylinositol-4,5-bisphosphate 3-kinase
PMEL	premelanosome protein
PMN	polymorphonuclear
PMSF	Phenylmethylsulfonylfluorid
PPARGγ	peroxisome proliferator-activated receptor gamma
PRR	pattern recognition receptors
PSA	prostate-specific antigen
PTEN	phosphatase and tensin homolog
PVDF	polyvinylidenfluorid
RAG	recombination-activating gene
RIG	retinoic acid-inducible gene
RNA	ribonucleic acid
ROCK2	Rho-dependent kinase-2
ROS	reactive oxygen species
RPKM	reads per kilobase million
rpm	revolutions per minute
RT	room temperature
s	second
s.c.	subcutaneously
SCID	severe combined immunodeficiency

SD	standard deviation
SDS	sodium dodecyl sulfate
SEM	standard error of the mean
sgRNA	single guide RNA
SOCS	suppressor of cytokine signaling
STAT	signal transduced and activator of transcription proteins
Syk	spleen tyrosine kinase
TAA	Tumor-associated antigen
TAB	TAK1 binding proteins
TAE	Tris-acetate-EDTA
TAK1	transforming growth factor beta-activated kinase 1
TALEN	transcription activator-like effector nuclease
TAM	tumor associated macrophages
TANK	TRAF family member-associated NF-κB activator
TAP	transporter associated with antigen processing
TBK1	TANK binding kinase 1
TBS	Tris-buffered saline
TCR	T cell receptor
TERT	telomerase reverse transcriptase
Tet1	ten-eleven translocation methylcytosine dioxygenase 1
TF	transcription factor
TGF	transforming growth factor
TIL	tumor infiltrating lymphocyte
TIM-3	T-cell immunoglobulin and mucin-domain containing-3
TIR	toll/interleukin-1 receptor
TLCK	N-alpha-tosyl-L-lysinyl-chloromethylketone
TLR	toll-like receptor
TME	tumor microenvironment
TNF	tumor necrosis factor
TNFAIP3	tumor necrosis factor alpha-induced protein 3
TNM	tumor-node-metastasis
TPTE	transmembrane phosphatase with tensin homology
TRAF	TNF-receptor associated factor
TRAIL	TNF-related apoptosis-inducing ligand
TRAM	TRIF-related adaptor molecule
Treg	regulatory T cell
TRIF	TIR-domain containing adapter inducing interferon-β
u	upstream
UTR	untranslated region
V	volt
VEGF	vascular endothelial growth factor
WT	wildtype
ZFN	zinc finger nuclease

1 Introduction

1.1 The immune system and cancer

1.1.1 General principles of the immune system

The human body is constantly exposed to putative pathogenic microorganisms and has evolved immune defense mechanisms to eliminate intruding pathogens. The human immune system is composed of many different effector cells and effector molecules that enable the human body to differentiate between foreign and self-antigens. In addition, the generation of memory cells upon primary infection allows an accelerated and more robust immune response in case of re-infection. At least as important as the establishment of an appropriate immune reaction, is the termination of such a response, returning the immune system to a basal state after the antigen has been cleared. Disorders in one of the described mechanisms can result in autoimmune diseases, inflammatory diseases and cancer.
The human immune system is divided in two branches: innate and adaptive immunity. The innate immune system represents the first line defense against pathogens and is responsible for the discrimination between self and a variety of pathogens. The innate immune system consists of specialized cells such as macrophages, mast cells, granulocytes and dendritic cells (DCs) that recognize microorganisms with a limited number of germline-encoded pattern recognition receptors (PRRs). These include toll-like receptors (TLRs), cytosolic nucleotide-binding oligomerization domain (NOD)-like receptors (NLRs) and retinoic acid-inducible gene (RIG)-I-like receptors. All PRRs recognize so called pathogen-associated molecular patterns (PAMPs) which are conserved microbial components indispensable for the survival of microorganisms. Once activated through PRRs, a series of signaling events lead to the production of immune mediators such as interleukins (ILs) that have the potential to regulate an immune response. Another first line defense mechanism of innate immune cells is the expression and secretion of antimicrobial peptides, which either weaken or even kill pathogens [1]. The upregulation of both, major histocompatibility complex (MHC)/peptide complexes as well as costimulatory molecules (e.g. B7-1 and B7-2) on the surface of antigen presenting cells (APCs; e.g. macrophages and dendritic cells) allow subsequent priming of naive T cells and thereby activation of adaptive immunity. The adaptive immune system is characterized by high specificity, develops by clonal selection from a vast repertoire of B and T lymphocytes bearing antigen-specific receptors and has the capacity to establish an immunological memory. Three signals are required for a naïve T cell to become fully activated [2, 3]. The interaction between the unique T cell receptor (TCR) and its ligand (MHC/peptide complex) presented on the surface of an APC represents the first signal. The second signal is provided by an interaction between costimulatory molecules on the same APC and their corresponding ligands on the T cell surface (e.g. cluster of differentiation (CD) 28). Thereafter, $CD4^+$ T cells can differentiate into a variety of effector subsets (e.g. Th1, Th2, Th17, regulatory T cells (Tregs)) which fulfill different effector functions. The differentiation decision is mainly triggered by the cytokines in the microenvironment produced by cells of the innate immune system (“signal 3”) [4, 5]. Primed T helper cells can for instance trigger B cell differentiation into antibody secreting plasma cells [6]. In contrast, $CD8^+$ T cells differentiate into cytotoxic T lymphocytes (CTLs), which are able to kill target cells directly through the release of cytotoxic granules.

1.1.2 Cancer immunoediting

Whether the immune system has the capacity to control tumor growth was debated for over a century. Based on an enhanced understanding of the human immune system and the demonstration that tumor antigens do exist [7], Burnet and Thomas constructed the hypothesis of immunosurveillance in the 1950s. According to their hypothesis the development of cancer is controlled or even prevented in immunocompetent hosts by the adaptive immune system [8, 9]. However, this concept was abandoned shortly afterwards as subsequent studies in nude mice (major but not totally immunodeficient) demonstrated similar susceptibility to carcinogen induced tumor development compared to immunocompetent mice [10].

In the 1990s, immunodeficiency mouse models on pure genetic backgrounds became available and facilitated more precise experimental validations of the immunosurveillance hypothesis. Kaplan *et al.* demonstrated in an interferon-gamma receptor (IFNGR) deficient mouse model that spontaneously arising and chemically induced tumors are controlled by the endogenous production of interferon-gamma (IFNγ). They furthermore showed that tumors developed faster and more frequently in signal transduced and activator of transcription protein (Stat) 1 deficient mice, lacking sensitivity to all IFN family members, compared to wild type (WT) mice [11]. Three years later, similar experiments were performed in recombination-activating gene-2 (Rag2) immunodeficient mice that fail to generate mature T or B lymphocytes [12]. These results demonstrated that lymphocytes and IFNγ are required to induce an effective anti-tumor immune response. Furthermore, the authors showed that the immune system selects for those tumor cells which have reduced immunogenicity. The awareness, that the immune system not only protects the host from the cancer development, but also modulates the immunogenicity of tumor cells was the basis for the cancer immunoediting hypothesis. The process of immunoediting was divided into three consecutive phases termed “elimination”, “equilibrium” and “escape” (three “Es”) as illustrated in Figure 1.1 [13]. In the elimination phase, innate and adaptive immunity are capable to recognize and destroy transformed cells before a tumor becomes clinically apparent. Tumor cells that survive the elimination phase enter into the equilibrium phase in which the adaptive immune system controls tumor development and shapes the tumor cells immunogenicity. Experimental evidence for the existence of the equilibrium phase arose from experiments in immunocompetent mice [14]. If those mice were treated with low dose carcinogen but did not develop a palpable tumor, they still harbored occult cancer cells which started to grow out when T cells and IFNγ were depleted by the administration of monoclonal antibodies. The cells isolated from these tumors were highly immunogenic. Further investigations demonstrated that keeping occult tumor cells in the equilibrium phase is exclusively mediated by the adaptive immune system, more precisely by IL-12, IFNγ, $CD4^+$ and $CD8^+$ T cells. The equilibrium phase is assumed to be the longest phase within the process of immunoediting and may even persist throughout the life of the host. However, due to the constant immune selection pressure the tumor cell population changes and altered variants may arise and enter the escape phase. These altered tumor cell variants often show a reduced immunogenicity and at the same time an increased resistance to immune mediated cytotoxicity, which eventually facilitates tumor outgrowth. The loss of antigens is one of the best studied escape mechanisms resulting in a reduced susceptibility of tumor cells to $CD8^+$ T cell recognition. Different mechanisms, all driven by the process of immunoselection and the inherent genetic instability of tumor cells, are known to be

responsible for the loss of tumor antigen expression. Some tumor cells lose expression either of strong rejection antigens [15] or of MHC I molecules which are necessary to present antigen derived epitopes [16]. Another possible way of losing epitope presentation are defects in the antigen processing machinery (e.g. low molecular mass protein (LMP) 7, transporter associated with antigen processing (TAP) 1 or TAP2), which is essential to produce the epitopes and load them on MHC molecules [17, 18]. Eventually, these “naturally selected” tumor cells are poorly immunogenic and can only be hardly detected by cytotoxic T lymphocytes.

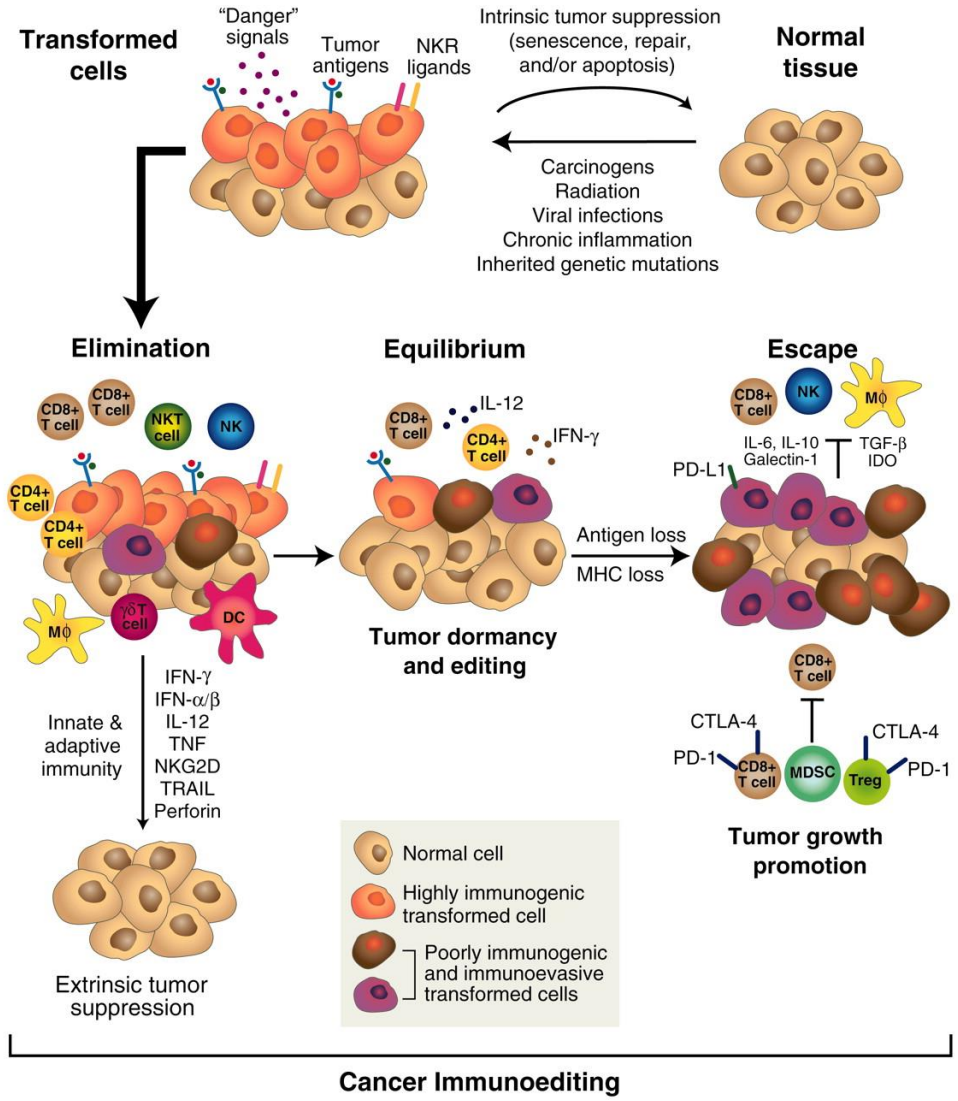

Figure 1.1: The cancer immunoediting concept.
The process of cancer immunoediting consists of three consecutive phases: elimination, equilibrium and escape. If transformed cells escape intrinsic tumor suppression mechanisms like induction of senescence or apoptosis, they enter the elimination phase in which innate and adaptive immunity destroy the developing tumor before it becomes clinically apparent. If the destruction fails, the tumor cells enter into the equilibrium phase in which further tumor development is controlled exclusively by the adaptive immune system. The equilibrium phase might persist for the entire lifetime of the host and thus represents an end stage of the immunoediting process. However, as a result of the constant immune selection pressure within the equilibrium phase, some tumor cell variants which are not recognized anymore by the adaptive immune system might emerge and enter the escape phase. As these tumor cells are not eliminated any longer by the immune system, they most likely cause clinically apparent tumors. Figure was taken from [19].

Alternatively to the aforementioned escape mechanism, tumor cells can promote the establishment of an immunosuppressive microenvironment in which adaptive immune cells are impaired in fulfilling their function. Mechanisms by which tumor cells establish such a microenvironment include the production of immunosuppressive cytokines like transforming growth factor-β (TGF- β), vascular endothelial growth factor (VEGF) [20] or indoleamine 2,3-dioxygenase (IDO) [21]. Additionally, tumor cells can recruit immunosuppressive immune cells such as Tregs and myeloid-derived suppressor cells (MDSCs). Immunosuppressive M2 macrophage recruitment and polarization is mediated by IL-13 and IL-4 secretion [19, 22]. A more comprehensive description of the tumor microenvironment composition and its role in promoting tumor growth is given in section 1.1.4.

1.1.3 T cell responses against tumors

In 1863, Rudolf Virchow noted for the first time that tumors contain lymphocytes, which nowadays are referred to as tumor infiltrating lymphocytes (TILs) [23]. A first link between prognosis and the extend of TIL infiltration was observed 1949 in breast cancer patients [24]. Twenty years later, infiltration of melanomas by lymphocytes was described for the first time [25] and was subsequently found to be of prognostic significance [26]. The 5 year survival rate of patients with highly infiltrated primary melanoma was 3 times higher compared to patients with low numbers of immune cells in the tumor [27]. Clemente *et al.* further demonstrated a negative correlation between the probability to get lymph node metastases and TIL infiltration [28]. More comprehensive analysis of the tumor microenvironment in melanoma revealed that the T cell composition of infiltrated TILs in individual patients ranged from 90 % $CD4^+$ T cells to 90 % $CD8^+$ T cells [29-31]. Several studies demonstrated that the infiltrated $CD8^+$ T cells show an anergic or exhausted phenotype as they often lack the expression of perforin and only produce low amounts of IFNγ upon stimulation with peptide-pulsed target cells [32, 33]. Nevertheless, the presence of $CD8^+$ T cells in the tumor microenvironment was shown to positively correlate with patients' outcome [34]. While a lot is known about CTLs and their function in the tumor microenvironment, the role of $CD4^+$ T cells is not well understood yet. Several studies demonstrated that melanoma specific $CD4^+$ T cells possess the ability to lyse tumor cells through cognate interaction [35, 36]. Moreover, the adoptive transfer of autologous New York esophageal squamous cell carcinoma (NY-ESO) 1 antigen specific $CD4^+$ T cells induced durable responses in some patients with metastatic melanoma [37]. Additional work revealed that regressing melanoma lesions are mainly infiltrated by Th1 $CD4^+$ T cells secreting immunostimulatory cytokines (e.g. IFNγ, IL-2 and IL-15). In contrast, the presence of $CD4^+$ regulatory T cells or Th2 T cells is predominantly associated with non-regressing lesions [38, 39]. Furthermore, the accumulation of Tregs, which was shown to be associated with a higher risk of melanoma recurrence [40], might at least in part, explain the high frequency of anergic and exhausted $CD8^+$ T cells in these tumors. These results reveal the important roles of the different $CD4^+$ T cell subsets present in the tumor microenvironment and should serve as a basis for more comprehensive analyses of these cell populations.

The above mentioned prognostic value of TILs emphasizes the importance of the immune system in controlling tumor development. However, it was uncertain for decades what kinds of antigens were recognized by tumor-reactive T cells. The development of new techniques, including mass spectrometry analysis of peptides eluted from purified MHC molecules [41, 42] and screenings of tumor-reactive T cells against cDNA expression libraries [43, 44],

facilitated the identification of tumor-associated antigens (TAAs) and their respective epitopes. Use of these techniques resulted in the identification of a vast amount of TAAs as well as their T cell epitopes. TAAs can be grouped into several categories which are listed below in decreasing order of tumor specificity:

1. Neoantigens
   Nonsynonymous mutations in the genome of tumor cells are a frequent source of tumor-specific antigenic peptides. Examples of proteins of which mutated epitopes derived from include neuroblastoma rat sarcoma (NRAS) [45], cyclin-dependent kinase (CDK) 4 [46], v-Raf murine sarcoma viral oncogene homolog B1 (BRAF) [47] and a fusion protein composed of breakpoint cluster region protein (BCR) and abelson murine leukemia viral oncogene homolog (ABL) 1 [48].

2. Viral antigens
   Proteins from oncogenic viruses are another source of antigenic peptides which can be considered as tumor-specific. Two of the best studied viral oncoproteins that give rise to tumor-specific T cell epitopes are E6 and E7 of human papillomavirus (HPV) [49].

3. Cancer-testis antigens
   Cancer-testis antigens are exclusively expressed in male germ cells and trophoblastic cells [50], which are not recognized by T cells as they have no detectable MHC I or II surface expression. In many cancers, cancer-testis genes are expressed as a result of genome-wide hypomethylation [51, 52] and can therefore give rise to tumor associated epitopes. Examples of cancer-testis antigens include NY-ESO-1 [53] and proteins belonging to the melanoma-associated antigen (MAGE) family (MAGE-A, MAGE-B, MAGE-C) [54].

4. Differentiation antigens
   These are proteins which are only expressed in a certain healthy tissue or cell type and in tumor cells arising from them. For instance, CTLs recognizing epitopes derived from melanocyte-specific proteins, such as tyrosinase, premelanosome protein (PMEL) 17 and melanoma antigen recognized by T cells (MART) 1 were detected in melanoma patients [55, 56].

5. Overexpressed antigens
   These antigens are overexpressed on tumor cells but also present on normal cells. One example is the telomerase reverse transcriptase (TERT) which was shown to be highly expressed in more than 85 % of all human cancers [57]. Immunogenic TERT epitopes facilitating efficient CTL activation were identified in preclinical studies and make TERT an attractive target for cancer immunotherapy [58].

1.1.4 The tumor microenvironment

For a long time, cancer was considered as a disease that mainly results from genetic mutations and genomic instability. However, the strong influence of stromal cells on tumor progression is nowadays widely accepted. Tumors are highly complex tissues not only consisting of malignant tumor cells, but also stromal cells including cancer-associated fibroblasts (CAFs), various immune cell types as well as endothelial cells and pericytes which form the tumor vasculature [59]. All these different cell types together with the extracellular matrix are referred to as tumor microenvironment (TME). The different

components of the TME interact with the tumor cells, thus playing a pivotal role in tumor development and disease progression as described in more detail in the following paragraphs.

Fibroblasts are a component of the connective tissue in which they are embedded in fibrillar matrix. These cells are specialized in producing components of the extracellular matrix and are especially important in the process of wound healing [60]. Tumor resident fibroblasts that became activated, for instance by reactive oxygen species, growth factors or cell-cell contact are known as CAFs [61]. Activated CAFs were shown to promote tumor growth by inducing angiogenesis, cell invasion and proliferation [61, 62]. Moreover, CAFs can mediate epithelial to mesenchymal cell transition and produce matrix metalloproteinases (MMPs) [63, 64], thereby facilitating metastatic spread of tumor cells. These cells do also have the capacity to mediate immunosuppression as they express programmed death-ligand (PD-L) 1 and PD-L2 [65]. Besides CAFs, all types of immune cells are part of the TME and can have tumor promoting or repressing properties depending on the particular cell type and their activation state.

Immune cells originated from a common lymphoid progenitor

$CD8^+$ T cells infiltrating into the tumor are often impaired in their effector function due to the immunosuppressive TME and terminally differentiate into a so called exhausted phenotype. Such exhausted T cells express elevated levels of inhibitory receptors (including programmed cell death protein 1 (PD-1), cytotoxic T-lymphocyte-associated protein-4 (CTLA-4) and T-cell immunoglobulin and mucin-domain containing-3 (TIM-3) [66, 67] and secrete less IL-2, tumor necrosis factor (TNF) alpha, IFNγ and granzyme B [68, 69]. Restoring anti-tumor reactivity of exhausted T cells is an attractive strategy to treat cancer and is discussed more in detail in section 1.3.

Regulatory T cells (Tregs), traditionally defined as $CD4^+$ T cells expressing forkhead box P3 (FoxP3) and CD25 [70, 71] contribute to the establishment of an immunosuppressive microenvironment, thereby promoting tumor progression. Tregs can be either recruited in response to chemokines secreted by the tumor or generated from conventional T cells mediated by tumor derived adenosine and TGF-β [72]. The mechanisms by which Tregs exert their immunosuppressive function include the secretion of IL-10 [73], TGF-β [74] and adenosine [75]. In addition, these cells constitutively express the high affinity IL-2 receptor (CD25) and are dependent on exogenous IL-2 which limits the amount of available IL-2 for surrounding cells [76]. By constitutive expression of CTLA-4 Tregs mediate downregulation of co-stimulatory molecules (CD80 and CD86) on dendritic cells and deprive all other T cell subsets of co-stimulatory signals [77].

Natural killer (NK) cells were originally discovered as a subset of cells that kill cancer cells of certain tumor entities *in vitro* [78]. Tumor cells which have downregulated MHC expression or overexpress ligands (e.g. MHC class I chain-related protein (MIC) A and MICB) for activating receptors on NK cells (e.g. natural killer group 2D (NKG2D)) serve as ideal NK cell targets [79]. In a NK cell deficient mouse model Kim and colleagues demonstrated the importance of NK cells in controlling tumor outgrowth and suppressing tumor metastases [80]. The infiltration of NK cells positively correlated with increased overall survival in patients with squamous cell lung carcinoma [81] and colorectal carcinoma [82].

Patients with gastric carcinoma and a high rate of NK cell infiltration showed less metastases and have a better prognosis compared to patients with low level of NK cell infiltration [83].

B cells infiltrating into the tumor microenvironment were associated with good prognosis and positively correlated with patient survival in ovarian, breast, non-small cell lung and cervical cancer. The tumor infiltrating B cell populations were demonstrated to comprise oligoclonal, antigen-experienced cells producing autoantibodies against TAAs [84]. In theory, these autoantibodies could induce an anti-tumor response by direct inhibition of the target protein or by mediating complement-dependent cytotoxicity (CDC) and antibody-dependent cellular cytotoxicity (ADCC). However, the exact contribution of B cells in mediating an anti-tumor response is not fully understood.
B cells also exert several tumor promoting functions, including the secretion of cytokines to inhibit T cell activity. Further, B cells have been shown to promote angiogenesis and secrete factors which directly mediate enhanced tumor cell survival [85].

Immune cells originated from a common myeloid progenitor

Neutrophils are the most abundant circulating leukocytes and are known to be part of the TME in many tumor entities, including melanoma [86], colorectal cancer [87] and renal cell carcinoma [88]. In 2009, Fridlender and colleagues demonstrated that neutrophils show a certain plasticity and can have a pro- or anti-tumor phenotype (N1 or N2, respectively) which is dependent on the environmental factors [89]. However, most studies reported that the presence of neutrophils per se correlates with a poor prognosis of cancer patients [90-92]. Several mechanisms of how neutrophils contribute to tumor progression have been described. By the release of matrix metalloproteinases (MMP8 and MMP9) neutrophils can remodel the extracellular matrix which was shown to modulate tumor cell invasion in skin cancer models [93]. Moreover, neutrophils can release reactive oxygen species (ROS; induces DNA damage) [94], Oncostatin M (increases angiogenesis) [95] and prostaglandin E2 (supports proliferation) [96].

Mast cells, eosinophils and basophils play an important role in defending the human body against parasites by exerting different effector functions [97]. The role of these three cell types in promoting or inhibiting tumor growth is still controversial. Several studies have shown a poor prognosis for patients with high numbers of mast cells in the TME (e.g. in colorectal cancer [98], melanoma [99] and pancreatic cancer [100]), while others found mast cell infiltration to be correlated with a good prognosis (e.g. in breast cancer [101] and hepatocellular carcinoma [102]). The mechanisms by which mast cells act within the TME are diverse and include the release of soluble mediators through degranulation. For instance, Histamine classically released by mast cells can have pleiotropic effects within the TME and modulate both innate and adaptive immunity [103]. By binding to the histamine receptor type 2 (H2R) it inhibits T cell reponses [104] and induces IL-10 secretion by peripheral monocytes [105]. Moreover, the release of histamine was shown to recruit Tregs to the site of inflammation thereby contributing to the establishment of an immunosuppressive TME [106]. Similar to mast cells, the infiltration of eosinophils into the TME has been shown to be associated with a good or poor prognosis depending on the tumor entity. An improved prognosis was shown for instance in colon tumors [107] and prostate cancer [108], whereas eosinophil infiltration was associated with poor prognosis in Hodgkin lymphoma [109]. By secretion of proteins like eosinophil peroxidase and eosinophil

cationic protein stored in the secondary granules, eosinophils can disrupt lipid bilayer integrity and were shown to have cytotoxic effects on tumor cells [110, 111]. While there is evidence for direct anti-tumor activity of eosinophils *in vitro*, data showing similar effects *in vivo* are in large part missing [112]. Carretero *et al.* demonstrated that eosinophils secrete chemokines (e.g. CXCL9, CXCL10) which facilitated recruitment of adoptively transferred $CD8^+$ T cells. Moreover, eosinophils induced normalization of the tumor vasculature and polarized TAMs into a M1-like phenotype [113]. In contrast to their anti-tumorigenic activities, eosinophils may also support tumorigenesis by promoting tissue remodeling, angiogenesis and activation of fibroblasts mediated through the release of growth factors (e.g. VEGF, FGF) and cytokines (e.g. TGF-β, IL-8) [112]. Basophils are the least abundant granulocytes in the peripheral blood and are rapidly recruited to inflamed tissue. They are important in promoting a protective immune response against multicellular parasites. However, the role of basophiles in the TME of solid tumors is largely unknown.

Myeloid-derived suppressor cells (MDSCs) are another subset of myeloid cells present in the TME. The population of MDSCs comprises immature mononuclear cells (M-MDSCs), immature polymorphonuclear (PMN) cells (PMN-MDSCs) as well as a third, small population of other myeloid precursors and cells with colony-forming activity [114]. M-MDSCs and PMN-MDSCs are morphologically and phenotypically similar to monocytes and neutrophils, respectively [115]. MDSCs possess strong immunosuppressive capacities and have been shown to directly support tumorigenesis (reviewed in [116]). Some of the main features of MDSCs include secretion of IL-10 [117] and TGF-β [118] as well as expression of inducible nitric oxide synthase (iNOS) and arginase 1 [119]. Furthermore, the expression of angiogenesis mediators such as VEGF and MMP9 by MDSCs promote angiogenesis and tumor cell invasion [120, 121]. In general, increased numbers of MDSCs in the circulation of cancer patients was shown to be associated with poor outcomes [122]. A positive correlation between tumor burden and the frequency of circulating MDSCs was demonstrated in colorectal [123], non-small-cell lung [124], bladder [125] and breast cancer [126] as well as in melanoma [114, 127].

Macrophages constitute another major population of tumor infiltrating leukocytes. Due to their importance within this study, their role in the tumor microenvironment will be described in detail in section 1.2.4.

1.2 Polarization of macrophages

Macrophages are a subset of myeloid cells that show phenotypic and functional plasticity. Depending on the environmental signals, they are involved in a variety of processes such as tissue remodeling, tumor growth promotion/inhibition, clearance of pathogens and immunoregulation [128]. In the early 1990s, two macrophage phenotypes were established based on studies comparing gene expression upon treatment of macrophages with IL-4 compared to IFNγ and/or lipopolysaccharide (LPS) [129]. Activation of macrophages with IFNγ and/or LPS resulted in the classically activated phenotype with increased expression of proinflammatory cytokines (e.g. TNF-α, IL-1β, IL-6, C-X-C motif chemokine (CXCL) 9, CXCL10) and an elevated microbicidal as well as tumoricidal activity. In contrast, treatment with IL-4 polarized macrophages to the alternatively activated state in which the cells secrete immunosuppressive cytokines (e.g. IL-10, TGF-β) and are involved in tissue repair, matrix

remodeling, angiogenesis and parasite clearance. A few years later, Mills and colleagues demonstrated that macrophages derived from Th1 mouse strains (e.g. C57BL/6) show substantial differences in their arginine metabolism compared to macrophages derived from Th2 mouse strains (e.g. BALB/c) [130]. In response to IFNγ or LPS, macrophages derived from Th1 strains metabolized arginine to nitric oxide, whereas those from Th2 strains metabolized arginine to ornithine. In addition, they showed that C57BL/6 and BALB/c macrophages, both stimulated with IFNγ or LPS induced differential cytokine secretion of CB6F1 (hybrid mice: C57BL/6 X BALB/c) lymphocytes. While macrophages from C57BL/6 mice induced Th1 cytokine secretion, BALB/c derived macrophages mediated a Th2 cytokine response. Based on their results, the authors proposed to term these different macrophage responses “M1” and “M2”, respectively.
These observations were combined with the aforementioned concept of classically and alternatively activated macrophages to propose a general scheme of macrophage polarization [131]. Within this widely accepted scheme, classical activation represents M1, whereas alternatively activated macrophages represent the M2 state. However, due to the plasticity of macrophages the M1 and M2 state should only be considered as the two extremes within a spectrum of functional phenotypes. Within the next sections, the signaling pathways (section 1.2.1), miRNAs (section 1.2.2) and metabolic changes (section 1.2.3) involved in macrophage polarization will be described. Moreover, the contribution of macrophages to the establishment of an immunosuppressive tumor microenvironment will be discussed in section 1.2.4. Some key characteristics of classically and alternatively activated macrophages are summarized and illustrated in Figure 1.2.

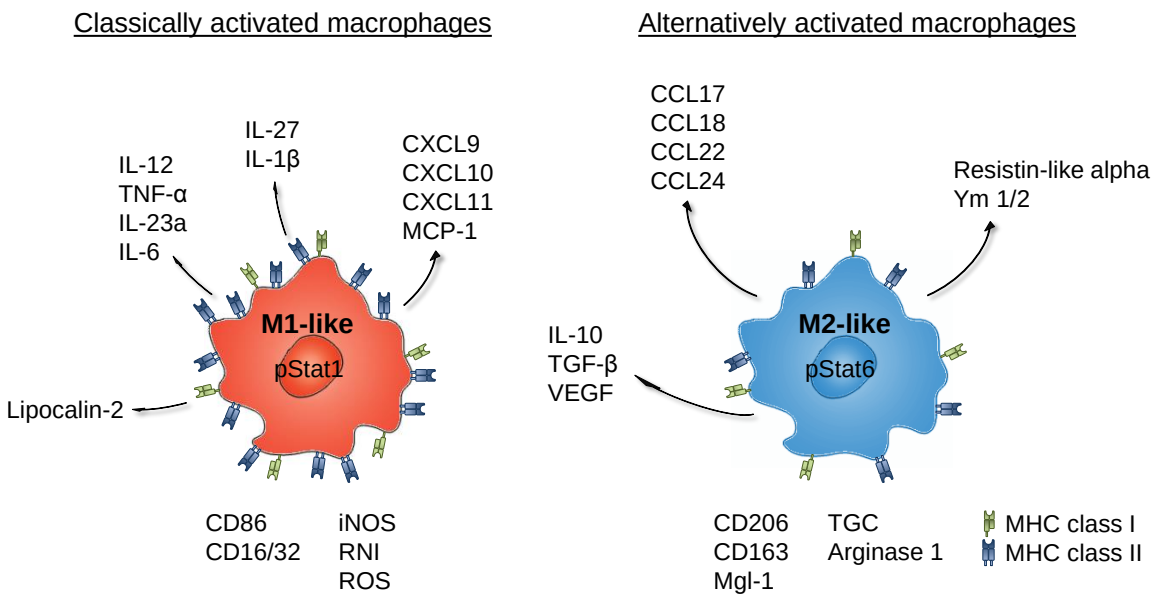

- also known as M1-like macrophages
- activated by IFNγ + LPS
- produce pro-inflammatory and immunostimulatory cytokines
- involved in Th1 responses to infection
- display microbicidal and tumoricidal activity
- anaerobic glycolytic pathway
- iron-retention (CD163^{low}, Ferritin^{high}, Ferroportin^{low})

- also known as M2-like macrophages
- activated by Th2 cytokines (IL-4, IL-10, IL-13)
- can promote tissue repair, matrix remodelling and angiogenesis
- tumor promotion
- protection from parasite infection
- immunosuppressive phenotype
- increased phagocytic activity
- iron-export (CD163^{high}, Ferritin^{low}, Ferroportin^{high})

Figure 1.2: Classical versus alternative macrophage activation.

1.2.1 Transcription factors

Extensive research has led to a detailed understanding of the signaling pathways that underlie macrophage polarization. Some of these pathways are described in the following paragraphs and are illustrated in Figure 1.3.

Alternative activation:

Besides IL-4, several other cytokines have been shown to induce alternative macrophage polarization, including IL-13, IL-10, IL-33 and TGF-β [132]. IL-4 and IL-13 are closely related cytokines which share the same receptors. IL-4 utilizes both, type I (IL-4Rα or IL-4Rγc) and type II (IL-4Rα or IL-13Rα1) IL-4 receptors, whereas IL-13 signals only through the type II receptor [133]. Junttila and colleagues demonstrated that PECs, bone marrow-derived macrophages (BMMs) as well as mouse and human monocytes express both receptors and have a greater sensitivity to IL-4 than to IL-13 [133]. The cytoplasmic domains of the receptor subunits are associated with janus kinase (JAK) tyrosine kinases. Upon binding of a ligand, two receptor subunits dimerize and bring two JAKs in close proximity, facilitating trans-phosphorylation. Phosphorylated JAKs have an increased kinase activity and therefore the capacity to phosphorylate additional targets including the receptor, thereby generating docking sites for STATs. Subsequently, recruited STATs are phosphorylated by JAKs which permits STAT dimerization and their subsequent entry into the nucleus. In the nucleus, STAT dimers bind to regulatory sequences in order to activate or repress target gene expression [134]. IL-4 and IL-13 binding to either type I or type II IL-4 receptors eventually results in activation of STAT6, which is known to be one of the master regulators for M2-associated gene expression [135]. Moreover, IL-4 induces STAT6 mediated expression of the demethylase Jmjd3, which demethylates histone H3 lysine-27 and histone H3 lysine-4 in the promoter regions of M2-associated genes thereby additionally promoting their expression [136]. These results demonstrate the importance of epigenetic regulation and chromatin remodeling in the context of macrophage polarization. Additional key transcription factors involved in M2 polarization are interferon regulatory factor (IRF) 4 [137] and peroxisome proliferator-activated receptor gamma (PPARγ) [138]. Bouhlel and colleagues reported a positive correlation between PPARγ and M2 marker expression [138]. Further, they demonstrated that treatment of primary human monocytes with PPARγ agonists enhanced the activation of M2-associated gene expression.

IL-10 acts through binding to its receptor IL-10R followed by activation of JAKs. The immunosuppressive effects of IL-10 are mainly mediated through the activation of STAT3. A consequence of IL-10 signaling is the upregulation of suppressor of cytokine signaling (SOCS) 3 which inhibits proinflammatory cytokine signaling pathways. Accordingly, SOCS3 deficient macrophages (isolated from LysM Cre-SOCS3$^{fl/fl}$ mice) express elevated levels of M1-associated cytokines, such as IL-6, IL-12 and IL-1β [139].

IL-33 is a cytokine belonging to the IL-1 family and acts through binding to its receptor interleukin 1 receptor-like 1 (IL1RL1 also known as ST2). IL-33 was reported to induce expression of Th2-associated cytokines by activating nuclear factor kappa-light-chain-enhancer of activated B cells (NF-κB) and mitogen-activated protein (MAP) kinases [140]. A study of Kurowska-Stolarska and colleagues showed that treatment of BMMs with IL-33 had no significant effect on macrophage polarization [141]. However, macrophages treated with IL-33 in combination with IL-13 or IL-4 expressed significantly higher levels of typical M2

markers (*Mrc1*, *Arg1* and *Ym1*) compared to macrophages treated with IL-13 or IL-4 alone. These results indicate that IL-33 synergizes with IL-13 and IL-4 to induce alternative macrophage polarization.

The spleen tyrosine kinase (Syk) is activated through phosphorylation upon binding of immune complexes to Fc-gamma receptor (FcγR) on macrophages. The signaling pathways induced by activated Syk induce expression of IL-10, SOCS3 and other negative regulators which results in the inhibition of both, type I IFN signaling as well as TLR4 signaling [142]. Ligation of immune complexes to the FcγRIIb on macrophages inhibits secretion of proinflammatory cytokines by inducing the production of prostaglandin E_2 [143]. These data suggest that immune complexes can participate in the modulation of macrophage polarization by inhibiting pathways involved in classical activation.

Classical activation:

Classical activation of macrophages is induced by binding of LPS or type I IFNs or IFNγ to TLR4 or IFN-α/β (IFNAR) receptor or IFN-γ (IFNGR) receptor, respectively. After binding to its ligand, TLR4 dimerizes and undergoes conformational changes. These changes facilitate subsequent recruitment of toll/interleukin-1 receptor (TIR) domain containing adaptor molecules including myeloid differentiation primary response 88 (MyD88), TRIF-related adaptor molecule (TRAM), TIR-domain containing adapter inducing interferon-β (TRIF) and MyD88-adapter like (Mal). Mal functions as bridging molecule between TLR4 and MyD88. Upon stimulation, MyD88 recruits IL-1 receptor associated kinase (IRAK) 4 and IRAK1. After the recruitment of several other IRAKs, they dissociate from MyD88 to interact with TNF-receptor associated factor (TRAF) 6. TRAF6 builds up a complex with the transforming growth factor beta-activated kinase 1 (TAK1) and several proteins belonging to the family of TAK1 binding proteins (TABs). This complex in turn activates the IκB kinase (IKK) complex (composed of IKK-α, IKK-β and NF-kappa-B essential modulator (NEMO)) which subsequently phosphorylates the NF-κB inhibitory molecule IκB. As a consequence, IκB is degraded by the proteasome and NF-κB (heterodimer of p50 and p65) is released. After translocation into the nucleus, NF-κB induces expression of proinflammatory genes [144]. Besides recruiting MyD88, TLR4 additionally recruits TRAM, serving as bridging molecule between TLR4 and TRIF. The recruited TRIF binds to TRAF3, which is important for the activation of IKK-related kinases (including TRAF family member-associated NF-kappa-B activator (TANK) binding kinase 1 (TBK1) and IKK-i). These kinases eventually phosphorylate IRF3 and IRF7 which subsequently translocate into the nucleus and induce the expression of additional proinflammatory genes [144, 145].

Binding of IFNs to their corresponding receptors induce the JAK/STAT signaling pathway as described above. This results in the activation of several transcription factors such as STAT1, STAT2 and IRF-1 which subsequently induce M1-associated gene expression [146].

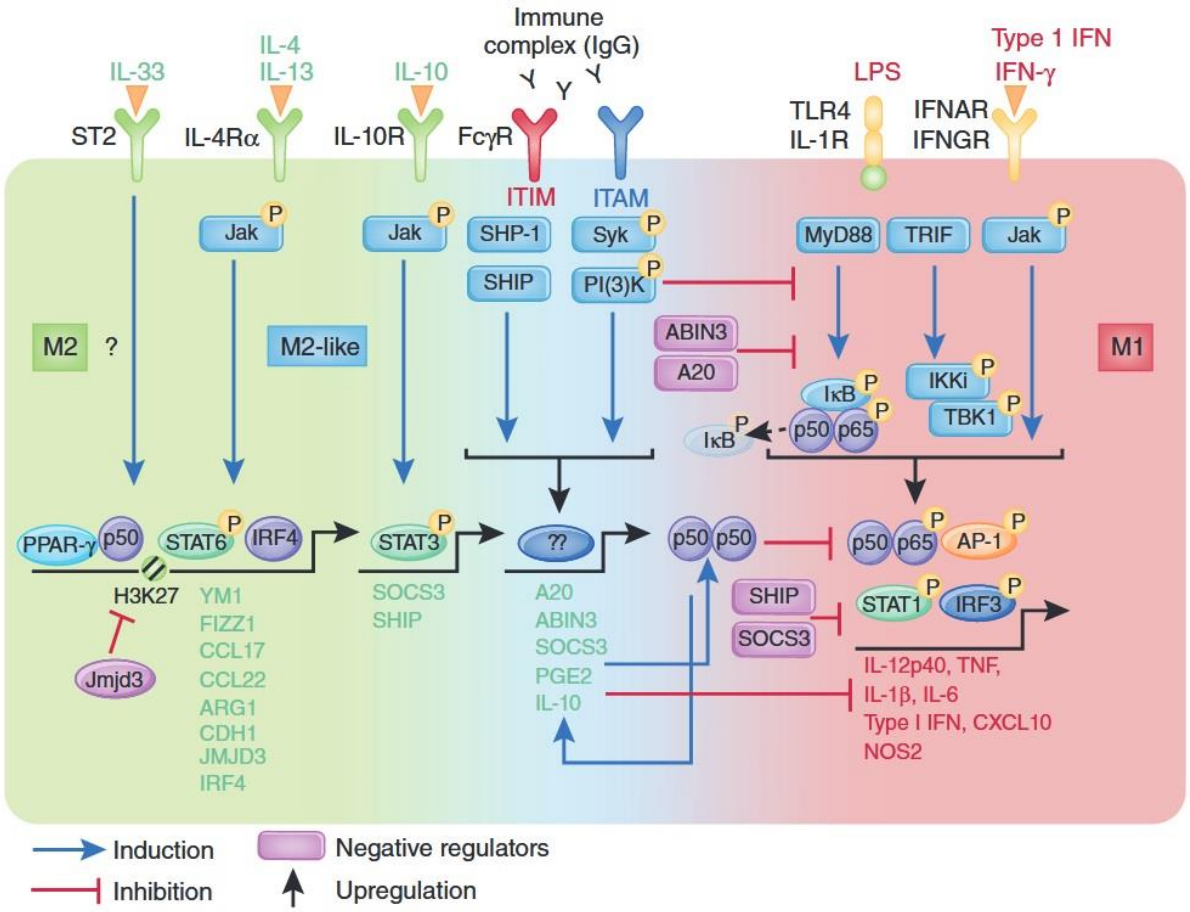

Figure 1.3: Molecular pathways of classical and alternative macrophage activation.
M1- and M2-associated genes transcribed upon macrophage activation are indicated by red and green lettering, respectively. Figure was taken from [147].

1.2.2 MicroRNA-mediated control of macrophage polarization

MicroRNAs (miRNAs) are small non-coding RNA molecules approximately 20 - 24 nucleotides in length. They play an important role in post-transcriptional gene regulation by binding to the 3'-untranslated region (UTR) of target mRNA sequences, mediating their translational repression or cleavage. Regulation of gene expression by miRNAs is a highly conserved mechanism present in most eukaryotic cells and involved in virtually all biological processes. Deregulated miRNA expression can result in pathological conditions such as cancer and normalization of miRNA expression might be a valuable therapeutic approach in the near future [132]. The following paragraph describes several miRNAs which have been identified to play a major role in macrophage polarization by regulating the expression of some key transcription factors. The expression and clinical relevance of miRNAs in TAMs has been described elsewhere [148].

MiR-125a and miR-125b were shown to be highly expressed in human monocyte-derived macrophages [149]. However, LPS treatment was accompanied by a downregulation of miR-125b in the murine macrophage cell line Raw264.7 cells [150] and an upregulation of miR-125a in murine monocyte-derived macrophages [149]. Interestingly, transfection of THP-1 cells with miR-125a-5p mimics increased the expression of several M1-associated genes [149]. In a cohort of diffuse large B-cell lymphoma biopsies, miR-125a and miR-125b have been shown to constitutively stimulate the NF-κB pathway by targeting one of its

negative regulators tumor necrosis factor alpha-induced protein 3 (TNFAIP3) [151]. In accordance with these findings, macrophages (BMMs or RAW264.7 cells) transfected with miR-125b show an increased responsiveness to IFNγ, upregulate CD80 expression and have the capacity to activate T cells more efficiently compared to untransfected macrophages [152]. Further, the transcription factor IRF4 which plays an important role in the alternative activation of macrophages was identified to be a direct target of miR-125b [152]. Thus, miR-125a and miR-125b seem to be important regulators of macrophage polarization, driving macrophages preferentially into the M1 state.

Expression of miR-155 was shown to be induced upon activation of macrophages by TLR ligands and IFNs [153]. In PECs and RAW264.7 cells miR-155 downregulates suppressor of cytokine signaling-1 (SOCS1) and B-cell lymphoma-6 protein (BCL6), both of which are inhibitors of the classical macrophage activation [154, 155]. SOCS1 is a direct inhibitor of type I IFN signaling, whereas BCL6 is a transcription factor known to repress NF-κB signaling. Downregulation of these proteins mediated by miR-155 induces the expression of proinflammatory cytokines and drives M1 polarization. Further, miR-155 was shown to directly target the IL-13 receptor, thereby reducing phosphorylation and activation of STAT6, which is one of the key transcription factors promoting M2 polarization [156]. Cai and colleagues demonstrated that transfection of M2 polarized (IL-4) BMMs as well as M2 TAMs with miR-155 resulted in repolarization into M1 macrophages [157]. However, miR-155 was also shown to downregulate SHIP1, a negative regulator of the phosphatidylinositol-4,5-bisphosphate 3-kinase/RAC-alpha serine/threonine-protein kinase (PI3K/AKT1) pathway. The resulting increased activation of AKT1 signaling is associated with alternative BMM polarization [158]. Further, miR-155 expression correlates with poor survival of lung adenocarcinoma patients [159] as well as higher tumor grade and lymph node metastases in breast cancer patients [160] and was shown to be overexpressed in several other tumor entities [161]. These results indicate that miR-155 can have both, tumor suppressive as well as tumor promoting potential depending on the cell type in which it is expressed.

Another miRNA which was reported to have substantial effects on macrophage polarization is miR-146a. Treatment of THP-1 cells with LPS results in a strong NF-κB dependent upregulation of miR-146a as demonstrated by Taganov and colleagues [162]. Of note, miR-146a has been demonstrated to target TRAF6 and IRAK1 mRNA, both of which are adapter molecules downstream of cytokine and TLR signaling pathways. Thus, miR-146a expression is induced in classically activated macrophages to control cytokine and TLR signaling in a negative feedback loop and reduce the release of proinflammatory cytokines [162]. In accordance with these results, inhibition of miR-146a in polarized PECs promoted the expression of M1-associated genes (*Il6* and *Il1b*) and decreased expression of M2-associated genes (*Pdgf* and *Arg1*). Furthermore, miR-146a transfected RAW264.7 cells mixed with 4T1 cells and injected subcutaneously (s.c.) into BALB/c mice significantly promoted tumor growth [163].

Similar regulatory feedback loops as described above were reported for miR-21, miR-9, miR-187 and miR-147 [132, 164]. The expression of these miRNAs is induced upon TLR stimulation and all of them target different molecules involved in promoting classical macrophage activation. While miR-21 is regulating the tumor suppressor programmed cell death protein-4 (PDCD4) [165], miR-9 and miR-187 are regulating different components involved in NF-κB signaling (NF-κB subunit p50 (NFKB1) [166] and NF-κB inhibitor zeta (NFKBIZ) [167], respectively).

miR-124 expression was shown to be induced in PECs, BMMs and RAW264.7 cells upon stimulation with IL-4 and IL-13 [168]. Inhibition of miR-124 and subsequent polarization of macrophages with IL-4 was accompanied by decreased expression levels of M2-associated genes (*Mrc1, Ym1*) and increased expression of several M1 markers (CD86, TNF, iNOS) when compared to a scrambled antagomir control. These results indicate that miR-124 has an important role in driving and maintaining a M2 phenotype.

The two miRNAs miR-511-3p and miR378-3p are upregulated upon stimulation of macrophages with IL-4 and act in a negative feedback loop by downregulating signaling molecules involved in alternative macrophage activation. miR378-3p directly targets the protein kinase AKT1 which is a component of the PI3K/AKT1 signaling pathway [169]. Interestingly, miR-511 is located within an intron of the *Mrc1* gene and its expression is co-regulated with *Mrc1* expression. *Mrc1* encodes for the mannose receptor CD206 and is typically associated with alternatively activated macrophages. As demonstrated by Zhou and colleagues, transfection of a miR-511-3p mimic into LPS treated BMMs resulted in reduced expression of proinflammatory cytokines such as IL-1β and IL-6 [170]. Conversely, expression of typical M2-associated genes (*Ym1, Arg1 and Fizz1*) were elevated in IL-4 treated and miR-511-3p transfected BMMs compared to mock transfected cells. Moreover, they showed that macrophages of *Mrc1*$^{-/-}$ mice express significantly lower amounts of miR-511-3p and have a more pronounced M1 phenotype when compared to wild type mice. The Rho-dependent kinase-2 (ROCK2), which phosphorylates the transcription factor IRF4 was identified to be a direct target of miR-155 [171].

All examples mentioned above illustrate the importance of miRNAs in the context of macrophage polarization. However, most of the studies focused only on single miRNAs, thereby neglecting that the interplay between multiple miRNAs is essential to orchestrate the complex process of alternative and classic activation of macrophages. Thus, experimental set ups should additionally include a variety of miRNA combinations to eventually define clusters of miRNAs which modulate macrophage phenotypes.

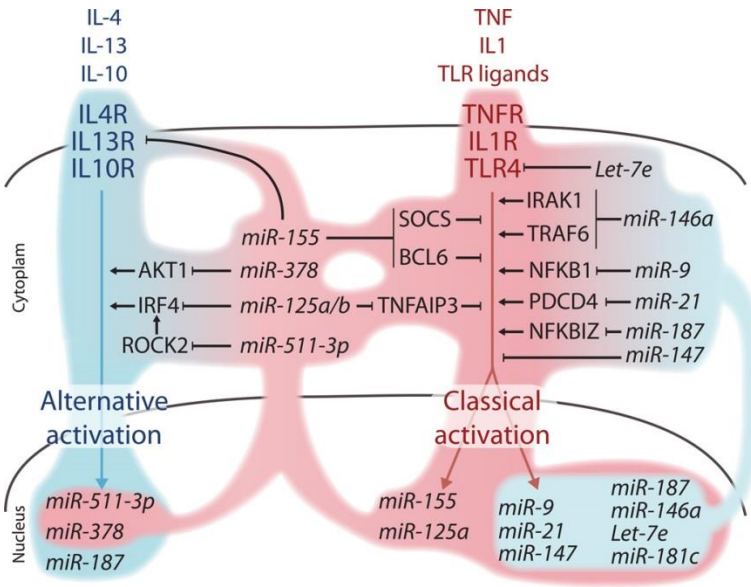

Figure 1.4: Regulation of macrophage polarization by miRNAs.
The figure illustrates receptor ligand interactions which are known to drive M2 (left, blue) or M1 (right, red) polarization of macrophages. miRNAs which primarily maintain the M1 phenotype are shaded in red, whereas blue shaded miRNAs are necessary to sustain alternative activation. Figure was taken from [132].

1.2.3 Metabolic changes during macrophage polarization

The polarization of macrophages is accompanied by metabolic changes, including a shift towards the anaerobic glycolytic pathway in M1 macrophages [172]. An increase in glycolysis is required to rapidly trigger anti-microbial activity and to survive in hypoxic microenvironments. In contrast, M2 macrophages predominantly use fatty acid oxidation which guarantees permanent energy supply required for processes like tissue repair or remodeling [173].

As already briefly mentioned, polarization of macrophages is also associated with changes in the arginine metabolism. While M1 macrophages use iNOS to metabolize arginine to nitric oxide, M2 macrophages metabolize arginine to ornithine and urea using arginase. Nitric oxide has antimicrobial activities and is an important effector molecule of M1 macrophages, whereas ornithine is the starting point for polyamine synthesis required for collagen synthesis and tissue remodeling [174].

Macrophages are constantly phagocytosing red blood cells, thereby recycling iron and making it available for erythropoiesis and other processes. Polarization of macrophages is associated with changes in their iron metabolism, with M1 macrophages showing low levels of CD163 (heme uptake) and ferroportin (iron export) and high levels of ferritin (iron storage) [174]. Thus, M1 polarized macrophages are in an iron-retention mode and efficiently keep away the iron from invading pathogens. Moreover, they secrete lipocalin-2 which was shown to inhibit siderophore-mediated iron uptake by pathogens [175]. As iron is an essential growth factor for many bacteria, the iron-retention mode together with the secretion of lipocalin-2 support bacteriostatic activity of M1 polarized macrophages. In contrast, M2 polarized macrophages are in an iron-export mode, with high expression level of CD163 and ferroportin, but low expression of ferritin [174]. The high heme concentrations within the cells facilitate expression of heme oxygenase by inhibiting the transcription repressor Bach1 [176]. Heme oxygenase catalyzes the degradation of heme into Fe^{2+}, biliverdin and carbon monoxide [177]. Biliverdin is subsequently converted into bilirubin which has anti-inflammatory properties and acts as antioxidant. Carbon monoxide inhibits the expression of TNF-α and IL-1β and increases expression of IL-10 [178], thus contributing to the immunosuppressive phenotype of M2-like macrophages.

1.2.4 Tumor-associated macrophages

Macrophages express the C-C chemokine receptor (CCR) 2 and can be recruited into the tumor microenvironment by C-C chemokine ligand (CCL) 2 expressing tumor cells [179]. The phenotype of infiltrated tumor associated macrophages (TAMs) is strongly dependent on the microenvironment of the developing tumor and the tumor progression stage. In an early stage of tumor development, TAMs resemble the M1 phenotype and have the capacity to induce anti-tumor immunity and to elicit tumor eradication. However, in later stages of tumor development TAMs receive signals from the tumor cells (e.g. IL-10 and TGF-β) and from surrounding stroma cells directing M1-like macrophages to the immunosuppressive M2 state [180-182]. TAMs with a M2 phenotype show low surface expression levels of MHC molecules and suppress anti-tumor immune responses by various mechanisms:

1. Release of immunosuppressive cytokines such as IL-10 and TGF-β, thereby impairing effector T cell activity.

2. Secretion of IL-10 and TNF-α induces PD-L1 expression on TAMs in an autocrine manner and suppresses tumor-specific T cell immunity [183].
3. Attraction of regulatory T cells by secretion of CCL22 [184].
4. Overexpression of the tryptophan degrading enzyme indoleamine 2,3-dioxygenase-1 (IDO1), thereby depriving T cells of tryptophan and suppressing their activation and proliferation [185].
5. Expression of B7-H4, a negative regulator of T cell activity that binds to an unknown receptor on activated T cells resulting in impaired T cell effector functions [186, 187].
6. Expression of arginase 1 inhibits antigen-specific T cell responses by depriving the cells of the semi-essential amino acid L-arginine [188].

However, M2 polarized TAMs do not only promote tumor growth by modulating the immune system, but also by inducing and controlling additional processes like angiogenesis, tumor cell proliferation and invasion. TAMs secrete high amounts of angiogenesis promoting factors such as VEGF and thymidine phosphorylase, thereby contributing to metastases formation [189, 190]. Moreover, they express a number of matrix metalloproteinases (e.g. MMP-2, MMP-9, MMP-12) which were shown to be important mediators of angiogenesis in a mouse model of human cervical carcinogenesis [191]. In accordance with this, high frequencies of TAMs were reported to be associated with an increased tumor vascularization in many tumor entities including breast [192], bladder [193] and prostate carcinoma [194]. Besides promoting tumor growth by inducing angiogenesis, TAMs can also directly affect tumor cell survival by secreting factors that are important for tumor cell proliferation, including epidermal growth factor (EGF) [195]. Further details about the clinical significance of TAMs in different tumor entities and the development of TAM targeting immunotherapeutic approaches are given in section 1.3.1.

1.3 Immunotherapy approaches to treat cancer

Tumor immunotherapy approaches comprise treatments which improve or restore functions of the immune system or involve the administration of immunological compounds, thereby facilitating tumor cell killing. In the following paragraphs, the modes of action and preclinical as well as clinical data of different immunotherapeutic strategies are described.

1.3.1 Targeting tumor associated macrophages

As already described in section 1.2.4, the majority of TAMs are in a M2 state and contribute to the establishment of an immunosuppressive microenvironment by various mechanisms. A high density of $CD68^+$ TAMs was shown to be associated with negative effects on overall survival (OS) in patients with gastric, breast, bladder, ovarian, oral and thyroid cancer [196]. In contrast, accumulation of TAMs had beneficial effects on overall survival in patients with colorectal cancer. However, not only the density of TAMs within the tumor, but also their localization and polarization are of clinical relevance. As demonstrated by Medrek and colleagues, the presence of $CD163^+CD68^+$ M2 macrophages in the tumor stroma positively correlated with increased tumor size and higher tumor grade [197]. Infiltration of TAMs into the tumor nest did not correlate with any clinicopathological features. Similar results were

obtained in melanomas where high densities of $CD163^+$ macrophages in the tumor stroma and $CD68^+$ cells at the invasive front were associated with poor overall survival [198]. In a retrospective study using paraffin-embedded non-small cell lung cancer (NSCLC) specimens, a high density of M1 macrophages ($CD68^+$HLA-DR^+) positively correlated with patients survival, whereas M2 densities did not correlate with overall survival [199].

As TAMs are generally associated with poor prognosis in most tumor entities they are considered as a promising new target for cancer therapy. As illustrated in Figure 1.5, TAM targeting approaches are either based on inhibiting TAM recruitment, suppressing TAM survival, enhancing tumoricidal activity of TAMs or inhibiting their tumor promoting activity. Recruitment of TAMs into the tumor microenvironment is mediated in great part by CCL2. High expression levels of CCL2 were shown to be associated with elevated numbers of TAMs and poor prognosis in breast [200] and prostate [201] cancer patients. Treatment with Bindarit, an inhibitor of CCL2 expression was shown to reduce tumor growth and macrophage recruitment in a human melanoma xenograft model [202]. Trabectedin (Yondelis) is a DNA binding chemotherapeutic drug which is approved for the treatment of patients with advanced soft-tissue sarcoma and relapsed ovarian cancer [203]. The mode of action of this compound seems to be different from other DNA intercalating agents used in cancer therapy and is not completely understood. Allavena and colleagues reported that Trabectedin inhibits macrophage differentiation and reduces CCL2 expression in freshly isolated ovarian tumor cells. The authors concluded that these immunomodulatory properties probably contribute to the antitumor activity of this drug [204]. Other chemoattractants such as macrophage colony-stimulating factor (M-CSF), CCL5 and CXCL12 might additionally serve as therapeutic targets to inhibit macrophage recruitment.

Another approach to reduce the number of TAMs is to kill them locally. This has been achieved by chemical drugs, immunotoxin-conjugated antibodies, attenuated bacteria or agents that trigger immune cells to recognize TAMs. Legumain, a stress protein overexpressed by TAMs was demonstrated to be an ideal target molecule for a legumain-based DNA vaccine [205]. Vaccination of tumor bearing mice induced a robust $CD8^+$ T cell response against TAMs and decreased the release of proangiogenic factors such as VEGF and MMP9. Decreasing the number of TAMs in the tumor microenvironment by legumain targeting $CD8^+$ T cells suppressed tumor growth and metastases formation in murine breast, colon and non-small cell lung cancer models.

Besides inhibiting macrophage recruitment or inducing their depletion, repolarization of TAMs into M1-like macrophages with tumoricidal activity is an attractive approach. Successful repolarization of TAMs was already achieved by the use of different compounds. Administration of CpG in combination with an anti-interleukin-10 receptor antibody was shown to repolarize tumor infiltrating macrophages from M2 to M1 in mammary adenocarcinoma bearing BALB/c mice [206]. Banerjee and colleagues achieved TAM repolarization in advanced stage B16F10 tumors by using a combination of heat-killed *Mycobacterium indicus pranii* and an agonistic glucocorticoid-induced TNFR-related protein (GITR) antibody [207]. A multidrug chemotherapy (vincristine, cyclophosphamide and doxorubicin) combined with an anti-CD40 antibody and CpG induced expression of M1-associated genes in TAMs from B16 tumors, delayed tumor growth and significantly increased survival of the mice [208]. Overexpression of histidine-rich glycoprotein (HRG) in T241 fibrosarcoma cells, PancO2 cells and 4T1 cells was demonstrated to inhibit tumor growth and metastases. HRG promoted repolarization of TAMs to a M1 phenotype which

was accompanied by vessel normalization and an effective anti-tumor immune response [209]. In Id-specific T cell receptor transgenic mice, $CD4^+$ T cells were reported to induce macrophage repolarization in s.c. MOPC315 myeloma tumors by secretion of IFNγ [210, 211]. Klug and colleagues showed that neoadjuvant local low-dose gamma irradiation induced accumulation of iNOS expressing M1 macrophages [212]. Moreover, iNOS was reported to mediate CTL recruitment into the tumors by inducing vascular normalization, endothelial activation and suppressing the production of immunosuppressive factors.
In addition to enhancing M1 mediated tumoricidal activity as described above, the inhibition of M2 tumor promoting features is another promising strategy. This might be achieved by inhibition of transcription factors known to be involved in maintaining a M2 phenotype, such as STAT3 [213], MYC [214], STAT6 and KLF4 [215].

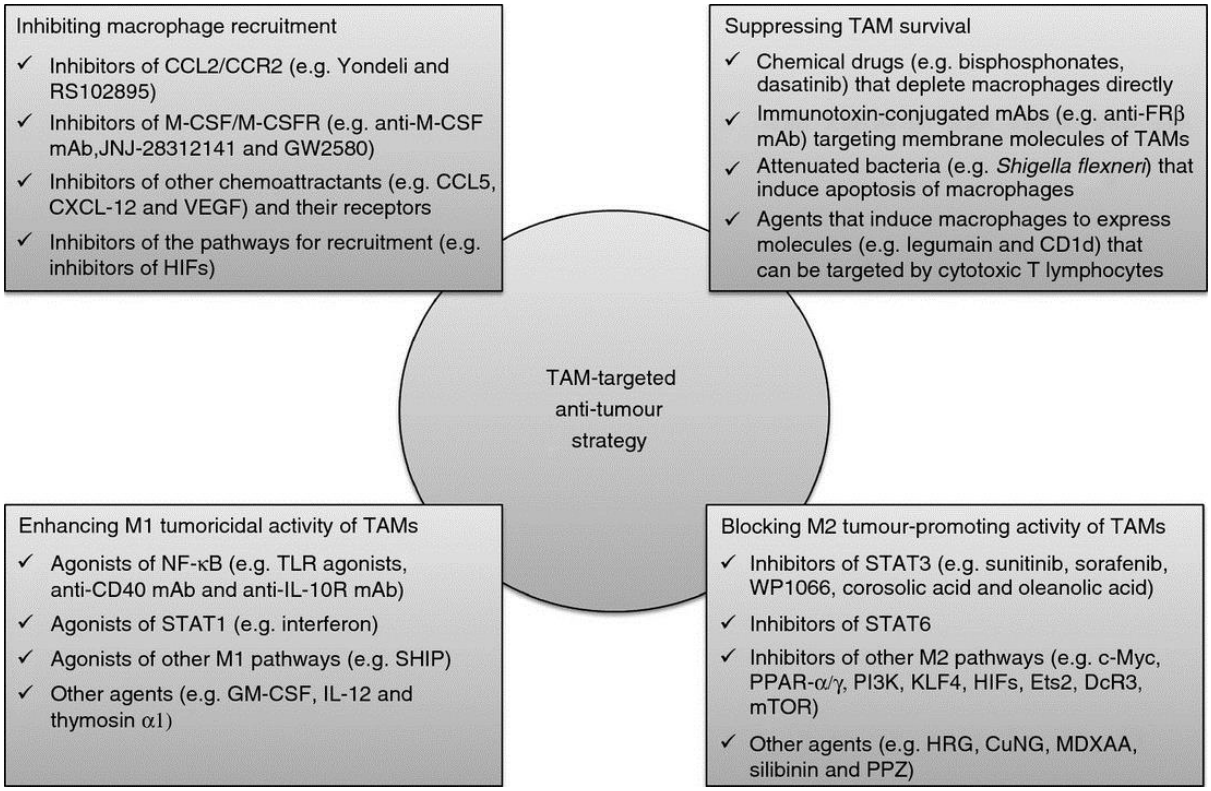

Figure 1.5: Strategies to target tumor-associated macrophages.
The strategies to target TAMs are either aiming for a reduction of TAM numbers in the tumor microenvironment (two upper rectangles) or a repolarization of TAMs from a tumor promoting to a tumoricidal state (two lower rectangles). Figure was taken from [216].

1.3.2 Adoptive cell therapy

Adoptive cell therapy (ACT) is a personalized cancer therapy approach that involves the administration of T cells with direct anti-tumor activity to the patient [217]. In 1987 Rosenberg and colleagues demonstrated for the first time that tumor-infiltrating lymphocytes (TILs) expanded from patients with metastatic melanoma were cytotoxic against autologous melanoma cells but not against normal cells [218]. Only one year later, patients with metastatic melanoma were treated by ACT using TILs and IL-2. An objective regression of the metastases in the lungs, liver, bone and skin was observed in 55 % of the patients and lasted from 2 to more than 13 months [30]. Nowadays, ACT using autologous TILs is

considered as an effective immunotherapy to treat patients with metastatic melanoma as it is more effective in inducing complete durable responses than any other available immunotherapy. As reported by several institutions, the objective response rates of melanoma patients treated with autologous TILs and IL-2 following lymphodepletion ranged from 38 % – 55 % [219-221]. In a study of Rosenberg and colleagues, 22 % of the patients with metastatic melanoma achieved a complete tumor regression beyond five to ten years after ACT demonstrating that the adoptive transfer of autologous TILs can induce durable complete responses [222]. Even though TILs can be expanded from almost all types of cancer, a consistent expansion of TILs with anti-tumor reactivity was so far only applicable for melanomas. Moreover, ACT using TILs is a very complex, expensive and time consuming approach making it unsuitable for general application until now. Another major limitation of this approach is the requirement of pre-existing tumor-reactive T cells within the tumors of the patients that can be expanded *ex vivo*.

Genetically engineered T cells, transduced with either high affinity T cell receptors against TAAs or chimeric antigen receptors (CARs) were developed to overcome these limitations. The first TCR engineered T cells used in the clinic were transduced with a TCR recognizing a human leukocyte antigen (HLA) A2 restricted peptide of the melanocytic differentiation antigen MART-1 [223]. In all 15 patients treated, the adoptively transferred T cells were detectable in the peripheral blood for at least 2 months. Moreover, in 2 patients who both showed regression of metastatic melanoma lesions TCR transduced cells were still detected in the circulation 1 year after T cell transfer. In another study, T cells were engineered to express a high affinity TCR recognizing a peptide derived from the cancer-testis antigen NY-ESO-1 [224]. In 16 out of 20 patients with advanced multiple myeloma promising clinical responses were observed upon adoptive T cell transfer.

CAR T cells overcome some limitations associated with TCR engineered T cells as they are independent of costimulatory signals (starting from the second generation CARs) and expression of MHC molecules on the surface of tumor cells. CARs are fusion proteins consisting of an extracellular protein binding domain and intracellular signaling domains. The extracellular binding domain is most commonly derived from an antibody single chain variable fragment directed against a tumor-associated antigen. The intracellular signaling domains derive from proteins involved in TCR signaling. First generation CARs contain only a single intracellular signaling module composed of CD3ζ. Second and third generation CARs possess one or more costimulatory domains (e.g. CD28 or 4-1BB) fused to CD3ζ, respectively. In August 2017, autologous T cells expressing a CAR specific for CD19 were approved by the Food and Drug Administration (FDA) for treatment of diffuse large B cell lymphoma and refractory pre-B cell acute lymphoblastic leukemia (Kymriah; Novartis). Complete remission was achieved in 83 % of treated patients [225]. Only 2 months later, a second CD19 CAR T cell therapy was approved for treatment of adults with relapsed/refractory large B cell lymphoma (Yescarta; Kite Pharma). The FDA approval was based on a study showing an overall response rate (ORR) of 82 %, including a complete response in 58 % of the patients [225]. Using CAR T cells to target tumor-associated antigens also in solid tumors is more difficult and has achieved only limited success so far, due to the immunosuppressive tumor microenvironment and antigen heterogeneity.

1.3.3 Vaccination strategies

Vaccination of cancer patients with recombinant TAAs, whole tumor cell lysates, TAA encoding RNAs or synthetic peptides encompassing T cell epitopes are strategies to induce an anti-tumor immune response. However, most clinical trials based on one of these vaccination approaches demonstrated limited therapeutic efficiencies [226].
Several studies demonstrated that vaccinations with peptides derived from TAAs can induce T cell responses and even result in durable clinical responses [227, 228]. However, the overall clinical response rates were low revealing the need for improved peptide vaccination strategies. The outcome of peptide vaccinations might be improved by including long peptides, modifying the adjuvants, including new antigens and combining peptide vaccination with other immunotherapies. Short peptides might directly bind to MHC molecules on the surface of non-professional antigen presenting cells and thereby induce T cell anergy. In contrast, long peptides (30-mer) need to be internalized and processed by APCs and might harbor both, CD4 and CD8 T cell epitopes which was demonstrated to be essential to establish a long-term T cell memory [229, 230].

During the last years, several clinical studies testing the efficiency of RNA-based vaccination strategies have been set up. mRNAs encoding TAAs have been used to elicit anti-tumor immune responses primarily in two ways. The first approach is based on loading of autologous dendritic cells *ex vivo* with mRNA and subsequent transfer of these cells into the patient where the encoded protein is expressed and TAA derived epitopes are presented. A second approach relies on the presentation of epitopes by APCs upon direct injection of mRNA into the patient (either systemically or locally). A study by Fotin-Mleczek and colleagues reported a robust TAA specific $CD4^+$ and $CD8^+$ T cell response upon intradermal administration of an ovalbumin (OVA) encoding self-adjuvanted mRNA vaccine [231]. After two intradermal vaccinations, C57BL/6 mice s.c. injected with E.G7 cells were completely protected against tumor outgrowth. A self-adjuvanted mRNA vaccine encoding for various prostate cancer associated antigens was safe and well tolerated as demonstrated in a phase I/IIa study [232]. Further, tumor antigen specific T cells could be detected in 79 % of the patients, with 58 % showing an immunological response against multiple antigens. Even though other studies could also demonstrate the induction of antigen specific T cell responses upon vaccination with mRNA formulations, the anti-tumor activity remains low [233]. Recently, the intravenous (i.v.) administration of OVA encoding RNA-lipoplexes with optimal net charge has been shown to protect RNA from degradation and mediate its uptake, translation and epitope presentation by dendritic cells [234]. Further, the authors showed an induction of strong effector and memory T cell responses resulting in B16-OVA tumor rejection. The systemic delivery was more effective in T cell priming compared to local vaccine administration and thus appears to have greater therapeutic potential. In a phase I dose-escalation trial RNA-lipoplexes encoding four tumor antigens (Tyrosinase, Transmembrane phosphatase with tensin homology (TPTE), NY-ESO-1 and MAGE-A3) are currently tested in patients with malignant melanoma.

The use of whole tumor cell lysates represents an attractive alternative to synthetic peptide or RNA based immunotherapies. In contrast to TAA derived peptides or TAA encoding mRNA, tumor lysates comprise a huge amount of potential T cell epitopes which have the capacity to activate $CD4^+$ and $CD8^+$ T cells. The activation of a variety of anti-tumor reactive T cell clones increases the likelihood of durable tumor control. Further, vaccination with

whole tumor lysates is suitable for treatment of virtually all cancer patients due to the broad polyclonal immune response. Treatment of melanoma patients with Canvaxin, an allogenic whole cell vaccine composed of three irradiated melanoma cell lines resulted in improved overall survival rates [235]. However, two phase 3 clinical trials in patients with stage III and IV melanoma were discontinued due to low efficiency [236]. Another example is GVAX vaccine which was developed for the treatment of prostate cancer. GVAX is composed of two allogenic prostate tumor cell lines which were transduced with an adenoviral vector encoding for granulocyte macrophage colony-stimulating factor (GM-CSF) to increase DC recruitment to the site of vaccination [237]. The cell lines were irradiated and subsequently injected intradermally in prostate cancer patients. Safety and clinical activity of GVAX were confirmed in phase I and II studies [238]. However, a phase III trial comparing GVAX with the standard of care treatment (docetaxel and prednisone) was terminated due to increased number of deaths in the GVAX arm compared to the control arm. Another phase III trial, comparing a combination of GVAX and docetaxel with a combination of docetaxel and prednisone was terminated in the same year. This decision was based on a study of the Independent Data Monitoring Committee which stated that the trial has only a low chance (< 30 %) of meeting the predefined end point [238].

1.3.4 Monoclonal antibodies

Within the last 20 years, a variety of monoclonal antibodies for the treatment of solid and haematological cancers have been established. Antibodies can mediate tumor cell killing in various ways as explained by the following examples. Trastuzumab (anti-HER2/neu) is a humanized IgG1 antibody approved for the treatment of human epidermal growth factor receptor 2 (HER2/neu) positive breast cancer patients [239]. The monoclonal antibodies Cetuximab [240] and Panitumumab [241] target epidermal Growth Factor Receptor (EGFR) and are approved for the treatment of EGFR-positive metastatic colorectal cancer. These three antibodies act by inhibiting the downstream signaling pathways required for rapid tumor cell proliferation. Moreover, Trastuzumab and Cetuximab can induce antibody-dependent cellular cytotoxicity (ADCC) by recruiting NK cells.

Rituximab (anti-CD20) is a chimeric human-murine IgG1 antibody approved for treating patients with B cell non-Hodgkin’s lymphoma and chronic lymphocytic leukemia [242]. This antibody facilitates tumor cell killing by directly inducing apoptosis and ADCC as well as complement-dependent cytotoxicity (CDC). Other antibodies conjugated to radioisotopes or to toxic drugs, such as Yttrium-90 ibritumomab-tiuxetan (anti-CD20) and Iodine-131 tositumomab (anti-CD20) or Brentuximab vedotin (anti-CD30), respectively have been applied to induce tumor cell killing [243].

Besides targeting tumor-associated antigens to induce direct tumor cell killing, some antibodies function by either activating or antagonizing immunological pathways which are involved in cancer immune surveillance. For instance, an agonistic CD40 antibody was shown to induce tumor regressions in pancreatic ductal adenocarcinoma patients. This effect was mediated through the activation of macrophages, which rapidly infiltrated into the tumors and became tumoricidal [244]. Moreover, several antibodies blocking negative regulators of immune activation such as CTLA-4 and PD-1 resulted in durable responses and have been approved by the FDA for the treatment of melanoma. A detailed description of these immune checkpoint inhibitors is given in section 1.4.3.3.

1.3.5 Oncolytic viruses

Oncolytic viruses act by selective tumor cell killing as well as by establishing anti-tumor immunity. Selective targeting of tumor cells is driven by at least three factors. First, tumor cells often overexpress viral entry receptors. Second, viral replication benefits from the high metabolic activity of tumor cells compared to normal cells. Third, many tumor cells have deficiencies in antiviral type I IFN signaling. The release of viral antigens and cell debris by dying tumor cells promotes the development of the aforementioned anti-tumor immunity [245].

Most of the oncolytic viruses which are tested in clinical trials are engineered to improve selective targeting of tumor cells. For instance, many variants of the Herpes simplex virus type 1 with deletion of the infected cell protein (ICP) genes *ICP34.5* and *ICP6* have been constructed and showed increased anti-tumor and immune stimulating activity [246, 247]. The viral ribonucleotide reductase ICP6 is substantial for the generation of a nucleotide pool which is required for viral replication in quiescent cells. Deletion of *ICP6* results in selective viral replication in tumor cells with inactivated $p16^{INK4A}$ tumor suppressor. PROSTVAC is a prime-boost regimen using vaccinia virus as primary vaccination followed by booster injections with fowlpox virus. Both virus types are engineered to express costimulatory molecules (lymphocyte function-associated antigen (LFA) 3, B7.1 and intercellular adhesion molecule (ICAM) 1) and prostate-specific antigen (PSA). Subcutaneous injection of vaccinia viruses induces a strong immune response against the tumor-associated antigen PSA, resulting in PSA specific CTLs that can kill prostate cancer cells. As neutralizing antibodies against the vaccinia virus are produced rapidly, booster vaccinations with fowlpox viruses are required to enhance the anti-tumor T cell immunity. Treatment with PROSTVAC and GM-CSF in a Phase II trial was well tolerated and significantly improved median overall survival of prostate cancer patients [248].

In 2015, the first oncolytic virus (talimogene laherparepvec) was approved by the FDA for treatment of unresectable melanoma lesions. Talimogene laherparepvec is a herpes simplex virus type I engineered to express GM-CSF and deleted for *ICP34.5* and *ICP47*. ICP47 inhibits the TAP mediated transfer of viral derived peptides across the endoplasmic reticulum (ER) membrane, thereby preventing MHC restricted presentation of viral peptides on the infected cell surface which eventually results in immune evasion [249]. Melanoma patients that received intralesional injections of talimogene laherparepvec showed a significantly higher durable response rate compared to GM-CSF injections (16.3 % vs. 2.1 %) [250]. Moreover, the overall response rate as well as the median overall survival was higher and the therapy was well tolerated.

Many other viruses, including adenoviruses, vaccinia viruses, measles viruses and coxsackieviruses are now tested in clinical trials with some of them showing encouraging data [251].

1.3.6 Toll-like receptor agonists and cytokines

The two immunostimulatory cytokines IL-2 and IFN-α2b have been shown to improve an anti-tumor immune response and were approved by the FDA as standalone therapy for the treatment of advanced melanoma (described more in detail in section 1.4.3.3). However, most of the times administration of cytokines is combined with other immunotherapies to enhance their immunogenic potential. GM-CSF is a cytokine which promotes recruitment,

proliferation and maturation of antigen presenting cells, such as DCs and macrophages. As described in previous sections, the immunomodulatory properties of GM-CSF were already utilized in combination with several immunotherapeutic approaches such as vaccination with oncolytic viruses [248, 250], whole tumor cells [237] or with synthetic peptides [252].
Until today, only three TLR agonists have been approved by the FDA for the treatment of cancer patients. Bacillus Calmette-Guérin (BCG) is a weakened strain of the bovine tuberculosis bacterium *Mycobacterium bovis* which was initially used as a vaccine against tuberculosis. Currently, the TLR2/TLR4 agonist BCG is approved for the treatment of bladder cancer [253]. Monophophoryl lipid A (a derivative of LPS) is another TLR2/TLR4 agonist which is used as an adjuvant in prophylactic vaccination regimens against human papillomavirus 16 and 18 [254]. The imidazoquinoline derivative imiquimod exerts its proinflammatory functions mainly through binding to TLR7 and is currently approved for the treatment of superficial basal cell carcinoma, genital warts and actinic keratosis [255].

1.4 Melanoma

Skin cancers comprise of three main types including basal cell carcinoma, squamous cell carcinoma as well as melanoma. Basal cell carcinoma and squamous cell carcinoma together are called non-melanoma skin cancers. These two types are the most common forms of skin cancer, are rarely lethal and are both from epithelial origin (basal cell keratinocytes or squamous epithelial keratinocytes, respectively) [256]. In contrast, melanoma is a deadly skin cancer arising from melanocytes which are the melanin producing cells found in the basal layer of the epidermis [257]. Even though melanoma only accounts for approximately 5 % of the skin cancer cases, it is responsible for the majority of skin cancer related deaths due to its aggressiveness and resistance to various forms of therapy [258, 259]. In 2012, 232,000 new cases of melanoma were reported which accounted for 1.6 % of all diagnosed cancers worldwide. This makes melanoma the 16th and 15th most common malignancy in females and males, respectively, and accounts for 0.7 % (55,000 total deaths) of all cancer related deaths worldwide [260].

1.4.1 Pathophysiology

Melanomas are often associated with so called precursor lesions. These are melanocytic neoplasms of the skin ranging from benign naevi and dysplastic naevi to melanoma *in situ* which bear an increased risk of progressing into melanoma. Simplified melanoma progression models often suggest a single path of evolution from benign naevi, to dysplastic naevi, to melanoma *in situ* and eventually to metastatic melanoma. However, different evolutionary paths have been described which are dependent on the melanoma type and the precursor lesion the melanoma originated from. The molecular events taking place in several of these paths were reviewed in detail by Shain and Bastian and will not be discussed within this thesis [261].

Large-scale analyses revealed that melanomas have a relatively high mutational load when compared to other tumor entities, with a frequency that exceeds 100 somatic mutations per mega base [262]. The first mutations in melanoma commonly occur in genes belonging to the MAP kinase signaling pathway, with *BRAF* and *NRAS* being the most frequently mutated genes [263]. Besides these mutations in genes controlling cell proliferation, invasive and

metastatic melanomas additionally harbor mutations in genes involved in growth and metabolism (phosphatase and tensin homolog (*PTEN*) and *KIT*), apoptosis and genetic integrity (*TP53*), chromatin remodeling (AT-rich interactive domain-containing protein 1A (*ARID1A*)), cell cycle control (cyclin-dependent kinase Inhibitor 2A (*CDKN2A*)) and telomere length (*TERT*) [261, 263-266].

1.4.2 Staging systems

Stratification of patients into clinically relevant stage groups is essential for therapeutic decision making and eventually to improve patients' course of disease and overall survival. Three classification systems to determine the progress of melanoma are applied in clinics. The Clark scale can be used to evaluate how deep the neoplastic cells have grown into the skin and which skin layers are affected. In contrast, the Breslow scale considers the overall melanoma depth within the skin without taking the different skin layers into account. Third, the tumor-node-metastasis (TNM) staging, which determines the thickness of the melanoma (T), the presence of tumor cells in the nearby lymph nodes (N) and the formation of metastases (M). Based on the TNM classification system tumors are divided into clinical stages I to IV. Melanomas that have not spread to lymph nodes or other organs are designated as stage I or II depending on the thickness of the primary lesion as well as on the absence or presence of ulceration. In stage III melanomas, tumor cells have spread to regional lymph nodes and/or so called satellite (within 2 cm of the primary lesion) and/or in-transit metastases (more than 2 cm distance to primary lesion but before the first draining lymph node) have developed. Stage IV melanomas are defined by metastatic spread to distant organs such as lung, liver, brain or areas of the skin [259, 267-269].

1.4.3 Current therapeutic options

While traditional therapies against melanoma including surgery, chemotherapy and radiotherapy are often curative in an early stage of disease (Stage I and II), they are not effective in combating advanced metastatic melanoma (Stage III and IV). However, the development of new targeted therapy and immunotherapy approaches during the last years has dramatically improved clinical outcome of melanoma patients. The following paragraphs describe chemo-, targeted-, and immunotherapies currently approved by the FDA for the treatment of patients with stage III or IV metastatic melanoma.

1.4.3.1 Chemotherapy

The only FDA approved chemotherapeutic drug for the treatment of advanced melanoma is dacarbazine, an alkylating agent which executes its cytotoxic function by methylation of O^6-guanine. The presence of methylguanine containing DNA causes mismatches with thymine and cytosine which eventually leads to cell death [270]. Tumor cells are more susceptible to alkylating agents compared to healthy cells as they divide faster and their DNA repair mechanisms are often defective. The determined response rate of patients with advanced melanoma is about 20 % with complete responses in only 5 % of the patients (OS: 6.5 month). Common side effects include nausea and vomiting [271, 272].

1.4.3.2 Targeted therapy

The second class of therapeutic agents to treat stage III and IV melanoma are so called targeted therapies composed of small molecules which are designed to selectively target one of the kinases (either BRAF or MEK) involved in the MAP kinase signaling pathway. The inhibition of molecules within this pathway demonstrated improved clinical outcome compared to chemotherapy, as approximately 50 % of all melanoma patients harbor a mutation within the BRAF kinase ($BRAF^{V600}$) resulting in a constitutively active MAP kinase signaling [273]. Vemurafenib, which selectively targets V600 mutated BRAF was the first small molecule approved by the FDA for the treatment of advanced melanoma in 2011 (ORR: 50 - 51 %; OS: 17.8 - 18 month) [274-276]. Treatment with dabrafenib, another $BRAF^{V600}$ targeting small molecule approved by the FDA two years later showed similar response rates (53 %) and overall survival (18.7 month) compared to vemurafenib [277, 278]. The most common resistance mechanism in patients treated with BRAF inhibitors is the reactivation of the MAP kinase signaling pathway, thus treatment regimens in which BRAF and MEK inhibitors are used in combination were tested in clinical trials. In 2014, the first dual treatment approach using the BRAF inhibitor dabrafenib and the MEK inhibitor trametinib in combination was approved by the FDA and demonstrated an increase in the overall response rates (64 - 69 %) and overall survival (25.1 - 26.1 month) compared to the monotherapies [274, 276-278]. One year later, a second combination therapy including vemurafenib and the MEK inhibitor cobimetinib was approved showing comparable response rates (70 %) and overall survival (22.3 month) compared to dabrafenib and trametinib [275, 279]. Even though the rates of treatment associated adverse events were similar for both combination regimens, the toxicity profiles differed substantially. The most common side effects observed for the combination of dabrefenib and trametinib included fever, headache and vomiting [280], whereas treatment with vemurafenib and cobimetinib resulted in photosensitivity reactions, rash and increased liver enzymes [275].
The advantages of targeted therapy include the high response rates, the fast and deep tumor response as well as the fact that the treatment is not impaired by continuous administration of immunosuppressive agents like corticosteroids. However, tumor cells develop resistance mechanisms in a majority of the patients [264].

1.4.3.3 Immunotherapy

As described above (see section 1.4.1), melanomas have a high mutational load which increases the likelihood for the generation of neoepitopes that might induce anti-tumor T cell responses [281]. Thus, melanomas are an attractive target for immunotherapeutic approaches that involve the activation and expansion of T cells. Immunotherapy approaches that have been approved by the FDA for the treatment of advanced melanoma include IFNα-2b, IL-2 and monoclonal antibodies against CTLA-4 and PD-1 [282]. IFNα-2b activates the JAK/STAT signaling pathway by binding to the interferon α/β receptor. The binding triggers dimerization of the receptor subunits (IFNARI and IFNAR2) and subsequent activation and phosphorylation of JAKs and STATs. The phosphorylated STATs then bind to IRF9 to form the interferon-stimulated gene factor-3 (ISGF-3). ISGF-3 translocates into the nucleus to induce transcription of INF-inducible genes. The induced changes in gene expression are responsible for the pleiotropic, immunomodulatory functions of IFNs and include the upregulation of MHC I molecules on tumor cells thereby facilitating anti-tumor attack by CTLs [282-284]. Treatment of melanoma patients with IFNα-2b has been shown to

increase relapse-free survival but not overall survival. Common side effects include flu-like symptoms, vomiting, neutropenia, leukopenia and elevated transaminase levels [285].
A second cytokine approved by the FDA for the treatment of stage IV melanoma is IL-2. This cytokine induces a variety of effects on cells of the immune system. Most importantly, it induces the expansion of antigen-specific $CD4^+$ and $CD8^+$ T cells [286], enhances antibody secretion by B cells [287] and promotes proliferation and enhances cytolytic activity of natural killer (NK) cells [288, 289]. Treatment with IL-2 showed an overall response rate of 16 % with a complete response in 6 % of the patients [290]. However, IL-2 related cytotoxicity is high and none of the conducted clinical trials could show an overall survival benefit [291]. Common side effects include flu-like symptoms, hypotension, arrhythmias and vomiting.
Ipilimumab, a monoclonal antibody targeting CTLA-4 was approved by the FDA in 2011 for treatment of stage IV melanoma. CTLA-4 is upregulated in conventional T cells upon activation and constitutively expressed on the surface of Tregs. It serves as a negative regulator of T cell activation by binding to its ligands CD80 and CD86 which are expressed on the surface of antigen-presenting cells. Monoclonal antibodies targeting CTLA-4 were shown to increase T cell activation and expansion by blocking the inhibitory signals. At the same time these antibodies mediate Treg depletion which eventually results in an increased T effector/Treg ratio [292]. While the response rates of ipilimumab alone are relatively low (11 - 19 %), the treatment improved overall survival of advanced melanoma patients as demonstrated in a clinical phase III study (28 % decreased mortality rate compared to dacarbazine) [293-297]. Common side effects including rash, nausea, and fatigue might be accompanied by more severe autoimmune side effects like enterocolitis, hypophysitis and pancreatits which can be life threatening [298].
Two monoclonal antibodies (nivolumab and pembrolizumab), targeting PD-1, were approved by the FDA in 2014 for the treatment of stage IV melanoma. Similar to CTLA-4, PD-1 is involved in maintaining peripheral tolerance and is thus referred to as immune checkpoint molecule. The PD-1 receptor is expressed on the surface of lymphocytes and binds to its ligand PD-L1 which is frequently expressed on tumor cells (40 - 50 % of melanomas). The interaction between PD-1 and its ligand eventually leads to T cell exhaustion. The use of pembrolizumab and nivolumab improved the overall response rates up to 40 % and increased the median overall survival of melanoma patients to 32.3 and 37.6 months, respectively [294-297, 299, 300]. Only 10 - 16 % of the patients developed grade 3 or 4 toxicities when treated with a monoclonal antibody against PD-1 [294, 295, 299]. In contrast, such toxicities were induced in approximately 30 % of the patients when treated with ipilimumab, showing that anti-PD-1 treatment is tolerated better [293, 301].
The combination of ipilimumab and nivolumab improved the overall response rates further (57 - 58 %) and was approved by the FDA in 2015 for the treatment of stage IV melanoma [294, 297, 302]. However, the combinatorial therapy is accompanied by grade 3 or 4 side effects in up to 59 % of the patients [297].
In summary, immunotherapies have the highest chance to induce a durable response against tumors compared to other treatment options. In addition, this reponse can be ongoing even after stopping the therapy. However, lower response rates and the prolonged period of time it takes to induce a potent anti-tumor response are the current major disadvantages of immunotherapies [264].

1.5 Aims of the study

The immunosuppressive TME established by inhibitory immune cells such as myeloid derived suppressor cells (MDSC), regulatory T cells (Treg) and tumor associated macrophages (TAM) forms a major obstacle for successful immunotherapy. Combining available tumor immunotherapies with approaches to repolarize immunosuppressive M2-like macrophages might overcome this hurdle. The aim of this study is to investigate three strategies to repolarize M2-like macrophages (illustrated in Figure 1.6).

Strategy I: Repolarization of macrophages through cognate interaction with $CD4^+$ T cells.
The goal of this part of the project is to answer the question whether tumor antigen specific $CD4^+$ T cells are able to polarize M2-like macrophages into immunostimulatory M1 *in vitro*. Another goal was to clarify whether adoptively transferred $CD4^+$ T cells have the capacity to reprogram M2-like TAMs *in vivo*, thereby neutralizing the immunosuppressive tumor microenvironment and facilitating anti-tumor attack by tumor antigen specific $CD8^+$ CTLs.

Strategy II: Repolarization of M2-like PECs by transcription factor knock down.
This part of the study focuses on the identification of key transcription factors (TFs) mediating macrophage polarization. Identification of such TFs should reveal new insights into the metabolic and transcriptional reprogramming of macrophages and might be useful for the identification of therapeutic targets to reprogram M2-like macrophages

Strategy III: Repolarization of M2-like PECs by miRNA transfection.
This strategy aims at repolarizing M2-like PECs by miRNA transfection, thereby further elucidating the regulation of miRNA-mediated macrophage polarization.

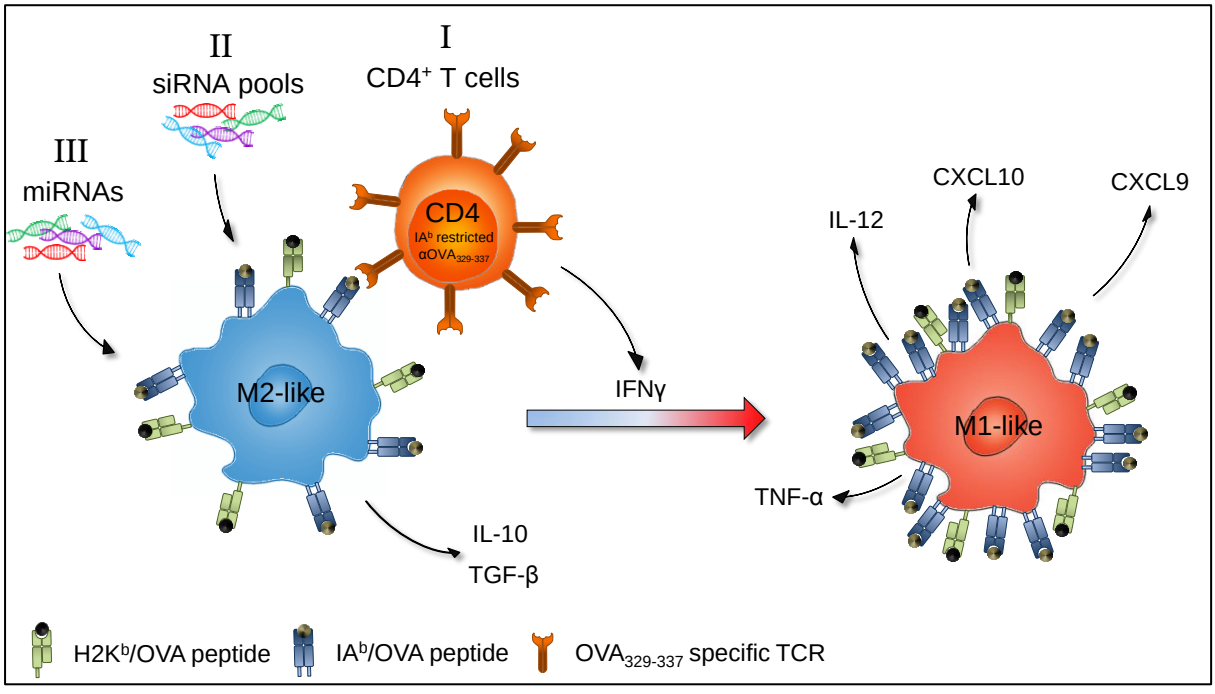

Figure 1.6: Investigated strategies to induce macrophage repolarization.
Strategy I: Repolarization of macrophages through cognate interaction with $CD4^+$ T cells. IFNγ secretion by activated $CD4^+$ T cells (orange) induces M2-like macrophages (blue) to polarize to proinflammatory M1 (red). Strategy II: Repolarization of M2-like macrophages by knocking down transcription factors involved in maintaining the M2 state using transcription factor targeting siRNA pools. Strategy III: Repolarization of M2-like macrophages by transfecting miRNAs that mediate M1 polarization.

2 Materials & Methods

2.1 Materials

2.1.1 General instrumentation

Table 2.1: General instrumentation

Instrument	Manufacturer
7300 Real time PCR system	Applied Biosystems, Foster City, USA
accu-jet pro Pipette Controller	VWR International, Radnor, USA
Biological Safety Cabinet	Heraeus, Hanau, Germany
CASY Cell counter	OMNI Life Science, Bremen, Germany
CB 150 incubator	BINDER, Tuttlingen, Germany
Centrifuge 5415 D	Eppendorf, Hamburg, Germany
Centrifuge 5424	Eppendorf, Hamburg, Germany
Centrifuge 5424 R	Eppendorf, Hamburg, Germany
Centrifuge 5810R	Eppendorf, Hamburg, Germany
Dynal (MPC-L)	Thermo Fischer Scientific, Waltham, USA
Dynal (MPC-S)	Thermo Fischer Scientific, Waltham, USA
ELISpot Reader System	Cellular Technology Limited, Sharker Heights, USA
FACS Aria I Cell Sorter	Becton Dickinson, Franklin Lakes, USA
FACS Aria II Cell Sorter	Becton Dickinson, Franklin Lakes, USA
FACS Calibur1 Flow Cytometer	Becton Dickinson, Franklin Lakes, USA
FACS Canto II Flow Cytometer	Becton Dickinson, Franklin Lakes, USA
Gammacell 1000 Elite	MDS, Ottawa, Canada
Gel Documentation System	Bio-Rad Laboratories, Hercules, USA
Gel iX Imager system	Intas Science Imaging Instruments, Göttingen, Germany
Innova 4230 Refrigerated Benchtop Incubator	New Brunswick Scientific, Edison, USA
IVIS Lumina Series III	PerkinElmer, Waltham, USA
LSR II Flow Cytometer	Becton Dickinson, Franklin Lakes, USA
Megafuge 2.0R	Heraeus, Hanau, Germany
Micro-centrigue 2 CMG-060	neoLab Migge, Heidelberg, Germany
Microscope Olympus CK40	Leica Camera, Wetzlar, Germany
Microwave intellowave	LG, Seoul, South Korea
Mini Laboratory Centrifuge	neoLab Migge, Heidelberg, Germany
Mithras LB940	Berthold Technologies, Bad Wildbad, Germany
Mixer Mill MM301	Retsch, Haan, Germany
MR 3002 S Magnetic stirring hot plate	Heidolph Instruments, Schwabach, Germany
Multipipette E3x	Eppendorf, Hamburg, Germany
Neubauer counting chamber	Brand, Wertheim, Germany
pH Meter 766 Calimatic	Knick, Berlin, Germany
PIPETBOY acu 2	INTEGRA Biosciences, Biebertal, Germany

Pipette (P2, P10, P20, P100, P200, P1000)	Gilson, Middleton, USA
PowerPac™ Basic Power Supply	Bio-Rad Laboratories, Hercules, USA
Spectrophotometer NanoDrop 2000	Thermo Fischer Scientific, Waltham, USA
Sterilgard class II Type A/B3	The Baker Company, Sanford, USA
Syro II	MultiSynTech, Witten, Germany
Tecan Infinite 200 PRO	Tecan Group, Männedorf, Switzerland
Thermo Finnigan LCQ Deca XP LCMS System	Thermo Fischer Scientific, Waltham, USA
thermomixer comfort	Eppendorf, Hamburg, Germany
Trans-Blot Turbo Transfer System	Bio-Rad Laboratories, Hercules, USA
Veriti 96-Well Thermal Cycler	Applied Biosystems, Foster City, USA
Vortex-Genie 2	Scientific Industries, New York, USA
Water bath	GFL, Burgwedel, Germany
Wet Blotting System Mini Trans-Blot Cell	Bio-Rad Laboratories, Hercules, USA
xCELLigence® RTCA SP System	ACEA Biosciences, San Diego, USA

2.1.2 General consumables

Table 2.2: General consumables

Material	Manufacturer
14mL Round Bottom High Clarity PP Test Tube	Corning, New York, USA
3MM CHR Blotting Paper	neoLab Migge, Heidelberg, Germany
5 ml Polystyrene round bottom tube with cell strainer cap	Corning, New York, USA
BD Discardit II disposable syringe (5, 10 ml)	Becton Dickinson, Franklin Lakes, USA
BD Mircolance 3 (21G, 27G)	Becton Dickinson, Franklin Lakes, USA
Bepanthen	Bayer, Leverkusen, Germany
Cap for PCR microcentrifuge tubes	nerbe plus, Winsen, Germany
CASY ton	OMNI Life Science, Bremen, Germany
CASYcups	OMNI Life Science, Bremen, Germany
Cell culture flask 50 ml	Greiner Bio-One, Kremsmünster, Austria
cell scraper	Corning, New York, USA
Centrifuge tube pp with screw cap PE (15, 50 ml)	nerbe plus, Winsen, Germany
Corning® 96 Well Solid Polystyrene Microplate	Sigma-Aldrich, St. Louis, USA
Cover glasses	Thermo Fischer Scientific, Waltham, USA
Cryogenic vials	Thermo Fischer Scientific, Waltham, USA
Disposable scalpel	Feather, Osaka, Japan
Disposable serological pipette (5, 10, 25, 50 ml)	Corning, New York, USA
easystrainer (40, 70 µm)	Greiner Bio-One, Kremsmünster, Austria
Einmal-Drigalskispatel Dreiecksform	neoLab Migge, Heidelberg, Germany
Enthaarungscreme	dm-drogerie markt, Karlsruhe, Germany
E-Plate 96	ACEA Biosciences, San Diego, USA
Eppendorf Combitips advanced (0.1, 1, 5, 25 ml)	Eppendorf, Hamburg, Germany
Eppendorf Micro test tube 3810X 1.5 ml	Eppendorf, Hamburg, Germany
Eppendorf Safe-Lock microtubes, PCR clean 2.0 ml	Eppendorf, Hamburg, Germany
Eppendorf Tubes 3810X 1.5 ml	Eppendorf, Hamburg, Germany
Eppendorf tubes 5.0 ml	Eppendorf, Hamburg, Germany

LS columns	Miltenyi Biotech, Bergisch Gladbach, Germany
LumaPlate 96	PerkinElmer, Waltham, USA
Messpipetten	BRAND, Wertheim, Germany
MicroAmp Optical 96-Well Reaction plate	Applied Biosystems, Foster City, USA
Mini-PROTEAN® Combs, 15-Well, 1.5 mm, 40 µl	Bio-Rad Laboratories, Hercules, USA
Mini-PROTEAN® Short Plates (1.5 mm integrated spacers)	Bio-Rad Laboratories, Hercules, USA
Mini-PROTEAN® Tetra Handcast Systems, 1.5 mm	Bio-Rad Laboratories, Hercules, USA
Mouse restrainer	Braintree Scientific, Braintree, USA
MS columns	Miltenyi Biotech, Bergisch Gladbach, Germany
MultiScreenHTS-IP, 0,45 µm, transparent, nicht steril	Merck KGaD, Darmstadt, Germany
Neubauer Zählkammer	BRAND, Wertheim, Germany
Nunc™ MaxiSorp™ ELISA Plates, uncoated	BioLegend, San Diego, USA
Parafilm M	Pechiney Plastic Packaging, Chicago, USA
PCR microcentrifuge tube PP, 0.2 ml, without cap	nerbe plus, Winsen, Germany
Pipette filter tips (10, 20, 100, 200, 1250 µl)	nerbe plus, Winsen, Germany
Pipette tips PP refill system (10, 200, 1000 µl)	nerbe plus, Winsen, Germany
Plastic serum pipette	Greiner Bio-One, Kremsmünster, Austria
Premium Aluminum Foil	VWR International, Radnor, USA
Protran BA 85	GE Healthcare, Little Chalfont, UK
Reagent Reservoir	Corning, New York, USA
Safe-lock microcentrifuge tubes (1.5, 2 ml)	Eppendorf, Hamburg, Germany
Sealing Tape	Thermo Fischer Scientific, Waltham, USA
Soft-Ject single use syringes	Henke-Sass, Wolf, Tuttlingen, Germany
Tissue culture dish 100	TPP, Trasadingen, Switzerland
Tissue culture flask (75, 150 cm^2)	TPP, Trasadingen, Switzerland
Tissue culture test plate (96F, 96U)	TPP, Trasadingen, Switzerland
Tissue culture test plates (6, 12, 24, 96 Wells)	TPP, Trasadingen, Switzerland

2.1.3 Chemicals and Reagents

2.1.3.1 Cell culture

Table 2.3: Cell culture

Component	Cat. No.	Manufacturer
2-Mercaptoethanol	M6250	Sigma-Aldrich, St. Louis, USA
Accutase cell detachment solution	SCR005	Merck KGaA, Darmstadt, Germany
ACK Lysing Buffer	A10492-01	Thermo Fisher Scientific, Waltham, USA
Biocoll	L6115	Merck KGaA, Darmstadt, Germany
Dimethyl sulfoxide (DMSO) Cell culture grade	A3672	AppliChem , Darmstadt, Germany
DMEM, high glucose, GlutaMAX™ Supplement	61965-026	Thermo Fisher Scientific, Waltham, USA
DPBS, no calcium, no magnesium	14190-094	Thermo Fisher Scientific, Waltham, USA
Dynabeads® Mouse T-Activator CD3/CD28	11452D	Gibco, Waltham, USA

Fetal calf serum	S 0115	Biochrom , Darmstadt, Germany
Fluorescein isothiocyanate–dextran	FD40-100MG	Sigma-Aldrich, St. Louis, USA
FluoSpheres™ Carboxylate-Modified Microspheres, 2.0 µm	F8827	Thermo Fisher Scientific, Waltham, USA
HEPES solution	H0887	Sigma-Aldrich, St. Louis, USA
Iscove's Modified Dulbecco's Medium (IMDM)	12440053	Thermo Fisher Scientific, Waltham, USA
Lactacystin	L6785	Sigma-Aldrich, St. Louis, USA
L-Glutamine (200 mM)	25030-081	Thermo Fisher Scientific, Waltham, USA
Lympholyte®-M Cell Separation Media	CL5035	Cedarlane Laboratories, Burlington, Canada
Methyl α-D-mannopyranoside	M6882	Sigma-Aldrich, St. Louis, USA
Minimum Essential Medium Eagle	M4526	Sigma-Aldrich, St. Louis, USA
Opti-MEM™ I Reduced Serum Medium	31985070	Thermo Fisher Scientific, Waltham, USA
Penicillin-Streptomycin	P0781	Sigma-Aldrich, St. Louis, USA
RPMI 1640 Medium, GlutaMAX™ Supplement	61870-010	Thermo Fisher Scientific, Waltham, USA
Sodium Pyruvate	S8636	Sigma-Aldrich, St. Louis, USA
Trypsin-EDTA (0.25%), phenol red	25200-056	Thermo Fisher Scientific, Waltham, USA
X-VIVO™ 20 Chemically Defined, Serum-free Hematopoietic Cell Medium	BE04-448Q	Lonza Group, Basel, Switzerland

2.1.3.2 Transfection reagents

All transfection reagents used within this thesis to transfect miRNAs or plasmids into tumor cell lines and PECs are listed in Table 2.4. The reagents were used according to manufacturer's instructions, unless otherwise stated.

Table 2.4: Transfection reagents

Transfection Reagent	Cat. No.	Manufacturer
DharmaFECT 4 Transfection Reagent	T-2004-01	Dharmacon, Lafayette, USA
DharmaFECT Duo Transfection Reagent	T-2010-01	Dharmacon, Lafayette, USA
Effectene Transfection Reagent Kit	301425	Qiagen, Venlo, Netherlands
Lipofectamine 3000 Transfection Reagent	L3000001	Thermo Fisher Scientific, Waltham, USA
Lipofectamine LTX Reagent	15338030	Thermo Fisher Scientific, Waltham, USA
Lipofectamine RNAiMAX Transfection Reagent	13778-100	Thermo Fisher Scientific, Waltham, USA
METAFECTENE® PRO	T040-1.0	Biontex Laboratories , München, Germany
METAFECTENE® SI$^+$	T100-1.0	Biontex Laboratories , München, Germany
PromoFectin-Macrophage	PK-CT-2000-MAC-10	Promokine, Heidelberg, Germany
siLentFect Lipid Reagent for RNAi	1703361	Bio-Rad Laboratories, Hercules, USA
TransIT Dynamic Delivery System	MIR-6003	Mirus Bio LLC, Madison, USA

TransIT-2020 Transfection Reagent	MIR-5404	Mirus Bio LLC, Madison, USA
TurboFect Transfection Reagent	R0533	Thermo Fisher Scientific, Waltham, USA
Viromer Red	230151	Biozym Scientific, Hessisch Oldendorf, Germany

2.1.3.3 Reagents for flow cytometry

Table 2.5: Reagents for flow cytometry

Component	Cat. No.	Manufacturer
7-AAD Viability Staining Solution	420403	BioLegend, San Diego, USA
BD Perm/Wash™ - Perm/Wash Buffer	51-2091KZ	Becton Dickinson , Franklin Lakes, USA
CountBright™ Absolute Counting Beads	C36950	Thermo Fisher Scientific, Waltham, USA
Cytofix/Cytoperm™ - Fixation/Permeabilization Solution	51-2090KZ	Becton Dickinson , Franklin Lakes, USA
LIVE/DEAD® Fixable Blue Dead Cell Stain Kit	L-23105	Thermo Fisher Scientific, Waltham, USA
LIVE/DEAD® Fixable Yellow Dead Cell Stain Kit	L-34959	Thermo Fisher Scientific, Waltham, USA
Normal Syrian Hamster Serum	007-000-120	Jackson Laboratory, Bar Harbor, USA
OneComp eBeads	01-1111-42	eBioscience, Waltham, USA
Purified Rat Anti-Mouse CD16/CD32	553142	Becton Dickinson , Franklin Lakes, USA
Rat serum	GTX73216	GeneTex, Irvine, USA

2.1.3.4 Reagents for protein biochemistry

Table 2.6: Reagents for protein biochemistry

Component	Cat. No.	Manufacturer
10% SDS	51206	Lonza Group, Basel, Switzerland
30% Acrylamide/Bis Solution, 37.5:1	161-0158	Bio-Rad Laboratories, Hercules, USA
Acetic acid	9526	Avantor, Center Valley, USA
Albumin from chicken egg white	A5503	Sigma-Aldrich, St. Louis, USA
Albumin from chicken egg white	A2512	Sigma-Aldrich, St. Louis, USA
Albumin, from bovine serum	A7030	Sigma-Aldrich, St. Louis, USA
Amersham ECL Prime Western Blotting Detection Reagent	RPN2232	GE Healthcare Life Sciences, Chalfont St Giles, UK
Ammonium Persulfate	1610700	Bio-Rad Laboratories, Hercules, USA
Bromophenol blue	B0126	Sigma-Aldrich, St. Louis, USA
Cell Lysis Buffer (10X)	9803	Cell Signaling Technology, Cambridge, UK
Glycerol	A3561	AppliChem , Darmstadt, Germany
Glycine	33226	Sigma-Aldrich, St. Louis, USA
Isopropanol	33539	Sigma-Aldrich, St. Louis, USA
Methanol	32213	Sigma-Aldrich, St. Louis, USA
Milk powder	T145.2	Carl Roth, Karlsruhe, Germany

N,N,N',N'-Tetramethylethylendiamin, 1,2-Bis(dimethylamino)-ethan	2367.3	Carl Roth, Karlsruhe, Germany
Phenylmethanesulfonyl fluoride	P7626	Sigma-Aldrich, St. Louis, USA
Precision Plus Protein™ Dual Color Standards	161-0374	Bio-Rad Laboratories, Hercules, USA
Protein-Marker IV ('Prestained')	27-2110	VWR International, Radnor, USA
Sodium chloride	31434	Sigma-Aldrich, St. Louis, USA
Substrate Reagent A	51-2606KC	Becton Dickinson , Franklin Lakes, USA
Substrate Reagent B	51-2607KC	Becton Dickinson , Franklin Lakes, USA
Trizma base	T1503	Sigma-Aldrich, St. Louis, USA
Tween 20	A4974	AppliChem , Darmstadt, Germany

2.1.3.5 Restriction enzymes

The type II restriction endonucleases listed in Table 2.7 were used as advised by the manufacturer.

Table 2.7: Restriction enzymes

Enzyme	Cat. No.	Manufacturer
EcoRI (10 U/µL)	ER0271	Thermo Fisher Scientific, Waltham, USA
FastDigest ScaI	FD0434	Thermo Fisher Scientific, Waltham, USA

2.1.3.6 Antibiotics

Table 2.8: Antibiotics

Antibiotic	Cat. No.	Manufacturer
Blasticidine S hydrochloride	15205	Sigma-Aldrich, St. Louis, USA
Geneticin® Selective Antibiotic	10131035	Thermo Fisher Scientific, Waltham, USA
Hygromycin B (50 mg/mL)	10687010	Thermo Fisher Scientific, Waltham, USA
Puromycin Dihydrochloride	A1113803	Thermo Fisher Scientific, Waltham, USA

2.1.3.7 Reagents for polymerase chain reaction

Table 2.9: Reagents for polymerase chain reaction

Component	Cat. No.	Manufacturer
dNTP-Mix Long Range	20-3111	PEQLAB Biotechnologie, Erlangen, Germany
$MgCl_2$ (magnesium chloride)	R0971	Thermo Fisher Scientific, Waltham, USA
Nuclease free water	W4502	Sigma-Aldrich, St. Louis, USA
Taq Buffer with $(NH_4)_2SO_4$ (10X)	B33	Thermo Fisher Scientific, Waltham, USA
Taq DNA Polymerase	EP0401	Thermo Fisher Scientific, Waltham, USA

2.1.3.8 Reagents for tumor digestion

All reagents used for tumor digestion were resolved/diluted in Hanks' Balanced Salt solution to reach the desired stock concentrations and stored at -80 °C.

Table 2.10: Reagents for tumor digestion

Component	Cat. No.	Manufacturer
Collagenase D	1108885800	Hoffmann-La Roche, Basel, Switzerland
Deoxyribonuclease I from bovine pancreas	D5025	Sigma-Aldrich, St. Louis, USA
Nα-Tosyl-L-lysine chloromethyl ketone hydrochloride (TLCK)	90182	Sigma-Aldrich, St. Louis, USA
Hanks' Balanced Salt solution	H9269	Sigma-Aldrich, St. Louis, USA

2.1.3.9 Reagents for gel electrophoresis

Table 2.11: Reagents for gel electrophoresis

Component	Cat. No.	Manufacturer
Agarose Basic	A8963	AppliChem , Darmstadt, Germany
EcoRI Buffer (10X)	B12	Thermo Fisher Scientific, Waltham, USA
Ethidiumbromidlösung 0,025 %	HP47.1	Carl Roth, Karlsruhe, Germany
FastDigest Green Buffer (10X)	B72	Thermo Fisher Scientific, Waltham, USA
O'GeneRuler 1 kb DNA Ladder	SM1163	Thermo Fisher Scientific, Waltham, USA
Quick-Load® 100 bp DNA Ladder	N0467G	New England Biolabs, Ipswich, USA
6X Orange DNA Loading Dye	R0631	Thermo Fisher Scientific, Waltham, USA

2.1.3.10 Bacteria

Table 2.12: Bacteria

Bacteria	Cat. No.	Manufacturer
One Shot® TOP10 Chemically Competent E. coli	C4040-06	Thermo Fisher Scientific, Waltham, USA

2.1.3.11 Reagents for transformation of bacteria

Table 2.13: Reagents for transformation of bacteria

Component	Cat. No.	Manufacturer
S.O.C. Medium	15544-034	Thermo Fisher Scientific, Waltham, USA
Tryptone	T7293	Sigma-Aldrich, St. Louis, USA
Yeast extract	70161	Sigma-Aldrich, St. Louis, USA
Ampicillin sodium salt	A9518	Sigma-Aldrich, St. Louis, USA
Agar-Agar	5210.3	Carl Roth, Karlsruhe, Germany

2.1.3.12 Cytokines and TLR ligands

Table 2.14: Cytokines and TLR ligands

Component	Cat. No.	Manufacturer
Lipopolysaccharides from Salmonella typhosa	L2387	Sigma-Aldrich, St. Louis, USA
Mouse IFN gamma Recombinant Protein Carrier-Free	34-8311-82	eBioscience, Waltham, USA
ODN 1826 (CpG)	tlrl-1826-1	InvivoGen, San Diego, USA

Recombinant Mouse IL-2 (carrier-free)	575402	Biolegend, San Diego, USA
Recombinant Mouse IL-4 (carrier-free)	574302	Biolegend, San Diego, USA

2.1.4 Cell lines and culture medium

All cell lines used and generated within this thesis are listed in Table 2.15. The "Medium Index" column shows the index of the cell line specific culture medium (listed in Table 2.16).

2.1.4.1 Cell lines

Table 2.15: Cell lines

Cell line	Cell type	Modification	Provider	Medium Index	Antibiotic
771 B cell lymphoma	BL	-	Offringa, Rienk	5	-
B16F10 ATCC	M	-	ATCC	2	-
B16F10 ATCC/Acceptor 10	M	FRT site in Rosa26 locus	generated in this thesis	2	1 mg/ml G418
B16F10 ATCC/Acceptor 10/Ctrl.	M	Fluorophore in Rosa26 locus (isogenic)	generated in this thesis	2	1 mg/ml G418
B16F10 ATCC/Acceptor 10/OVA-F	M	OVA in Rosa26 locus (isogenic)	generated in this thesis	2	1 mg/ml G418
B16F10 ATCC/Acceptor 10/OVA-T	M	OVA in Rosa26 locus (isogenic)	generated in this thesis	2	1 mg/ml G418
B16F10 ATCC/Acceptor 35	M	FRT site in Rosa26 locus	generated in this thesis	2	1 mg/ml G418
B16F10 ATCC/Acceptor 35/Ctrl.	M	Fluorophore in Rosa26 locus (isogenic)	generated in this thesis	2	1 mg/ml G418
B16F10 ATCC/Acceptor 35/M2KO	M	FRT site in Rosa26 locus/MHC-class II KO	generated in this thesis	2	1 mg/ml G418
B16F10 ATCC/Acceptor 35/OVA-F	M	OVA in Rosa26 locus (isogenic)	generated in this thesis	2	1 mg/ml G418
B16F10 ATCC/Acceptor 35/OVA-T	M	OVA in Rosa26 locus (isogenic)	generated in this thesis	2	1 mg/ml G418
B16F10 ATCC/M1KO	M	MHC-class I KO	generated in this thesis	2	-
B16F10 ATCC/M2KO	M	MHC-class II KO	generated in this thesis	2	-
B16F10 ATCC/M2KO/OVA-F	M	MHC-class II KO/OVA	generated in this thesis	2	1 mg/ml G418
B16F10 ATCC/M2KO/OVA-F/Luci	M	MHC-class II KO/OVA/Luciferase	generated in this thesis	2	1 mg/ml G418, 1 µg/ml Puromycin
B16F10 ATCC/M2KO/OVA-T	M	MHC-class II KO/OVA	generated in this thesis	2	1 mg/ml G418
B16F10 ATCC/M2KO/OVA-T/Luci	M	MHC-class II KO/OVA/Luciferase	generated in this thesis	2	1 mg/ml G418, 1 µg/ml Puromycin
B16F10 ATCC/OVA-F	M	OVA	generated in this thesis	2	1 mg/ml G418
B16F10 ATCC/OVA-F/Luci	M	OVA/Luciferase	generated in this thesis	2	1 mg/ml G418, 1 µg/ml Puromycin
B16F10 ATCC/OVA-T	M	OVA	generated in this thesis	2	1 mg/ml G418
B16F10 ATCC/OVA-T/Luci	M	OVA/Luciferase	generated in this thesis	2	1 mg/ml G418, 1 µg/ml Puromycin
B16F10/M1KO	M	MHC-class I KO	generated in this thesis	2	-
$CD4^+$ T cell line ($OVA_{323-339}$; IA^b)	T	-	generated in this thesis	7	-

CTL ($OVA_{257-264}$; K^b)	T	-	Osen, Wolfram	7	-
E.G7	TL	OVA	unknown	2	0.8 mg/ml G418
EL-4	TL	-	unknown	2	-
EO771	BC	-	unknown	1	-
EO771/Luci	BC	Luciferase	generated in this thesis	1	1 µg/ml Puromycin
EO771/Luci/OVA-F	BC	Luciferase/OVA	generated in this thesis	1	1 µg/ml Puromycin 0.2 mg/ml G418
EO771/Luci/OVA-T	BC	Luciferase/OVA	generated in this thesis	1	1 µg/ml Puromycin 0.2 mg/ml G418
EO771/OVA-F	BC	OVA	generated in this thesis	1	0.2 mg/ml G418
EO771/OVA-T	BC	OVA	generated in this thesis	1	0.2 mg/ml G418
MC-38	CC	-	unknown	6	-
MC-38/OVA-T	CC	OVA	Offringa, Rienk	6	25 µg/ml G418
Panc02	PC	-	Offringa, Rienk	2	-
PDAC (30364)	PC	-	Offringa, Rienk	3	-
PDAC/OVA-F (30364 Klon #7 m14865)	PC	OVA	Offringa, Rienk	3	10 µg/ml Blasticidin

All cell lines are of mouse origin. BL: B lymphoma; M: melanoma; T: T cell line; TL: T lymphoma; BC: breast cancer; CC: colon carcinoma; PC: pancreatic cancer

2.1.4.2 Culture medium

Table 2.16: Culture medium

Index	Name	Medium	Supplements
1	RPMI Complete Medium with HEPES	RPMI 1640 Medium, GlutaMAX™ Supplement	10 % FCS 10 mM HEPES 100 U/ml Penicillin 100 µg/ml Streptomycin
2	RPMI Complete Medium	RPMI 1640 Medium, GlutaMAX™ Supplement	10 % FCS 100 U/ml Penicillin 100 µg/ml Streptomycin
3	DMEM Complete Medium with sodium pyruvate	DMEM, high glucose, GlutaMAX™ Supplement	10 % FCS 1 mM sodium pyruvate 100 U/ml Penicillin 100 µg/ml Streptomycin
4	DMEM Complete Medium for PECs	DMEM, high glucose, GlutaMAX™ Supplement	10 % FCS 100 U/ml Penicillin 100 µg/ml Streptomycin
5	IMDM Complete Medium with Glutamine	Iscove's Modified Dulbecco's Medium (IMDM)	10 % FCS 2 mM L-Glutamine 100 U/ml Penicillin 100 µg/ml Streptomycin

6	IMDM Complete Medium with 2-Mercaptoethanol	Iscove's Modified Dulbecco's Medium (IMDM)	10 % FCS 50 µM 2-Mercaptoethanol 100 U/ml Penicillin 100 µg/ml Streptomycin
7	Complete T cell Medium	Minimum Essential Medium Eagle	10 % FCS 2 mM L-Glutamine 50 µM 2-Mercaptoethanol 12.5 mM Methyl α-D-mannopyranoside 12.5 ml ConA culture supernatant 100 U/ml Penicillin 100 µg/ml Streptomycin

2.1.5 Plasmids

All plasmids used in this thesis are listed in Table 2.17. Plasmids were stored in double-distilled water (ddH_2O) at -20 °C.

Table 2.17: Plasmids

Designation	Insert	Promotor	Backbone	Resistance	Source
pDEST26_pHIS_6_N_OVAK1_Klon1	OVA-F	CMV	pDEST26	Neomycin	Rainer Will (German Cancer Research Center, Heidelberg, Germany)
pDEST26_pHIS_6_N_OVA Trunc_Klon1	OVA-T	CMV	pDEST26	Neomycin	Rainer Will (German Cancer Research Center, Heidelberg, Germany)

2.1.6 Guide RNA sequences

All nucleotide sequences used for the generation of target specific guide RNAs were purchased from Sigma-Aldrich (St. Louis, USA) and are shown in Table 2.18. On-target scores obtained from the CRISPR Design Tool (https://crisper.mit.edu/) are shown in the right column.

Table 2.18: H2-IA^b targeting guide RNA sequences

exon 1 guide #1	sense	5'-CACCGACTCCGAAAGTAAGTGCCG-3'	95
	antisense	5'-AAACCGGCACTTACTTTCGGAGTC-3'	
exon 1 guide #4	sense	5'-CACCGAGACTCCGAAAGTAAGTGC-3'	80
	antisense	5'-AAACGCACTTACTTTCGGAGTCTC-3'	
exon 1 guide #5	sense	5'-CACCGAGCCATCTCTAAGGCAC-3'	61
	antisense	5'-AAACGTGCCTTAGAGATGGCTC-3'	
exon 2 guide #3	sense	5'-CACCGAAATGCCCTGCGGACGGACG-3'	94
	antisense	5'-AAACCGTCCGTCCGCAGGGCATTTC-3'	
exon 2 guide #12	sense	5'-CACCGCGAGTGCTACTTCACCAAC-3'	87
	antisense	5'-AAACGTTGGTGAAGTAGCACTCGC-3'	
exon 1 up guide #1	sense	5'-CACCGGCTCTCTATGCGCGGCA-3'	96
	antisense	5'-AAACTGCCGCGCATAGAGAGCC-3'	
exon 1 up guide #2	sense	5'-CACCGTTACAAAGGCTCTCTATGCG-3'	88
	antisense	5'-AAACCGCATAGAGAGCCTTTGTAAC-3'	
exon 6 down	sense	5'-CACCGCCCGCCCTTACATGGAGTTC-3'	82

guide #1	antisense	5'-AAACGAACTCCATGTAAGGGCGGGC-3'	
exon 6 down guide #2	sense	5'-CACCGAACCTCCACAACTGAGC-3'	81
	antisense	5'-AAACGCTCAGTTGTGGAGGTTC-3'	

2.1.7 siRNA pools

siRNA pools purchased from siTools Biotech contain 30 siRNAs targeting the same gene of interest. Each siRNA is only present in picomolar working concentrations which dilutes the off-target effect of each individual siRNA, increases on-target specificity and ensures a co-operative knock-down of the target gene. The lyophilized siRNA pools were resolved in nuclease free water to reach a stock concentration of 10 µM. The ON-TARGET plus siRNA pools obtained from Dharmacon contain 4 individual siRNAs with a dual-strand modification to reduce off-target effects. The lyophilized siRNA pool targeting MYC was resolved in nuclease free water to reach a stock concentration of 50 µM.

Table 2.19: siRNA pools

siPool target	NCBI Gene ID	Description	Manufacturer
Myc	17869	myelocytomatosis oncogene	Dharmacon, Lafayette, USA
E2f1	13555	E2F transcription factor 1	siTools Biotech, Planegg, Germany
Ctcf	13018	CCCTC-binding factor	siTools Biotech, Planegg, Germany
Stat6	20852	signal transducer and activator of transcription 6	siTools Biotech, Planegg, Germany
Pparg	19016	peroxisome proliferator activated receptor gamma	siTools Biotech, Planegg, Germany

2.1.8 miRNA sequences

The miRIDIAN miRNA Mimics were purchased from Dharmacon (Lafayette, USA) and resolved in nuclease free water to reach a stock concentration of 10 µM.

Table 2.20: miRNA sequences

miRNA	Cat. No.	Sequence
mmu-let-7e-5p	C-310507-07-0005	5'-UGAGGUAGGAGGUUGUAUAGUU-3'
mmu-let-7i-5p	C-310375-07-0005	5'-UGAGGUAGUAGUUUGUGCUGUU-3'
mmu-miR-1198-5p	C-311047-00-0005	5'-UAUGUGUUCCUGGCUGGCUUGG-3'
mmu-miR-210-3p	C-310570-05-0005	5'-CUGUGCGUGUGACAGCGGCUGA-3'
mmu-miR-221-5p	C-311234-00-0005	5'-ACCUGGCAUACAAUGUAGAUUUCUGU-3'
mmu-miR-222-3p	C-310584-07-0005	5'-AGCUACAUCUGGCUACUGGGU-3'
mmu-miR-27b-3p	C-310380-05-0005	5'-UUCACAGUGGCUAAGUUCUGC-3'
mmu-miR-30e-3p	C-310467-07-0005	5'-CUUUCAGUCGGAUGUUUACAGC-3'
mmu-miR-674-5p	C-310694-01-0005	5'-GCACUGAGAUGGGAGUGGUGUA-3'
mmu-miR-744-5p	C-310776-03-0005	5'-UGCGGGGCUAGGGCUAACAGCA-3'
mmu-miR-99b-5p	C-310387-05-0005	5'-CACCCGUAGAACCGACCUUGCG-3'

2.1.9 Primers

All primers used within this thesis were obtained from Sigma-Aldrich (St. Louis, USA) and are listed in Table 2.21 and Table 2.22. The lyophilized primers were resolved in ddH_2O to a stock concentration of 100 µM and stored at -20 °C.

2.1.9.1 Primers for quantitative real-time polymerase chain reaction (qPCR)

All primers used for qPCR were tested for their amplification efficiency using a standard curve that is based on four 10 fold dilutions of a cDNA sample. The efficiency was calculated using the slope of the standard curve and the following formula:
Efficiency = (10(-1/slope)-1)*100

Table 2.21: Primers for quantitative real-time PCR

Target	Primer	Sequence (5'-3')	Product size [bp]	Efficiency	Source
Ym1	Ym1_qPCR_FP1	CACCATGGCCAAGCTCATTCTTGT	114	97.23	Tatano *et al.* 2014 [303]
	Ym1_qPCR_RP2	TATTGGCCTGTCCTTAGCCCAACT			
Fizz1	Fizz1_qPCR_FP3	ACTGCCTGTGCTTACTCGTTGACT	82	100.08	
	Fizz1_qPCR_RP4	AAAGCTGGGTTCTCCACCTCTTCA			
Cd163	CD163_fw35	TCCACACGTCCAGAACAGTC	107	83.98	
	CD163_rev36	CCTTGGAAACAGAGACAGGC			
Il6	IL-6_qPCR_FP5	GTCTTCTGGAGTACCATAGC	368	81.02	Movahedi *et al.* 2010 [181]
	IL-6_qPCR_RP6	GTCAGATACCTGACAACAGG			
Cxcl10	CXCL10_qPCR_FP7	TCTGAGTCCTCGCTCAAGTG	228	92.34	
	CXCL10_qPCR_RP8	CCTTGGGAAGATGGTGGTTA			
Cxcl9	CXCL9_qPCR_FP9	TCAACAAAAGAGCTGCCAAA	263	85.72	
	CXCL9_qPCR_RP10	GCAGAGGCCAGAAGAGAGAA			
Il12b	IL12b_qPCR_FP11	GAAAGACCCTGACCATCACT	314	81.3	
	IL12b_qPCR_RP12	CCTTCTCTGCAGACAGAGAC			
Il1b	IL1b_qPCR_FP13	GTGTGGATCCAAAGCAATAC	282	80.19	
	IL1b_qPCR_RP14	GTCTGCTCATTCATGACAAG			
Nos2	NOS2_qPCR_FP15	GCTTCTGGTCGATGTCATGAG	506	60.92	
	NOS2_qPCR_RP16	TCCACCAGGAGATGTTGAAC			
Vegfa	VEGFA_qPCR_FP17	CAGGCTGCTGTAACGATGAA	187	97.23	
	VEGFA_qPCR_RP18	AATGCTTTCTCCGCTCTGAA			
Arg1	ARG1_qPCR_FP19	TCACCTGAGCTTTGATGTCG	257	83.29	
	ARG1_qPCR_RP20	TTATGGTTACCCTCCCGTTG			
Mrc1	Mrc1_qPCR_FP21	GCAAATGGAGCCGTCTGTGC	299	83.29	
	Mrc1_qPCR_RP22	CTCGTGGATCTCCGTGACAC			
Mrc1	CD206_qPCR_FP23	TTGGACGGATAGATGGAGGG	182	96.84	Zhu *et al.* 2014 [304]
	CD206_qPCR_RP24	CCAGGCAGTTGAGGAGGTTC			
Hprt	HPRT_qPCR_FP25	AGTACAGCCCCAAAATGGTTAAG	203	95.29	
	HPRT_qPCR_RP26	CTTAGGCTTTGTATTTGGCTTTTC			
Actb	bACTIN_qPCR_FP27	TGGAATCCTGTGGCATCCATGAAAC	348	79.39	Davis *et al.* 2013 [305]
	bACTIN_qPCR_RP28	TAAAACGCAGCTCAGTAACAGTCCG			
Itgax	CD11c_fw29	CTGGATAGCCTTTCTTCTGCTG	113	94.91	Shaul *et al.* 2010 [306]
	CD11c_rev30	GCACACTGTGTCCGAACTC			

Il10	IL10_fw31	GCTCTTACTGACTGGCATGAG	105	111.66	Shaul *et al.* 2010 [306]
	IL10_rev32	CGCAGCTCTAGGAGCATGTG			
Il13	IL13_fw33	CCAGGTCCACACTCCATACC	117	not tested	
	IL13_rev34	TGCCAAGATCTGTGTCTCTCC			
Stat6	STAT6_fw37	CTGGGGTGGTTTCCTCTTG	94	112.03	
	STAT6_rev38	TGCCCGGTCTCACCTAACTA			
Il1b	IL1β_fw39	CTGGTGTGTGACGTTCCCATTA	76	90.25	
	IL1β_rev40	CCGACAGCACGAGGCTTT			
Stat1	STAT1_fw41	CTGAATATTTCCCTCCTGGG	103	96.06	
	STAT1_rev42	TCCCGTACAGATGTCCATGAT			
Vegfa	VEGF_fw43	CCTTCGTCCTCTCCTTACCC	117	94.17	
	VEGF_rev44	AAGCCACTCACACACACAGC			
Cd86	CD86_fw45	TCTCCACGGAAACAGCATCT	100	95.29	
	CD86_rev46	CTTACGGAAGCACCCATGAT			
Cd80	CD80_fw47	GGCAAGGCAGCAATACCTTA	94	104.43	
	CD80_rev48	CTCTTTGTGCTGCTGATTCG			
Tgfb1	TGFβ1_fw49	AAGTTGGCATGGTAGCCCTT	128	93.8	
	TGFβ1_rev50	GCCCTGGATACCAACTATTGC			
Nos2	iNOS_fw51	CAGAGGACCCAGAGACAAGC	300	80.47	designed by David Eisel
	iNOS_rev52	TGCTGAAACATTTCCTGTGC			
Arg2	ARG_fw53	AGGAACTGGCTGAAGTGGTTA	215	100.9	
	ARG_rev54	GATGAGAAAGGAAAGTGGCTGT			
Cxcl9	CXCL9_fw55	CGAGGCACGATCCACTACAA	265	80.47	
	CXCL9_rev56	TCTTCCTTGAACGACGACGAC			
Il12b	IL12b_fw57	AGTGACATGTGGAATGGCGT	285	105.35	
	IL12b_rev58	CAGGAGTCAGGGTACTCCCA			
Il1b	IL1b_fw59	GGACAGAATATCAACCAACAAGACT	190	134.6	
	IL1b_rev60	TTGCTTGGGATCCACACTCTC			
Actb	bactin_fw61	ACCCTAAGGCCAACCGTGA	193	91.28	
	bactin_rev62	ATGGCGTGAGGGAGAGCATA			
Rpl19	Rpl19_fw69	TACCGGGAATCCAAGAAGATTGA	89	98.13	PrimerBank ID 226958656c3
	Rpl19_rev70	AGGATGCGCTTGTTTTTGAAC			
Ldha	Ldha_fw71	TGTCTCCAGCAAAGACTACTGT	155	98.11	PrimerBank ID 6754524a1
	Ldha_rev72	GACTGTACTTGACAATGTTGGGA			
Ppat	Ppat_fw75	TTCAGGGTGCATAAGGGAATGG	104	98.73	PrimerBank ID 247301190c1
	Ppat_rev76	GCGTACCTCGTATGTCCGA			
Ppia	Ppia_fw79	GAGCTGTTTGCAGACAAAGTTC	125	95.62	PrimerBank ID 6679438c1
	Ppia_rev80	CCCTGGCACATGAATCCTGG			
Nos2	Nos2_fw81	GTTCTCAGCCCAACAATACAAGA	127	90.33	PrimerBank ID 6754872a1
	Nos2_rev82	GTGGACGGGTCGATGTCAC			
Cxcl9	CXCL9_fw83	GGAGTTCGAGGAACCCTAGTG	82	99.68	PrimerBank ID 162287427c1
	CXCL9_rev84	GGGATTTGTAGTGGATCGTGC			
Myc	Myc_fw89	ATGCCCCTCAACGTGAACTTC	78	100.47	PrimerBank ID 293629266c1
	Myc_rev90	GTCGCAGATGAAATAGGGCTG			
Pparg	Pparg_fw99	TTTTCCGAAGAACCATCCGATT	139	91.86	PrimerBank 187960104c3
	Pparg_rev100	ATGGCATTGTGAGACATCCCC			

Stat6	Stat6_fw103	TGGAGAGCATCTATCAGAGGGA	95	95.3	PrimerBank ID 128485773c3
	Stat6_rev104	GCGGAACTCTTCTATAACAGCTT			
Ctcf	Ctcf_fw125	GATCCTACCCTTCTCCAGATGAA	175	91.41	PrimerBank ID 31044459a1
	Ctcf_rev126	GTACCGTCACAGGAACAGGT			
E2f1	E2f1_fw127	TGCAGAAACGGCGCATCTAT	122	95.45	PrimerBank ID 158517881c2
	E2f1_rev128	CCGCTTACCAATCCCCACC			

M1-like
M2-like
TF
Housekeeping gene

2.1.9.2 Primers for PCR

Table 2.22: Primers for PCR

Target	Primer	Sequence (5'-3')	Length [bp]	Product size [bp]
OVA-F	forward	CGCAGCAAGCATGGAATTTTG	21	229 bp
	reverse	GTGAACGTTTACAGATGTGCCA	22	
OVA-F and OVA-T	forward	TCAAAGTGTACTTACCTCGCATGA	24	323 bp
	reverse	AGGGGAAACACATCTGCCAA	20	
Actb	forward	ACCCTAAGGCCAACCGTGA	19	193 bp
	reverse	ATGGCGTGAGGGAGAGCATA	20	
H2-Ab1	forward	TTTGCTTTCTGAAGGGGGCA	20	309 bp
	reverse	AGAATGGAGTCTCACTCTCTCTT	23	

2.1.10 Antibodies

All antibodies used in this study are listed in Table 2.23, Table 2.24 and Table 2.25. If not stated otherwise, the listed antibodies react against mouse antigens and were stored according to manufacturer's recommendations.

2.1.10.1 Antibodies used for flow cytometry

Table 2.23: Flow cytometry antibodies

Index	Antigen	Coupled	Cat. No.	Manufacturer	Clone	Isotype Index
101	CD11b	PerCP-Cy 5.5	101228	BioLegend	M1/70	100
109	CD11c	V450	560521	Becton Dickinson	HL3	108
125	CD19	PE	115508	BioLegend	6D5	126
175	CD2	APC	100111	BioLegend	RM2-5	-
112	CD206	Brilliant Violet 605	141721	BioLegend	C068C2	111
201	CD206	PE-Cy7	141719	BioLegend	C068C2	87
165	CD25	PE	102008	BioLegend	PC61	167
44	CD3	PerCP-Cy 5.5	100217	BioLegend	17A2	100
110	CD4	V450	560468	Becton Dickinson	RM4-5	148
117	CD44	Brilliant Violet 421	103039	BioLegend	IM7	164

53	CD45	PE	553081	Becton Dickinson	30-F11	158
154	CD45.1	APC	110714	BioLegend	A20	155
99	CD45.2	Alexa Fluor 488	109816	BioLegend	104	98
116	CD49b	Alexa Fluor 647	108912	BioLegend	DX5	-
174	CD49d	PE	103705	BioLegend	9C10 (MFR4.B)	126
166	CD69	PerCP-Cy 5.5	104522	BioLegend	H1.2F3	168
89	CD8	PE-Cy7	100722	BioLegend	53-6.7	87
145	Egr2	APC	17-6691-80	ebioscience	erongr2	146
97	F4/80	APC-Cy7	123118	BioLegend	BM8	119
107	F4/80	Alexa Fluor 647	123122	BioLegend	BM8	106
156	F4/80	PE-Cy7	123114	BioLegend	BM8	87
159	F4/80	Brilliant Violet 421	123137	BioLegend	BM8	160
94	Gr-1	Alexa Fluor 700	108422	BioLegend	RB6-8C5	93
202	Gr-1	Alexa Fluor 488	108417	BioLegend	RB8-8C5	203
144	H2-Db	PerCP-Cy 5.5	111517	BioLegend	KH95	150
143	H2-Kb	FITC	116505	BioLegend	AF6-88.5	151
152	H-2Kb SIINFEKL	PE-Cy7	141607	BioLegend	25-D1.16	153
10	I-A[b]	PE	553552	Becton Dickinson	AF6-120.1	122
104	I-A[b]	Alexa Fluor 647	116412	BioLegend	AF6-120.1	103
176	LFA-1	PerCP-Cy 5.5	141007	BioLegend	H155-78	177
88	NOS2	PE-Cy7	25-5920-82	eBioscience	CXNFT	87
42	TCR Vα2	FITC	127805	BioLegend	B20.1	-
43	TCR Vβ5.1	APC	139505	BioLegend	MR9-4	198

Index	Antigen	Coupled	Cat. No.	Company	Clone
87	Isotype Ctrl.	PE-Cy7	400522	BioLegend	RTK2758
93	Isotype Ctrl.	Alexa Fluor 700	400628	BioLegend	RTK4530
98	Isotype Ctrl.	Alexa Fluor 488	400233	BioLegend	MOPC-173
100	Isotype Ctrl.	PerCP-Cy 5.5	400632	BioLegend	RTK4530
103	Isotype Ctrl.	Alexa Fluor 647	400234	BioLegend	MOPC-173
106	Isotype Ctrl.	Alexa Fluor 647	400526	BioLegend	RTK2758
108	Isotype Ctrl.	V450	560552	Becton Dickinson	G235-2356
100	Isotype Ctrl.	PerCP-Cy 5.5	400632	BioLegend	RTK4530
111	Isotype Ctrl.	Brilliant Violet 605	400539	BioLegend	RTK2758
119	Isotype Ctrl.	APC-Cy7	400523	BioLegend	RTK2758
122	Isotype Ctrl.	PE	553457	Becton Dickinson	G155-178
126	Isotype Ctrl.	PE	400507	BioLegend	RTK2758
146	Isotype Ctrl.	APC	17-4321-41	ebioscience	eBR2a
148	Isotype Ctrl.	V450	560377	Becton Dickinson	R35-95
150	Isotype Ctrl.	PerCP-Cy 5.5	400337	BioLegend	MPC-11
151	Isotype Ctrl.	FITC	400209	BioLegend	MOPC-173
153	Isotype Ctrl.	PE-Cy7	400125	BioLegend	MOPC-21
155	Isotype Ctrl.	APC	400219	BioLegend	MOPC-173
158	Isotype Ctrl.	PE	553989	Becton Dickinson	A95-1

160	Isotype Ctrl.	Brilliant Violet 421	400535	BioLegend	RTK2758
164	Isotype Ctrl.	Brilliant Violet 421	400639	BioLegend	RTK4530
167	Isotype Ctrl.	PE	401905	BioLegend	G0114F7
168	Isotype Ctrl.	PerCP-Cy 5.5	400931	BioLegend	HTK888
177	Isotype Ctrl.	PerCP-Cy 5.5	400425	BioLegend	RTK2071
198	Isotype Ctrl	APC	17-4714-81	ebioscience	P3.6.2.8.1
203	Isotype Ctrl.	Alexa Fluor 488	400625	BioLegend	RTK4530

2.1.10.2 Antibodies used for Western blot

Table 2.24: Western blot antibodies

Antigen	Reactivity	Coupled	Dilution	Cat. No.	Manufacturer	Clone	Isotype	Organism
Actin	mouse	-	10000	691001	MP Biomedicals	C4	IgG1	mouse
IgG	mouse	HRP	5000	sc-2005	Santa Cruz Biotechnology	polyclonal	ns	goat
Ovalbumin	chicken	-	1000	sc-65984	Santa Cruz Biotechnology	3G2E1D9	IgG1	mouse

ns: not specified

2.1.10.3 Antibodies used for ELISpot assay

Table 2.25: ELISpot antibodies

Antigen	Coupled	Dilution	Cat. No.	Manufacturer	Clone	Isotype	Organism
IFN-γ	-	200	551216	Becton Dickinson	R4-6A2	IgG1, κ	Rat
IFN-γ	Biotin	500	554410	Becton Dickinson	XMG1.2	IgG1, κ	Rat

2.1.11 Peptides

Parts of the following paragraph have been taken from reference [307] and were originally written by myself. Peptides were synthesized by Fmoc chemistry using the fully automated multiple synthesizer Syro II, followed by HPLC purification on a Kromasil 100–10C 10 µm 120 A reverse phase column (20 x 150 mm). Eluted peptides were analyzed by HPLC and MS using the Thermo Finnigan LCQ Deca XP LCMS System. The lyophilized peptides were dissolved in DMSO to a stock concentration of 20 mg/ml and subsequently diluted in culture medium to the desired working concentration.

Table 2.26: Peptides

Sequence	Position	Length	MHC Restriction	Protein
AAHAEINEA	329-337	9	H2-IA^b	Ovalbumin
ISQAVHAAHAEINEAGR	323-339	17	H2-IA^b	Ovalbumin
SIINFEKL	257-264	8	H2-K^b	Ovalbumin
SVYDFFVWL	180-188	9	H2-K^b	Tyrosinase-related protein 2
TPPAYRPPNAPIL	128-140	13	H2-IA^b	HBV core antigen

2.1.12 Kits

Commercially available kits used within this study are listed in Table 2.27. All kits were used according to the manufacturer's protocols, unless otherwise stated.

Table 2.27: Kits

Kit	Cat. No.	Manufacturer
Anti-Mouse/Rat Foxp3 Staining Set APC	77-5775-40	eBioscience, Waltham, USA
CD4 (L3T4) MicroBeads, mouse	130-049-201	Miltenyi Biotec , Bergisch Gladbach, Germany
CD4+ T Cell Isolation Kit, mouse	130-104-454	Miltenyi Biotec , Bergisch Gladbach, Germany
CD8a (Ly-2) MicroBeads, mouse	130-049-401	Miltenyi Biotec , Bergisch Gladbach, Germany
ELISA Kit for Ovalbumin (OVA)	MBS2000240	MyBioSource, San Diego, USA
iScript cDNA Synthesis Kit	1708890	Bio-Rad Laboratories, Hercules, USA
Luciferase Assay System	E1500	Promega, Madison, USA
miRNeasy Mini Kit	217004	Qiagen, Venlo, Netherlands
Mouse IFN gamma ELISA Ready-SET-Go!	88-7314-88	eBioscience, Waltham, USA
Mouse IFN-γ Secretion Assay – Detection Kit (PE)	130-090-516	Miltenyi Biotec , Bergisch Gladbach, Germany
Pierce™ BCA Protein Assay Kit	23225	Thermo Fisher Scientific, Waltham, USA
QIAamp DNA Blood Mini Kit	51104	Qiagen, Venlo, Netherlands
QIAprep Spin Miniprep Kit	27104	Qiagen, Venlo, Netherlands
QIAquick Gel Extraction Kit	28704	Qiagen, Venlo, Netherlands
QIAquick PCR Purification Kit	28106	Qiagen, Venlo, Netherlands
RNase-Free DNase Set	79254	Qiagen, Venlo, Netherlands
RNeasy Plus Mini Kit	74134	Qiagen, Venlo, Netherlands
TaqMan™ MicroRNA Reverse Transcription Kit	4366596	Thermo Fisher Scientific, Waltham, USA
TaqMan™ Universal PCR Master Mix	4304437	Thermo Fisher Scientific, Waltham, USA
TOPO® TA Cloning® Kit for Sequencing	450030	Thermo Fisher Scientific, Waltham, USA
Transcriptor First Strand cDNA Synthesis Kit	04379012001	Hoffmann-La Roche, Basel, Switzerland

2.1.13 Software

Table 2.28: Software

Software	Provider
ApE - A plasmid Editor v2.0.47	M. Wayne David
EndNote X7.0.1	Thomson Reuters, Toronto, Canada
FlowJo V10	Becton Dickinson , Franklin Lakes, USA
GraphPad Prism 5	GraphPad Software, Inc., San Diego, USA
Living Image Software 4.4	PerkinElmer, Waltham, USA
Microsoft Office 2010	Microsoft, Redmont, USA
RTCA Software 2.0	ACEA Biosciences, San Diego, USA

2.2 Methods

2.2.1 Cell culture

Working with cell lines or primary cells was performed under sterile conditions in a tissue culture hood. Cells were maintained by incubation at 37 °C in a CO_2 incubator (5 % CO_2). A commercially available hemocytometer was used for cell number adjustments. Reagents used for cell culture work are listed in Table 2.3. All cell lines used or generated within this thesis and their corresponding culture medium are listed in Table 2.15 and Table 2.16, respectively.

2.2.2 Generation of single guide RNA encoding plasmids

Parts of the following paragraph have been taken from reference [307] and were originally written by myself. Single guide (sg)RNAs targeting exon 1 of the murine IA^b beta chain gene were designed by Ashish Goyal (German Cancer Research Center, Heidelberg, Germany) using the online sgRNA design tool available at https://crispr.mit.edu/. In order to maximize specificity, guide sequences with high scores for on-target activity and at least 3 base pair mismatches to any predicted off-targets in the genome were selected. The corresponding sense and antisense DNA oligomers are shown in Table 2.18. Annealed oligomers were cloned downstream of the U6 promoter of PX458 (Addgene, Plasmid 48138, Middlesex, UK) as described earlier [308]. A plasmid map of PX458 is depicted in supplementary Figure 6.1 [307].

2.2.3 Transfection of B16F10 cells with single guide RNA encoding plasmids

B16F10 cells were transfected using the Effectene Transfection Reagent Kit (Table 2.4). The transfection protocol was optimized to achieve the highest possible transfection efficiency. Briefly, 2 x 10^5 B16F10 cells were seeded in a 6-Well plate in a total volume of 2.5 ml culture medium and incubated overnight at 37 °C and 5 % CO_2. The following day, 0.8 µg DNA were diluted in DNA-condensation buffer (Buffer EC) to reach a total volume of 100 µl. In case of double transfection with two guide RNA constructs, 0.5 µg of each plasmid was used. After adding 6.5 µl Enhancer the solution was vortexed for 1 second and incubated at room temperature (RT) for 4 minutes. Subsequently, 8 µl of Effectene Transfection Reagent were added to the DNA-Enhancer mixture and the solution was mixed by pipetting up and down 5 times. The mixture was incubated at RT for 10 min to allow transfection-complex formation. While complex formation took place, the culture medium of B16F10 cells was aspirated and the adherent cells were washed once with PBS. Fresh culture medium (1600 µl per well) containing serum and antibiotics was added. After adding 600 µl of culture medium to the transfection-complex tube, the solution was mixed by pipetting up and down twice and immediately dispensed in the 6-Well plates dropwise (714.4 µl/well). The cells were incubated at 37 °C and 5 % CO_2 and analyzed 24, 48 or 72 h post transfection without changing the transfection-complex containing culture medium.

2.2.4 IFNγ treatment of tumor cells

Tumor cells were seeded at a density of 2 x 10^5 cells per well in a 6-Well plate in 2 ml of culture medium. After overnight incubation at 37 °C and 5 % CO_2, Mouse IFNγ (Table 2.14)

was added to the culture medium at a final concentration of 20 U/ml. The cells were incubated for 24, 48 or 72 h and subsequently analyzed by flow cytometry as described in detail in the corresponding figure legends.

2.2.5 Genomic DNA isolation and PCR

Parts of the following paragraph have been taken from reference [307] and were originally written by myself. Genomic DNA of various cell lines, including the generated IA^b knockout (KO) B16F10 cells, was isolated using the QIAamp DNA Blood Mini Kit according to manufacturer's instructions. The sequences of interest were amplified by PCR using 0.5 µM of forward and reverse primer (Table 2.22), 0.2 mM dNTP-Mix Long Range, 2.5 mM $MgCl_2$, 1.25 U Taq DNA Polymerase, and 160 ng genomic DNA resolved in Taq Buffer (compare Table 2.29). The desired genomic loci were amplified with the Veriti 96-Well Thermal Cycler using the cycler protocol shown below (Table 2.30). All reagents required to perform PCRs are listed in Table 2.9.

Table 2.29: Pipetting scheme for PCR

Component	Volume per reaction
Forward primer (10 µM)	2.5 µl
Reverse primer (10 µM)	2.5 µl
Taq Buffer with $(NH_4)_2SO_4$ (10X)	5 µl
dNTP-Mix Long Range (10 mM)	1 µl
$MgCl_2$ (25 mM)	5 µl
Taq DNA Polymerase (5 U/µl)	0.25 µl
DNA template (160 ng)	x µl
Nuclease free water	50 - (16.25 + x) µl
Total volume	50 µl

Table 2.30: Cycler protocol for PCR

Step	Temp.	Time
Initial	95 °C	1 min
Amplification (40 cycles)	95 °C	30 s
	60 °C	30 s
	72 °C	1 min
Final	72 °C	5 min

2.2.6 TOPO TA cloning

Parts of the following paragraph have been taken from reference [307] and were originally written by myself. The CRISPR/Cas9 (clustered regularly interspaced short palindromic repeats/CRISPR-associated 9) induced mutations in the generated IA^b knockout clones were analyzed on genomic DNA level. Therefore, genomic DNA was isolated and the sequences of interest containing the predicted cutting sites of the Cas9 nuclease were amplified by PCR using IA^b specific primers (Table 2.22) as described in section 2.2.5. The PCR products were purified using the QIAquick PCR Purification Kit according to manufacturer's instructions. Subsequently, the purified PCR products were cloned into the

TOPO vector using the TOPO® TA Cloning® Kit for Sequencing. In order to set up the TOPO cloning reaction, 2.5 µl of purified PCR product were mixed with 1 µl of the supplied salt solution and filled up with water to a total volume of 5 µl. After the addition of 1 µl TOPO vector, the reaction was gently mixed, incubated for 10 min at RT and either used immediately for subsequent transformation (section 2.2.7) or stored at -20 °C.

2.2.7 Transformation, plasmid isolation and sequencing

LB Medium (pH 7.5):	1 % Tryptone 0.5 % Yeast extract 170 mM NaCl
LB-Amp Medium:	LB Medium 50 µg/ml Ampicilin
LB-Amp Plates:	LB-Amp Medium 1.5 % Agar

Parts of the following paragraph have been taken from reference [307] and were originally written by myself. In order to amplify the TOPO vectors with the integrated PCR products (refer to section 2.2.6), 2 µl of the plasmids were added to one vial of One Shot competent TOP10 bacteria (Table 2.12). After incubating the vial for 10 min on ice, the cells were heat-shocked for 30 seconds at 42 °C without shaking. The cells were immediately transferred to ice and 250 µl of room temperature S.O.C medium were added. Next, the vial was shaken horizontally at 37 °C and 200 revolutions per minute (rpm) for 1 h. The bacteria were subsequently dispensed (10, 30 or 50 µl) on pre-warmed LB-Amp Plates and incubated overnight. To verify that the PCR product was successfully integrated into the TOPO vector of growing colonies, several clones were picked to perform a colony PCR. For this, the picked colonies were transferred into 10 µl ddH_2O and incubated at 95 °C for 10 minutes. The lysate (4 µl per reaction) was used as DNA template for amplifying the insert by PCR (protocol as described in section 2.2.5) using IA^b specific primers (Table 2.22) or M13 primers which are part of the TOPO® TA Cloning® Kit for Sequencing. After verifying that all picked colonies carried the insert, several additional clones were picked and expanded for 24 h in LB-Amp Medium at 37 °C and 200 rpm. Plasmids were isolated using the QIAprep Spin Miniprep Kit according to manufacturer's instructions and sent to GATC Biotech (Konstanz, Germany) for sequencing. The sequences were analyzed using the ApE-A plasmid Editor Version 2.0.47. All reagents used for transformation of bacteria are listed in Table 2.13.

2.2.8 Titration of Geneticin and Puromycin on tumor cells

EO771 or B16F10 cells were seeded into a 12-Well plate (10^5 cells per well) and incubated overnight at 37 °C and 5 % CO_2. On the following day, the culture medium was replaced by medium supplemented with different concentrations of the corresponding selection antibiotic (Table 2.8). Puromycin concentrations ranged from 0.5 µg/ml to 5 µg/ml with increments of 0.25 µg/ml. Geneticin concentrations ranged from 3 mg/ml to 0.4 mg/ml with 0.2 mg/ml increments. Cell viability was assessed every day using an optical microscope. The minimal

concentration of each antibiotic that was lethal to 100 % of the cells was used for selection and subsequent culturing of transduced clones.

2.2.9 Generation of stable transduced clones

The transduction of tumor cell lines using retroviral particles was done by the Genomics and Proteomics Core Facility of the German Cancer Research Center in Heidelberg, Germany.
The wild type OVA encoding sequence (RefSeq NM_205152.2.) as well as a truncated sequence of OVA lacking the first 150 base pairs flanked by attL recombination sites were synthesized and cloned into a pMX plasmid (Thermo Fisher Scientific, Waltham, USA). The sequences were shuttled in lentiviral expression vectors adding a C-terminal IRES sequence coupled to a neomycin resistance gene by gateway recombination. For generation of lentiviral particles, HEK293FT cells (Thermo Fisher Scientific, Waltham, USA; Cat. No. R70007) were co-transduced with the lentiviral OVA expression constructs and 2nd generation viral packaging plasmids VSV.G (Addgene #14888) and psPAX2 (Addgene #12260). Transduction of B16F10, B16F10 IA^b knockout and EO771 cells with luciferase was performed using a retroviral construct expressing red Firefly luciferase and a puromycin selection marker under control of a SV40 promoter. Retroviral particles were produced by co-transduction of HEK293FT cells with pBabe-Puro red Firely luciferase expression vector and the packaging plasmids pHIT60 and pMD2G (Addgene #12259). Two days after transduction, the virus containing supernatants were collected and cleared by centrifugation at 500 g (gravitational force) for 5 minutes. After the supernatants were passed through a 0.45 µm filter to remove remaining cellular debris, B16F10, B16F10 IA^b knockout and EO771 cells were transduced with viral particles at 70 % confluency in the presence of 10 µg/ml polybrene (Merck KGaA, Darmstadt, Germany; Cat. No. TR-1003-G). The virus containing medium was replaced by the corresponding selection medium one day post transduction. After two weeks, clones were picked and expanded.

2.2.10 Lactacystin treatment

In order to block the proteasome, transduced cell clones and their respective parental cell lines were seeded in a 6 well plate (10^5 cells per well) one day prior lactacystin treatment (Table 2.3). The cells were incubated in the presence of 10 µM or 25 µM lactacystin for 6 or 13 h. Finally, the culture supernatants were collected and whole cell protein samples were prepared (see section 2.2.25) for subsequent Western blot analysis.

2.2.11 Magnetic activated cell sorting (MACS) for positive and negative selection

MACS buffer (pH 7.2): PBS
0.5 % BSA
2 mM EDTA

OVA specific $CD4^+$ T cells were isolated from either OT-II splenocytes or restimulated T cell cultures using either CD4 (L3T4) MicroBeads (positive selection) or the $CD4^+$ T Cell Isolation Kit (negative selection) according to manufacturer's instructions. If purification of $CD8^+$ T cells was required, CD8a (Ly-2) MicroBeads were used according to manufacturer's instructions.

2.2.12 Generation of OVA specific CD4+ T cell lines

In order to generate an OVA specific $CD4^+$ T cell line that can be kept in culture through recurring restimulations, three different strategies were implemented as described in the following sections.

2.2.12.1 Peptide immunization of C57BL/6 mice

C57BL/6 mice were immunized subcutaneously (s.c.) with 100 µg of IA^b restricted OVA peptide ISQAVHAAHAEINEAGR (aa 323–339; compare Table 2.26) diluted in complete Freund's Adjuvant (Sigma-Aldrich, St. Louis, USA). After 7 or 13 days, mice were sacrificed and 6×10^6 splenocytes were cultured in Minimum Essential Medium Eagle Alpha Modification supplemented with 2 µg/ml peptide, 2 mM L-Glutamine, 10 % FCS, 50 µM beta-Mercaptoethanol, 100 U/ml Penicillin and 100 µg/ml Streptomycin. Every 7 days, half of the supernatant was exchanged with the above mentioned supplemented medium, additionally containing 12.5 mM Methyl α-D-mannopyranoside and 2.5 % (v/v) culture supernatant from ConA stimulated rat-spleen cells, as a source of interleukin-2 (Complete T cell Medium). Spleen cell cultures were restimulated every 4 weeks by the addition of 6×10^6 irradiated (33 Gray (Gy)) syngeneic feeder cells together with antigenic peptide (2 µg/ml). All reagents needed for culturing OVA specific $CD4^+$ T cells are listed in Table 2.3.

2.2.12.2 OT-II $CD4^+$ T cell expansion using peptide

In the homozygous T cell receptor transgenic OT-II mice, all T cells express the mouse alpha- and beta-chain T cell receptor specifically recognizing the IA^b restricted OVA peptide (aa 323-339). Therefore, an OVA specific $CD4^+$ T cell line can be generated without the need to perform *in vivo* immunizations. The strategy described in this section included the isolation of splenocytes from naïve OT-II mice which were cultured in 24-Well plates in 2 ml Complete T cell Medium containing 2 µg/ml IA^b restricted OVA peptide (aa 323-339). Spleen cell cultures were restimulated every 4 weeks by the addition of 6×10^6 irradiated (33 Gy) syngeneic feeder cells together with antigenic peptide (2 µg/ml).

2.2.12.3 OT-II $CD4^+$ T cell expansion using CD3/CD28 Dynabeads

As all $CD4^+$ T cells in OT-II mice bear the same T cell receptor, it is possible to expand those cells using CD3/CD28 Dynabeads without the risk of unwanted T cell clones expanding. To avoid co-expansion of $CD8^+$ T cells, the isolated OT-II splenocytes were negatively selected using the $CD4^+$ T Cell Isolation Kit (compare section 2.2.11), adjusted to the desired cell concentration in Complete T cell Medium and dispensed in 24-Well plates (1×10^6 cells in 2 ml). Next, 25 µl of CD3/CD28 Dynabeads were added to each well. Three days later, the proliferated T cells were harvested, counted and 8×10^5 T cells per well were seeded in a fresh 24-Well plate (without the addition of fresh Dynabeads). After additional 5 days of culturing, 1 ml of old medium was aspirated and replaced by 6×10^6 irradiated (33 Gy) syngeneic feeder cells together with IA^b restricted OVA peptide (2 µg/ml). The T cell culture was restimulated every 4 weeks using the aforementioned amounts of irradiated syngeneic feeder cells and antigenic peptide.

2.2.13 *In vitro* propagation of ovalbumin specific CD8$^+$ T cells

OVA specific CTLs (CTL ($OVA_{257-264}$; K^b)) were cultured in 24-Well plates using 2 ml Complete T cell Medium. Every 7 days, half of the supernatant was aspirated and replaced by 5 x 10^6 irradiated (33 Gy) syngeneic feeder cells together with 2 x 10^5 irradiated (200 Gy) stimulator cells (E.G7). All reagents needed for culturing OVA specific CD8$^+$ T cells are listed in Table 2.3.

2.2.14 Isolation, purification and polarization of peritoneal exudate cells (PECs)

C57BL/6 mice were injected intraperitoneally (i.p.) with 1 ml of 3 % (w/v) Thioglycolate medium (Applichem, Darmstadt, Germany; Cat. No. A3869) using a 27 G needle. Four days later, mice were sacrificed by gradual CO_2 exposition and 8 ml of ice cold PBS were injected into the peritoneal cavity using a 21 G needle. PECs containing fluid was aspirated and centrifuged at 300 g for 10 minutes. PECs were resuspended in DMEM containing 10 % FCS and 2 x 10^6 or 0.5 x 10^6 cells were seeded to each well of a 6 well or 24 well plate. After two hours (h), the medium was removed and adherent cells were washed three times with PBS. To induce M2 or M1 polarization, cells were cultured in DMEM supplemented with either 10 ng/ml IL-4 or a combination of 100 ng/ml LPS and 50 ng/ml IFNγ, respectively for 4, 24, 48 or 72 h. For subsequent analysis, cells were detached with 500 µl Accutase at 37 °C for 5 minutes and harvested using a cell scraper. The reagents and cytokines used for PECs isolation and polarization are listed in Table 2.3 and Table 2.14, respectively.

2.2.15 Peptide loading of PECs

Adherent, polarized PECs were incubated at 37 °C for 45 min in X-VIVO™ 20 serum free medium containing 1 µg/ml IA^b restricted OVA specific peptide (aa 323–339) or HBV core antigen derived peptide (aa 128–140; compare Table 2.26) as control. Cells were washed 3–5 times with PBS to remove unbound peptides. Tumor cell lines (B16F10 derived or 771 B cell lymphoma) were harvested, adjusted to a cell concentration of 2 x 10^6 cells/ml in X-VIVO™ 20 serum free medium containing the relevant peptides as mentioned above. After 45 minutes of incubation at 37 °C, the cells were washed 3-5 times with PBS, resuspended in culture medium and used for co-culture experiments.

2.2.16 Co-culture of PECs and OVA specific CD4$^+$ T cells

M2 polarized PECs (24 h) were loaded with peptide (5 µg/ml) and co-cultured with OVA specific CD4$^+$ T cells for 24 h (ratio 4:1). Supernatants were collected to measure IFNγ concentrations and macrophages were washed 3 times to remove the non-adherent T cells. The cells were subsequently detached as described above (section 2.2.14) and analyzed by flow cytometry or lyzed for the preparation of cell lysates (as described in sections 2.2.21 and 2.2.27).

2.2.17 Phagocytosis and pinocytosis assay

PECs were seeded in a 24-Well plates (5 x 10^5) and polarized for 72 h as described in section 2.2.14. In case of co-culture experiments, PECs were polarized for 24 h into M2-like macrophages, loaded with peptide (section 2.2.15) and subsequently cultured for additional

24 h with OVA specific $CD4^+$ T cells (section 2.2.16). After washing three times with PBS, the cells were maintained in DMEM containing 10 % FCS and either 1 mg/ml FITC-dextran (pinocytosis) or 1.25 x 10^6/ml FluoSpheres™ Carboxylate-Modified Microspheres (2.0 µm; phagocytosis) [309, 310]. Thereafter, PECs were detached, harvested, stained with LIVE/DEAD® Fixable Yellow dye and analyzed by flow cytometry (section 2.2.27). Background values were determined upon incubation of cells with FITC labeled particles at 4 °C and subtracted from the values measured after culturing at 37 °C. All reagents needed to perform phagocytosis and pinocytosis assays are listed in Table 2.3.

2.2.18 Transfection of PECs with plasmids

Plasmid transfection of PECs was carried out using Lipofectamine LTX Reagent, Lipofectamine 3000 Transfection Reagent, PromoFectin-Macrophage, TransIT Dynamic Delivery System, TransIT-2020 Transfection Reagent, TurboFect Transfection Reagent, Viromer Red, Effectene Transfection Reagent Kit, DharmaFECT Duo Transfection Reagent or METAFECTENE® PRO (Table 2.4). All Reagents were used according to manufacturer's instructions. Detailed information about the exact transfection conditions (cell density, amount of DNA and transfection reagent) is specified in the corresponding figure legends.

2.2.19 Transfection of PECs with siRNAs and miRNAs

PECs were transfected with a custom-made fluorescently labeled siRNA (Sigma-Aldrich, St. Louis, USA) using DharmaFECT 4 Transfection Reagent, Lipofectamine RNAiMAX Transfection Reagent, METAFECTENE® SI^+ or siLentFect Lipid Reagent for RNAi (Table 2.4). Based on these results DharmaFECT 4 Transfection Reagent was determined to be the most suitable Reagent to deliver siRNAs in macrophages (high transfection efficiency and low cytotoxicity) and was used for all experiments according to manufacturer's instructions. Briefly, siRNAs or miRNAs were diluted in serum-free DMEM medium to a total volume of 200 µl and a concentration that was 10 times higher than the desired final concentration. Next, 4 µl of DharmaFECT 4 Transfection Reagent were diluted in 196 µl serum-free DMEM medium. Both tubes were gently mixed by pipetting carefully up and down and incubated for 5 min at RT. The contents of both tubes were mixed and incubated for 20 min at RT. Meanwhile, the old PECs culture medium was aspirated and replaced by 1600 µl antibiotic-free DMEM medium containing 10 % FCS. Finally, 400 µl of the transfection reagent/siRNA or miRNA mixture were added dropwise and the cells were incubated at 37 °C and 5 % CO_2. Analysis was performed 24, 48 or 72 h post transfection. The transfection reagent was not replaced since cytotoxicity could not be observed. The protocol was applied to transfect 2 x 10^6 PECs seeded in 6-Well plates.

2.2.20 miRNA isolation and quantification of miRNA expression level

Micro RNA of PECs was isolated using the miRNeasy Mini Kit according to manufacturer's instructions. Reverse transcription was performed using the TaqMan™ MicroRNA Reverse Transcription Kit according to the pipetting scheme shown below (Table 2.31). Each miRNA was reverse transcribed using its specific RT primer pair by incubating in a thermal cycler at 16 °C for 30 minutes, then at 42 °C for 30 minutes and finally at 85 °C for 5 minutes.

Table 2.31: cDNA synthesis using the TaqMan™ MicroRNA Reverse Transcription Kit

Component	Volume per reaction
Deoxynucleotide Mix (100 mM)	0.15 µl
MultiScribe Reverse Transcriptase (50 U/µl)	1 µl
Reverse Transcription Buffer (10 X)	1.5 µl
Rnase Inhibitor (20 U/µl)	0.19 µl
nuclease free water	4.16 µl
RT primer	3 µl
RNA template (40 ng)	5 µl
Total volume	15 µ

Gene expression was quantified using quantitative real-time PCR. Therefore, 2 µl of the undiluted cDNA was mixed with the matching TaqMan Probes, the TaqMan™ Universal PCR Master Mix and nuclease free water to reach a total volume of 20 µl as shown in Table 2.32. The selected miRNAs were amplified using the ABI 7300 Real-time PCR System and the cycler protocol shown in Table 2.33. Gene expression was quantified by normalization to small nucleolar RNA 202 (snoRNA202). Primer pairs for reverse transcription as well as TaqMan Probes were obtained from Thermo Fisher Scientific, Waltham, USA (Cat. No. 4427975).

Table 2.32: qPCR pipetting scheme using TaqMan™ Universal PCR Master Mix

Component	Volume per reaction
cDNA (undiluted)	2 µl
TaqMan Probe	1 µl
TaqMan™ Universal PCR Master Mix (2 X)	10 µl
nuclease free water	7 µl
Total volume	20 µl

Table 2.33: Cycler protocol for qPCR using TaqMan™ Universal PCR Master Mix

Step	Temp.	Time
Pre-incubation (1 cycle)	50 °C	2 min
	95 °C	10 min
Amplification (45 cycles)	95 °C	15 s
	60 °C	1 min

2.2.21 RNA isolation and quantitative real-time PCR

RNA of tumor cell lines was isolated using the RNeasy Plus Mini Kit according to manufacturer's instructions. RNA of primary macrophages sorted from tumor tissue was isolated using the RNeasy Micro Kit according to manufacturer's instructions. RNA of PECs was isolated using phenol-chloroform extraction followed by solid-phase anion-exchange chromatography. Briefly, PECs in 6-Well plates were washed twice with PBS, lyzed by the addition of 1 ml QIAzol Lysis Reagent (Qiagen, Venlo, Netherlands; Cat. No. 79306) per well and transferred into a 1.5 ml Eppendorf tube. After the addition of 200 µl chloroform (VWR International, Radnor, USA; Cat. No. 22711.29) and a subsequent centrifugation step at

maximum speed and 4 °C for 15 minutes, the aqueous phase was transferred into a fresh tube containing 600 µl 75 % Ethanol. The mixture was transferred on RNeasy columns and RNA extraction was carried out using the RNeasy Plus Mini Kit according to manufacturer's instructions (including on-column DNA digestion).
The isolated RNA of tumor cell lines or PECs was quantified using Nanodrop Spectrophotometer. In case of low 260/230 ratios, the RNA was purified by ethanol precipitation (see section 2.2.22) prior reverse transcription using the Transcriptor First Strand cDNA Synthesis Kit according to the pipetting scheme shown in Table 2.34. The reaction mix from step 1 was incubated at 65 °C for 10 min to ensure denaturation of RNA secondary structures. After the additional components were added, the reaction mix from step 2 was incubated at 50 °C for 1 h followed by a 5 min incubation at 85 °C. The cDNA was cooled down to 4 °C and stored at -80 °C.

Table 2.34: cDNA synthesis using the Transcriptor First Strand cDNA Synthesis Kit

Step 1

Component	Volume per reaction
RNA template (500 ng)	x µl
nuclease free water	(12 - x) µl
Anchored-oligo$(dT)_{18}$ primer (50 pmol/µl)	1 µl
Total volume	13 µl

Step 2

Component	Volume per reaction
Reaction mix from Step 1	13 µl
Reverse Transcriptase Reaction Buffer (5 X)	4 µl
Protector RNase Inhibitor (40 U/µl)	0.5 µl
Deoxynucleotide Mix (10 mM each)	2 µl
Transcriptor Reverse Transcriptase (20 U/µl)	0.5 µl
Total volume	20 µl

The yield of RNA isolated from sorted macrophages was too low for accurate quantification. Therefore, the whole volume was used for reverse transcription using the iScript cDNA Synthesis Kit according to the protocol in Table 2.35. The complete reaction mix was incubated at 25 °C for 5 min, at 42 °C for 30 min and at 85 °C for 5 min. The cDNA was cooled down to 4 °C and stored at -80 °C until further use.

Table 2.35: cDNA synthesis using the iScript cDNA Synthesis Kit

Component	Volume per reaction
RNA template	15 µl
5x iScript reaction mix	4 µl
iScript reverse transcriptase	1 µl
Total volume	20 µl

Gene expression was measured using quantitative real-time PCR. Therefore, 2 X Power SYBR® Green PCR Master Mix (Thermo Fisher Scientific, Waltham, USA; Cat. No. 4367659), 10 ng cDNA, 400 nM of each primer pair and nuclease free water were mixed to a total volume of 20 µl (see also Table 2.36). The selected genes were amplified using the ABI

7300 Real-time PCR System and the cycler protocol shown in Table 2.37. Gene expression was quantified by normalization to the corresponding housekeeping gene. All primers used for quantitative real-time PCR are shown in Table 2.21.

Table 2.36: qPCR pipetting scheme using Power SYBR® Green PCR Master Mix

Component	Volume per reaction
cDNA (diluted 1:5 in nuclease free water)	2 µl
Power SYBR® Green PCR Master Mix (2X)	10 µl
Forward primer (10 µM)	0.4 µl
Reverse primer (10 µM)	0.4 µl
nuclease free water	7.2 µl
Total volume	20 µl

Table 2.37: Cycler protocol for qPCR using Power SYBR® Green PCR Master Mix

Step	Temp.	Time
Pre-incubation (1 cycle)	50 °C	2 min
	95 °C	10 min
Amplification (40 cycles)	95 °C	15 s
	60 °C	1 min
	72 °C	30 s
Melting curve (1 cycle)	98 °C	15 s
	60 °C	1 min
	95 °C	15 s
	60 °C	15 s

2.2.22 Ethanol precipitation of RNA samples

RNA samples with low 260/230 ratios (below 1.8), indicating phenol contamination, were purified by ethanol precipitation as described in the following. After adding 0.1 volume of 3 M sodium acetate and 2.75 volumes of ice cold 100 % ethanol to the RNA, the samples were stored overnight at -80 °C to allow RNA precipitation. The following day, the samples were centrifuged at full speed and 4 °C for 30 minutes and the ethanol was carefully aspirated. The precipitated RNA pellet was washed by the addition of 500 µl ice cold 75 % ethanol followed by a 10 minute centrifugation at full speed and aspirating the ethanol carefully. After repeating the washing step once, the RNA pellet was air dried and resolved in an appropriate amount of nuclease free water.

2.2.23 Whole RNA and small RNA sequencing

Whole RNA sequencing as well as small RNA sequencing of polarized PECs was done by the Genomics and Proteomics Core Facility of the German Cancer Research Center in Heidelberg, Germany using a HiSeq 2000 Sequencing System from Illumina (San Diego, USA). The sequencing data were analyzed by Franziska Hoerhold (Integrated Research and Treatment Center, Center for Sepsis Control and Care (CSCC), Jena, Germany). Briefly, Reads were mapped against the mouse GRCm38/mm10 reference genome by using TopHat [311]. The read counts of whole RNA sequencing data were calculated with

featureCounts [312, 313]. The read counts of small RNA sequencing data were calculated with customized scripts. Subsequently, DESeq2 [314] was used to determine differentially expressed genes.

2.2.24 SDS-PAGE gel casting

4 X Lower buffer:
1.5 M Trizma Base
0.4 % SDS
adjust pH to 8.8

4 X Upper buffer:
0.5 M Trizma Base
0.4 % SDS
adjust pH to 6.8

The amounts of required reagents for one gel with dimensions 0.15 x 8 x 8 cm are given in Table 2.38. The polymerized separating gel was overlaid by 2 ml of the 5% stacking gel and a 1.5 mm x 5 mm gel strip was introduced. All reagents required to cast the gels are listed in Table 2.6.

Table 2.38: SDS-PAGE gel casting

Component	5 % stacking gel	12 % separating gel
30% Acrylamide/Bis Solution [µl]	425	4000
4 X Upper Buffer [µl]	312.5	-
4 X Lower Buffer [ml]	-	2.5
Ammonium Persulfate [µl]	25	100
TEMED [µl]	2.5	4
Add water to final volume [ml]	2.5	10

2.2.25 Protein detection by Western blot

5 X Protein loading buffer:
0.02% Bromophenol blue
30 % Glycerol
10 % SDS
250 mM Trizma Base (adjusted with HCL to pH 6.8)
10 % β-Mercaptoethanol (just before usage)

10 X Running buffer:
0.25 M Trizma Base
1 % SDS
1.9 M Glycine

10 X Transfer buffer:
0.25 M Trizma Base
0.4 % SDS
1.9 M Glycine

1 X Transfer buffer:
10 X Transfer buffer
20 % Methanol

Blocking buffer:
1 X TBS
5 % Milk powder
0.05 % Tween 20

10 X TBS:	0.2 M Trizma Base 1.37 M NaCl adjust pH to 7.6
Washing buffer (TBS-T):	1 X TBS 0.05 % Tween 20

In order to detect secreted proteins in the medium of cultured tumor cell lines, the cell culture supernatants were collected, mixed with 5 X protein loading buffer and heat denatured at 95 °C for 10 min. For the preparation of whole cell protein samples, cells were harvested, counted and resuspended in an appropriate amount of Cell Lysis Buffer (2.5×10^4 cells per µl) supplemented with 1 mM Phenylmethylsulfonylfluorid (PMSF). The samples were stored on ice for 10 min and subsequently centrifuged at 4 °C and 14000 g for 20 min. The protein containing supernatants were transferred into fresh tubes, mixed with 5 X protein loading buffer and heat denatured at 95 °C for 10 minutes. Cell culture supernatants as well as whole cell protein samples were separated on a 12 % polyacrylamide gel (20 min at 80 V followed by 1.5 h at 120 V) and the proteins were electro-transferred onto nitrocellulose membranes using the Trans-Blot Turbo Transfer System. The membranes were blocked with 5 % of non-fat milk in Tris-buffered saline containing 0.05 % Tween (Blocking buffer) for 1 h. Subsequently, the membranes were incubated overnight at 4 °C on a shaking platform with an OVA specific antibody diluted 1:1000 in blocking buffer. Next, membranes were washed 3 times for 5 min with 10 ml TBS-T and incubated at RT for 1 h with a horseradish peroxidase (HRP) conjugated secondary antibody 1:5000 diluted in blocking buffer. After 3 additional washing steps with TBS-T as described above, protein signals were detected by adding ECL Prime Western Blotting Detection Reagent directly on the membrane and exposing blots to a charge-coupled device (CCD)-camera. Afterwards the membranes were washed 5 times for 5 min using TBS-T and incubated at RT for 1 h with an actin specific antibody diluted 1:10000 in blocking buffer. After 3 additional washing steps for 5 min using TBS-T, the membranes were incubated a second time at RT for 1 h with a HRP conjugated antibody diluted 1:5000 in blocking solution and analyzed using the ChemiDoc™ XRS+ System after adding detection reagent. Data were analyzed using the Image Lab Software. The material and antibodies used for Western blot analysis are listed in Table 2.6 and Table 2.24, respectively.

2.2.26 Gel electrophoresis

1 X Tris-acetate-EDTA (TAE) buffer (pH 8.6):	40 mM Trizma Base 20 mM Acetate 1 mM EDTA

For the electrophoretic separation of PCR products according to their size, the samples were mixed with DNA Ladder and loaded on a 1 % agarose gel. For gel preparation, appropriate amounts of agarose were boiled in Tris-acetate-EDTA (TAE) buffer. After cooling down to approximately 50 °C, Ethidiumbromide (5 drops per 100 ml) was added and the agarose poured into a gel chamber. An appropriate volume of sample and DNA Ladder were loaded as soon as the agarose gel was completely polymerized. After separation at a constant voltage of 120 V for 60 minutes in TAE buffer, the nucleic acid intercalating Ethidiumbromide

was excited with ultraviolet light and light emission was measured using the Gel iX Imager system.

2.2.27 Immunofluorescence staining for flow cytometry and cell sorting

FACS buffer: PBS
3 % FCS

Immunofluorescence staining of cells was performed using monoclonal antibodies listed in Table 2.23. The respective isotype matched antibodies against irrelevant epitopes were included as controls. All centrifugation steps were carried out for 2 min at 300 g and RT. After harvesting the cells and resuspending the cell pellet in an appropriate amount of FACS buffer, 200 µl of the cell suspension were dispensed per well in a 96-Well U-bottom plate. The plate was centrifuged, the supernatant was discarded and the pellet was incubated at 4 °C for 20 min in a mixture of rat anti-mouse CD16/CD32 (50 µg/ml), normal Syrian Hamster serum (1:100) and Rat serum (1:100) in a total volume of 100 µl to block Fc-receptors. The Fc-receptor blocking step was not performed if tumor cells or T cells were stained. Subsequently, the cells were centrifuged and washed using 180 µl FACS buffer. After an additional centrifugation, the cells were incubated at 4 °C for 1 h in FACS buffer containing fluorochrome conjugated antibodies and LIVE/DEAD Fixable Yellow Dead Cell dye (1:1000). Finally, the cells were washed twice, resuspended in 200 µl FACS buffer and analyzed with a FACSCanto II or LSR II cytometer or sorted using a FACS Aria I or II. The data were evaluated with FlowJo software (Version 10). If absolute quantification was required, 33 µl of CountBright Absolute Counting Beads were added to the cell suspension prior measurement. Absolute quantification was calculated based on the following formula:

$$\frac{\text{No. of cell events}}{\text{No. of Bead events}} \times \frac{\text{No. of Beads added per sample}}{\text{Volume of sample [µl]}} = \text{concentration of sample as cells/µl}$$

In case of intracellular staining of proteins the cells were fixed and permeabilized using FoxP3 staining Kit according to manufacturer's instructions. Briefly, the cell pellets were resuspended in 100 µl Fixation/Permeabilization solution and incubated at 4 °C for 20 min. After washing the cells twice with 200 µl Perm/Wash buffer, they were incubated with 100 µl fluorochrome conjugated antibodies diluted in Permeabilization Buffer at 4 °C for 1 h. The cells were washed twice with 200 µl Perm/Wash buffer and resuspended in 200 µl FACS buffer for subsequent analysis. The different buffers, compensation beads and Fc-blocking reagents are listed in Table 2.5.

2.2.28 xCELLigence

The xCELLigence® RTCA SP System was set up by measuring the background signal of an E-Plate 96 filled with 50 µl of RPMI 1640 per well supplemented with Glutamax, 10 % FCS, 100 U/ml Penicillin and 100 µg/ml Streptomycin. Afterwards, 2×10^3 cells per well were dispensed to reach a final volume of 200 µl and the impedance as a measure of cell proliferation was recorded for 10 days. Data were analyzed using the RTCA Software 2.0. All reagents used to perform the xCELLigence assay are listed in Table 2.3.

2.2.29 IFNγ ELISpot assay

Washing buffer: PBS
0.5 % Tween 20

IFNγ ELISpot assays were performed in order to investigate IFNγ secretion by activated T cells. The Polyvinylidenfluorid (PVDF) membrane of MultiScreenHTS-IP ELISpot plates was activated by incubating each well with 50 µl 80 % Ethanol for 2 min. After 2 washing steps with 200 µl PBS per well, the membrane was coated with 1 µg/ml goat anti-mouse IFNγ capture antibody (100 µl per well) overnight at 4 °C. The ELISpot plate was washed once with PBS and blocked with 200 µl serum containing medium. Next, graded numbers of antigen-specific T cells were added to 5 x 10^4 target cells in a total volume of 200 µl per well. Alternatively, 1.5 x 10^6 splenocytes of immunized mice in combination with a relevant peptide were dispensed. The plates were incubated for 16–18 h at 37 °C and 5 % CO_2 and subsequently washed 5 times with washing buffer followed by an additional washing step using PBS only. After washing 4 times with PBS, the plates were incubated with 2 µg/ml biotinylated rat anti-mouse IFNγ antibody (100 µl per well) for 1 h at 4 °C followed by additional 4 washing steps using PBS. Next, 100 µl avidin-conjugated alkaline phosphatase (Becton Dickinson, Franklin Lakes, USA; Cat. No. 554065) was added to each well and the plate was incubated for 30 min at RT. Finally, IFNγ-specific spots were visualized by adding 100 µl of BCIP/NBT (Sigma-Aldrich, St. Louis, USA; Cat. No. B1911). The reaction was stopped after 3 min of incubation at RT in the dark with distilled water. Spots were counted using the CTL ELISpot Reader System as soon as the membranes were dry. All antibodies used for the ELISpot Assay are depicted in Table 2.25.

2.2.30 IFNγ ELISA

Supernatants of co-cultured PECs were collected and IFNγ secretion of T cells was quantified using Mouse IFN gamma ELISA Ready-SET-Go! Kit according to manufacturer's instructions. The IFNγ concentrations of the samples were determined based on the standard curve generated in GraphPad Prism.

2.2.31 Luciferase assay

The luciferase expression of transduced clones was tested using the luciferase Assay System (Table 2.27). Tumor cells were dispensed in 96-Well F-bottom plates at a density of 5 x 10^4 cells per well and incubated overnight at 37 °C and 5 % CO_2. On the next day, the culture medium was aspirated and the cells were washed once with 200 µl PBS per well. After adding 20 µl 1 X Lysis Reagent to each well and incubating for 10 min at RT, 10 µl of the lysates were transferred into a white 96-Well F-bottom plate. Light emission was measured immediately after the addition of 100 µl luciferase Substrate using the Mithras LB940 system.

2.2.32 *In vivo* tumor growth

In order to measure tumor growth of tumor cells *in vivo*, cells were harvested, washed 3 times using PBS and adjusted to the desired concentration in PBS. C57BL/6 or C57BL/6 Ly5.1 mice were injected s.c. into the right flank with 100 µl of B16F10 (2 x 10^5) or PDAC

(2×10^6) or EO771 cells (3.5×10^5 or 2×10^6) or their corresponding transduced/knock out cell lines. Tumor growth was monitored at least twice per week by caliper measurement and mice were killed after the tumor had achieved a size of 1.5 cm in diameter. Mice were sacrificed by gradual CO_2 exposition.

2.2.33 *In vivo* imaging

C57BL/6 Ly5.1 mice were injected s.c. with luciferase expressing B16F10 clones (2×10^5) and tumor growth was monitored every 2-4 days using a caliper (as described in section 2.2.32). In order to determine the individual luciferase expression kinetic for each cell line, 30 gram heavy mice were shaved, sedated (1.5 vol. % Isofluoran (Zoetis, Parsippany-Troy Hills Township, USA)) and injected i.p. with 300 µl StayBrite D-Luciferin (15 mg/ml; BioCat, Cat. No. 7903-100-BV), which corresponds to 150 mg/kg body weight, 13 days post tumor cell injection. After substrate injection, the total Flux (p/s) was measured using auto exposure time, medium binning, F/stop of 1 and subject height of 1.5 cm every two minutes for 1 h using the IVIS Lumina Series III. The data were analyzed using the Living Image Software 4.4. to determine the percentages of max. Flux. Each total Flux value was divided by the highest total Flux value measured within a sequence of pictures.

2.2.34 Adoptive cellular therapy

Tumor bearing C57BL/6 Ly5.1 mice received adoptive cellular therapy 8-10 days post tumor cell injection. Therefore, splenocytes of OT-II mice were used either in their naïve state or after 3 days of expansion using CD3/CD28 Dynabeads or IA^b restricted OVA peptide as described in the following.

Naïve OT-II $CD4^+$ T cells:

OT-II splenocytes were isolated and underwent positive selection using CD4 (L3T4) MicroBeads (section 2.2.11). After adjusting the cell concentration to 50×10^6 cells/ml in PBS, 100 µl of the cell suspension were administered intravenously (i.v.) into the lateral tail vein of tumor bearing C57BL/6 Ly5.1 mice.

Pre-activation using CD3/CD28 Dynabeads:

OT-II splenocytes were isolated, positively selected using CD4 (L3T4) MicroBeads (section 2.2.11) and resuspended in an appropriate amount of Complete T cell Medium. Next, 1.5×10^6 $CD4^+$ T cells were dispensed into each well of a 24-Well plate and 37.5 µl CD3/CD28 Dynabeads were added. After 2 days of incubation, 1 ml of the old culture medium was replaced by fresh medium. Three days post $CD4^+$ T cell isolation, the cells were harvested and the Dynabeads were removed according to manufacturer's instructions. The cells were washed 3 times using PBS and adjusted to a cell concentration of 50×10^6 cells/ml in PBS. The cell suspension (100 µl per mouse) was administered i.v. into the lateral tail vein of tumor bearing C57BL/6 Ly5.1 mice.

Pre-activation using peptide:

OT-II splenocytes were isolated, resuspended in Complete T cell medium and dispensed in 24-Well plates (6×10^6 cells per well in 2 ml). The cells were cultured in the presence of 1 µg/ml IA^b restricted OVA peptide (aa 323-339) for 3 days. On day 2, 1 ml of old culture medium was replaced by fresh medium. After 3 days of incubation, the cells were harvested, positively selected using CD4 (L3T4) MicroBeads (section 2.2.11) and were adjusted in PBS

to a cell concentration of 50 x 10^6 cells/ml. A total of 5 x 10^6 $CD4^+$ T cells were injected i.v. into the lateral tail vein of tumor bearing C57BL/6 Ly5.1 mice.

2.2.35 Spleen and lymphnode preparation

Spleens and lymphnodes were harvested, transferred into PBS and passed through a 70 µm and 40 µm cell strainer, respectively. The single cell suspensions were centrifuged at 300 g for 10 min, the supernatants were discarded and the pellets resuspended in either 4 ml ACK lysing buffer (spleens) or an appropriate amount of FACS buffer for subsequent immunofluorescence staining (lymphnodes). After incubating the splenocytes for 2 min at RT in ACK lysing buffer, the 50 ml falcon tubes were filled up to a total volume of 50 ml using RPMI 1640 Medium. The cell suspension was centrifuged at 300 g for 10 min and the pellet was resuspended in an appropriate amount of RPMI 1640 Medium for subsequent cell counting. If necessary, the erythrocyte lysis step was repeated until the splenocyte pellet was completely white.

2.2.36 Tumor digestion and isolation of tumor infiltrating leukocytes

Tumors were harvested, transferred into hanks' balanced salt solution (HBSS) and cut into small pieces using a pair of scissors. Next, the tumors were digested for 1 h at 37 °C by shaking at 200 rpm using 0.5 mg/ml collagenase D, 10 µg/ml DNAse I, 0.1 µg/ml TLCK and 10 mM HEPES buffer diluted in HBSS (components listed in
Table 2.10). After passing the digested solution through a 70 µm cell strainer and then through a 40 µm cell strainer, the single cell suspension was centrifuged at 300 g for 10 minutes. The cell pellet was resuspended in 4 ml ACK lysing buffer and incubated for 2 min at RT. The erythrocyte lysis was stopped by filling up the 50 ml falcon tube to a total volume of 50 ml with RPMI 1640 Medium. After another centrifugation step at 300 g for 10 min, the cell pellet was resuspended in an appropriate amount of FACS buffer and the cell suspension was transferred into 96-Well U-bottom plates for subsequent immunofluorescence staining.

3 Results

3.1 Generation of ovalbumin and luciferase expressing, IA^b deficient B16F10 cells

The project aims for answering the question whether adoptively transferred tumor antigen specific $CD4^+$ T cells are able to polarize TAMs into immunostimulatory M1, thereby neutralizing the immunosuppressive tumor microenvironment and facilitating efficient tumor attack by tumor antigen specific $CD8^+$ CTLs.
An IA^b deficient variant of the murine melanoma cell line B16F10 was established to avoid possible interactions between transferred $CD4^+$ T cells and tumor cells and promote cognate interaction between $CD4^+$ T cells and TAMs *in vivo*. The IA^b KO B16F10 clone was generated using the CRISPR/Cas9 system (section 3.1.1). Therefore, nine guide RNAs (Table 2.18) targeting the beta chain of IA^b were designed and cloned into PX458 (supplementary Figure 6.1) downstream of the U6 promotor by Goyal Ashish (German Cancer Research Center, Heidelberg, Germany). Five of these guide RNAs target either Exon 1 (guide# 1, 4 and 5) or Exon 2 (guide# 3 and 12) creating a double strand break within the coding region of the gene. The target sequence of the remaining four guide RNAs is either upstream (u) of Exon 1 (guide# 1u and 2u) or downstream (d) of Exon 6 (guide# 1d and 2d), both in non-coding regions. These guide RNAs need to be combined, thus inducing two individual double strand breaks which result in the deletion of the intermediate region. The PX458 plasmid additionally encodes for a Cas9-GFP transcript which is cleaved by a self-cleaving T2A peptide. As Cas9 is flanked by nuclear localization sequences, the enzyme localizes to the nucleus whereas GFP remains in the cytoplasm allowing the determination of transfection efficiency.
In a next step, nucleotide sequences encoding two variants of the model antigen OVA were either transduced into the parental B16F10 cell line or into the IA^b KO clone (M2KO) (section 3.1.2). The first variant represents the full length sequence of OVA (OVA-F), whereas the second variant lacks the annotated signal peptide (amino acids 22-48 [315]) and is retained within the cytosol (OVA-T). The different OVA variants (either secreted or not) allow us to clarify whether induced changes in macrophage polarization upon adoptive $CD4^+$ T cell transfer are dependent on secretion of the tumor-associated antigen or not. As outlined in Figure 3.1, OVA transduced cells were characterized by quantification of OVA expression/secretion, MHC surface expression, susceptibility to $CD8^+$ T cell recognition and efficient tumor growth in C57BL/6 mice.
Finally, the OVA expressing clones (B16F10/OVA-F, B16F10/OVA-T, M2KO/OVA-F and M2KO/OVA-T) were transduced with retroviral particles encoding Red Firefly Luciferase (section 3.1.3). After expansion, luciferase expression levels of individual clones were analyzed and used to establish the *in vivo* bioluminescence imaging protocol. The luciferase expressing clones B16F10/OVA-F/Luci, B16F10/OVA-T/Luci, M2KO/OVA-F/Luci and M2KO/OVA-T/Luci can be used for subsequent *in vivo* experiments, in which the effect of adoptively transferred $CD4^+$ and/or $CD8^+$ T cells on tumor outgrowth is analyzed. The whole process of generating OVA and luciferase expressing B16F10 cells deficient in MHC II expression is illustrated in Figure 3.1. The designations of clones finally selected are given in brackets.

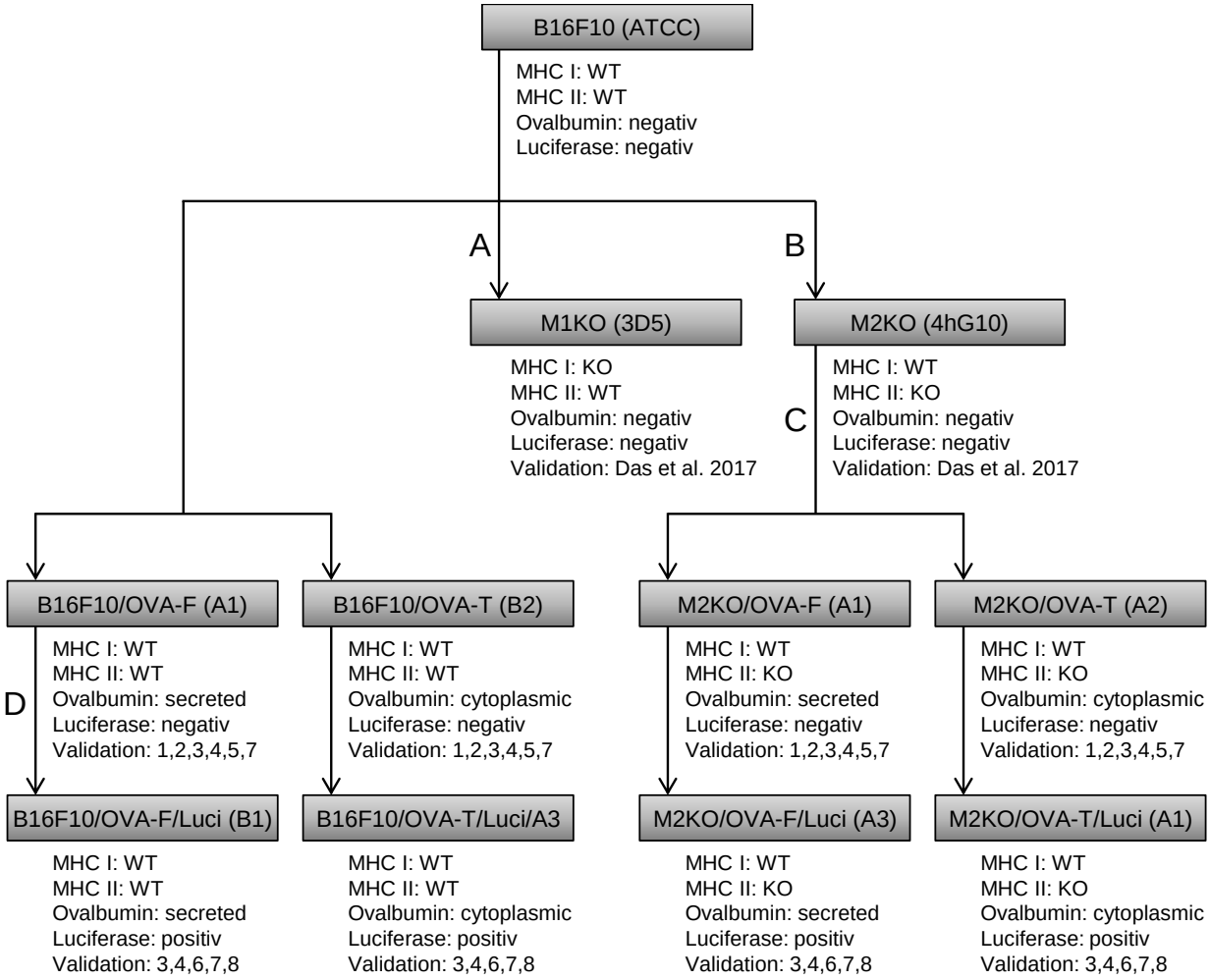

A. MHC I knock out using a β2m-specific single guide RNA
B. MHC II knock out using a single guide RNA specific for the β-chain encoding locus of the IA^b molecule
C. Transduction using lentiviral particles (rwpLX305-Ovalbumin-IRES-Neo)
D. Transduction using retroviral particles (rwpBABE-Puro-Red Firefly Luciferase)

Validation legend:

1. Ovalbumin expression level (qPCR and WB; Figure 3.6)
2. Ovalbumin secretion (WB; Figure 3.10)
3. MHC expression profile (FC; Figure 3.9)
4. Recognition by OVA spec. $CD8^+$ T cells (ELISpot; Figure 3.7 and Figure 3.12)
5. *In vitro* growth curve (xCELLigence; Figure 3.8)
6. Luciferase expression level (LA; Figure 3.12)
7. Tumor growth curve (Figure 3.11 and Figure 3.13)
8. Luciferase expression kinetic *in vivo* (IVIS; Figure 3.13)

Figure 3.1: Workflow for the generation of OVA and luciferase expressing B16F10 clones deficient in MHC II expression.
The corresponding clone names are enclosed in brackets.

3.1.1 Establishment of B16F10 cells deficient in MHC II expression

3.1.1.1 Transfection optimization of B16F10 cells

The first step in generating MHC II KO B16F10 cells was to transfect the tumor cell line with a guide RNA and Cas9 encoding plasmid. In order to guarantee optimal plasmid transfection efficiency in B16F10 cells, the cells were transfected with guide #1 or PX458 backbone using different amounts of DNA as well as different DNA:Enhancer (µg:µl) and DNA:Effectene (µg:µl) ratios (Figure 3.2 A).

A

Reaction	1	2	3	4	5	6	7	8	9	10	11	12	13	14
DNA [µg]	0.4	0.4	0.4	0.2	0.2	0.2	0.6	0.8	0.8	0.4	0.2	0.8	mock	untr.
DNA:Enhancer	1:8	1:8	1:8	1:8	1:8	1:8	1:8	1:8	1:8	1:8	1:8	1:8		
DNA:Effectene	1:25	1:50	1:10	1:25	1:50	1:10	1:25	1:50	1:10	1:25	1:25	1:25		
Effectene:Volume	1:231	1:116	1:577	1:461	1:231	1:1152	1:155	1:59	1:290	1:231	1:461	1:116	1:116	
	guide #1									PX458 backbone			w/o DNA	

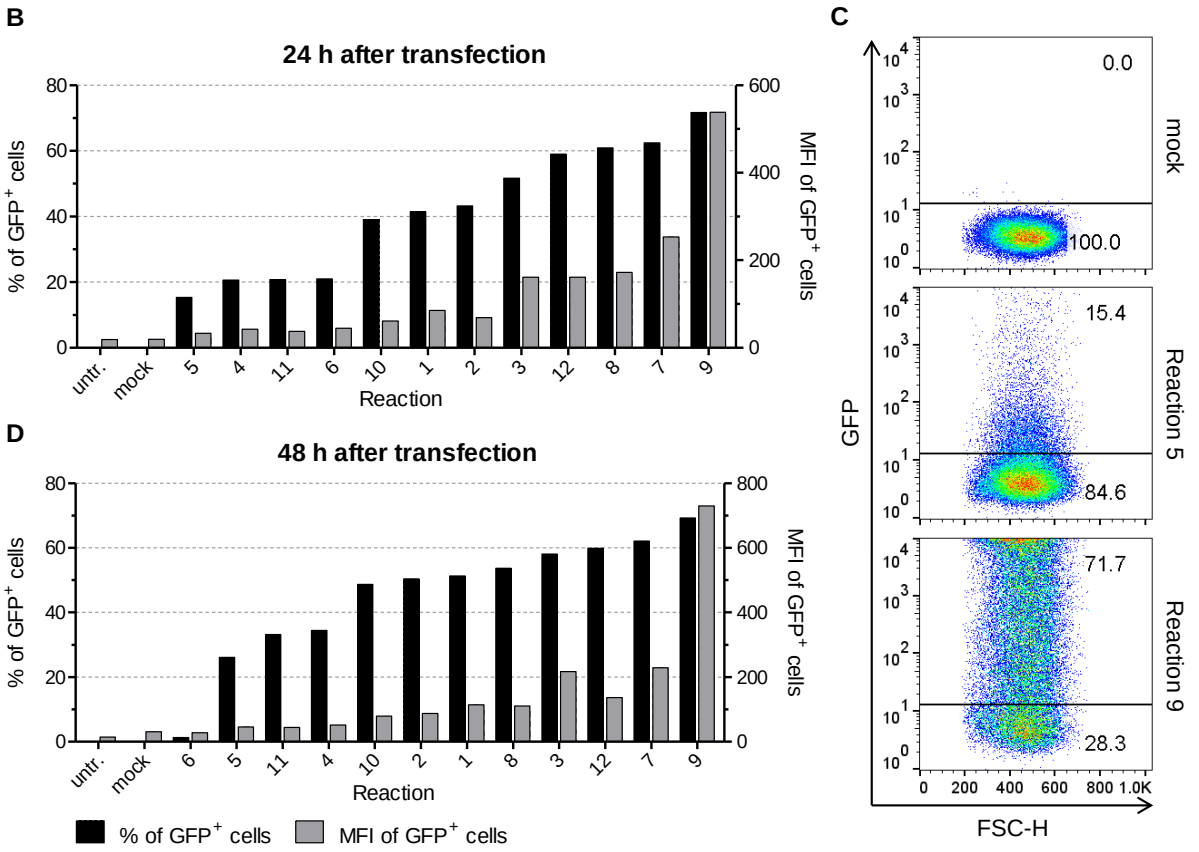

Figure 3.2: Optimization of the transfection protocol for B16F10 cells using Effectene transfection reagent.
One day after seeding 2 x 10^5 B16F10 cells into 6-Well plates, the cells were transfected either with guide #1 (approach 1-9) or the empty PX458 plasmid (approach 10-12) using different amounts of DNA and transfection reagent. **(A)** Table displaying all tested transfection conditions. **(B)** Cells were harvested 24 h after transfection and analyzed by flow cytometry. The bar graph shows the percentage of GFP^+ cells (left y-axis) as well as the median fluorescence intensity values of GFP^+ cells (right y-axis). **(C)** Representative dot plots of the mock control as well as of Reaction 5 and 9 24 h after transfection. **(D)** Analysis of B16F10 cells 48 h after transfection. Gating strategy: FSC-A vs. SSC-H → GFP vs. FSC-H.

Transfection of the plasmids yielded between 15.4 % and 71.7 % GFP positive cells, as determined by flow cytometry 24 h post transfection (Figure 3.2 B and C). The highest percentage of transfected cells was detected in reaction 9, in which 0.8 µg of DNA and a DNA:Effectene ratio of 1:10 was used. Cell viability was assessed 24 h after transfection using the CASY cell counting technology. The overall viability was high (between 72.4 % and 87.8 %) with the exception of cells transfected using reaction 8 (data not shown). These cells showed a viability of only 61.2 % which was probably due to the large volume of transfection reagent used (40 µl). Two days after transfection the ranking of the different reactions according to the percentage of GFP^+ cells changed only slightly (Figure 3.2 D). Based on those results, the conditions tested in reaction 9 were used for all subsequent experiments.

3.1.1.2 Determination of guide RNA knock out efficiencies

In a next step, the guide RNA knock out efficiencies were determined. Therefore, B16F10 cells were transfected with the different guide RNA constructs using the optimized transfection protocol (see section 3.1.1.1). Two days after transfection, parts of the bulk cultures were analyzed by flow cytometry to determine transfection efficiencies. As expected, the percentages of GFP^+ cells among the different constructs appeared similar ranging from 46.8 % to 62.4 % (Figure 3.3 A). However, big differences in the median fluorescence intensities were detected, being lowest in cells transfected with PX458 backbone (MFI: 137) and highest after transfection with a combination of guide #1d and #2u (MFI: 373). The remaining cells were expanded for 7 days and treated with IFNγ for 72 h, to induce IA^b surface expression. As shown in Figure 3.3 B, the percentage of IA^b negative B16F10 cells increased upon transfection with one of the single guide RNAs compared to PX458 backbone transfected cells. In contrast, no differences in IA^b expression were observed when combinations of guide RNAs were transfected (e.g. 1d + 1u). The analysis revealed that transfection of guide #4 resulted in the most prominent subpopulation of IA^b negative cells (51.4 %) compared to 29.6 % IA^b negative cells in PX458 backbone transfected cells (Figure 3.3 C). Based on the transfection efficiencies and the percentages of IA^b negative cells, the knock out efficiencies of the different guide RNA constructs were calculated, revealing the guide #4 containing construct as the most effective one (Figure 3.3 D).

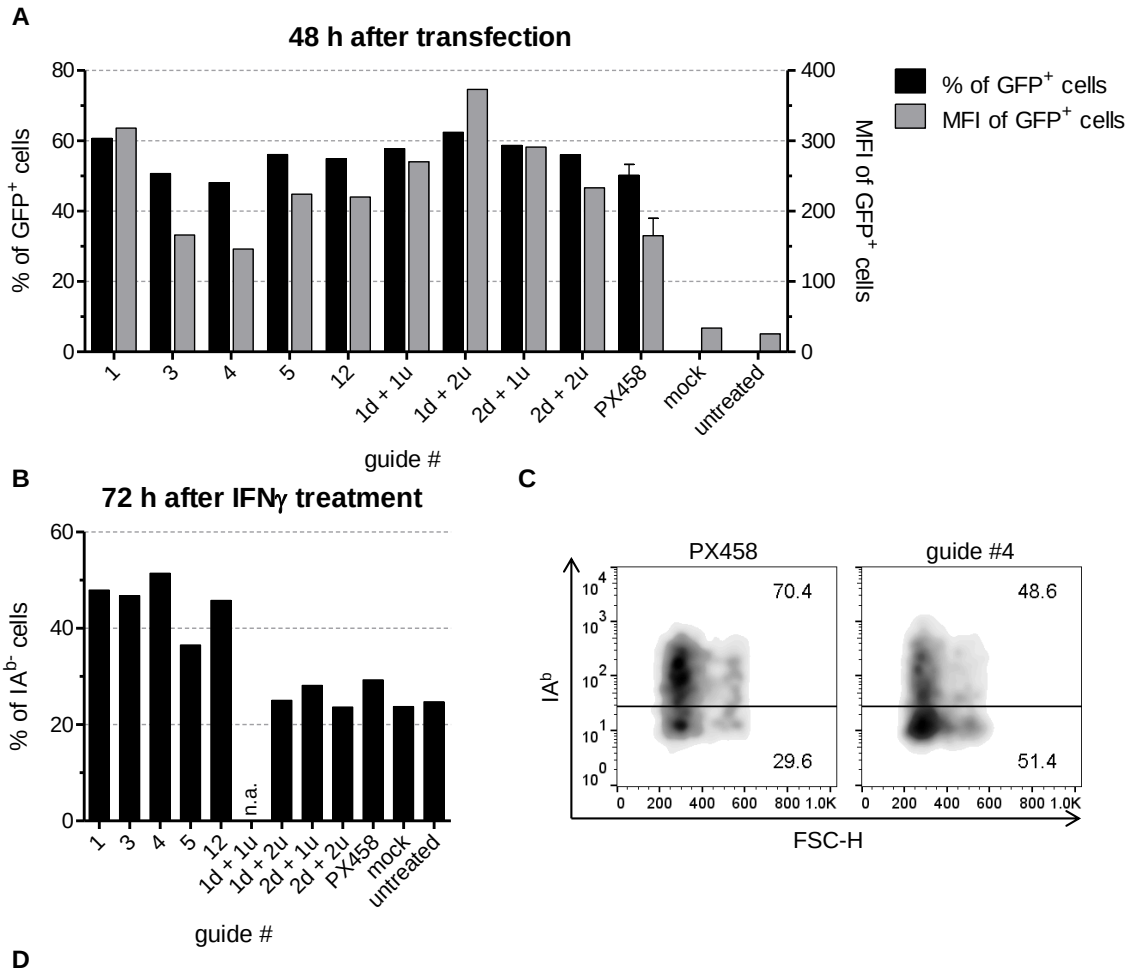

D

Guide #	Transfection efficiency [%]	% of IA^{b-} cells	% of IA^{b-} cells minus background	% of CRISPR/Cas efficiency
1	59.6	47.9	18.65	31.3
3	49.9	46.8	17.55	35.2
4	48.6	51.4	22.15	45.6
5	55.1	36.5	7.25	13.2
12	55.1	45.8	16.55	30.0
1d + 1u	56.2	n.a.	n.a.	n.a.
1d + 2u	61	25	0	0.0
2d + 1u	57.2	28.1	0	0.0
2d + 2u	54.7	23.6	0	0.0
PX458	48.95	29.25	0	0.0
mock	0.05	23.7	0	0.0
untreated	0.026	24.7	0	0.0

n.a. = not available

Figure 3.3: Different guide RNA constructs have different knock out efficiencies.
B16F10 cells (2 x 10^5 cells/well) were transfected with all available guide RNA constructs using the optimized transfection protocol (Reaction 9). In case of double transfection with two guide RNA constructs, 0.5 µg of each plasmid was used. **(A)** Cells were harvested 48 h after transfection with the annotated guide RNA and analyzed by flow cytometry. The bar graph shows the percentage of GFP^+ cells (left y-axis) as well as the median fluorescence intensity values of GFP^+ cells (right y-axis). Gating strategy: FSC-A vs. SSC-H → GFP^+ vs. FSC-H. **(B)** The cells were expanded and 7 days post transfection treated with 20 U/ml IFNγ for 72 h. The percentage of IA^{b-} cells was determined after staining with IA^b specific monoclonal antibody. **(C)** Density plots of B16F10 cells transfected either with guide #4 or empty PX458 plasmid and subsequently treated with IFNγ for 72 h. Gating strategy: FSC-A vs. SSC-H → living cells → IA^b vs. FSC-H. **(D)** Table displaying calculated guide RNA construct knock out efficiencies. The percentage of IA^{b-} cells in PX458 transfected cells was considered as background and subtracted from the other values.

3.1.1.3 Generation of a stable MHC II negative B16F10 clone

Parts of the following paragraph have been taken from reference [307] and were originally written by myself.

For the generation of a stable IA^b negative clone, B16F10 cells were transfected with the two guide RNA constructs which resulted in the highest percentage of IA^b negative cells (guide #1 and #4). The GFP expressing transfectants were isolated by FACS and further expanded *in vitro* (Figure 3.4 A). After 9 days, the cells were treated with IFNγ to stimulate IA^b surface expression, thus creating most stringent conditions for subsequent selection of IA^b KO clones. Indeed, flow cytometry analysis revealed that transfection of guide #1 resulted in a subpopulation of 25.3 % IA^b negative cells, whereas the proportion of IA^b negative cells induced with guide #4 was 32.8 % (Figure 3.4 B). In contrast, no IA^b negative population was observed within parental B16F10 cells treated with IFNγ. Upon single cell sorting, 24 individual clones were established from the IA^b negative subpopulations of the transfected bulk cultures, resulting in 23 clones with stable loss of IA^b surface expression (supplementary Figure 6.2). Finally, clone #4G10 was selected, from now on termed M2KO, and expanded for subsequent experiments. Flow cytometry analysis confirmed lack of IA^b surface expression on IFNγ treated M2KO cells, in contrast to parental B16F10 cells that upregulated IA^b expression upon IFNγ treatment (Figure 3.4 C).

In order to confirm, that the stable IA^b KO clone had lost susceptibility to $CD4^+$ T cell recognition, IFNγ ELISpot assays with an OT-II derived $CD4^+$ T cell line were performed (expanded with CD3/CD28 Dynabeads as explained in section 2.2.12.3). As expected, IFNγ treated parental B16F10 cells, but not M2KO cells loaded with the IA^b restricted $OVA_{323-339}$ peptide were recognized by OVA specific $CD4^+$ T cells (Figure 3.5 A). These results show that M2KO cells had lost both, surface expression of IA^b and susceptibility to $CD4^+$ T cell recognition, even when cell had been treated with IFNγ concentrations that induce MHC II expression on parental cells.

Next, tumorigenic capacity of the established IA^b knockout clone was tested in C57BL/6 mice. After s.c. injection into syngeneic C57BL/6 mice, parental B16F10 cells and M2KO transfectants showed almost superimposing tumor growth curves, reaching a tumor size of approximately 135 mm^2 within 15 days (Figure 3.5 B). As the absence of MHC II on the surface of M2KO cells did not alter their tumor growth behavior *in vivo,* these cells resemble a suitable tool for additional modifications (integration of OVA and luciferase) and subsequent *in vivo* experiments.

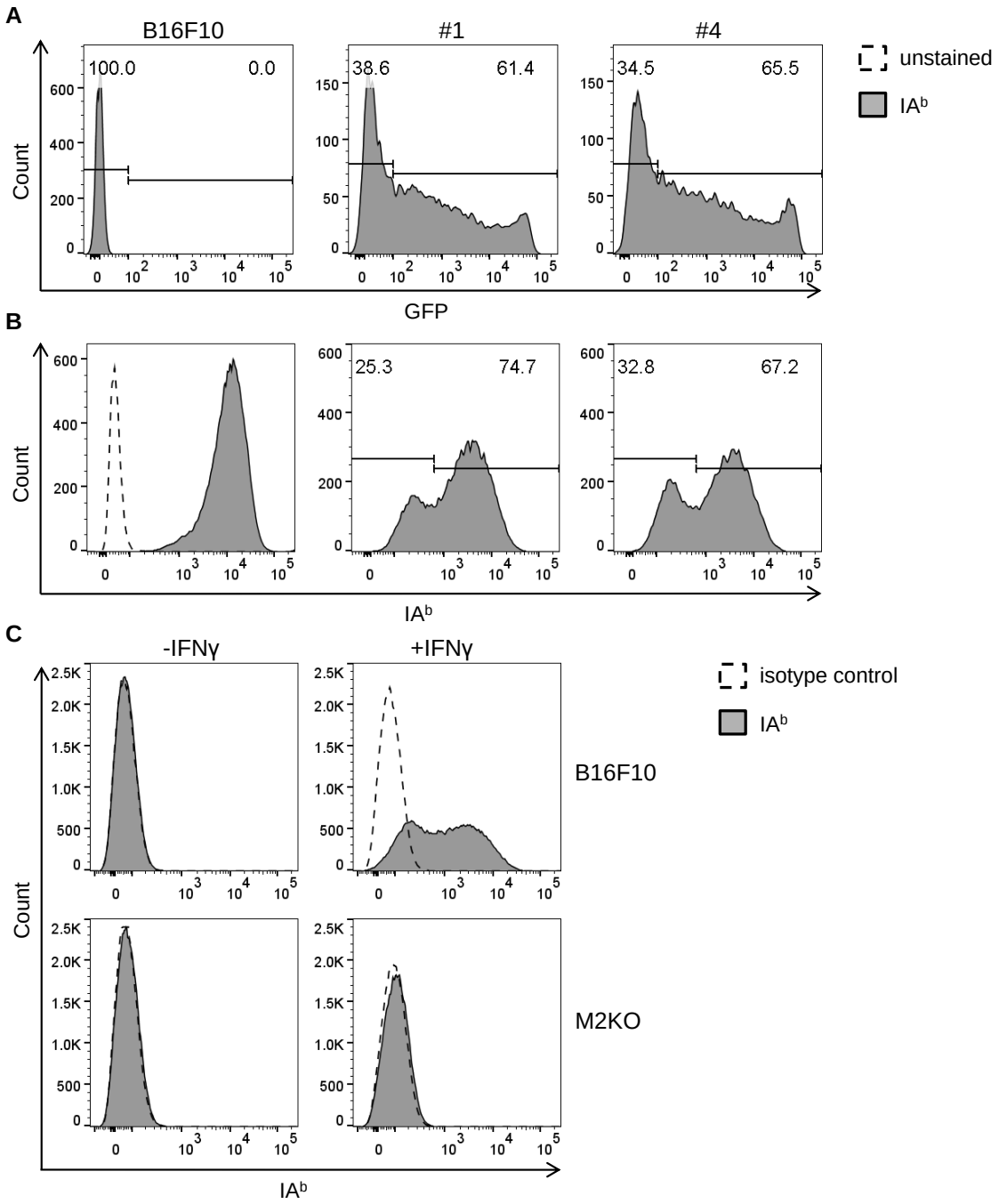

Figure 3.4: Transfection of B16F10 cells with guide #4 encoding constructs results in generation of a stable B16F10 IA^b KO clone.
(A) B16F10 cells were transfected with guide #1 or guide #4 encoding constructs. Two days later, GFP$^+$ cells were sorted and expanded. Gating strategy: FSC-A vs. SSC-H → GFP$^+$ vs. FSC-H. **(B)** Sorted bulk cultures were treated with IFNγ (20 U/ml) 9 days post transfection, followed by surface staining with IA^b specific monoclonal antibody. **(C)** Immunofluorescence staining confirmed complete loss of IA^b surface expression on the selected B16F10 KO clone (M2KO), even when treated with IFNγ. Gating strategy: FSC-A vs. SSC-H → living cells → IA^b vs. FSC-H.

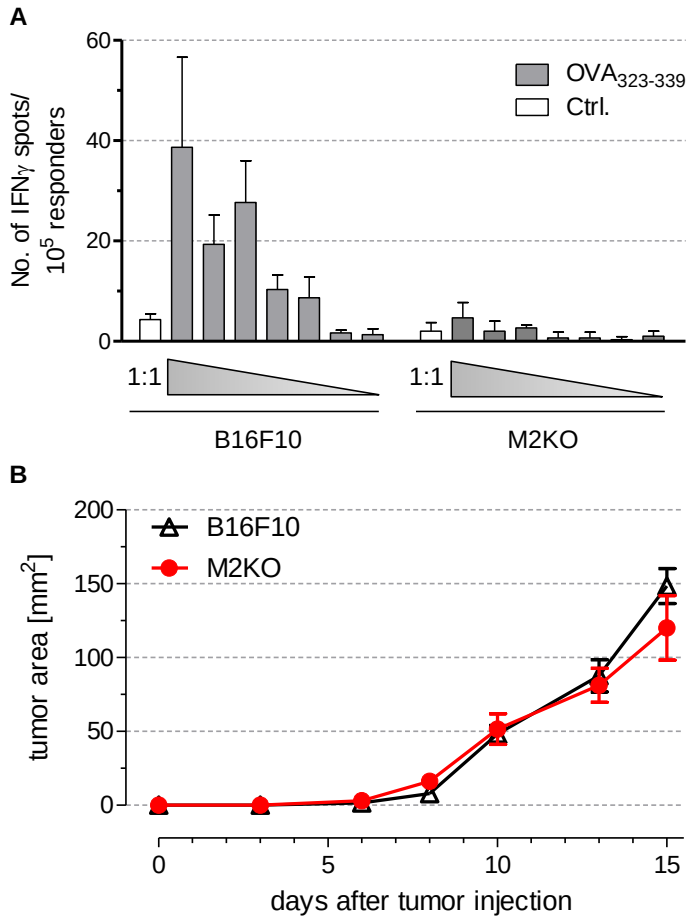

Figure 3.5: Stable IA^b KO clone loses susceptibility to cognate CD4$^+$ T cell recognition and gives rise to tumors in C57BL/6 mice.
(A) Peptide loaded B16F10 cells but not M2KO cells were recognized by OVA-specific CD4$^+$ T cells. Target cells were treated with IFNγ (20 U/ml) prior to the assay to upregulate IA^b expression. Empty bars (Ctrl.) represent the recognition of target cells loaded with IA^b restricted HBV core antigen control peptide 128-140 (TPPAYRPPNAPIL). Error bars represent standard deviation (SD) of technical triplicates. **(B)** C57BL/6 mice (n = 10) were injected s.c. with the parental B16F10 cells or the stable IA^b KO clone (2 x 10^5) and tumor growth was monitored every 2-4 days. Error bars represent standard error of the mean (SEM) within each animal collective.

3.1.1.4 Analysis of CRISPR/Cas9 induced mutations in M2KO cells

Parts of the following paragraph have been taken from reference [307] and were originally written by myself.

Finally, we analyzed the CRISPR/Cas9 induced mutations within IA^b KO clone M2KO. Therefore, the Cas9 target region within exon 1 of the IA beta chain gene was amplified by PCR and the resulting PCR products were cloned into TOPO vectors. After transformation of these vectors into One Shot competent TOP10 bacteria and subsequent plasmid isolation, the plasmids were sequenced as described in section 2.2.7. As shown in Table 3.1, all plasmids isolated from a total of 26 bacterial colonies showed the same 11 bp deletion, occurring at the vicinity of the putative Cas9 cutting site (highlighted in green) which is located 3 base pairs upstream of the PAM sequence (highlighted in blue). The deletion caused a frameshift in exon 1, thereby generating a stop codon resulting in a truncated protein. In contrast, no sequence changes were observed within the exon 1 of the IA beta chain gene in the parental B16F10 cell line as compared to the wild type C57BL/6 genome.

Table 3.1: guide RNA sequence and sequence analysis of the mutated M2KO clone

Cell line	Bacterial colony	Sequence
B16F10	30	5'-GGAGACTCCGAAAGTAAG|TGCCGGGGGCAGGGC-3'
M2KO	1	5'-GGAGACTCCGA-------|------GGGGGCAGGGC-3'
	2	5'-GGAGACTCCGA-------|------GGGGGCAGGGC-3'
	3	5'-GGAGACTCCGA-------|------GGGGGCAGGGC-3'
	6	5'-GGAGACTCCGA-------|------GGGGGCAGGGC-3'
	10	5'-GGAGACTCCGA-------|------GGGGGCAGGGC-3'
	18	5'-GGAGACTCCGA-------|------GGGGGCAGGGC-3'
	23	5'-GGAGACTCCGA-------|------GGGGGCAGGGC-3'
	25	5'-GGAGACTCCGA-------|------GGGGGCAGGGC-3'
	26	5'-GGAGACTCCGA-------|------GGGGGCAGGGC-3'
-	guide RNA	5'-~GAGACTCCGAAAGTAAGTGC-3'

3.1.2 Establishment of ovalbumin expressing B16F10 derived clones

3.1.2.1 Transduced B16F10 clones express OVA on RNA and protein level

B16F10 and M2KO cells were transduced with either the native, full length version of OVA (OVA-F) or a truncated version of OVA (OVA-T), lacking the first 150 bp including the signal peptide. The transduced bulk cultures were selected with 1 mg/ml Geneticin, which was found to be the minimal concentration lethal to 100 % of untransduced B16F10 cells. After 7 days of culture, genomic DNA of the bulk cultures was isolated and the stable integration of the introduced OVA sequences was confirmed by PCR using two different primer pairs. One primer pair includes the amplification of the signal peptide and was therefore specifically amplifying OVA-F, whereas the second primer pair binds downstream of the signal peptide, thereby amplifying both, OVA-F as well as OVA-T. By using these primer pairs it was possible to distinguish between the two different OVA sequences and to prove that in each bulk culture the correct OVA version was integrated (supplementary Figure 6.3). After two weeks of culture, clones were picked and expanded. The expression of OVA-F on protein level in both, B16F10 and M2KO clones, was confirmed by Western blot analysis as shown in Figure 3.6 A and B. The full length OVA was detected at the expected molecular weight of 42.8 kDa in all OVA-F transfectant clones, except for M2KO/OVA-F clone B2. In contrast, no such band was detected in parental B16F10 or M2KO cells which served as negative controls (-). Quantification of the detected OVA-F signals revealed that B16F10/OVA-F clone A1 and C2 as well as M2KO/OVA-F clone A1 and C2 possessed the highest levels of OVA protein (Figure 3.6 B) which correlated well with OVA RNA expression results obtained by qPCR (Figure 3.6 C). In contrast to full length OVA, OVA-T could not be detected on protein level (molecular weight: 37.6 kDa) even though the used antibody is specific for an epitope outside the signal sequence (data not shown). However, qPCR analysis showed that in all clones, except for B16F10/OVA-T clone A2, the truncated OVA variant was expressed on RNA level. Notably, even though B16F10/OVA-T clone C2 possessed a higher OVA expression on RNA level than all B16F10/OVA-F clones, the truncated version was still not detected on protein level. These results indicate a rapid turnover of the truncated OVA protein due to the lacking signal peptide.

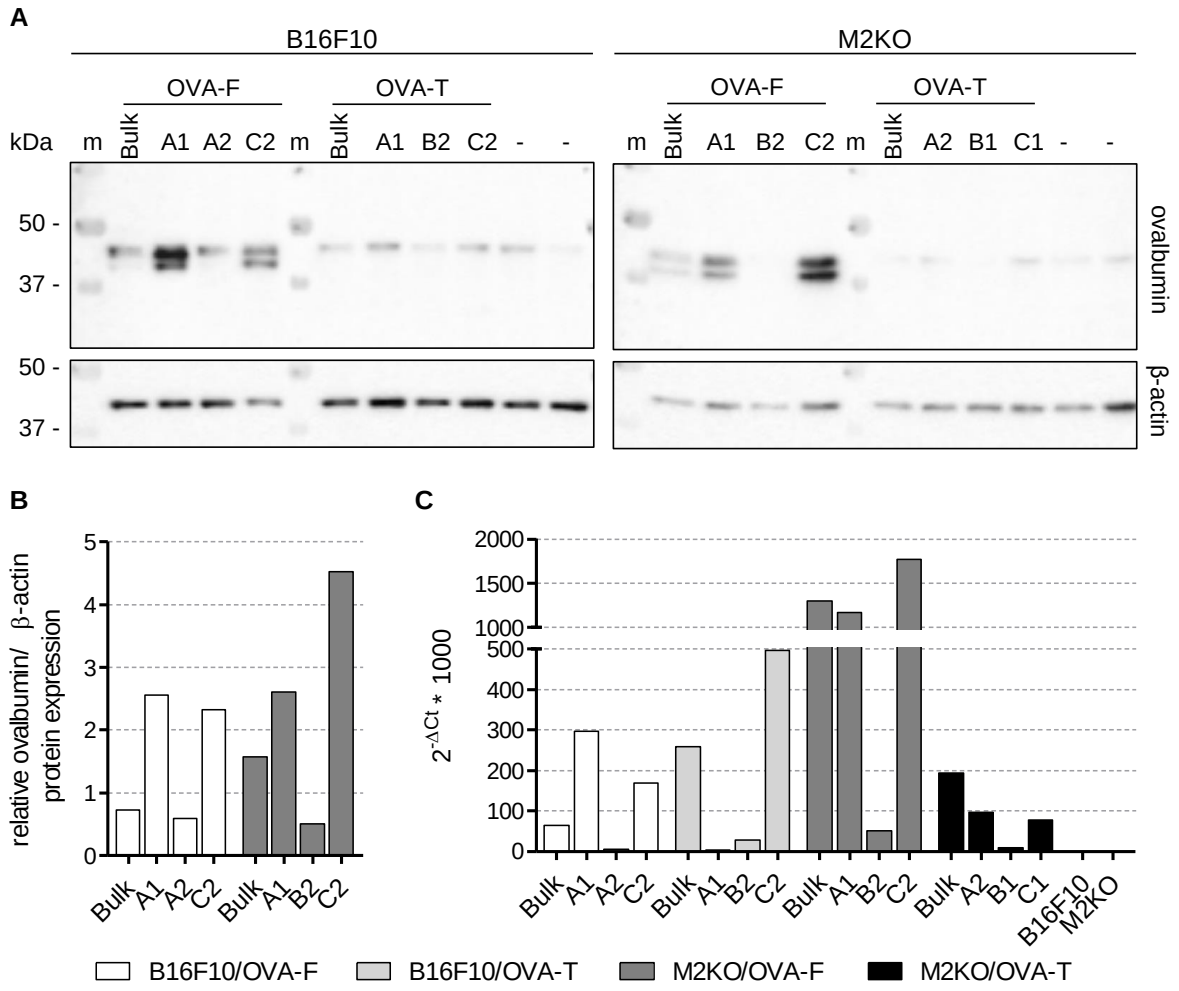

Figure 3.6: Transduced B16F10 derived clones express OVA on RNA and protein level.
(A) Expression of OVA in transduced B16F10 and M2KO cells was validated by Western blot. The full length version (42.8 kDa), but not the truncated version of OVA (37.6 kDa) is detected. As negative controls (-), whole cell protein samples of the parental cell lines were loaded (left: B16F10, right: M2KO). **(B)** Quantification of Western blot results. **(C)** Quantitative real-time PCR confirmed OVA expression on RNA level in all clones tested.

3.1.2.2 Transduced B16F10 clones are recognized by OVA specific CTLs

In order to investigate whether the truncated version of OVA is processed resulting in epitope presentation by MHC molecules, despite the assumed rapid degradation of the protein, an IFNγ ELISpot assay was performed. Therefore, the OVA expressing B16F10 derived clones were co-cultured with OVA specific CTLs for 16 h and the number of IFNγ spots was determined. As shown in Figure 3.7, all the transduced clones were susceptible to OVA specific CTL recognition, regardless of whether these clones expressed OVA-F or OVA-T. These results demonstrate that the truncated OVA RNA was not only successfully translated into protein, but also that the protein can be processed, thereby generating CTL epitopes that can be presented by MHC molecules on the cell surface. Both steps, the synthesis of the truncated protein as well as the presentation of OVA derived epitopes on MHC molecules, are essential for using these clones in subsequent *in vivo* experiments.
Based on the ELISpot results, four clones showing equal susceptibility to OVA specific CTL recognition, namely B16F10/OVA-F clone A1, B16F10/OVA-T clone B2, M2KO/OVA-F clone A1 and M2KO/OVA-T clone A2 were selected for subsequent experiments. For reasons of

clarity, the clone specifications in the clone designations are omitted from now on and can be looked up in Figure 3.1.

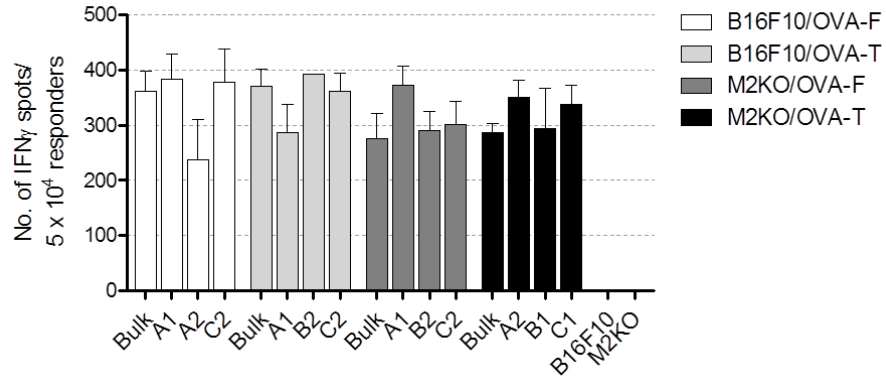

Figure 3.7: Transduced B16F10 derived clones are susceptible to OVA specific CTL recognition.
OVA transduced B16F10 derived clones (5 x 10^4) were incubated over night with 10^3 OVA specific CTLs. All transduced clones were susceptible to T cell recognition as measured by IFNγ ELISpot assay, whereas the parental B16F10 and M2KO cells were not recognized by CTLs. Error bars represent SD of technical triplicates.

3.1.2.3 *In vitro* proliferation and MHC expression of OVA expressing clones

Within the next set of experiments, the proliferative capacity *in vitro* as well as the MHC expression profile of the selected clones was characterized. In order to assess cell proliferation, the cells were seeded into a 96-Well plate and monitored over the course of eight days using the xCELLigence system. As shown in Figure 3.8 A, OVA transduced clones showed slower growth compared to the corresponding parental cell lines. However, the four clones that were finally selected showed similar proliferation capacity (Figure 3.8 B). Interestingly, the viability of B16F10 derived clones (green lines) drops one day earlier compared to the viability of M2KO derived clones (blue lines), suggesting that M2KO might be more resistant to nutrient deprivation.

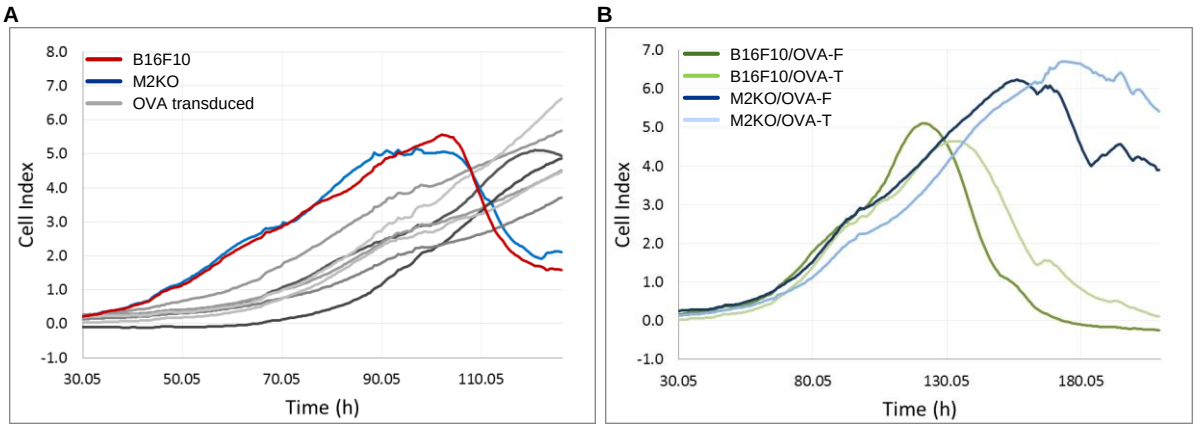

Figure 3.8: *In vitro* proliferation of B16F10 and M2KO OVA derived clones.
(A) The OVA transduced clones as well as their parental cell lines were seeded into a 96-Well F-bottom plate (2 x 10^3 cells/well) and proliferation was monitored using the xCELLigence system. All transduced clones (grey) show a decreased proliferation capacity compared to the corresponding parental cell lines (blue and red). **(B)** Growth curve comparison of clones finally selected.

The MHC expression profile of the selected clones was analyzed by immunofluorescence staining using H2-K^b, H2-D^b, and IA^b specific monoclonal antibodies. To make sure that M2KO derived clones still lack the MHC II molecule IA^b, the cells were treated for 48 h with 20 U/ml IFNγ in order to induce possible MHC expression. As an additional proof of successful OVA processing and MHC restricted epitope presentation (besides the ELISpot results shown in Figure 3.7), the clones were stained using a H2-K^b SIINFEKL specific monoclonal antibody. As shown in Figure 3.9, MHC expression on cells without IFNγ pre-treatment (solid line histograms) is almost absent (percentages of positive cells range between 0.2 and 0.5 %). In contrast, cells cultured in the presence of IFNγ for two days (dashed line histograms) highly upregulate MHC I as well as MHC II expression. Most importantly, IA^b expression was not detected on the cell surface of M2KO derived, OVA expressing clones even after IFNγ treatment. As expected, OVA transduced clones upregulated H2-K^b SIINFEKL expression to certain extent after IFNγ stimulation, whereas the parental B16F10 and M2KO cells did not show any H2-K^b SIINFEKL molecules on their surface.

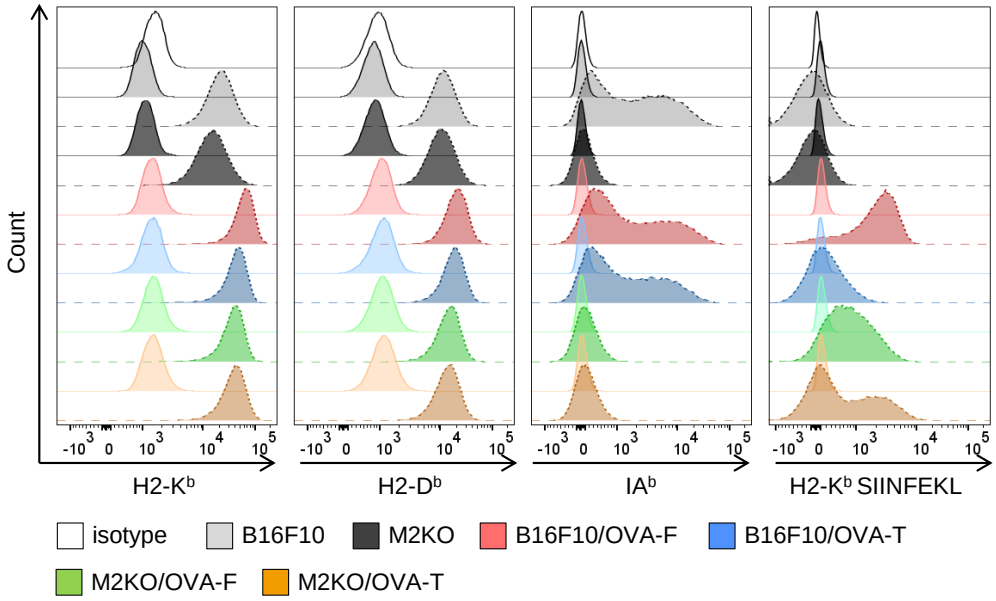

Figure 3.9: MHC expression profiles of B16F10 and M2KO OVA transduced clones.
The OVA expressing clones were treated with 20 U/ml IFNγ for 48 h (dashed line histograms) or left untreated (solid line histograms) and subsequently stained with H2-K^b, H2-D^b, IA^b and H2-K^b SIINFEKL specific monoclonal antibodies. Analysis was performed on living, single cells. The clones show a strong upregulation of H2-K^b SIINFEKL expression when treated with IFNγ. In contrast, the parental cells lack the MHC class I restricted presentation of the OVA derived SIINFEKL peptide.

3.1.2.4 The truncated version of OVA is not secreted

The clones expressing OVA-T were shown to present OVA derived SIINFEKL peptide (section 3.1.2.3) and to be susceptible to OVA specific CTL recognition (section 3.1.2.2), suggesting that the protein is expressed and processed. However, OVA-T could not be detected in whole cell protein samples, possibly due to proteasomal degradation (section 3.1.2.1). To test this hypothesis the clones were cultured in the presence of 10 µM lactacystin for 13 h in order to block proteasomal activity. After preparing whole cell protein samples, OVA expression was analyzed by Western blot (Figure 3.10 A and B). The inhibition of the proteasome increased the detectable amount of OVA-F and allowed the

detection of the truncated OVA version at 37.6 kDa after extended exposition time, confirming the suggested high turnover of that protein (Figure 3.10, middle panel).
In a next step, the culture supernatants of lactacystin treated, OVA expressing clones were analyzed by Western blot, in order to guarantee intracellular localization of OVA-T and at the same time secretion of OVA-F (Figure 3.10 C). The Western blot results demonstrated a strong OVA-F secretion which was unaffected by proteasome blockade. In contrast, OVA-T was not detectable in the culture supernatants even after lactacystin treatment and 20 min exposure time proving its intracellular localization.

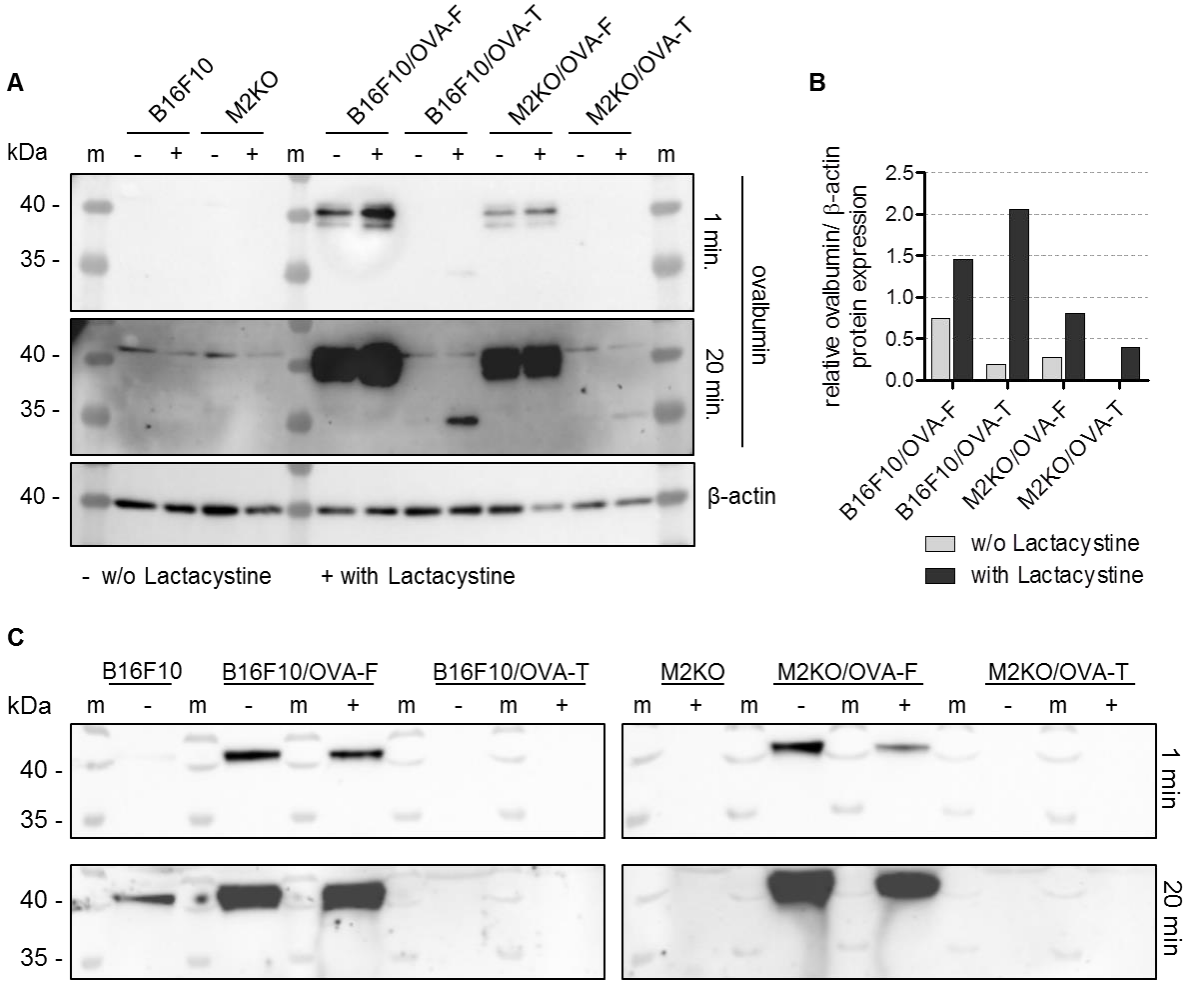

Figure 3.10: The truncated version of OVA is rapidly degraded by the proteasome and not secreted into the culture medium.
The selected OVA transduced clones as well as the parental cell lines were treated with 10 µM Lactacystin for 13 h in order to block proteasomal degradation of the truncated OVA version. OVA expression level in protein lysates (A-B) as well as cell culture supernatants (C) was analyzed by Western blot. **(A-B)** Due to degradation, the truncated version of OVA (37.6 kDa) is only detectable after treatment with lactacystin and an extended exposure time of 20 minutes. **(C)** Analysis of the culture supernatants revealed that OVA-F is secreted and can be detected independently of proteasomal blockade by lactacystin. In contrast, OVA-T is not secreted into the culture medium even after lactacystin treatment and extended exposition time (20 minutes). m = marker.

3.1.2.5 OVA transduced clones give rise to tumors in C57BL/6 mice

In a final step, the OVA transduced clones were s.c. injected into C57BL/6 mice to determine the tumor take rate as well as the individual tumor growth curves. As shown in Figure 3.11,

all clones gave rise to tumors reaching tumor volumes between 1300 (M2KO/OVA-F) and 1800 (B16F10 parental) mm^3 16 days post tumor cell injection. All transduced clones, except for B16F10/OVA-T, showed a delayed tumor growth compared to the parental B16F10 cell line, probably due to the expression of the foreign, immunogenic antigen OVA. Nevertheless, the tumor take rate of all tested clones was 100 % which makes them a useful tool for subsequent *in vivo* experiments.

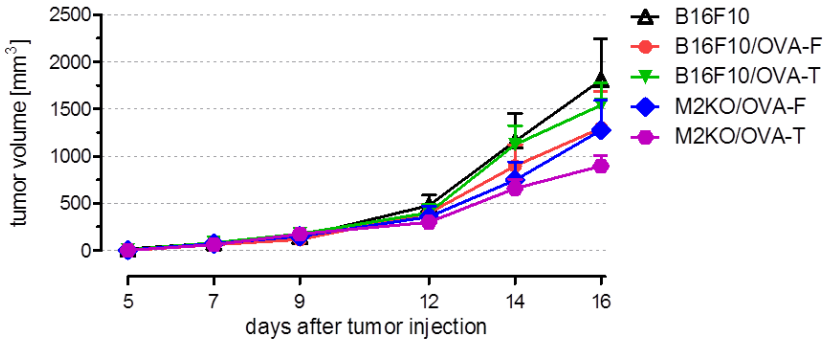

Figure 3.11: Transduced B16F10 and M2KO derived clones give rise to tumors *in vivo*.
C57BL/6 Ly5.1 mice (n = 7) were injected s.c. with B16F10/OVA or M2KO/OVA clones (2 x 10^5) and tumor growth was monitored every 2-3 days. Error bars represent SEM within each animal collective.

3.1.3 Establishment of ovalbumin and luciferase expressing B16F10 clones

3.1.3.1 Luciferase expression of transduced cells *in vitro*

In a final step, B16F10/OVA and M2KO/OVA clones were transduced using luciferase encoding retroviral particles and cultured in selection medium containing 1 µg/ml puromycin. After two weeks, individual clones were picked, expanded and the luciferase expression was analyzed by performing a luciferase assay. As shown in Figure 3.12 A, luciferase expression was detected in all clones (except for B16F10/OVA-F/Luci clone A2) as well as in the bulk cultures, but not in the parental OVA expressing clones B16F10/OVA-F and M2KO/OVA-F. An IFNγ ELISpot assay was performed to select for those luciferase expressing clones which are equally recognized by OVA specific CTLs, thereby allowing a better comparison between the different clones in subsequent *in vivo* experiments. As expected, all clones were susceptible to OVA specific CTL recognition, whereas the parental B16F10 and M2KO cells were not. The clones finally selected for subsequent experiments, are B16F10/OVA-F/Luci clone B1, B16F10/OVA-T/Luci clone A3, M2KO/OVA-F/Luci clone A3 and M2KO/OVA-T/Luci clone A1. For reasons of clarity, the specifications of the original clone designations omitted from now on and can be looked up in Figure 3.1.

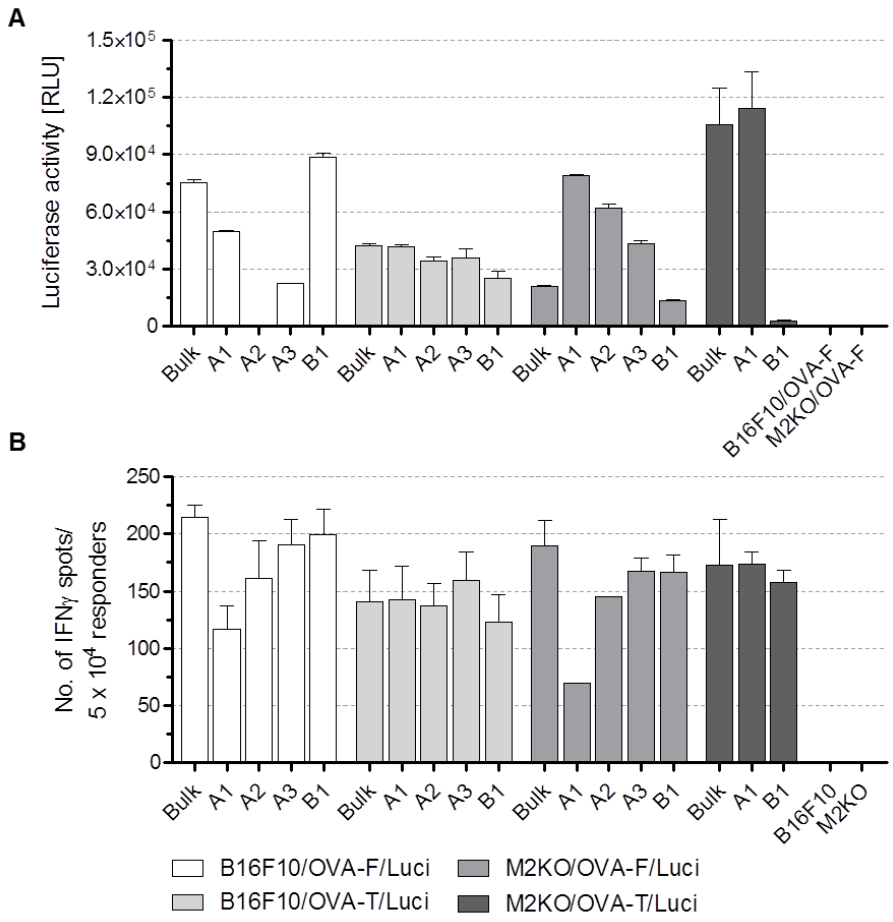

Figure 3.12: B16F10/OVA and M2KO/OVA cells transduced with luciferase encoding retroviral particles express luciferase *in vitro* and are recognized by OVA specific CTLs.
After generation of individual clones from luciferase transduced OVA expressing cells, the luciferase expression level (A) as well as the susceptibility to T cell recognition (B) was determined. **(A)** The cells were cultured in a 96-Well F bottom plate overnight and subsequently lyzed. After 5 minutes of incubation with luciferase substrate the light emission, which is proportional to luciferase activity was measured. **(B)** The clones (5 x 10^4) were co-cultured with 10^3 OVA specific CTLs overnight in order to perform an IFNγ ELISpot assay. Error bars represent SD of technical triplicates.

3.1.3.2 Characterization of luciferase expression kinetics *in vivo*

In a final validation step each of the selected clones were injected s.c. into C57BL/6 mice to determine tumor growth as well as the clone specific kinetics of luciferase expression *in vivo*. As shown in Figure 3.13 A, all clones gave rise to tumors with a tumor take rate of 100 %. However, remarkable differences in tumor growth were detected. Reduced tumor growth of M2KO/OVA-F/Luci, B16F10/OVA-F/Luci and M2KO/OVA-T/Luci were accompanied by higher luciferase expression levels compared to B16F10/OVA-F/Luci.
The individual luciferase expression kinetics in Figure 3.13 B revealed the optimal imaging time for each cell line after D-luciferin injection. The kinetics show a highly variable substrate distribution phase within the first 12-20 minutes after D-luciferin injection, followed by a stable plateau (in between the vertical, dotted lines) and a variable substrate clearance phase. To obtain optimal quantitative results, imaging must occur during the plateau phase which is specific for each clone.

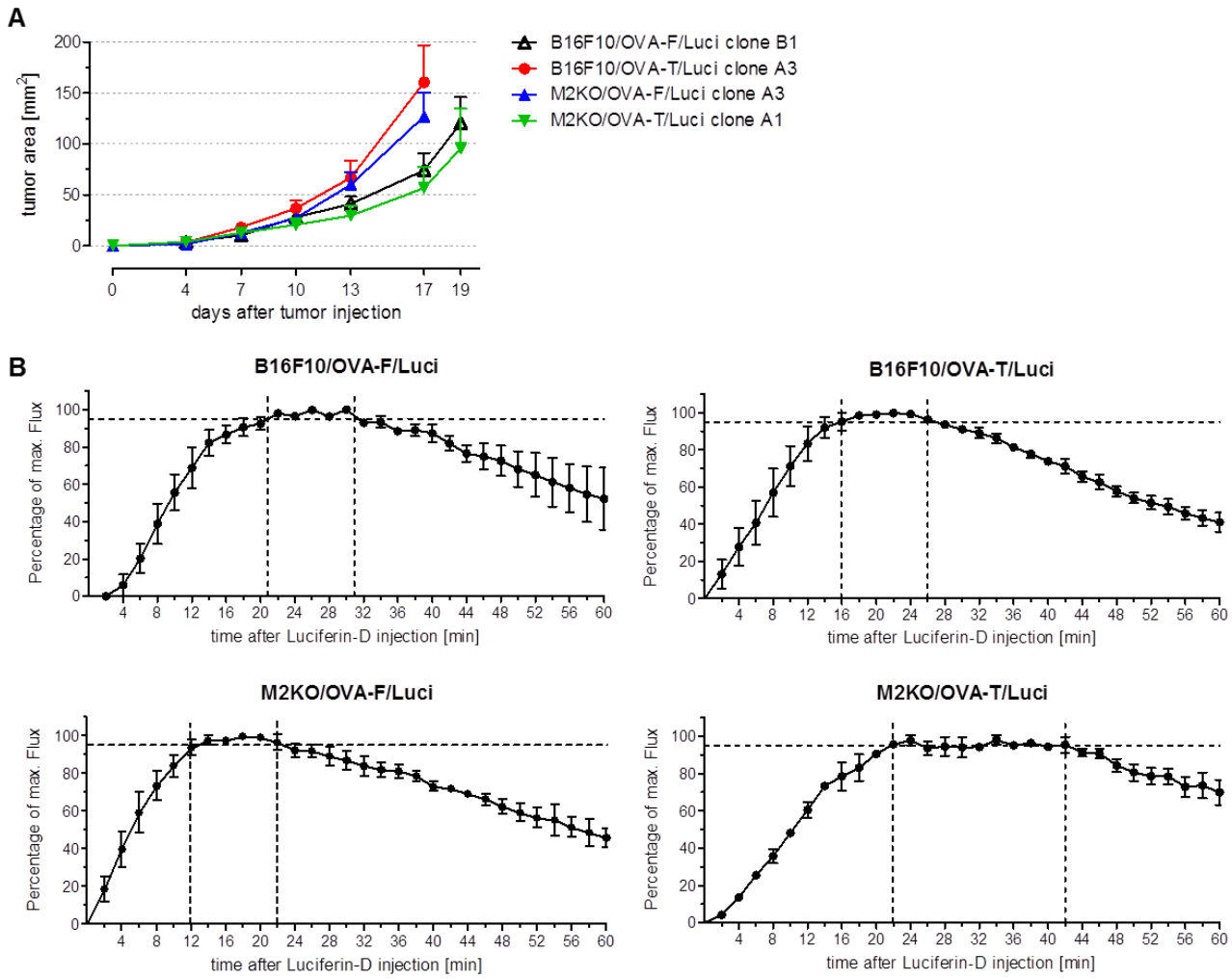

Figure 3.13: B16F10/OVA/Luci and M2KO/OVA/Luci clones form tumors in C57BL/6 mice and show individual luciferase expression kinetics.
(A) C57BL/6 Ly5.1 mice (n = 7-9) were injected s.c. with the finally selected OVA/Luci transduced clones (2 x 10^5) and tumor growth was monitored every 2-4 days. Error bars represent SEM within each animal collective. **(B)** In order to monitor tumor growth by *in vivo* luminescence imaging, it is essential to determine for each clone its individual luciferase expression kinetic. C57BL/6 Ly5.1 (n = 3) were injected s.c. with the luciferase expressing OVA transfectants (2 x 10^5). Thirteen days post tumor cell injection, mice were sedated and injected i.p. with 300 µl D-luciferin (15 mg/ml). Up to 60 minutes post substrate injection, the total Flux (p/s) was measured every two minutes to detect the clone specific luciferase expression plateau (% of max. Flux ≥ 95). Error bars represent SD within each animal collective.

3.2 Generation of an OVA specific $CD4^+$ T cell line

In order to generate an OVA specific $CD4^+$ T cell line that can be used to perform co-culture experiments with macrophages, three different strategies were implemented as already described in detail in section 2.2.12. Briefly, OVA specific $CD4^+$ T cells were generated either through peptide immunization of C57BL/6 mice (C57BL/6 immunized), or by activation of OT-II splenocytes using IA^b restricted peptide (OT-II peptide/feeder) or CD3/CD28 Dynabeads (OT-II CD3/CD28 beads). T cell cultures were restimulated every 4 weeks by the addition of irradiated syngeneic feeder cells together with antigenic peptide.

3.2.1 Peptide immunization results in OVA specific T cell response

C57BL/6 mice were immunized with IA^b restricted OVA specific T cell epitope ($OVA_{329-337}$ or $OVA_{323-339}$) to prime OVA specific $CD4^+$ T cells *in vivo*, followed by T cell expansion *in vitro*. The presence of OVA specific $CD4^+$ T cells was verified by culturing spleen cells of immunized mice in the presence of the respective peptide and measuring the number of IFNγ producing cells using IFNγ ELISpot assay. As shown in Figure 3.14 A, immunization using the core sequence of IA^b restricted epitope ($OVA_{329-337}$ [316]) did not result in T cell activation, even when high peptide concentrations (2 µg/ml) were used in the ELISpot assay. Between 156 and 210 IFNγ spots were detected upon unspecific stimulation of splenocytes using 20 µg/ml ConA, showing that the assay itself worked. In contrast, IFNγ producing, OVA specific $CD4^+$ T cells were detected in 4 out of 5 mice immunized with the complete IA^b restricted epitope ($OVA_{323-339}$) (Figure 3.14 B). The number of IFNγ secreting OVA specific $CD4^+$ T cells was higher in splenocytes of mice sacrificed 13 days compared to 7 days post immunization. Remaining spleen cells, not needed for the ELISpot assay, were cultured in Complete T cell Medium and $OVA_{323-339}$ peptide as described in section 2.2.12.1. After several weeks of culturing, T cells obtained from mice 7 days post immunization turned out to expand best and were compared to OT-II derived $CD4^+$ T cell lines (section 3.2.2).

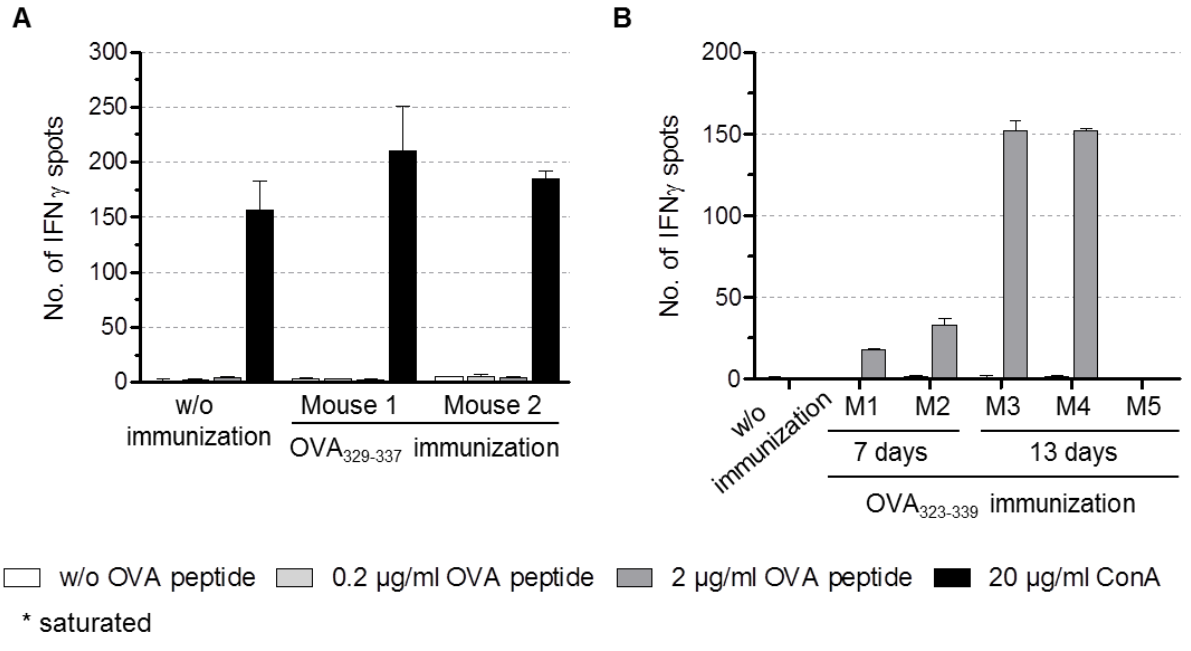

Figure 3.14: Immunization of C57BL/6 mice with IA^b restricted $OVA_{323-339}$ peptide results in OVA specific $CD4^+$ T cell priming.
(A) C57BL/6 were immunized s.c. with 100 µg $OVA_{329-337}$ peptide (AAHAEINEA) diluted in Freund's Adjuvant. Thirteen days post immunization the mice were sacrificed and 1.5 x 10^6 splenocytes were incubated with different OVA peptide concentrations to measure $CD4^+$ T cell activation using IFNγ ELISpot assay. **(B)** C57BL/6 mice were immunized s.c. with 100 µg $OVA_{323-339}$ peptide (ISQAVHAAHAEINEAGR) diluted in Freund's Adjuvant. Mice were sacrificed 7 or 13 days post immunization and 1.5 x 10^6 splenocytes were incubated with 2 µg/ml of the corresponding OVA peptide. OVA specific $CD4^+$ T cell activation was measured using IFNγ ELISpot assay. Error bars represent SEM of technical triplicates.

3.2.2 Testing of specificity and purity of established $CD4^+$ T cell lines

The OVA specific $CD4^+$ T cell line generated from immunized C57BL/6 mice was compared to OT-II derived $CD4^+$ T cell lines (generated as described in section 2.2.12) in terms of epitope specificity and purity. All three cell lines were generated from an individual mouse and restimulated once with irradiated syngeneic feeder cells and antigenic peptide prior to analysis of specificity and purity. The specificity was tested in an IFNγ ELISpot assay using peptide loaded 771 B cell lymphoma cells as targets, as these cells can be easily kept in culture and express high levels of IA^b. As shown in Figure 3.15 A, the maximum number of IFNγ spots detectable with this assay (i.e. > 500 IFNγ spots) was reached when the highest number of T cells (6250) was used. For each lower T cell number tested, the OT-II peptide/feeder cell line showed the highest number of IFNγ secreting cells compared to the other T cell lines. As expected, only a low number of OVA specific $CD4^+$ T cells were activated in the presence of 771 B cell lymphoma cells loaded with HBV core antigen control peptide (HBV) even though the highest T cell number was used, thereby emphasizing their high degree of specificity towards IA^b restricted OVA peptide.

To assess the purity of the OVA specific $CD4^+$ T cell lines, the cells were stained using CD3, CD4 and CD8 specific monoclonal antibodies and analyzed by flow cytometry (Figure 3.15 B, upper panel). The analysis revealed that only 48.6 % of the living, $CD3^+$ OT-II peptide/feeder cells were also stained positive for CD4. The remaining 51.4 % of the living, $CD3^+$ cell population consisted of $CD8^+$ as well as $CD4^-CD8^-$ cells. Similar frequencies were detected for the living, $CD3^+$ OT-II CD3/CD28 beads cells, with the exception that no $CD8^+$ T cells were present (resulting from $CD4^+$ T cell isolation prior CD3/CD28 beads addition). The highest purity was detected for cells derived from the C57BL/6 immunized cell line where all living, $CD3^+$ cells expressed CD4. For better characterization of the established T cell lines, the T cell receptor chain expression was analyzed (Figure 3.15 B, lower panel). As expected, all $CD4^+$ cells of both OT-II derived cell lines expressed the T cell receptor chains Vα2.1 and Vβ5.1, which are known to be the OVA specific transgenic T cell receptors of OT-II mice. In contrast, only a small fraction (0.9 %) of C57BL/6 immunized $CD4^+$ cells expressed both T cell receptor chains. The remaining cells belonged either to the $Vα2.1^+Vβ5.1^-$ (53.7 %) or to the $Vα2.1^-Vβ5.1^-$ (44.9 %) population, showing a high T cell receptor diversity within this $CD4^+$ T cell line.

Since the $CD4^+$ T cell line established by peptide immunization of C57BL/6 mice was the only one consisting of pure $CD4^+$ T cells, this cell line was used for subsequent co-culture experiments with PECs and TAMs.

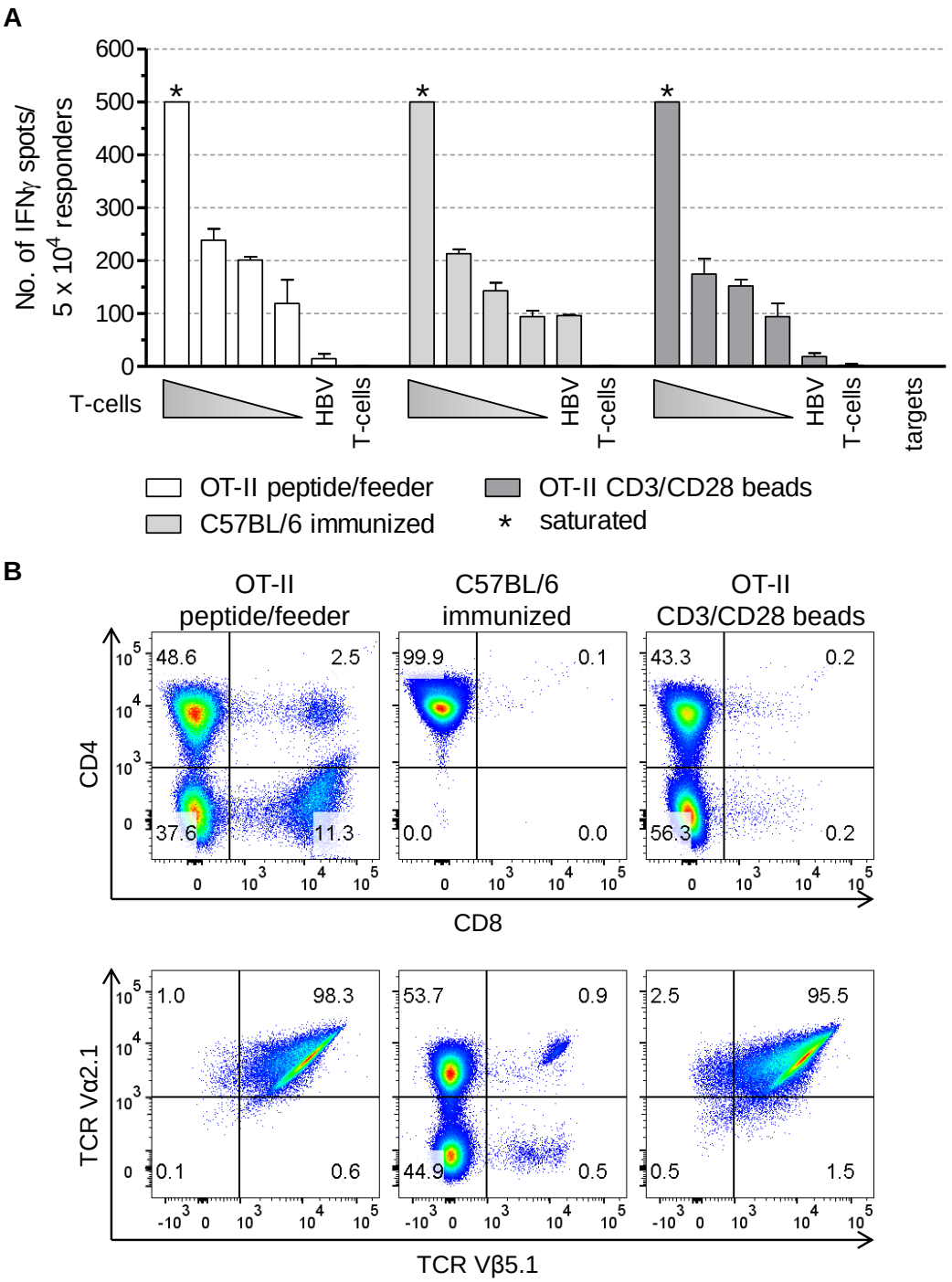

Figure 3.15: Specificity and purity comparison of the different OVA specific CD4$^+$ T cell lines. **(A)** Specificity of the generated T cell lines was tested in an IFNγ ELISpot assay. Therefore, 771 B cell lymphoma cells (5 x 10^4) were loaded with 1 µg/ml $OVA_{323-339}$ peptide or HBV core $antigen_{128-140}$ control peptide (HBV) and co-cultured with the different T cell lines for 16 h (highest T cell number: 6250, followed by serial 1:2 dilution). The highest number of T cells was used for all negative controls included in the assay (HBV, T cells). Error bars represent SD of technical triplicates. **(B)** The T cell lines were stained using monoclonal antibodies specific for CD3, CD4, CD8 and the two T cell receptor chains Vα2.1 and Vβ5.1. The cells were subsequently analyzed by flow cytometry. Gating strategy: living cells → single cells (FSC-A vs. FSC-H) → CD3$^+$ cells → CD4 vs. CD8 → TCR Vα2.1 vs. TCR Vβ5.1 (within CD4$^+$CD8$^-$ cells).

3.3 Repolarization of M2-like PECs into immunostimulatory M1-like PECs *in vitro*

As described in sections 1.1.4 and 1.2.4, the immunosuppressive tumor microenvironment still forms a major obstacle for successful cancer immunotherapy. In many tumor entities, TAMs with a M2-like phenotype contribute to the immunosuppressive tumor microenvironment by secreting inhibitory cytokines including IL-10 and TGF-β. Within this study several strategies to repolarize M2-like macrophages into immunostimulatory M1-like macrophages were investigated using PECs.

3.3.1 Phenotypic analysis of *in vitro* polarized PECs

In a first step, PECs were isolated from thioglycolate treated mice and analyzed by flow cytometry. Staining with F4/80 and CD11b specific monoclonal antibodies revealed co-expression of the macrophage markers by more than 99 % of the cells (Figure 3.16). Next, PECs were polarized into M1-like or M2-like macrophages using LPS/IFNγ or IL-4, respectively. Subsequently, the two phenotypes were characterized comprehensively by gene and protein expression analyses as well as functional assays.

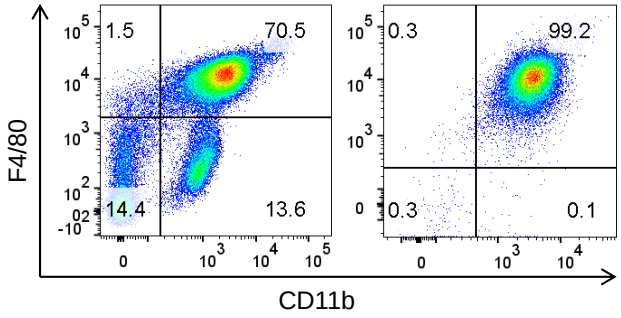

Figure 3.16: PECs contain a high percentage of macrophages.
Four days after C57BL/6 mice were injected i.p. with 1 ml of a 3 % thioglycolate solution, PECs were isolated and stained with F4/80 and CD11b specific monoclonal antibodies for subsequent flow cytometric analysis. **Left dot plot:** Cell suspension immediately after isolation. **Right dot plot:** The cells were cultured for 2 h, non-adherent cells were washed off and adherent cells were harvested and stained. More than 99 % of all adherent PECs are F4/80$^+$CD11b$^+$ and thus can be considered as pure macrophages. Gating strategy: living cells → single cells (FSC-A vs. FSC-H) → F4/80 vs. CD11b.

As shown in Figure 3.17 A treatment of PECs with a combination of LPS and IFNγ upregulated expression of the entire M1-associated gene panel within 4 h of stimulation as detected by qPCR. Some genes showed higher expression levels after prolonged stimulation periods (*Stat1, Cd86, Cd80, Nos2*), whereas expression of other M1-associated genes decreased after 24 h (*Il6, Il12b*) or 48 h (*Il1b*). Expression of *Cxcl10* was stable throughout all tested time points. As expected, no M2-associated marker expression was observed upon stimulation with LPS/IFNγ, except for *Il10 and Arg1* whose expression was transiently upregulated after 4 h or 24 h, respectively (Figure 3.17 B). On the other hand, IL-4 treatment of PECs decreased the expression of M1-associated genes being most pronounced after 24 h, with *Cxcl9* and *Cxcl10* showing strongest effects (Figure 3.17 A). Conversely, expression of M2-associated genes, such as *Ym1, Fizz1, Arg1, Mrc1* and

Cd163 was induced upon IL-4 stimulation. Their upregulation became apparent within 4 h after incubation and was further increased upon prolonged stimulation (Figure 3.17 B).

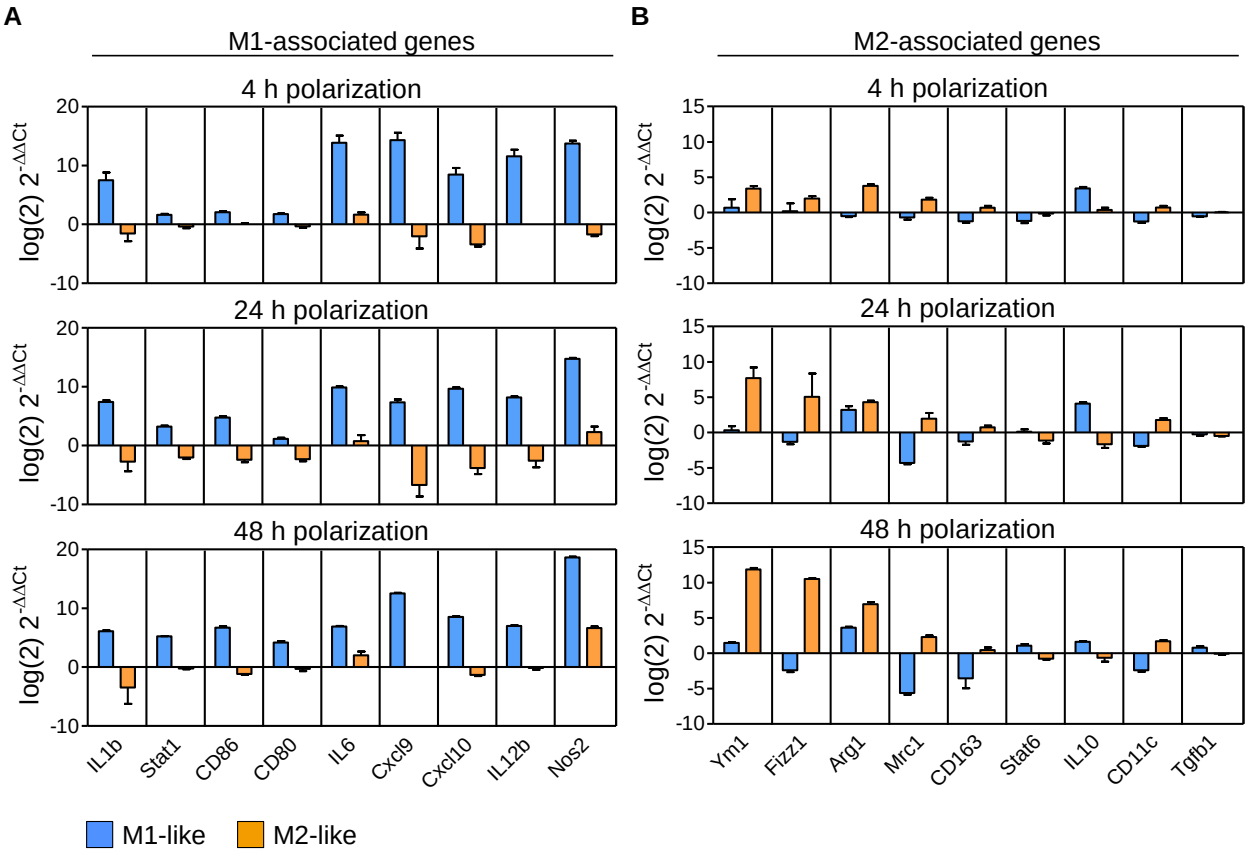

Figure 3.17: Gene expression analysis confirms polarization of *in vitro* polarized PECs.
After isolation, PECs were polarized into M1-like (blue) or M2-like (orange) macrophages for 4 h, 24 h and 48 h by LPS/IFNγ or IL-4 treatment, respectively. At each time point, RNA was isolated and the expression of M1- (A) and M2-associated genes (B) was measured using qPCR. The data obtained were first normalized to beta-actin ($2^{-\Delta Ct}$) and subsequently normalized to expression data obtained from untreated PECs ($2^{-\Delta\Delta Ct}$). **(A)** All M1-associated genes were upregulated in PECs treated with LPS and IFNγ, whereas most of the genes were downregulated in IL-4 treated PECs. **(B)** In contrast, most of the M2-associated genes were upregulated in PECs treated with IL-4 and downregulated in M1 polarized PECs. Error bars represent 95 % CI of technical triplicates. One representative out of three experiments is shown.

Next, the induced changes of M1/M2 *in vitro* polarization on protein level were analyzed by flow cytometry. Treatment with LPS/IFNγ for 48 h induced strong intracellular iNOS expression as well as surface expression of MHC II molecules, both representing classical M1-associated markers (Figure 3.18). As expected, expression of the M2-associated markers CD206 and Egr2 was decreased under these conditions. On the other hand, stimulation with IL-4 resulted in upregulated surface expression of the mannose receptor CD206 and in preserved Egr2 expression, whereas IA^b surface expression became present on a small subpopulation of PECs. Similar results were observed also after shorter (24 h) and extended (72 h) time periods of polarization (supplementary Figure 6.4). In addition, polarization of PECs could be followed morphologically, as M1 like PECs appeared round shaped whereas M2 like PECs showed an elongated phenotype (Figure 3.19).

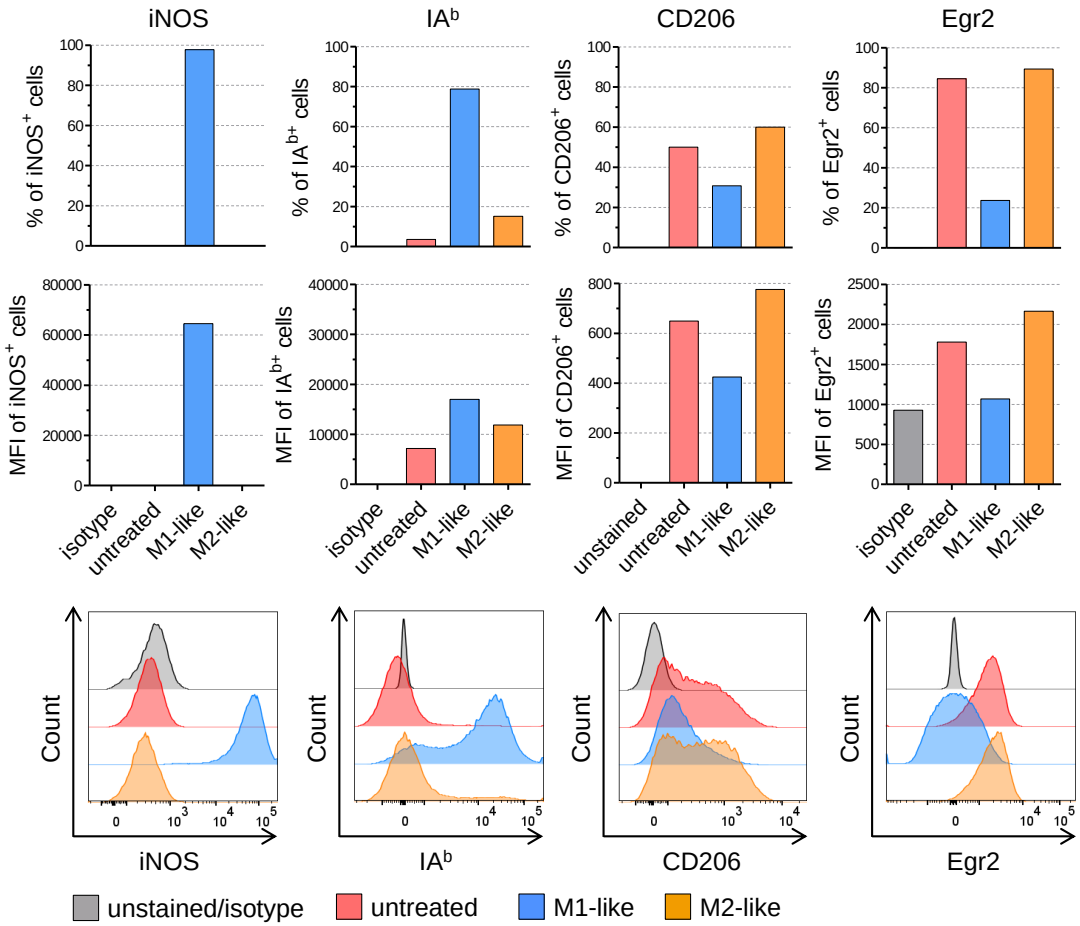

Figure 3.18: Protein expression analysis demonstrates successful polarization of PECs.
PECs were polarized for 48 h, harvested, stained with iNOS, IA^b, CD206 or Egr2 specific monoclonal antibodies and analyzed by flow cytometry. The percentage (upper panel) as well as the MFI (center) of marker positive cells is shown. In addition, the overlaid histograms are depicted in the lower panel. Gating strategy: living cells → single cells (FSC-A vs. FSC-H) → F4/80$^+$CD11b$^+$ → IA^b vs. FSC-H.

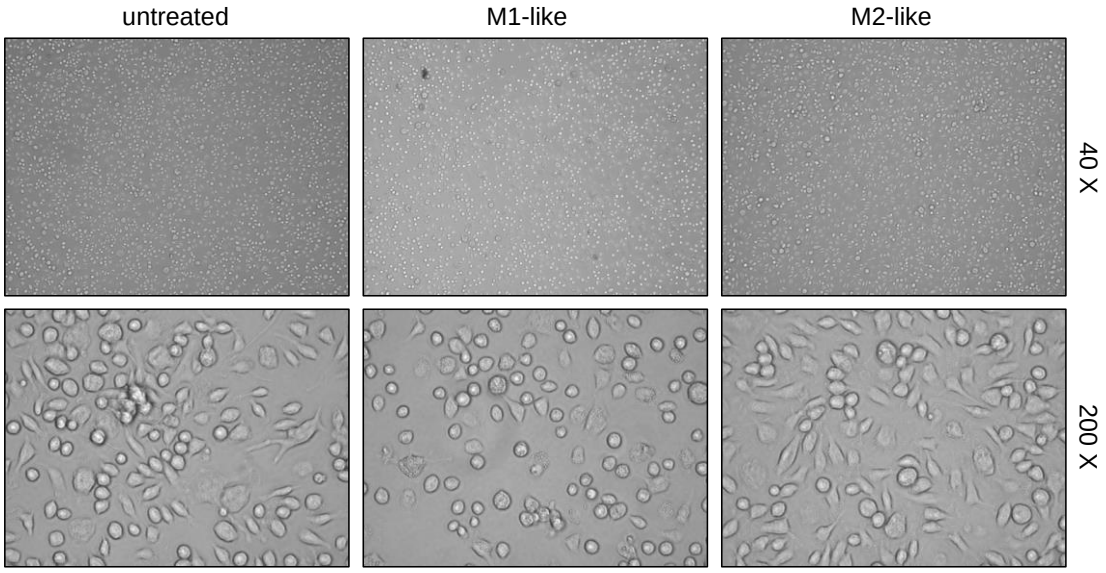

Figure 3.19: M1-like PECs differ phenotypically from M2-like PECs.
PECs were isolated and polarized in M1-like or M2-like PECs by using IL-4 or LPS/IFNγ for 72 h. The cells were subsequently analyzed microscopically. M1-like PECs show a rounded cell shape whereas M2-like PECs are more elongated.

In a last step, cytokine secretion profiles of *in vitro* polarized PECs were analyzed using the LEGENDplex Mouse Inflammation Panel (Figure 3.20). This investigation was part of a collaboration project with the Center for Sepsis Control and Care (CSCC) in Jena and was performed by our collaborator Daniela Röll. The Multiplex assay includes 13 cytokines which are associated with a M1-like phenotype, except for IL-10 which is known to be secreted predominantly by M2-like macrophages. The results show that secretion of most of the proinflammatory cytokines (IFNβ, IFNγ, IL-1α, IL-6, MCP-1, TNFα) was significantly increased after LPS/IFNγ treatment when compared to both, untreated or IL-4 treated PECs. As the culture medium of polarized PECs was not exchanged prior cytokine measurement, it must be assumed that the detected IFNγ is derived from the LPS/IFNγ containing medium used for PECs polarization. Therefore, the measured IFNγ levels only serve as internal positive control. Secretion of IL-12 and IL-27 was also increased in M1-like PECs but did not reach statistical significance. GM-CSF, IL-1β as well as IL-10 secretion was not affected by LPS/IFNγ or IL-4 treatment. As IL-17A and IL-23 were not detected in any of the culture supernatants these cytokines were excluded from the analysis.
In summary, these data demonstrate efficient *in vitro* polarization of PECs into macrophages with M1- or M2-like phenotype, as confirmed by quantitative gene and protein expression analyses as well as cytokine secretion analysis of M1- and M2-associated markers.

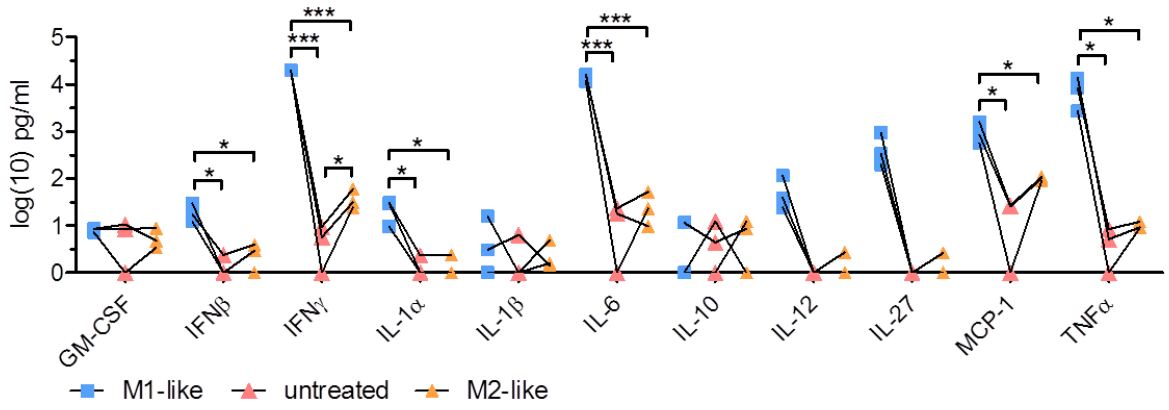

Figure 3.20: Cytokine secretion of polarized PECs.
The culture supernatants of 24 h polarized PECs were collected and analyzed using the LEGENDplex Mouse Inflammation Panel. The biological replicates (n = 3) are shown as individual dots and are connected with lines. PECs of 3-4 mice were pooled for each biological replicate. Significance was determined using One-way ANOVA with post-hoc Tukey test (95% CI, * $p \leq 0.05$, ** $p < 0.01$, *** $p \leq 0.001$). The presented data were generated jointly with Daniela Röll.

3.3.2 Functional analysis of *in vitro* polarized PECs

In order to analyze the functional capacities of putative M1- and M2- like PECs the phagocytic activity of polarized PECs using fluorescently labeled latex beads was measured. The whole assay was performed at 37 °C leading to phagocytosis mediated bead uptake. In comparison, PECs were incubated with beads at 4 °C, to control for unspecific binding of the beads to the cell surface (Figure 3.21 A). To guarantee proper quantification, the percentages of $FITC^+$ cells in the 4 °C control group were subtracted from the percentages obtained through 37 °C incubation.

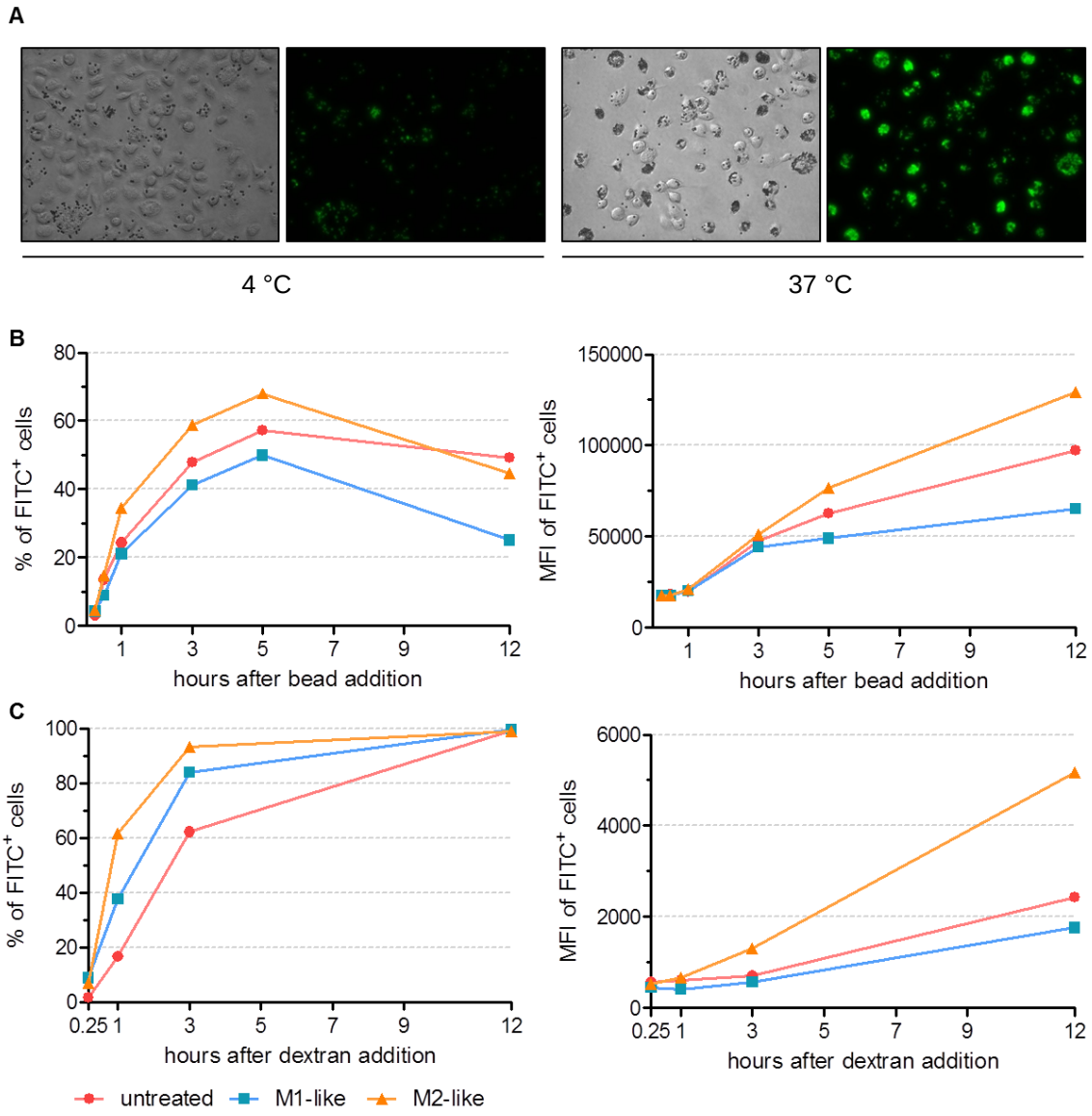

Figure 3.21: Differences in phagocytosis and pinocytosis confirm polarization of *in vitro* polarized PECs.
PECs were isolated and polarized either into M1-like or M2-like macrophages for 72 h. Subsequently, phagocytic and pinocytic activity was determined by using fluorescent latex beads and FITC-dextran, respectively. **(A)** PECs were incubated with fluorescent latex beads at 4 °C or 37 °C and analyzed microscopically. **(B)** PECs incubated with latex beads were harvested at various time points and analyzed by flow cytometry **(C)** Similar to the phagocytic activity, M2-like PECs show a greater pinocytic potential compared to M1-like and M0 PECs when treated with FITC-dextran. For both assays, background values were determined upon incubation of cells with FITC labeled particles at 4 °C and subtracted from the values measured after culturing at 37 °C. One out of three experiments with similar results is shown. Gating strategy: living cells → single cells (FSC-A vs. FSC-H) → FITC vs. FSC-H.

After incubation for 5 h, 68 % of M2-like PECs had taken up beads in comparison to 49.9 % of PECs polarized with LPS/IFNγ and 57.2 % of untreated macrophages (Figure 3.21 B, left). Moreover, after 12 h incubation M2-like PECs had taken up the double amount of beads compared to the LPS/IFNγ treated PECs as reflected by the MFI values (129,313 for M2-like macrophages versus MFI of 65,493 observed with M1 like PECs) (Figure 3.21 B, right). When the pinocytic activity of polarized PECs was analyzed using FITC-dextran [317, 318], IL-4 treated PECs turned out superior in pinocytosis compared to M1-like PECs (Figure

3.21 C). This effect became evident within 60 min after addition of FITC-dextran, showing that 61.5 % of M2-like PECs and 37.6 % of M1-like PECs had pinocytosed the compound. After overnight incubation with FITC-dextran, all PECs had taken up the particles, regardless of their polarization status. However, the median fluorescence intensity values revealed that M2-like PECs had taken up 2.9 fold more of the compound (MFI: 5,179) compared to M1-like PECs (MFI: 1,762) (Figure 3.21 C, right). Of note, the pinocytic capacity of untreated PECs was inferior to M1-like and M2-like PECs at all time points measured. All in all, both assays clearly showed an increased phagocytic and pinocytic capacity of M2-like PECs compared to untreated or M1 polarized macrophages, thereby supporting the gene and protein expression data presented in section 3.3.1.

3.3.3 Cognate interaction of $CD4^+$ T cells with M2-like PECs

Having observed that external addition of cytokines polarizes PECs *in vitro*, we next assessed whether cognate interaction with $CD4^+$ T cells (generated through peptide immunization as described in section 2.2.12.1) would induce IFNγ secretion by T cells and instruct PECs to acquire a M1-like phenotype.

3.3.3.1 Susceptibility of polarized PECs to $CD4^+$ T cell recognition

First, the susceptibility of peptide loaded PECs to OVA specific $CD4^+$ T cell recognition was examined. Therefore, PECs polarized for either 24 or 48 h were loaded with IA^b restricted OVA peptide and co-cultured over night with OVA specific $CD4^+$ T cells (Figure 3.22). As demonstrated by IFNγ ELISpot assays, peptide loaded PECs that had been polarized with LPS/IFNγ for 24 h were strongly recognized by OVA specific $CD4^+$ T cells resulting in saturating spot numbers (i.e. > 500 IFNγ spots) (Figure 3.22, top left). In contrast, M2-like peptide-pulsed PECs were significantly less susceptible to $CD4^+$ T cell recognition, similarly to untreated PECs loaded with antigenic peptide (119 and 100 spots, respectively). Flow cytometric analysis revealed IA^b surface expression by 52.5 % of PECs polarized with LPS/IFNγ, whereas only 9.7 % of IL-4 stimulated PECs and 8.7 % of untreated PECs showed cell surface expression of IA^b molecules (Figure 3.22, top right). When polarized for 48 h, more than 90 % of LPS/IFNγ treated PECs turned into IA^b expressing cells and the magnitude of MHC II surface expression increased 4 fold compared to untreated PECs (MFI 10350 vs. MFI 2586). As already observed with short term polarized PECs, maximal IFNγ spot formation was observed upon co-culture of T cells with peptide pulsed LPS/IFNγ treated macrophages. However, PECs treated for 48 h with IL-4 became less susceptible to $CD4^+$ T cell recognition compared to untreated PECs (23 spots versus 52 spots) (Figure 3.22, bottom left), which differs from the results obtained with short term polarized PECs. Of note, although IL-4 polarization for 48 h induced M2-like PECs with a higher MHC II surface expression compared to untreated PECs (8.4 % versus 3.1 %), M2-like PECs appeared less susceptible to $CD4^+$ T cell recognition, indicating that besides the amount of MHC II surface expression, further parameters impact on the T cell susceptibility of macrophages.

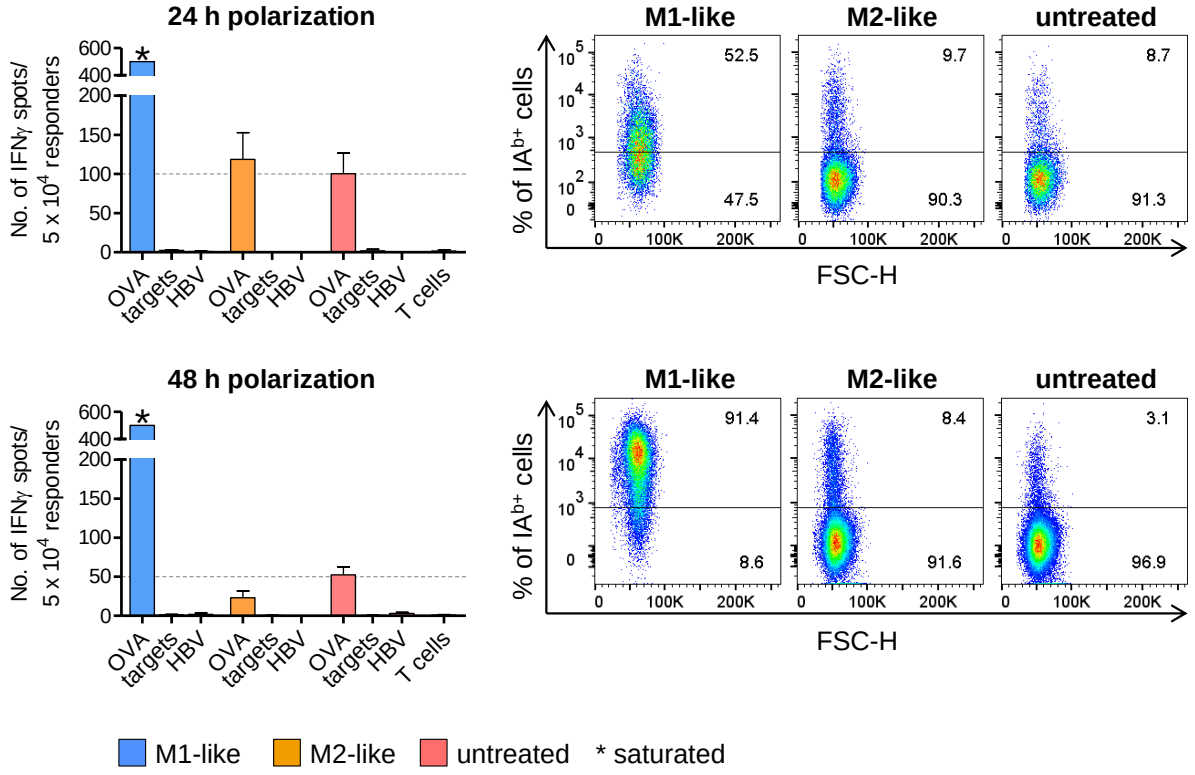

Figure 3.22: Susceptibility of polarized PECs to CD4$^+$ T cell recognition.
Polarized, peptide pulsed PECs were co-cultured with OVA specific CD4$^+$ T cells for 24 or 48 h and subsequently analyzed using an IFNγ ELISpot assay. After 24 h, M2 polarized PECs demonstrate equal susceptibility to recognition by CD4$^+$ T cells compared to untreated PECs. However, 48 h after co-culturing, recognition of M2-like PECs was lower compared to untreated PECs. The staining of PECs using an IA^b specific monoclonal antibody demonstrates that this difference was not due to a lower frequency of IA^b expressing M2-like PECs. One out of three experiments with similar results is shown. Gating strategy: living cells → single cells (FSC-A vs. FSC-H) → F4/80$^+$CD11b$^+$ → IA^b vs. FSC-H.

3.3.3.2 Cognate interaction with CD4$^+$ T cells repolarizes M2-like PECs

After showing that M2-like PECs efficiently interact with CD4$^+$ T cells, despite their immunosuppressive phenotype and low MHC II expression, the next set of experiments should clarify whether this interaction would instruct PEC derived M2-like macrophages to acquire M1-like phenotype and function. Thus, PECs were polarized for 24 h into M2-like macrophages as confirmed by flow cytometry (Figure 3.23 A and C, upper panel), loaded with IA^b restricted OVA peptide and co-cultured with OVA specific CD4$^+$ T cells. Subsequently, PECs were analyzed for iNOS and IA^b expression by flow cytometry. M2-like PECs co-cultured with CD4$^+$ T cells in the presence of OVA peptide showed a strong upregulation of both M1-associated markers when compared to M2-like PECs loaded with control peptide or to PECs cultured without T cells (Figure 3.23 A, lower panel). Interestingly, repolarization of M2-like PECs by cognate interaction with CD4$^+$ T cells was even more effective than polarization with LPS/IFNγ (compare with Figure 3.23 A, upper panel). Analysis performed on PECs 24 h after co-culture or treatment with LPS/IFNγ revealed that 80.3 % of PECs had turned into MHC II positive PECs upon co-culture with CD4$^+$ T cells, whereas only a 39.8 % of PECs showed IA^b expression upon treatment with LPS/IFNγ. Assuming IFNγ released by the T cells upon recognition of the M2-like PECs to be the key mediator responsible for macrophage repolarization, the supernatants from the co-cultures

were collected to determine their IFNγ concentrations by ELISA. As shown in Figure 3.23 B, the IFNγ concentration was increased 210 fold in supernatants of cultures that had included the OVA specific T cell epitope compared to supernatants from co-cultures with irrelevant epitope (HBV).

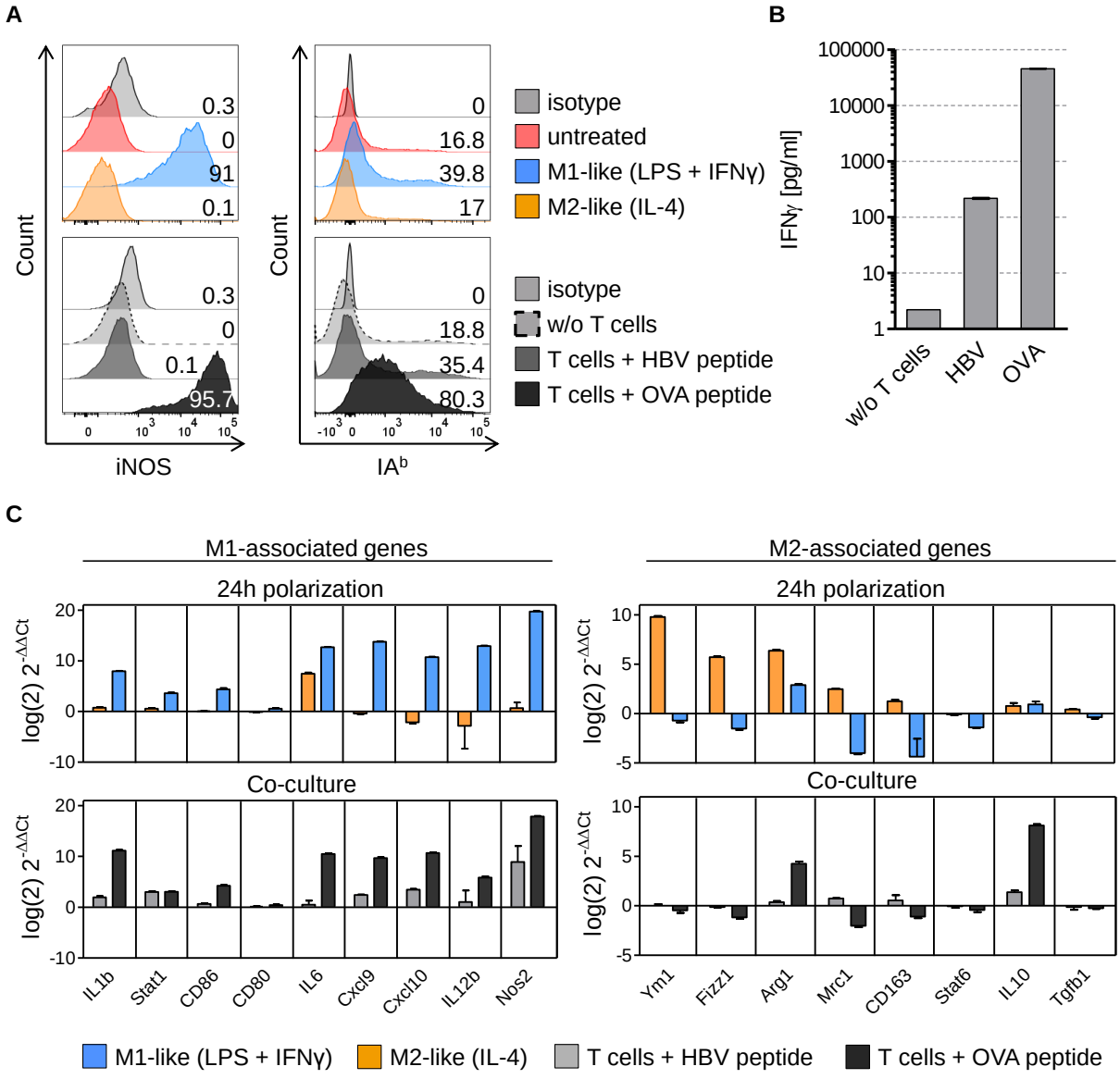

Figure 3.23: Repolarization of M2-like PECs by CD4$^+$ T cells.
PECs were polarized with IL-4 for 24 h, loaded with 1 µg/ml IA^b restricted OVA peptide and subsequently co-cultured with ovalbumin specific CD4$^+$ T cells for 24 h. **(A)** PECs were polarized by external cytokine addition (upper panel) or co-cultured with OVA specific CD4$^+$ T cells (lower panel). Cells were harvested and stained with iNOS and IA^b specific monoclonal antibodies for flow cytometry analysis. Gating strategy: living cells → single cells (FSC-A vs. FSC-H) → F4/80$^+$CD11b$^+$ → iNOS/IA^b vs. FSC-H. **(B)** Analysis of the co-culture supernatants by an IFNγ ELISA. Error bars represent SD of technical triplicates. **(C)** Gene expression analysis by qPCR after external cytokine addition (upper panel) or co-culture (lower panel). Data obtained by external cytokine addition were normalized to untreated PECs. Co-culture expression data were normalized to PECs w/o T cell addition. One out of three experiments with similar results is shown. Error bars represent 95 % CI of technical triplicates.

Next, we analyzed T cell mediated repolarization of M2-like PECs on gene expression level using the primer pairs described in Figure 3.17. The results show that all M1-associated genes were highly upregulated after co-culture with $CD4^+$ T cells in presence of the OVA specific epitope (Figure 3.23 C, lower panel). In contrast, most of the M2-associated genes were downregulated (with the exception of *Arg1* and *Il10*) when compared to M2-like PECs cultured with irrelevant peptide.

As detected by flow cytometry as well as qPCR, the co-culture using the control peptide (HBV) repolarizes M2-like PECs slightly into M1-like macrophages, most likely due to the steady release of low amounts of IFNγ by the $CD4^+$ T cell line even in the absence of its relevant peptide/MHC complex. This observation is additionally supported by the IFNγ ELISA results (Figure 3.23 B), showing increased IFNγ levels in co-cultures with $CD4^+$ T cells and HBV core antigen derived control peptide compared to PECs only (w/o T cells).

In a last step, it was tested whether the cognate interaction of M2-like PECs with $CD4^+$ T cells would also result in a switch toward M1-like functionality. Therefore, PECs were polarized into M2-like macrophages, loaded with 5 µg/ml IA^b restricted OVA peptide or irrelevant control peptide (HBV) and co-cultured with OVA specific $CD4^+$ T cells for 24 h. Subsequently, FITC-dextran or fluorescent latex beads were added in order to test phagocytic or pinocytic activity, respectively. As expected, the percentage of PECs taking up FITC-dextran was significantly reduced in macrophages cultured with $CD4^+$ T cells in the presence of the relevant peptide, pointing towards M1 repolarization (Figure 3.24 A, top). Of note, pinocytic activity remained unchanged in the presence of control peptide. However, the total amount of FITC-dextran taken up by macrophages was equal among the different groups (Figure 3.24 A, bottom).

Similar results were detected after incubation of PECs with fluorescent latex beads. Already 1 h after incubation, the proportion of FITC positive cells was significantly reduced among the population of M2-like PECs co-cultured with $CD4^+$ T cells in the presence of relevant peptide compared to the PECs from the two control groups (Figure 3.24 B, top). These effects became even more pronounced after incubation for 3 h with beads. No differences in the total amount of phagocytosed beads were detected among the three groups of PECs (Figure 3.24 B, bottom), similarly to the observations made when analyzing pinocytotic capacity (Figure 3.24 A, bottom).

In summary, these results clearly show that cognate interaction with $CD4^+$ T cells can instruct M2-like PECs to acquire M1-like phenotype and function as shown by extensive gene expression analyses and functional phagocytosis and pinocytosis assays. The data provided a solid basis for subsequent studies, in which the cognate interaction between $CD4^+$ T cells and TAMs was analyzed *in vivo* (see section 3.4).

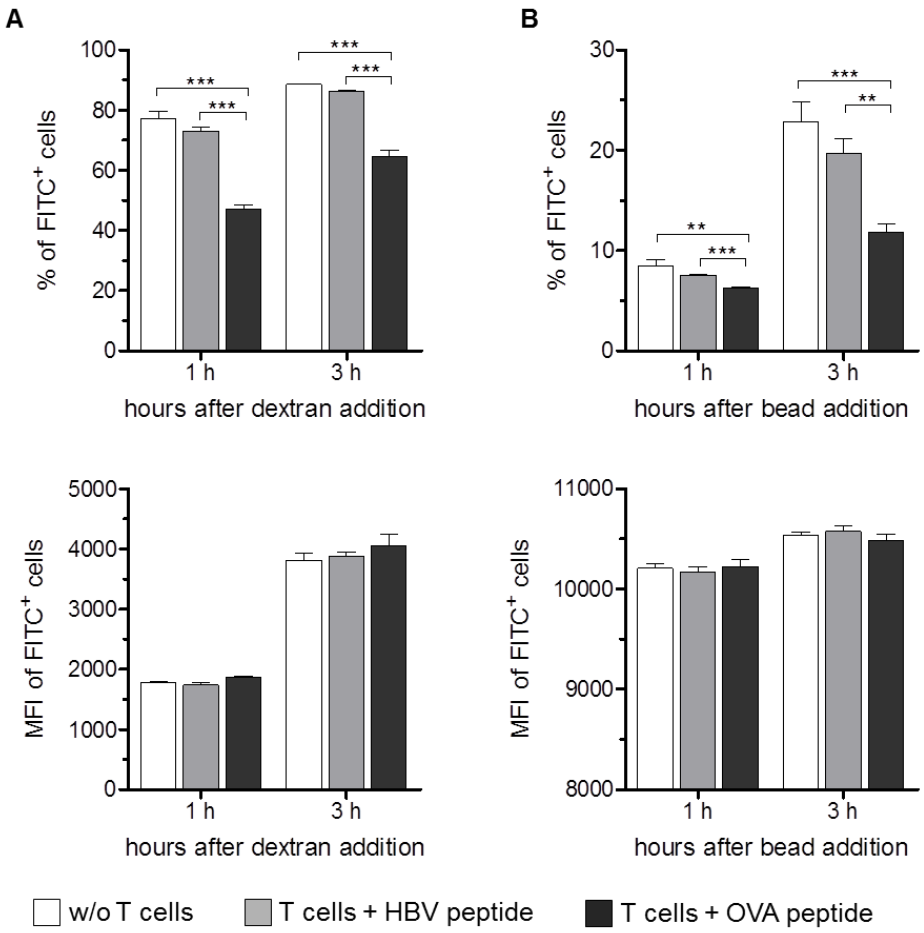

Figure 3.24: Functional repolarization of M2-like PECs by CD4$^+$ T cells.
PECs were polarized with IL-4 for 24 h, loaded with 5 µg/ml IA^b restricted OVA peptide or irrelevant control peptide (HBV) and subsequently co-cultured with OVA specific CD4$^+$ T cells for 24 h. Co-cultured PECs were either incubated with FITC-dextran **(A)** or with fluorescent latex beads **(B)** for 1 h or 3 h and subsequently harvested for flow cytometric analysis. Both, phagocytic as well as pinocytic activity of PECs co-cultured with CD4$^+$ T cells and relevant peptide significantly decreased compared to the control groups. Statistical analysis was done by unpaired Student's *t*-test (95% CI, * $p \leq 0.05$, ** $p < 0.01$, *** $p \leq 0.001$). Gating strategy: living cells → single cells (FSC-A vs. FSC-H) → FITC vs. FSC-H. Error bars represent SD of biological triplicates.

3.3.4 Identification of key transcription factors involved in PECs polarization

The analysis of *in vitro* polarized PECs described in sections 3.3.1 and 3.3.2 were extended in order to identify the key transcription factors (TFs) mediating macrophage polarization. Identification of such TFs should reveal new insights into the metabolic and transcriptional reprogramming of macrophages and might be useful for the identification of therapeutic targets to reprogram M2 macrophages into the proinflammatory M1-like macrophages.
Therefore, PECs were polarized either into a M1-like or a M2-like phenotype for 24 h, RNA was isolated and handed over to the Genomics and Proteomics Core Facility of the German Cancer Research Center (Heidelberg, Germany) to perform whole RNA sequencing. A detailed workflow as well as the purity and polarization check of isolated PECs is illustrated in Figure 3.25 A-C.
The sequencing data were analyzed by our collaboration partners at the Center for Sepsis Control and Care in Jena by using their previously published tool, which enables the investigation of transcriptional regulation of gene expression profiles [319]. At the same time

they used their newly developed method based on mixed-integer-linear programming which integrates gene expression data into flux balance models (unpublished). Based on these methods, five TFs responsible for the regulation of signaling genes and metabolic genes in polarized macrophages were determined (section 3.3.4.2). In order to validate the functional relevance of the transcription factors in PEC polarization, their expression was either knocked down by siRNA transfection or upregulated by transfecting TF encoding plasmids. Thereafter, the polarization of the macrophages was analyzed by qPCR and measuring cytokine secretion (section 3.3.4.4).

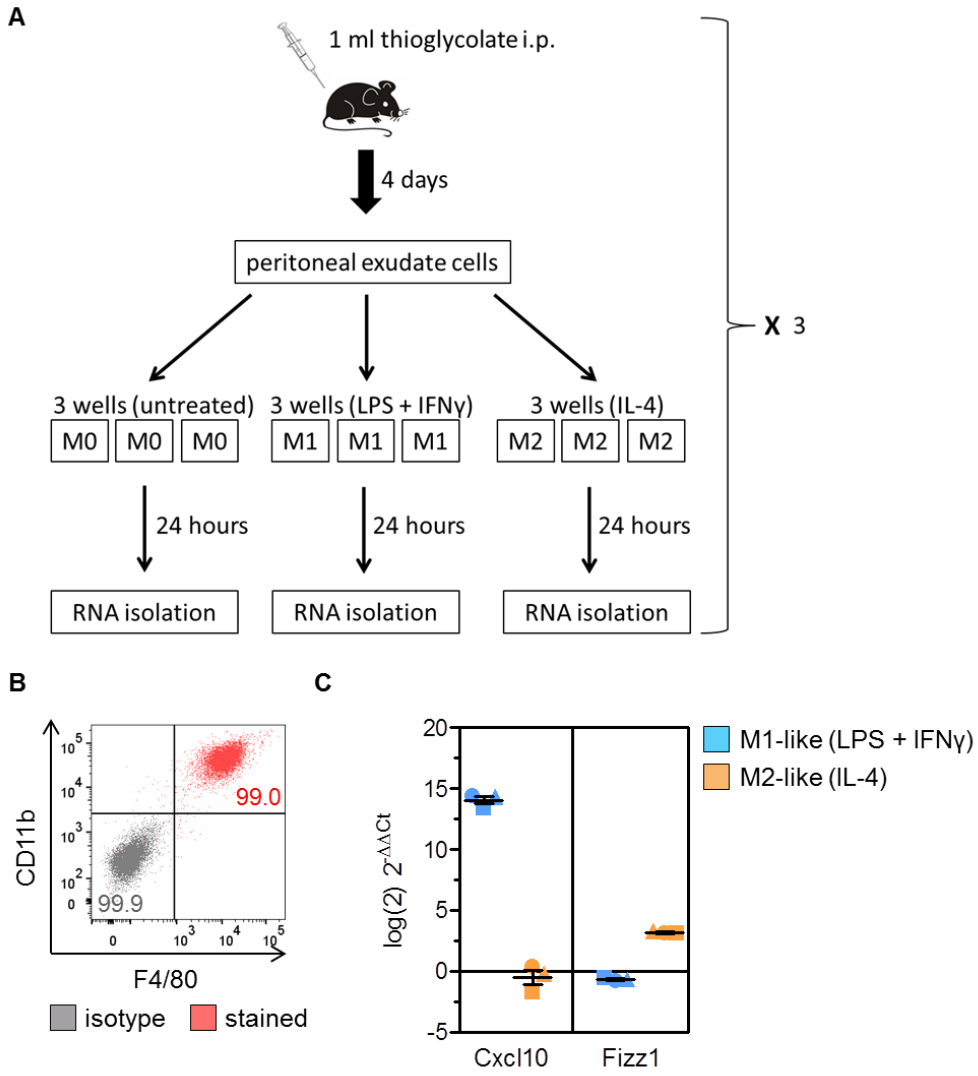

Figure 3.25: Experimental workflow for the generation of whole RNA sequencing data from polarized PECs.
(A) Three mice were injected i.p. with 1 ml of 3 % thioglycolate solution. Four days later, PECs were isolated and polarized into M1-like or M2-like macrophages or left untreated (three wells per condition per mouse). After overnight polarization, the triplicate wells were pooled for subsequent RNA isolation. The pooling was necessary to obtain the required amount of RNA for whole RNA sequencing. **(B)** The purity of isolated macrophages was assessed by flow cytometry after staining with F4/80 and CD11b specific monoclonal antibodies. **(C)** After the polarization of macrophages was confirmed by qPCR, the RNA samples were sent for sequencing. As example, expression of *Cxcl10* and *Fizz1* representing classical M1-like and M2-like markers, respectively are shown. Error bars represent SD of biological triplicates.

3.3.4.1 Correlation between RNA sequencing and qPCR data

In a first validation, the obtained RNA sequencing data were compared and correlated with the respective qPCR data (see Figure 3.17) to ensure that both methods yielded comparable results. In Figure 3.26 A, Log(10)RPKM (reads per kilobase million) values obtained from RNA sequencing were compared to log(10)$2^{-\Delta Ct}$ values measured by qPCR 24 h after PECs polarization. Both methods yielded corresponding results considering the upregulation of genes in polarized macrophages compared to untreated PECs (marked in red). However, qPCR analysis revealed a higher sensitivity in detecting downregulated genes in polarized macrophages (marked in blue) which resulted in differences between the two datasets.
The higher sensitivity of the qPCR method became even more apparent when the two datasets were plotted against each other, presenting each analyzed gene as an individual dot (Figure 3.26 B). Many genes with low expression level were located close to the y-axis (red dots showing little distribution across the x-axis) since the RNA sequencing sensitivity is not high enough to detect small differences in their expression level. In contrast, these small differences were still detected by qPCR as the same genes distribute throughout a wide range of the y-axis.

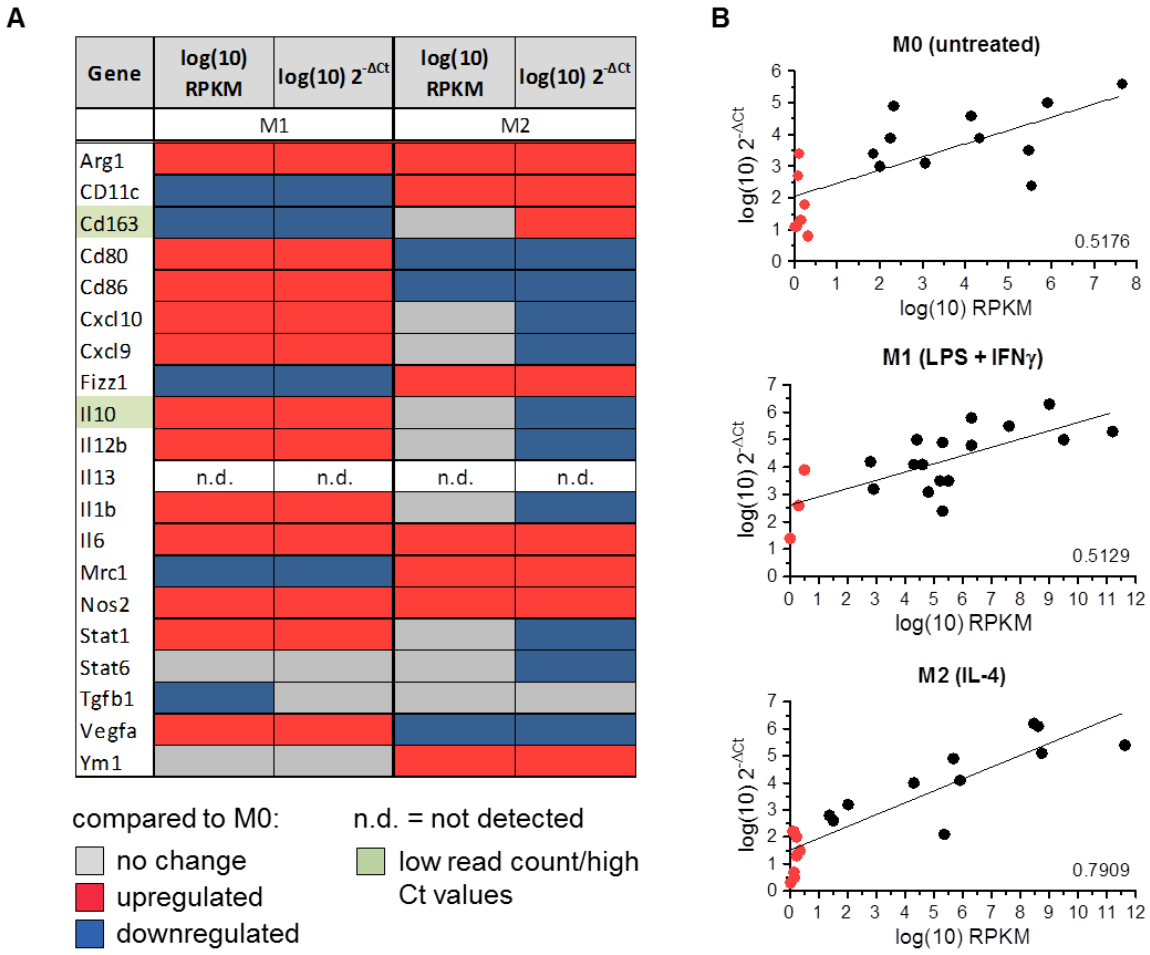

Figure 3.26: Correlation between RNA sequencing and qPCR data.
(A) Log(10)RPKM values obtained through RNA sequencing were compared to log(10)$2^{-\Delta Ct}$ values measured by qPCR 24 h after PECs polarization. Genes significantly upregulated or downregulated compared to M0 are highlighted in red and blue, respectively. Genes with no significant change compared to M0 are marked in grey. **(B)** The correlation between RNA sequencing and qPCR data was illustrated by plotting the two datasets against each other. Each dot represents one gene. Numbers depicted in the graphs give the calculated coefficients of determination (R^2).

In summary, both methods detected in 76 % (29/38) of all cases the same up- or downregulation compared to untreated PECs (Figure 3.26 A). In 18 % (7/38) of the cases, a downregulation was detected by qPCR, whereas no change in expression level was detected by RNA sequencing which can be explained by the aforementioned lower sensitivity of the latter method. Most importantly, the methods never showed contradictory results in terms of up- and downregulation of a given gene (e.g. upregulation detected by qPCR and downregulation detected by RNA sequencing) and as such support and supplement the qPCR data obtained from polarized PECs (Figure 3.17).

3.3.4.2 *In silico* predicted TFs are highly expressed in M2-like PECs

Based on the methods described in section 3.3.4, five TFs (CTCF, E2F1, MYC, PPARγ and STAT6) important for maintaining a M2-like phenotype in IL-4 treated PECs were identified. Analysis of the RNA sequencing data demonstrated a strong downregulation of all five TFs in LPS/IFNγ treated PECs compared to untreated cells (Figure 3.27 A). In contrast, the expression level in M2-like PECs was either upregulated (*Ctcf, Myc* and *Pparg*) or downregulated (*E2f1* and *Stat6*) compared to M0, but consistently higher as in M1-like macrophages.

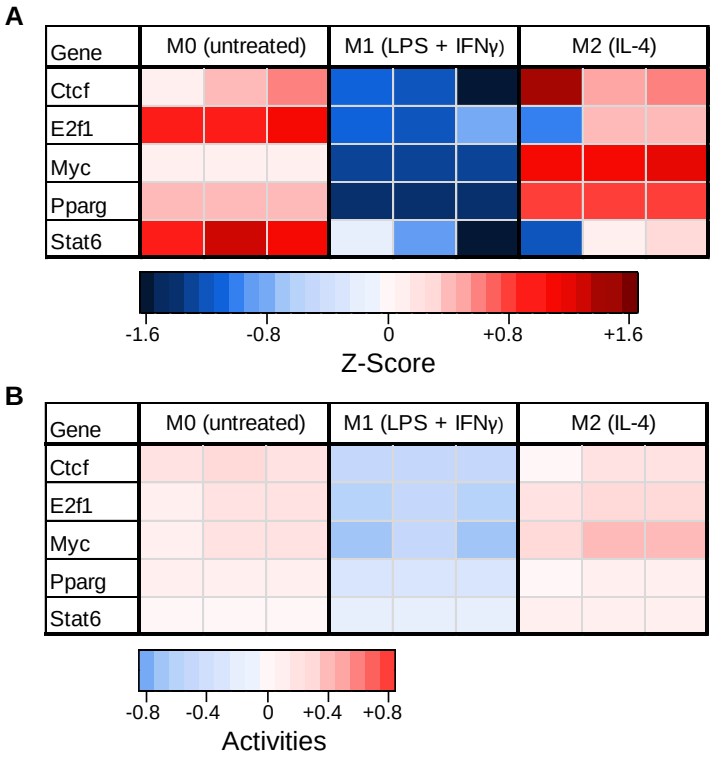

Figure 3.27: Expression level and activity of selected transcription factors.
PECs were polarized for 24 h into M1-like or M2-like macrophages and subsequently analyzed by RNA sequencing. **(A)** Z-scores and **(B)** activities of selected transcription factors revealed a higher expression level as well as a higher activity of all five factors in M2-like compared to M1-like PECs. Three biological replicates for each condition are shown. The presented data were generated jointly with Franziska Hörhold.

Similar results were obtained when the TF activities were calculated and plotted in a heatmap as shown in Figure 3.27 B. The activity is an estimation of the overall impact of a TF on its target genes and can differ substantially from the expression level [320]. For

instance, the expression level of *Stat6* is higher in untreated PECs compared to IL-4 treated cells, whereas the opposite is true for its calculated activity. Thus, the overall impact of STAT6 on its target genes is higher in M2-like PECs compared to untreated cells even though the expression level is lower.
All five *in silico* predicted TFs demonstrated a high activity in M2-like PECs and a low activity in M1-like PECs, supporting the gene expression data presented in Figure 3.27 A and emphasizing their importance in maintaining the M2-like phenotype.

3.3.4.3 Transfection of PECs with plasmids and siRNAs

Strategies to experimentally validate the TFs predicted *in silico* involve on the one hand their overexpression and on the other hand their knockdown. In both strategies, transfection of PECs using either TF encoding plasmids (overexpression) or TF targeting siRNAs (knockdown) is required. However, macrophages are generally considered as hardly transfectable cells as they are equipped with a large amount of potent degradative enzymes that can disrupt integrity of the delivered nucleic acids [321].
Based on that knowledge, PECs were transfected with a GFP encoding plasmid using 10 reagents developed for transfection of primary “hard-to-transfect” cells. Most of the transfection reagents were tested using two different cell densities and varying DNA:transfection reagent ratios. The specific conditions as well as the percentages of GFP^+ cells for all the tested approaches can be looked up in Table 6.1. As shown in Figure 3.28, only in 4 of 75 tested approaches the transfection efficiency exceeded 10 %. These included Lipo-LTX approach 3 (14.3 %), TransIT-2020 approach 1 and 2 (10.7 % and 11.1 %) and Viromer Red approach 5 (15.1 %), using 1×10^6 PECs. Even when GFP encoding RNA (pos. ctrl. RNA) in combination with Viromer Red was used, only 17.4 % of the macrophages were successfully transfected. In contrast, control transfection of B16F10 cells using the GFP encoding plasmid resulted in transfection efficiencies above 70 % for most of the transfection reagents, except for TurboFect (17.7 %) and Effectene (19.1 %), demonstrating that the plasmid as well as the reagents were working (supplementary Figure 6.5).

As the establishment of additional transfection strategies like electroporation or viral transduction would have taken too long, the strategy of TF overexpression was not pursued further.
Instead, the focus was placed on knocking down the TFs using siRNA pools. In order to find the most suitable transfection reagent to deliver siRNA to PECs, the cells were transfected with a fluorescently labelled (Cy3) siRNA testing four transfection reagents optimized for small RNA transfection. The transfection efficiency was determined by measuring the percentage of $Cy3^+$ cells by flow cytometry 24, 48 and 72 h post transfection. The histograms in Figure 3.29 A revealed an almost 100 % transfection efficiency for all tested transfection reagents already 24 h post transfection using either 25 or 50 nM Cy3 coupled siRNA. However, increasing cytotoxicity during the course of transfection was observed, with Lipofectamine and Metafectene being the most cytotoxic reagents (Figure 3.29 B; % of living cells). Comparing the Cy3 MFI values of the two transfection reagents with less cytotoxic effects (DharmaFect4 and siLentFect) showed that more siRNA is taken up if transfection was performed with DharmaFect4, no matter which siRNA concentration was used (Figure **3.29** B; MFI of $Cy3^+$ cells). Due to its low cytotoxicity and high transfection efficiency, DharmaFect4 was selected for subsequent knockdown experiments.

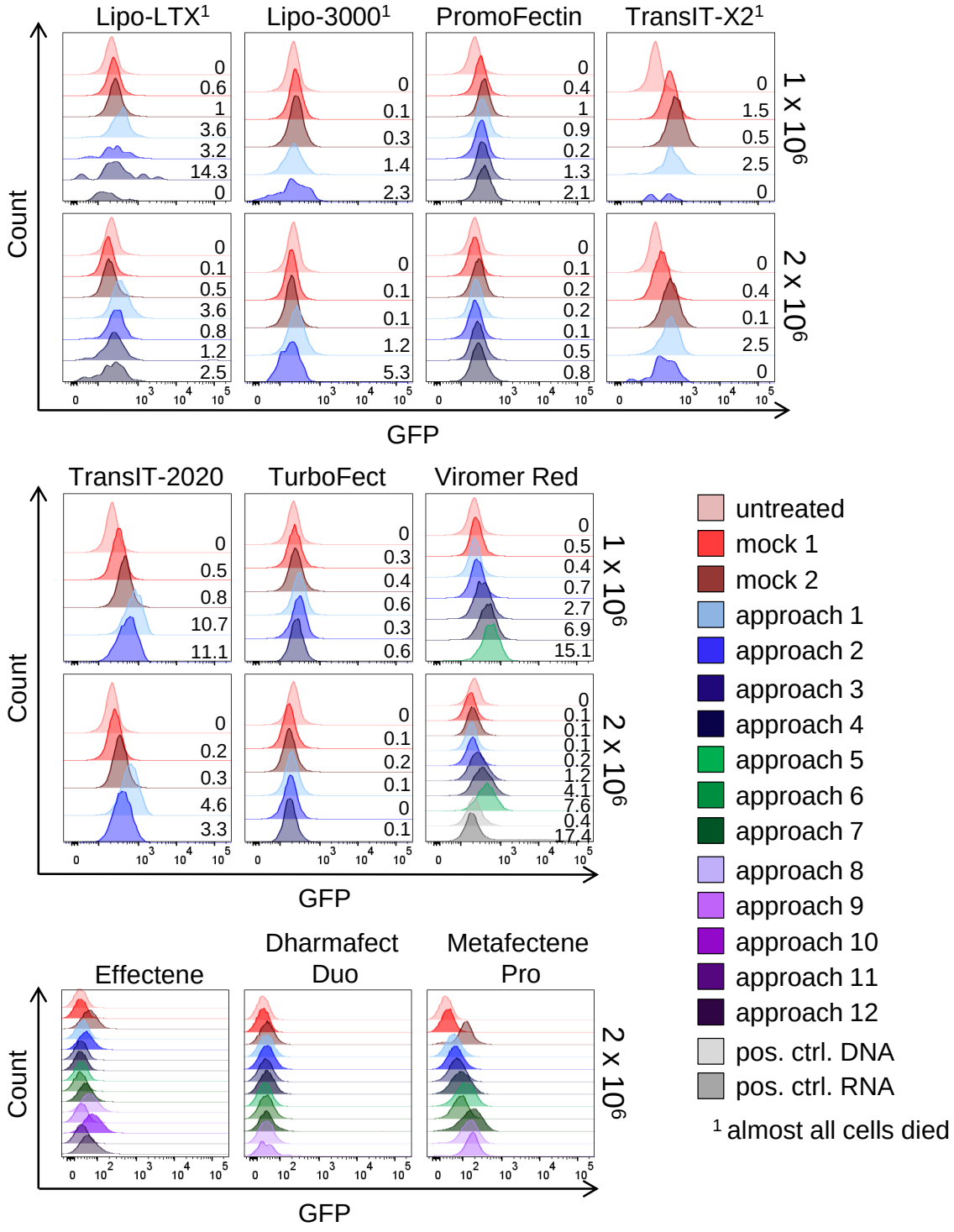

Figure 3.28: Transfection of PECs with GFP encoding plasmid.
Either 1 x 10^6 or 2 x 10^6 untreated PECs were transfected with a GFP encoding plasmid using 10 different transfection reagents. For each reagent several transfection approaches were tested as recommended by the manufacturer and shown in more detail in Table 6.1. Macrophages were harvested and analyzed by flow cytometry 48 h post transfection. The numbers given within the graphs represent the percentages of GFP positive cells. Gating strategy: living cells → single cells (FSC-A vs. FSC-H) → GFP vs. FSC-H.

A

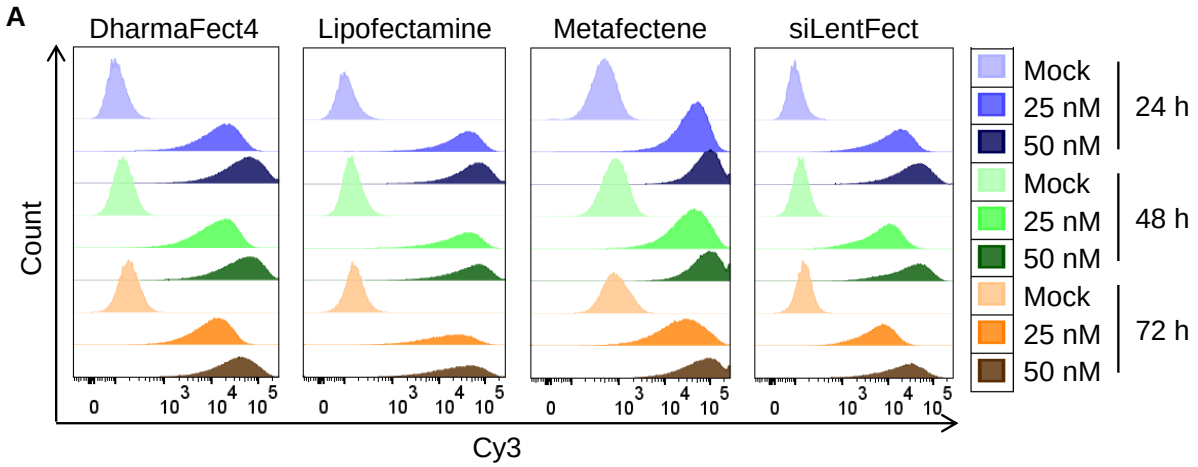

weak	strong	strong	weak	cytotoxicity
1.31	4.73	4.43	0.87	price per Well [€]
3	2	1	4	MFI Cy3

B

Sample		% of living cells			MFI of $Cy3^+$ cells			% of $Cy3^+$ cells		
Reagent	Condition	24 h	48 h	72 h	24 h	48 h	72 h	24 h	48 h	72 h
Dharmafect	Mock	85.9	90.7	84	108	150	195	0	0.1	0.2
	25 nM	84.5	89.5	78.4	14941	12594	10155	97.1	97.2	97.4
	50 nM	82.5	75.2	61.8	45988	42578	31998	98.4	98.6	98.6
Lipofectamine	Mock	70.9	85.2	68.5	109	148	167	0.1	0.2	0.2
	25 nM	57.5	48.1	40	30524	28333	15127	97.3	97.2	95.5
	50 nM	60.2	48.3	44.8	51047	45760	25465	98.1	98.1	96.6
Metafectene	Mock	63.7	60.8	44.2	477	803	823	0.1	1.5	3.5
	25 nM	62.8	60.9	50.5	39618	34904	22437	96.8	97.1	93.1
	50 nM	39.3	36.3	30	80653	80253	62587	98.4	99.3	98.5
siLentFect	Mock	85.7	93	81.9	102	135	160	0	0	0.4
	25 nM	83.7	88.6	71.7	13365	7797	5916	97.5	95.8	95.9
	50 nM	78	66.6	54.9	34218	29849	20984	97.7	97.5	97.4

Figure 3.29: Transfection of PECs with siRNA using different transfection reagents.
PECs were isolated from thioglycolate treated mice and dispensed in 6-Well plates (2×10^6). Cells were transfected either with 25 nM or 50 nM of Cy3 coupled siRNA using DharmaFect4, Lipofectamine, Metafectene or siLentFect transfection reagent. **(A)** 24, 48 and 72 h post transfection, PECs were harvested and analyzed by flow cytometry. Gating strategy: living cells → single cells (FSC-A vs. FSC-H) → $Cy3^+$ vs. FSC-H. **(B)** Table showing the percentages of living and $Cy3^+$ cells as well as the median fluorescence intensity values (MFI) of $Cy3^+$ cells.

The results shown in Figure 3.29 demonstrated an efficient uptake of small RNA molecules by macrophages. However, as mentioned before macrophages are specialized in degrading internalized molecules rapidly. Therefore, it is possible that transfected small RNAs are a target for degradation, whereas the fluorescent dye Cy3 remains stable in the cytoplasm, thus leading to false positive results when transfection efficiency is determined by Cy3 coupled siRNA. To rule out degradation of transfected small RNAs, a random miRNA which was available in the lab (miRNA-339-5p) was transfected into PECs. Small RNAs were isolated 24, 48 and 72 h post transfection and the presence of miRNA-339-5p was evaluated by qPCR. As shown in Figure 3.30, the detected endogenous expression of miRNA-339-5p measured in untreated PECs was low. As expected, the expression level measured in PECs

treated with the transfection reagent only (mock) was comparable to untreated PECs. In contrast, the detectable amount of miRNA-339-5p 24 h post PECs transfection was increased 2290 fold compared to the corresponding mock control, demonstrating successful transfection. As the miRNA was still detected in high quantities after prolonged culturing (48 and 72 h post transfection), it can be concluded that internalized small RNAs are stable in PECs for at least 3 days.

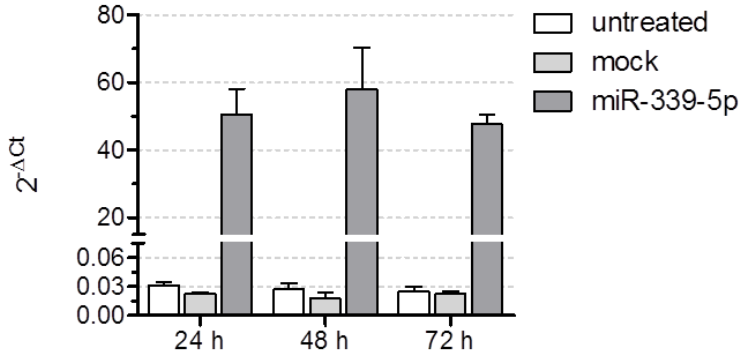

Figure 3.30: Transfected miRNA-339-5p is taken up by PECs and stable for at least 72 h.
Unpolarized PECs were isolated from thioglycolate treated mice, dispensed in 6-Well plates (2 x 10^6) and transfected with 25 µM of miRNA-339-5p using DharmaFect4 transfection reagent. 24, 48 and 72 h post transfection, PECs were harvested for subsequent miRNA isolation. The presence of miRNA-339-5p was analyzed by qPCR using a miRNA-339-5p specific primer pair. The data were normalized to snoRNA202 which serves as internal control. Error bars represent SD of technical triplicates.

3.3.4.4 Experimental validation of the *in silico* predicted transcription factors

In a last step, the *in silico* predicted TFs were experimentally validated. As described above, all five TFs were predicted to be involved in maintenance of the M2-like phenotype. Hence, knocking down these proteins should induce a repolarization into proinflammatory M1-like PECs. To investigate changes in PEC polarization upon TF knock down, PECs were polarized into M2-like macrophages using IL-4, transfected with TF targeting siRNA pools and analyzed by measuring gene expression (Figure 3.31) as well as cytokine secretion (Figure 3.32). All the obtained qPCR data were normalized to the housekeeping gene *Rpl19*, as *in silico* predictions from various sources [322-327] demonstrated that this gene is almost not regulated by the five TFs, thereby guaranteeing stable expression after TF knockdown (Table 3.2). Additionally, *Rpl19* expression was not affected by LPS/IFNγ or IL-4 treatment, making it a suitable and reliable housekeeping gene for subsequent knockdown experiments (Table 3.2, log2 fold change). As pilot experiments demonstrated inefficient knock down of CTCF (data not shown), subsequent experiments were performed either by knocking down all five TFs (5 TFs) or only four of them, excluding *Ctcf* (4 TFs).

Table 3.2: In search of an appropriate housekeeping gene for qPCR analysis of polarized PECs.

The BaseMean values were obtained from RNA sequencing data and serve as a measure of the expression level of a certain gene across all tested samples. The subsequent columns show whether the housekeeping genes are regulated by the different TFs. The numbers are based on *in silico* predicted as well as validated interactions between TFs and housekeeping genes (arbitrary unit: the higher the value the stronger the predicted regulation). The log(2) fold change values present the fold change expression between M1-like and M2-like PECs. A fold change of 0, showing that the housekeeping gene expression is not affected by LPS/IFNγ or IL-4 treatment, would be ideal. The presented data were generated jointly with Franziska Hörhold.

Gene	Full Name	Base Mean	Ctcf	E2f1	Myc	Pparg	Stat6	Sum	log(2) fold change
Actb	actin beta	48061	0	3.2	3.5	0	0	6.7	0.39
B2m	beta-2 microglobulin	125058	0	1	2	0	0	3	1.96
Gapdh	glyceraldehyde-3-phosphate dehydrogenase	2239	0	0.7	1	0	0	1.7	2.45
Gusb	glucuronidase, beta	15590	0	0.7	2.5	0	0	3.2	-1.27
Hmbs	hydroxymethylbilane synthase	409	0	0.7	2.5	0	0	3.2	-0.89
Hprt	hypoxanthine guanine phosphoribosyl transferase	2361	0	0	2	0	0	2	0.28
Ppia	peptidylprolyl isomerase A	2894	0	1.2	2	0	0	3.2	0.06
Rn18s	18S ribosomal RNA	n.a.	n.a.	n.a.	n.a.	n.a.	n.a.	n.a.	n.a.
Rpl13a	ribosomal protein L13a	4281	0.5	1.2	3.5	0	0	5.2	-0.08
Rpl19	ribosomal protein L19	1777	0	1.2	1.5	0	0	2.7	-0.08
Tbp	TATA-box binding protein	559	0.5	0	1	0	0	1.5	0.25
Ubc	ubiquitin C	28430	0	1.2	0.7	0	0	1.9	1.25

n.a. = not available

The knockdown efficiency for the different TFs was measured on RNA level by qPCR 24 h or 48 h post transfection as shown in Figure 3.31 A. In contrast to the results obtained in the aforementioned pre-experiments, the knockdown of all five TFs was successful and detected already 24 h after siRNA pool transfection. All TFs reached a log(2) $2^{-\Delta\Delta Ct}$ value of -0.5 and lower which corresponds to a knockdown efficiency of at least 30 % compared to the samples treated with a negative control siPool (knockdown efficiency = 100 – $2^{\log(2)\ 2\text{-}\Delta\Delta Ct}$). In some cases (e.g. *Myc* and *Pparg*) knockdown efficiencies of 75 %, corresponding to a log(2) $2^{-\Delta\Delta Ct}$ value of -2, were achieved. After 48 h the expression of all five TFs was still reduced when PECs were treated with all siRNA pools (5 TFs). In contrast, *E2f1* expression increased again, reaching physiological conditions if the *Ctcf* targeting pool was not transfected (4 TFs). As expected, knocking down all five TFs resulted in strong induction of M1-associated gene expression within 24 h of transfection (Figure 3.31 B). Some genes showed higher expression levels after prolonged transfection periods (*Arg2, Il1b, Stat1*) whereas expression of other genes decreased again after 48 h (*Cxcl9, Cxcl10, Il12b, Nos2*). In contrast expression of M2-associated genes was decreased upon siRNA transfection, except for *Ppat* and *Tgfb1* whose expression was upregulated after 48 h. Interestingly, using only *E2f1, Myc, Pparg* and *Stat6* targeting siRNA pools (knockdown of 4 TFs) resulted in almost the same gene expression patterns (Figure **3.31** C).

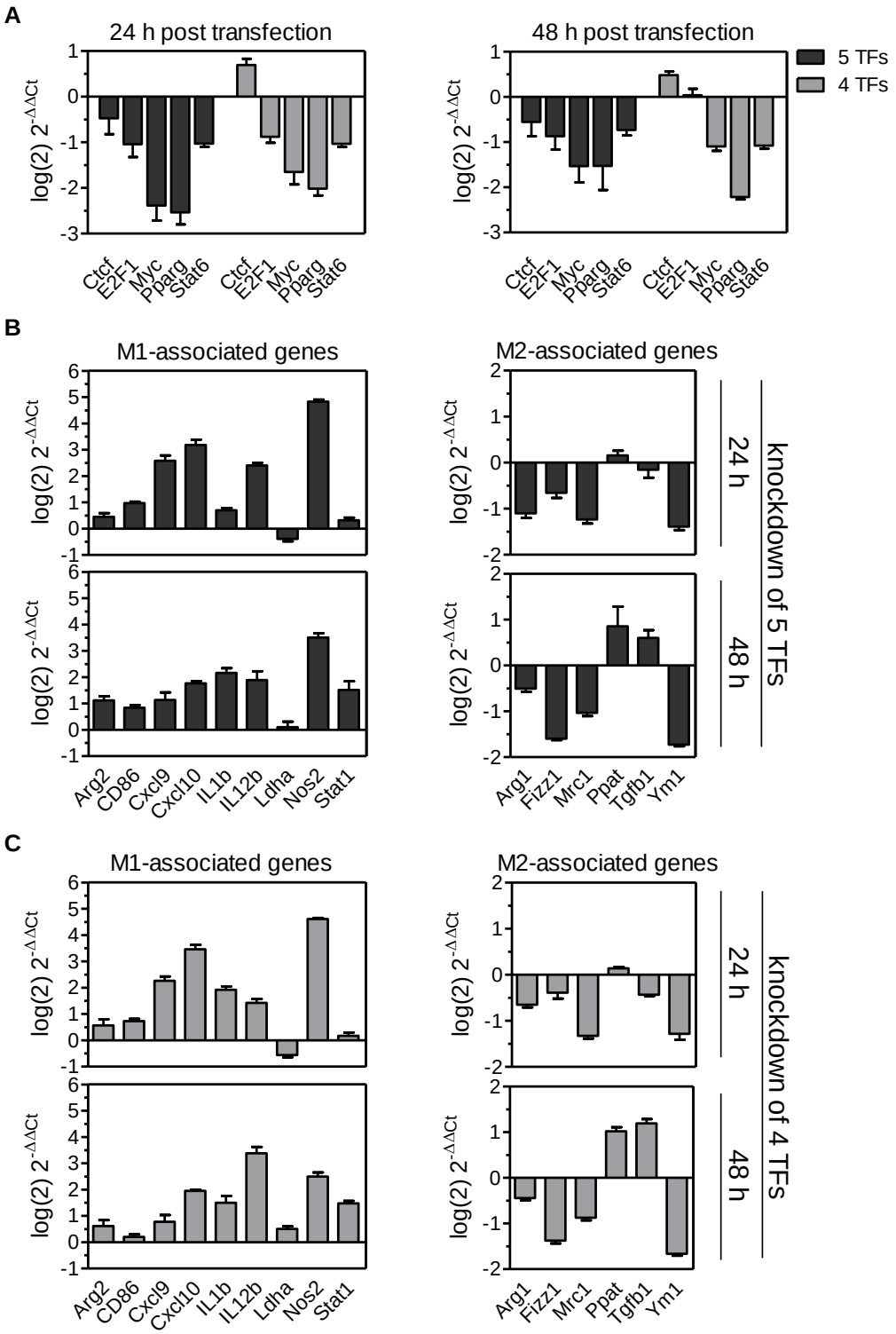

Figure 3.31: Transcription factor knockdown results in M1-associated gene expression.
PECs were polarized for 24 h into M2-like macrophages using IL-4 and subsequently transfected with siRNA pools targeting 5 (dark grey) or 4 (light grey) transcription factors. *Ctcf, E2f1, Pparg* and *Stat6* targeting siRNA pools were used in a final concentration of 10 nM, whereas the *Myc* targeting siRNA pool was used in a final concentration of 50 nM. **(A)** Gene expression analysis of the targeted transcription factors. **(B-C)** The expression of M1- and M2-associated genes was analyzed 24 and 48 h post transfection. The presented data was first normalized to the housekeeping gene Rpl19 ($2^{-\Delta Ct}$) and subsequently normalized to the data obtained after transfecting the negative siRNA pool ($2^{-\Delta\Delta Ct}$). The final concentration of the negative siRNA pool was 90 nM (5 TFs) or 80 nM (4 TFs). Error bars of qPCR data represent SD of technical triplicates. One representative out of three similar experiments is shown.

The gene expression analysis shown in Figure 3.31 revealed that knocking down *Ctcf* is not necessarily required for successful repolarization of M2-like PECs. Thus, the *Ctcf* targeting siRNA pool was excluded for subsequent experiments in which cytokine secretion of transfected PECs was analyzed. The measurement of the conditioned culture medium was done by Daniela Röll (Integrated Research and Treatment Center, Center for Sepsis Control and Care (CSCC), Jena, Germany) using the LEGENDplex Mouse Inflammation Panel. As already mentioned in section 3.3.1 all included cytokines, except for IL-10 are associated with a M1-like phenotype.

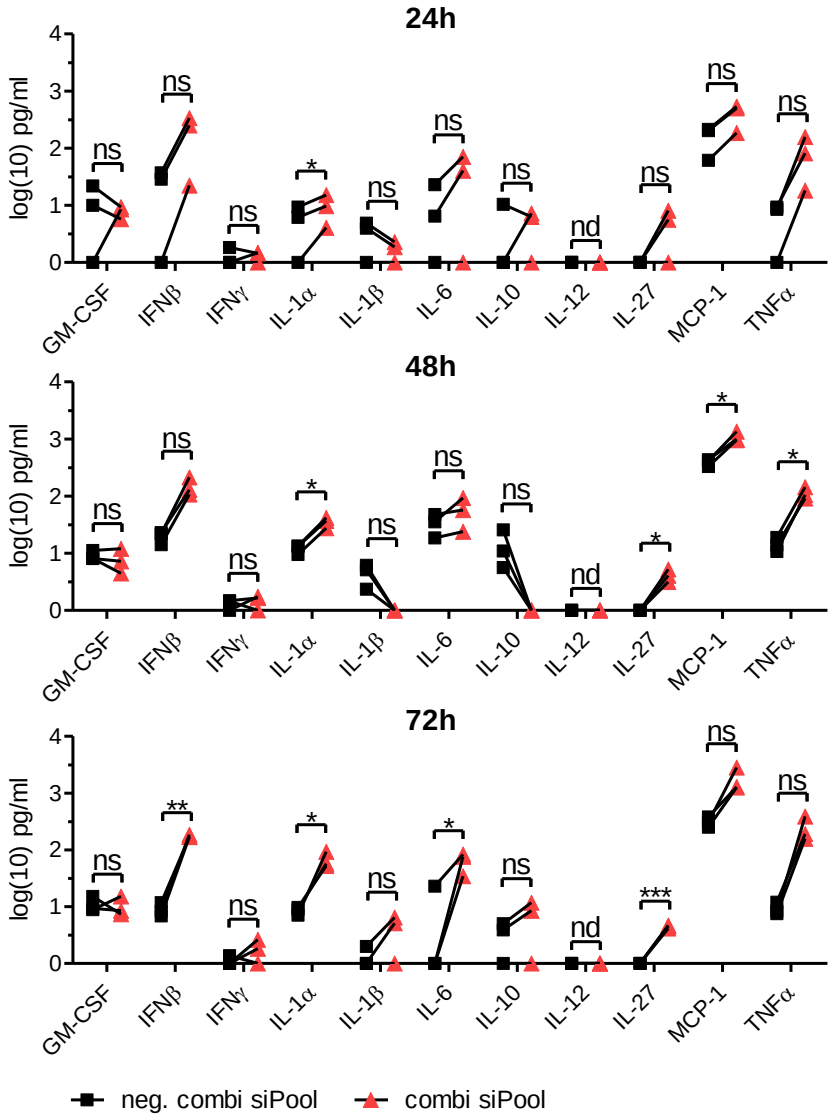

Figure 3.32: Cytokine secretion of PECs post transcription factor knockdown.
PECs were polarized with IL-4 for 24 h and transfected with siRNA pools targeting *E2f1, Myc, Stat6* and *Pparg* for 24, 48 and 72 h. *E2f1, Pparg* and *Stat6* targeting siRNA pools were used in a final concentration of 10 nM, whereas the *Myc* targeting siRNA pool was used in a final concentration of 50 nM. The final concentration of the negative siRNA pool was 80 nM. The culture medium was collected and analyzed using the LEGENDplex Mouse Inflammation Panel. The biological replicates (n = 3) are shown as individual dots and are connected with lines. PECs of 3-4 mice were pooled for each biological replicate. Significance was determined using paired Student's t-test (95% CI, ns = not significant, * $p \leq 0.05$, ** $p < 0.01$, *** $p \leq 0.001$). nd = not detected. The presented data were generated jointly with Daniela Röll.

As shown in Figure 3.32, already 24 h after transfecting M2-like PECs the quantities of several M1-associated cytokines (IFNβ, IL-1α, IL-6, IL-27, MCP-1, TNFα) were increased in culture medium of cells treated with the TF targeting siRNA pools (combi siPool) compared to the culture medium of cells that received the negative siRNA pool (neg. combi siPool). The differences between the two groups became even more prominent after prolonged transfection periods resulting in significantly higher amounts of all aforementioned cytokines upon TF knock down (48 h or/and 72 h post transfection). Secretion of IL-10, the only M2-associated cytokine within the tested panel was either not affected by TF knock down (24 h and 72 h) or decreased without reaching statistical significance (48 h). GM-CSF, IFNγ and IL-1β secretion did not change upon TF knock down at any of the tested time points.
In summary, these data demonstrate efficient *in vitro* repolarization of M2-like PECs into macrophages with M1-like phenotype mediated through TF knock down as confirmed by quantitative gene expression and cytokine secretion analysis.

3.3.5 Identification of key miRNAs involved in PECs polarization

In a next set of experiments, miRNA expression profiles of polarized PECs were generated in order to identify miRNAs involved in the process of polarization. Therefore, PECs were polarized either into M1-like or M2-like macrophages for 24 h using LPS/IFNγ or IL-4, respectively. In addition, M2 polarized PECs were loaded with $OVA_{323-339}$ epitope and subsequently co-cultured with ovalbumin specific $CD4^+$ T cells (T cells + OVA peptide) to induce repolarization into M1-like macrophages as described in section 3.3.3. Small RNAs were isolated and handed over to the Genomics and Proteomics Core Facility of the German Cancer Research Center (Heidelberg, Germany) to perform small RNA sequencing. A detailed workflow illustrating all tested conditions is shown in Figure 3.33 A. The polarization of PECs upon cytokine treatment Figure 3.33 B as well as the repolarization upon co-culture with OVA specific $CD4^+$ T cells Figure 3.33 C was confirmed by qPCR prior small RNA sequencing. In a first step, our collaboration partners at the Center for Sepsis Control and Care in Jena used the DESeq2 method [314] to identify differentially expressed miRNAs in each group (section 3.3.5.1). Next, the RNA sequencing data of previous experiments (section 3.3.4) were integrated in the analysis, thereby facilitating the identification of significantly enriched miRNAs as described in section 3.3.5.2. Finally, several significantly enriched miRNAs were transfected into PECs in order to validate their functional relevance in macrophage polarization (section 3.3.5.3).
The results of these experiments could reveal new insights into the regulation of macrophage polarization mediated by miRNAs. Additionally, the small RNA expression profile of PECs repolarized by cognate interaction with $CD4^+$ T cells was compared to that of PECs polarized by the addition of cytokines. Thereby it is possible to elucidate which changes in miRNA expression levels are dependent on T cell receptor signaling.

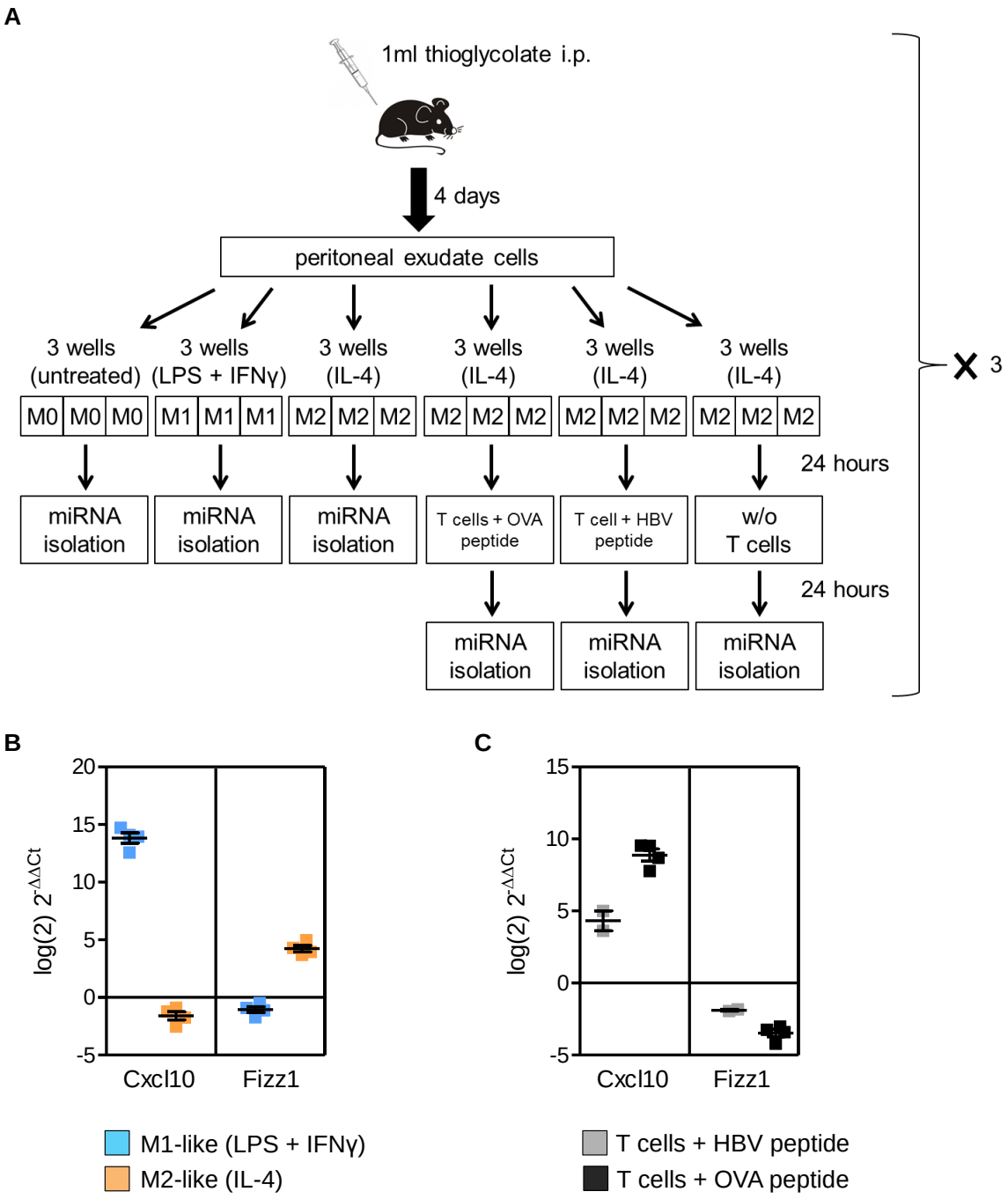

Figure 3.33: Experimental workflow for the generation of small RNA sequencing data from polarized PECs.
(A) Three mice were injected i.p. with 1 ml of 3 % thioglycolate solution. Four days later, PECs were isolated and dispensed in 6-Well plates (2 x 10^6). The cells were polarized into M1-like or M2-like macrophages or left untreated (three wells per condition per mouse). After overnight polarization, triplicate wells were pooled for subsequent miRNA isolation. Pooling was necessary to obtain the required amount of miRNA for small RNA sequencing. Additionally, some M2-like PECs were loaded with 5 µg/ml $OVA_{323-339}$ peptide (T cells + OVA peptide) or HBV core $antigen_{128-140}$ peptide (T cells + HBV peptide) and co-cultured using OVA specific $CD4^+$ T cells for 24 h. Next, triplicate wells were pooled and miRNA was isolated. **(B)** Polarization of macrophages by cytokine addition as well as **(C)** successful repolarization into M1-like PECs upon co-culture with OVA specific $CD4^+$ T cells was confirmed by qPCR. As example, expression of *Cxcl10* and *Fizz1* representing classical M1-like and M2-like markers, respectively are shown. Error bars represent SD of biological triplicates.

3.3.5.1 Differentially expressed miRNAs in polarized PECs

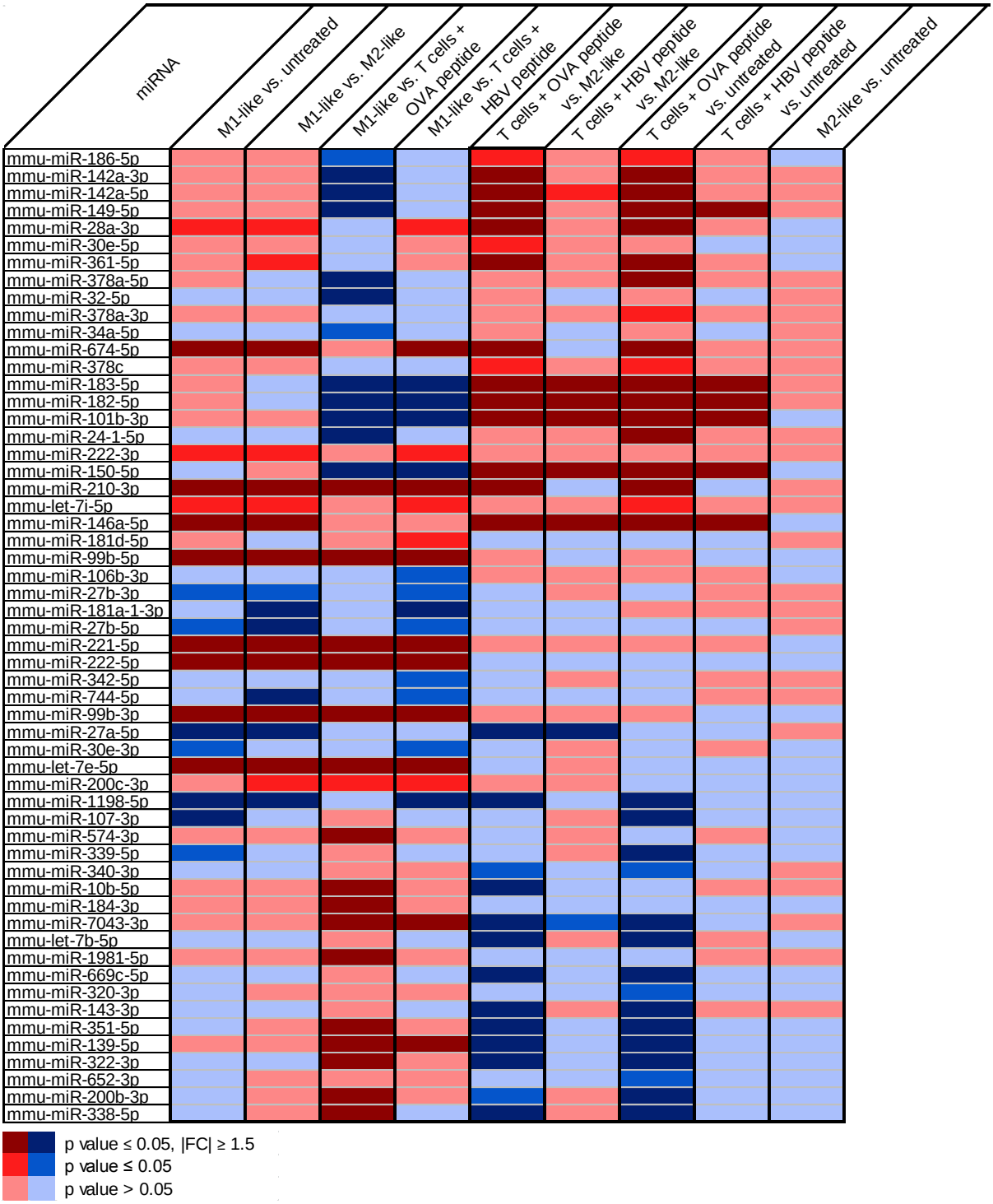

Figure 3.34: Differentially expressed miRNAs in polarized PECs.
PECs were left untreated or polarized for 24 h into M1-like or M2-like macrophages. In addition, M2-like PECs were loaded with $OVA_{323-339}$ peptide (T cells + OVA peptide) or HBV core antigen $peptide_{128-140}$ (T cells + HBV peptide) and co-cultured for 24 h with OVA specific $CD4^+$ T cells. RNA expression was analyzed by whole RNA sequencing. Differentially expressed miRNAs were determined by using the DESeq2 software package [314]. The presented data were generated jointly with Franziska Hörhold.

As shown in Figure 3.34, the tested conditions (untreated, M1-like, M2-like etc.) were arranged into respective groups (e.g. M1-like vs. untreated) to determine differential gene expression using the DESeq2 software package [314]. A miRNA was only considered as significantly differentially expressed if the average expression level was high enough (base mean ≥ 97.034) and the p-value less or equal than 0.05. Each of the listed miRNAs is significantly differentially expressed in at least one of the groups. The z-scores of all 56 differentially expressed miRNAs are shown in supplementary Figure 6.6.
As shown in Figure 3.34, none of the 56 listed miRNAs was significantly differentially expressed when M2-like PECs were compared to untreated cells. In accordance with that, the signatures of differentially expressed genes within the two groups M1-like vs. untreated and M1-like vs. M2-like were similar. The same holds true if the signatures of the groups T cells + OVA peptide vs. M2-like and T cells + OVA peptide vs. untreated were compared. Of note, 29 miRNAs were significantly differentially expressed in the group M1-like vs. T cells + OVA peptide, clearly demonstrating that M1-like PECs polarized by external cytokine addition (LPS/IFNγ) are different from M2-like PECs which were repolarized into M1-like by $CD4^+$ T cells. Interestingly, such differences were not detected by gene expression analysis already described in Figure 3.23 C (upper vs. lower panel).

3.3.5.2 Significantly enriched miRNAs in polarized PECs

miRNAs significantly up- or downregulated in M1-like vs. untreated and M1-like vs. M2-like are of particular interest as they might be important in maintaining a M1-like or M2-like phenotype, respectively. To narrow down the number of miRNAs to be validated in subsequent *in vitro* experiments, the RNA sequencing data obtained from previous experiments (section 3.3.4) were incorporated in the bioinformatics analysis to identify significantly enriched miRNAs within these two groups.
The first step to identify significantly enriched miRNAs was the collection of putative target genes of each differentially expressed miRNA using several prediction algorithms (Microcosm, miRanda, miRNAMap2, miRMap, miRDB, PITA, Pictar and TargetScan) as well as a database in which only validated targets are listed (MiRTarBase). A gene was only considered as target if a miRNA binding site was predicted by at least two of the aforementioned tools. Next, the fold change expression value of a miRNA within one of the groups (e.g. M1-like vs. M2-like) was compared to the fold change expression level of a certain differentially expressed target within the same group. Subsequently, the Fisher's exact test determines whether enough targets show opposing expression fold changes compared to the miRNA expression fold change. For instance, if a miRNA is upregulated in M1-like vs. M2-like (positive fold change), a certain number of its targets must show a downregulation in RNA expression level when comparing M1-like vs. M2-like (negative fold change). Only then, a miRNA was considered to be significantly enriched.
All of the 18 differentially expressed miRNAs in the group M1-like vs. untreated were identified to be significantly enriched. In the group M1-like vs. M2-like, 18 out of 19 differentially expressed miRNAs were significantly enriched with miR-221-5p being the only exception. Combining the results obtained from both groups revealed a total of 22 miRNAs enriched in M1-like PECs compared to either untreated PECs or M2-like PECs or both. As shown in Figure 3.35, plotting the z-scores of these 22 miRNAs in a heatmap resulted in 3 distinct clusters. The first cluster contains 6 miRNAs only upregulated in M1-like PECs, whereas the 7 miRNAs from the second cluster are upregulated in M1-like PECs and PECs

co-cultured with T cells and IA^{b} restricted OVA peptide (323-339). In contrast, miRNAs from the third cluster were downregulated in M1-like PECs as well as in PECs co-cultured with T cells and OVA peptide.

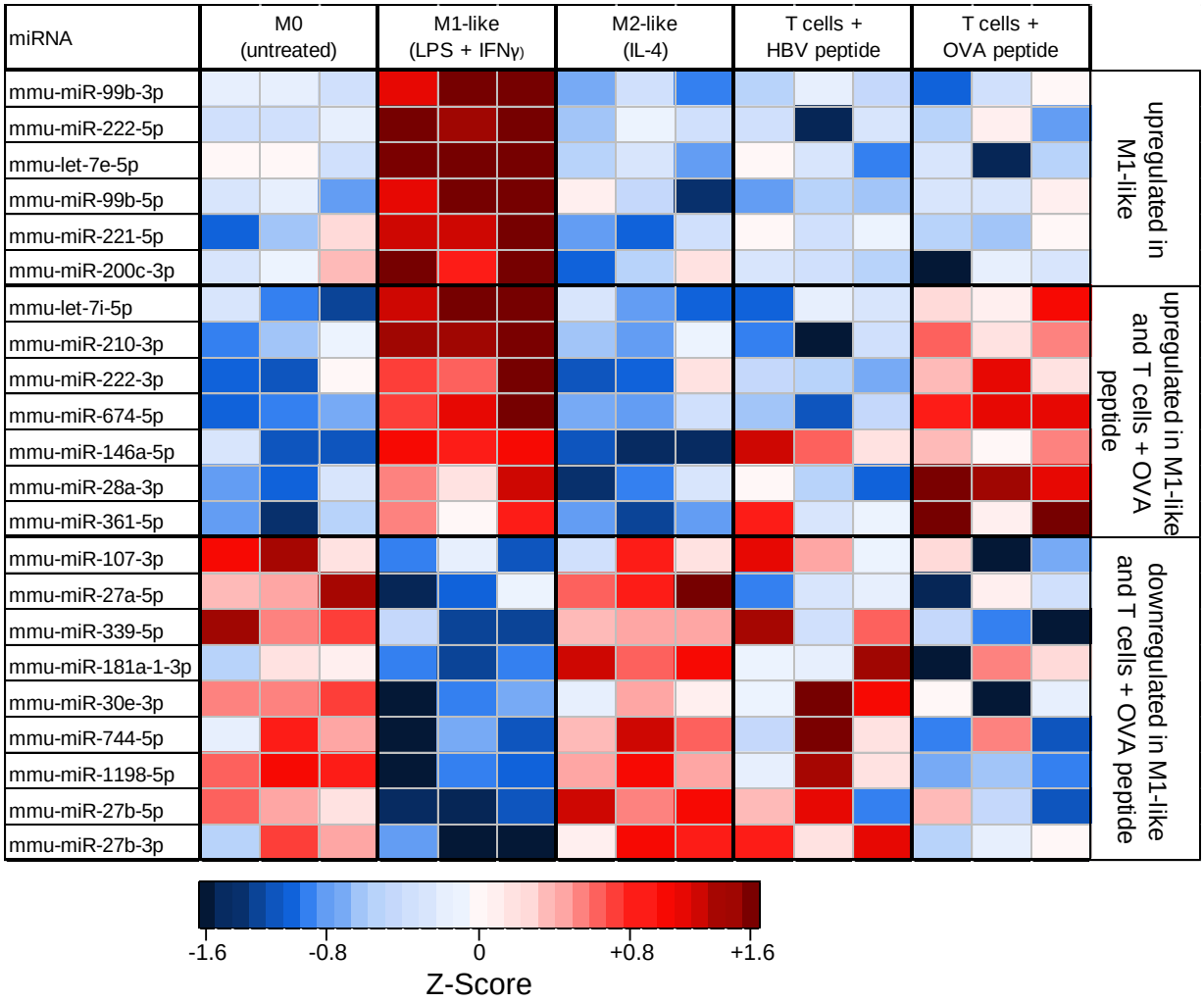

Figure 3.35: Significantly enriched miRNAs in PECs polarized by addition of cytokines or by cognate T cell interaction. The presented data were generated jointly with Franziska Hörhold.

In a last step, several significantly enriched miRNAs were selected for further validation based on their expression levels (base mean) and fold change expression in M1-like vs. untreated and M1-like vs. M2-like (Table 3.3, bold and italicized). miRNAs with a high expression level and high fold changes were preferentially selected as these are most likely the miRNAs causing the strongest changes in macrophage polarization.

Table 3.3: miRNAs significantly enriched in polarized PECs

The presented data were generated jointly with Franziska Hörhold.

miRNA	Base Mean	log(2) fold change		
		M1-like vs. untreated	M1-like vs. M2-like	
mmu-miR-99b-3p	***290,25***	***1.95***	***2.33***	upregulated in M1-like
mmu-miR-222-5p	98,37	0.64	0.65	
mmu-let-7e-5p	***1963,41***	***1.38***	***1.73***	
mmu-miR-99b-5p	***7944,62***	***1.05***	***1.09***	
mmu-miR-221-5p	***4826,18***	***0.81***	***n.a.***	
mmu-miR-200c-3p	156,91	n.a.	0.58	
mmu-let-7i-5p	***315259,46***	***0.47***	***0.45***	upregulated in M1-like and T cells + OVA peptide
mmu-miR-210-3p	***126,49***	***2.64***	***2.56***	
mmu-miR-222-3p	***3672,03***	***0.57***	***0.55***	
mmu-miR-674-5p	***210,19***	***1.9***	***1.64***	
mmu-miR-146a-5p	***27291,59***	***1.74***	***2.26***	
mmu-miR-28a-3p	***1473,67***	***0.47***	***0.52***	
mmu-miR-361-5p	217,77	n.a.	0.46	
mmu-miR-107-3p	98,27	-0.72	n.a.	downregulated in M1-like and T cells + OVA peptide
mmu-miR-27a-5p	2437,14	-0.75	-0.93	
mmu-miR-339-5p	255,71	-0.51	n.a.	
mmu-miR-181a-1-3p	213,54	n.a.	-0.94	
mmu-miR-30e-3p	***1653,18***	***-0.35***	***n.a.***	
mmu-miR-744-5p	***3323,79***	***n.a.***	***-0.67***	
mmu-miR-1198-5p	***4230,84***	***-0.95***	***-0.88***	
mmu-miR-27b-5p	292,09	-0.52	-0.66	
mmu-miR-27b-3p	***174854,19***	***-0.32***	***-0.39***	

n.a. = not available, since this miRNA was not differentially expressed in this comparison

3.3.5.3 Experimental validation of significantly enriched miRNAs

In a last step, the function of six miRNAs (miR-210-3p, miR-674-5p, miR-222-3p, let-7i-5p, miR-146a-5p and miR-28a-3p) which were upregulated in M2-like PECs upon $CD4^+$ T cell co-culture (T cells + OVA peptide) was further investigated. As the same miRNAs were also differentially expressed in M1-like PECs, transfection of these miRNAs in M0 or M2-like PECs might mediate polarization towards a M1-like phenotype.

To investigate changes in PEC polarization upon miRNA transfection, PECs were either left untreated (M0) or polarized into M2-like macrophages for 24 h using IL-4. Subsequently, a pool of the six miRNAs was transfected in which each miRNA had a final concentration of either 10 nM or 20 nM. The induced changes in macrophage polarization were analyzed 48 h post transfection by measuring expression of M1- and M2-associated genes (Figure 3.36). Similar to gene expression analysis after TF knockdown, all data obtained after miRNA transfection were first normalized to the housekeeping gene *Rpl19* and subsequently to expression data obtained from cells treated with transfection reagent only (mock). As

shown in Table 6.2, miR-222-3p was the only miRNA predicted to have a binding site in the 3' UTR region of *Rpl19*. However, as this binding site was only predicted by one out of nine *in silico* prediction tools, *Rpl19* was considered as a suitable housekeeping gene for gene expression analysis following transfection of the six miRNAs.

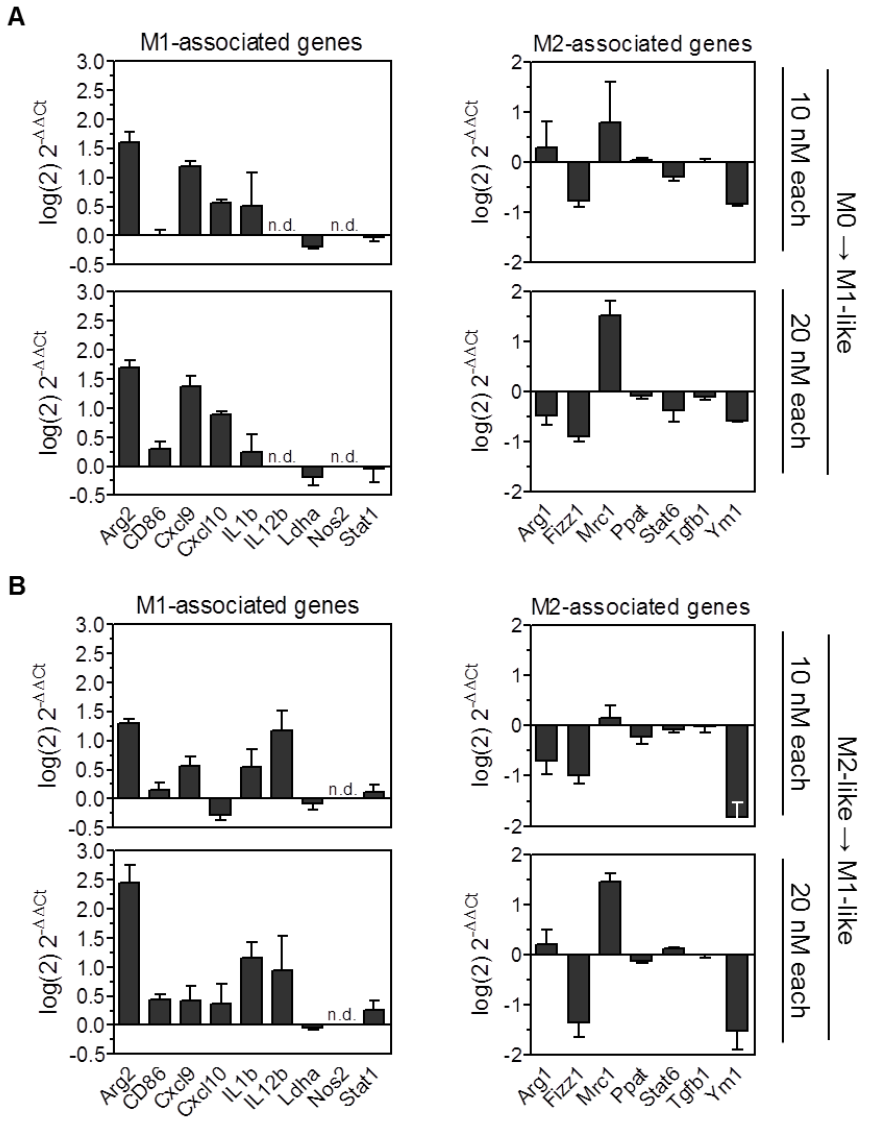

Figure 3.36: miRNA transfection results in M1-associated gene expression.
PECs were either left untreated (A) or polarized for 24 h into M2-like macrophages using IL-4 (B). Subsequently, the cells were transfected with a pool of miRNAs consisting of miR-210-3p, miR-674-5p, miR-222-3p, let-7i-5p, miR-146a-5p and miR-28a-3p, whereby each miRNA has a final concentration of either 10 or 20 nM. The expression of M1- and M2-associated genes was analyzed 48 h post transfection. Error bars represent SD of technical triplicates. One representative out of two similar experiments is shown. n.d. = not detected.

As expected, transfection of the miRNA pool in M0 PECs resulted in strong induction of M1-associated gene expression 48 h post transfection, except for *Ldha* and *Stat1* whose expression was slightly downregulated (Figure 3.36 A, left). Some genes showed higher expression levels after transfection with higher miRNA concentrations (*Cd86, Cxcl9* and *Cxcl10*) whereas expression of other genes decreased (*Il1b*). Expression of *Il12b* and *Nos2* was not detectable. On the other hand, expression of several M2-associated genes was

downregulated upon miRNA transfection being most pronounced when using 20 nM of each miRNA, with *Fizz1* and *Ym1* showing strongest effects (Figure 3.36 A, right). Unexpectedly, expression of *Mrc1* and *Arg1*, both representing typical M2-associated genes, were upregulated upon transfection with the pool containing 10 nM of each miRNA. *Mrc1* was expressed even to higher extend when the miRNA concentration was increased, whereas *Arg1* expression was downregulated. The second approach, in which M2-like PECs were transfected with the pool of miRNAs resulted in similar expression patterns (Figure 3.36 B), with some genes showing higher (*Il1b, Il12b* and *Stat1*) and others showing lower (*Cxcl9, Cxcl10, Fizz1* and *Ym1*) expression (compare to Figure 3.36 A).
In summary, these preliminary data demonstrate the potential of using only a small number of miRNAs to induce detectable changes in PEC polarization. However, additional analysis including cytokine secretion assays, flow cytometry analysis and functional assays are required to get a more comprehensive data set and to draw final conclusions.

3.4 Interaction of OVA specific CD4$^+$ T cells and TAMs

As presented in section 3.3, OVA specific CD4$^+$ T cells can efficiently interact with M2-like PECs inducing their repolarization *in vitro*, although these PECs showed a marked immunosuppressive phenotype and low MHC II expression. In a next set of experiments we investigated whether CD4$^+$ T cell mediated repolarization would also occur among tumor associated macrophages *in vivo*. We therefore transferred OVA specific CD4$^+$ T cells into syngenic M2KO/OVA-F tumor bearing mice and analyzed phenotypical changes of freshly isolated TAMs.

3.4.1 Characterization of TAMs in OVA expressing B16F10 tumors

In a first pilot experiment, B16F10/OVA-F cells expressing the full length OVA were used to determine TAM polarization at different tumor stages. Therefore, tumors generated in C57BL/6 mice upon s.c. injection were harvested and analyzed by flow cytometry either 12 or 14 days post tumor cell inoculation. As shown in Figure 3.37 A, tumors in a later stage (14 days) were larger, whereas tumors in an earlier stage (12 days) were smaller than 1000 mm^3. Tumors in a later stage contained higher proportions of CD206$^+$ (i.e. M2-like) TAMs (F4/80$^+$CD11b$^+$Gr1$^-$), but equal proportions of IA^b positive TAMs (i.e. M1-like) (Figure 3.37 B, left). Of note, the IA^b expression levels of TAMs were strongly reduced in larger tumors (Figure 3.37 B, right), thus pointing towards accumulation of CD206 positive TAMs with reduced IA^b expression in these tumors. The absolute number of TAMs in the whole tumor was significantly higher in late stage tumors (8.6×10^5 cells) with a fold change increase of about 2.5 compared to early stage tumors (3.3×10^5 cells) (Figure 3.37 C). Strikingly, CD206 expressing TAMs increased 4.6 fold whereas IA^b expressing TAMs did only increase 2.3 fold, showing that M2-like TAMs accumulated twice as much compared to M1-like TAMs (Figure 3.37 D).
These results show that TAMs with reduced expression of a typical M1-like marker (IA^b) and increased expression of a well characterized M2-like marker (CD206) are present in higher frequencies and total numbers in late stage B16F10/OVA-F tumors compared to tumors in an earlier stage.

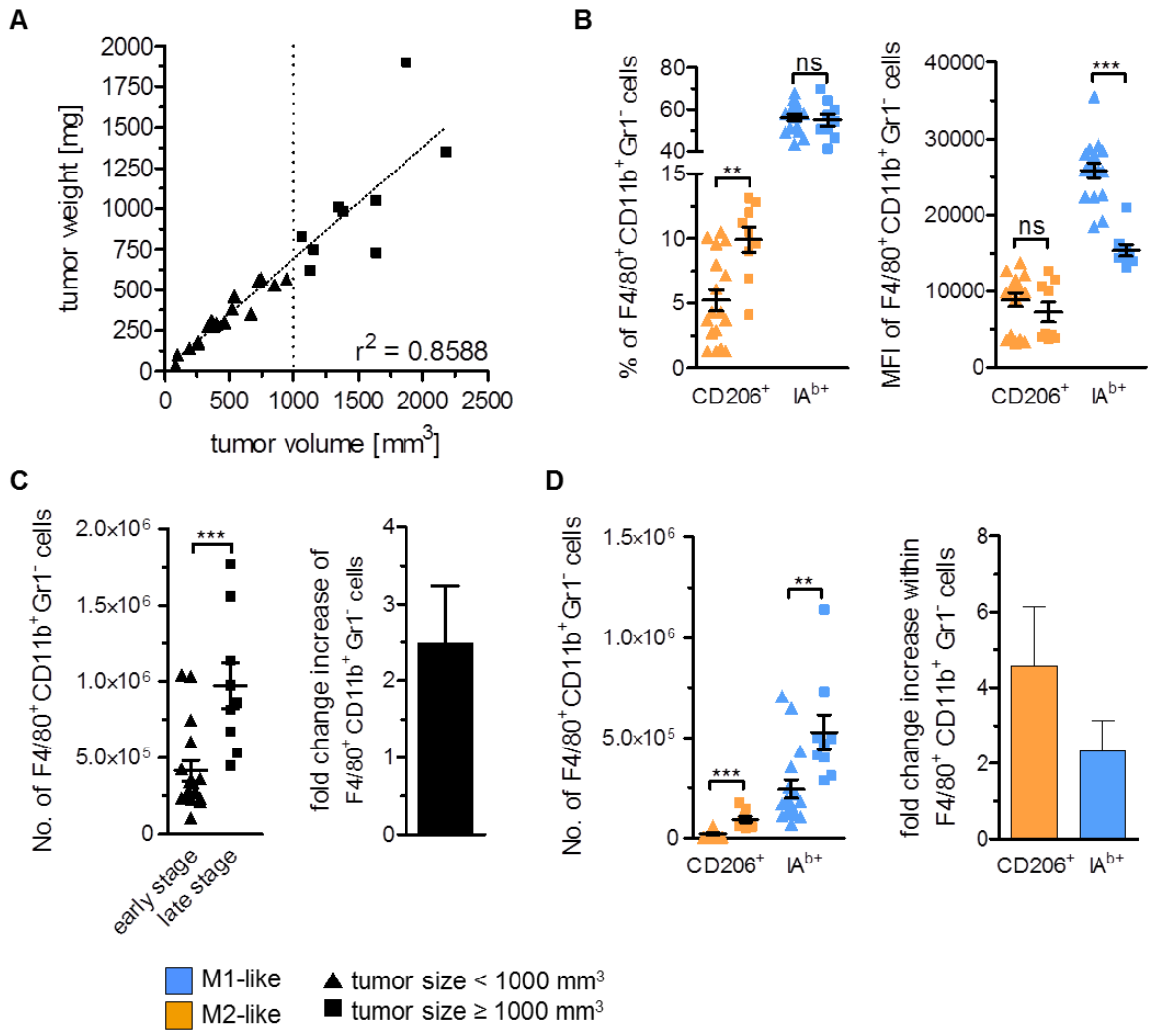

Figure 3.37: Analysis of TAMs in different B16F10/OVA-F tumor stages.
C57BL/6 mice were injected s.c. with 2 x 10^5 B16F10/OVA-F cells. Twelve or 14 days post tumor cell injection, tumors were isolated and analyzed by flow cytometry. **(A)** Correlation between tumor weight and tumor volume of all analyzed tumors. Early and late stage tumors are separated by the vertical dotted line. **(B)** Percentages and median fluorescence intensity values of CD206 and IA^b expressing TAMs. **(C)** Total numbers and fold change increase of TAMs. **(D)** Total numbers and fold change increase of CD206 or IA^b expressing TAMs. Error bars represent SEM within each animal collective. Statistical analysis was done by unpaired Student's *t*-test (95% CI, ns: not significant, * $p \leq 0.05$, ** $p < 0.01$, *** $p \leq 0.001$). Gating strategy: $CD45^+$ → living cells → single cells (FSC-A vs. FSC-H) → $F4/80^+CD11b^+Gr1^-$ → CD206 vs. IA^b.

3.4.2 Peptide loaded TAMs stimulate OVA specific $CD4^+$ T cells *ex vivo*

In the next set of experiments, we assessed the capacity of TAMs to take up B16F10 derived OVA in the tumor microenvironment and present MHC restricted OVA epitopes to OVA specific $CD4^+$ T cells. This process might induce polarization of TAMs into M1-like phenotype thereby facilitating CTL mediated tumor attack (compare detailed explanation in section 1.5).

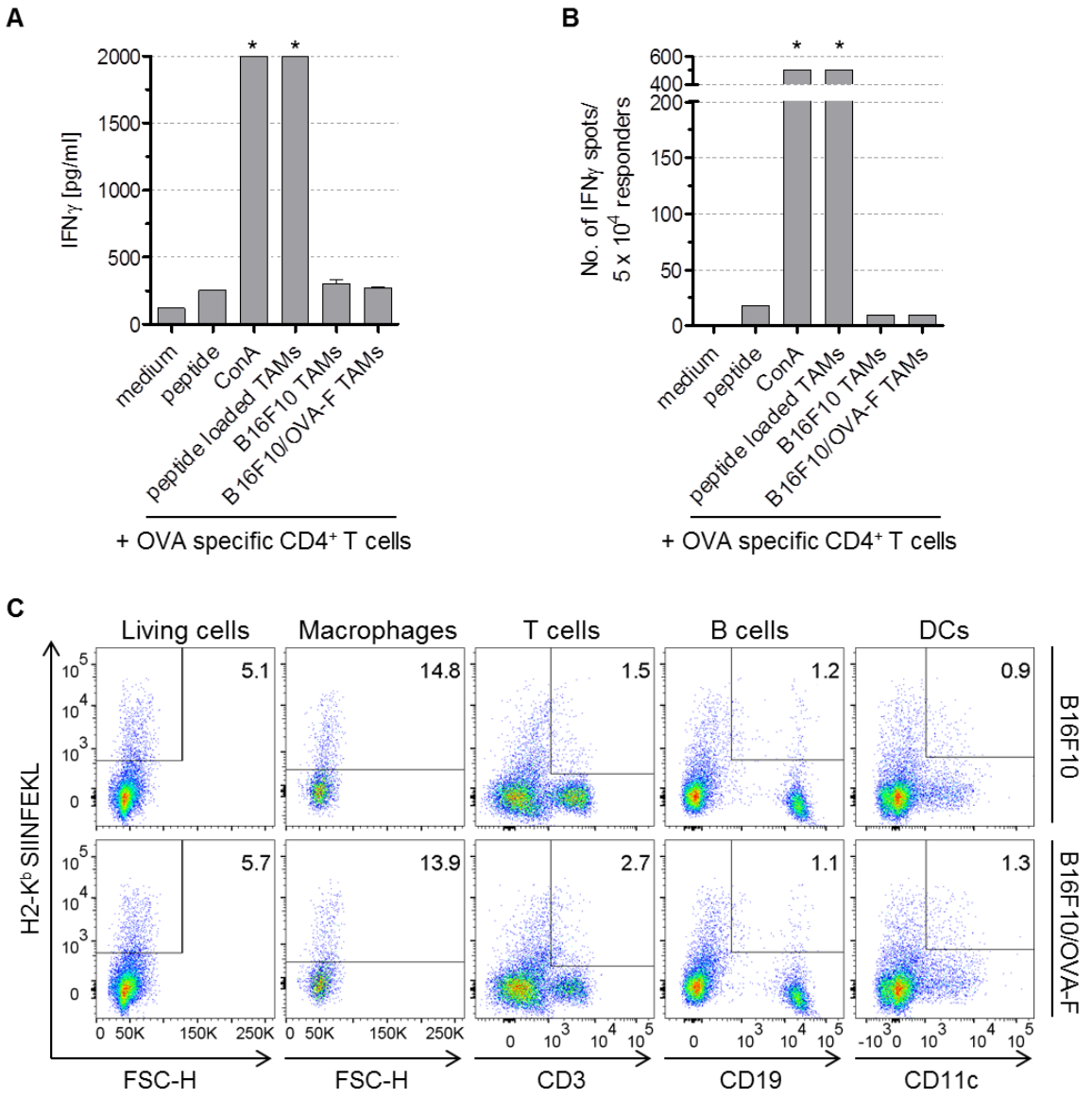

Figure 3.38: Peptide loaded TAMs stimulate OVA specific CD4$^+$ T cells *ex vivo*.
C57BL/6 mice were injected s.c. with either 2 x 10^5 B16F10 or B16F10/OVA-F cells. **(A)** Fourteen days after tumor inoculation, 10^4 TAMs from each tumor were isolated by FACS and co-cultured with the OVA specific CD4$^+$ T cells (1.5 x 10^5 cells). After 48 h, the culture supernatants were collected and analyzed using IFNγ ELISA. As positive controls, B16F10 derived TAMs were loaded with 1 µg/ml IA^b restricted $OVA_{323-339}$ epitope for 1 h prior co-culture (peptide loaded TAMs) or CD4$^+$ T cells were cultured in the presence of 20 µg/ml ConA (ConA). As negative controls, CD4$^+$ T cells were cultured with (peptide) or without (medium) 1 µg/ml $OVA_{323-339}$ peptide. * indicate saturated signal intensity. **(B)** Twelve days post tumor cell injection, 5 x 10^4 TAMs were co-cultured with OVA specific CD4$^+$ T cells (10^5 cells). IFNγ secretion by CD4$^+$ T cells was measured 24 h after co-culture using IFNγ ELISpot assay. Sort strategy: CD45$^+$ → single cells (FSC-A vs. FSC-H) → living cells → F4/80$^+$CD11b$^+$. **(C)** Thirteen days after tumor cell injection, tumors were isolated, stained with monoclonal antibodies and analyzed by flow cytometry. Gating strategy: CD45$^+$ → single cells (FSC-A vs. FSC-H) → living cells → (F4/80$^+$CD11b$^+$) → FSC-H/Marker vs. H2-K^b SIINFEKL.

To investigate OVA engulfment and epitope presentation by TAMs, B16F10 or B16F10/OVA-F tumors were isolated from C57BL/6 mice between 12 and 14 days post tumor cell injection. The tumors were stained using monoclonal antibodies and TAMs were subsequently sorted to perform co-culture experiments with OVA specific CD4$^+$ T cells or analyzed by flow cytometry. As measured by IFNγ ELISA, peptide ($OVA_{323-339}$) loaded

B16F10 derived TAMs stimulated strong IFNγ secretion of OVA specific $CD4^+$ T cells (T cell line established as described in section 2.2.12.1), showing that IA^b expression on TAMs was sufficient to facilitate interaction with CD4 TCRs (Figure 3.38 A). However, co-culturing $CD4^+$ T cells with TAMs from either B16F10 or B16F10/OVA-F tumors in the absence of synthetic peptide resulted in comparable IFNγ concentrations with 304.3 or 270.9 pg/ml, respectively. Similar results were obtained when the experiment was repeated using an IFNγ ELISpot as readout, demonstrating that TAMs sorted from OVA expressing tumors failed to stimulate OVA specific $CD4^+$ T cells (Figure 3.38 B).
In a next attempt, different cell populations in B16F10 and B16F10/OVA-F tumors were analyzed by flow cytometry using a H2-K^b SIINFEKL specific antibody in order to check OVA uptake and MHC I restricted presentation of the CTL epitope SIINFEKL (Figure 3.38 C). Staining of B16F10 tumors resulted in binding of the H2-K^b SIINFEKL antibody to 5.1 % of living cells. The same percentage was detected when the corresponding isotype control antibody was used (data not shown), indicating unspecific binding of the antibody. Staining of OVA-F expressing tumors revealed an increase of 0.6 % H2-K^b SIINFEKL positive cells. Analysis of the individual cell populations showed only a small increase of H2-K^b SIINFEKL expression in $CD3^+$ T cells (1.2 %) and $CD11c^+$ dendritic cells (0.4 %) in B16F10/OVA-F tumors compared to the parental tumors. In contrast, even lower frequencies of H2-K^b SIINFEKL positive cells were observed in B16F10/OVA-F tumors when macrophages (14.8 % vs. 13.9 %) or B cells (1.2 % vs. 1.1 %) were analyzed. Due to the fact that the antibody binds unspecifically and the staining did not result in a clear and separated population, the results should be treated with caution. The same H2-K^b SIINFEKL specific antibody was used to analyze OVA expression in B16F10 OVA transduced clones (see Figure 3.9), demonstrating that the antibody in principle works fine.
In summary, the data demonstrate that peptide pulsed TAMs isolated from B16F10 tumors have the capability to stimulate OVA specific $CD4^+$ T cells (Figure 3.38 A and B). However, TAMs from OVA expressing tumors that were not loaded with IA^b restricted OVA epitope failed to activate OVA specific $CD4^+$ T cells. In addition MHC I restricted OVA epitope presentation by TAMs was not detectable by flow cytometry (Figure 3.38 C).

3.4.3 Infiltration of adoptively transferred $CD4^+$ T cells in B16F10 tumors

As demonstrated in section 3.3.3.2, OVA specific $CD4^+$ T cells facilitated efficient repolarization of peptide pulsed M2-like PECs into immunostimulatory M1-like macrophages *in vitro*. Additionally, TAMs isolated from B16F10 tumors had the capability to stimulate $CD4^+$ T cells *ex vivo* as described in section 3.4.2. Based on these results, a set of experiments were performed to analyze the effects of adoptively transferred OVA specific $CD4^+$ T cells on TAM polarization in tumor bearing C57BL/6 Ly5.1 mice.
Pilot experiments showed that cells of the generated OVA specific $CD4^+$ T cell line (section 2.2.12.1) which was used for co-culture experiments with PECs and TAMs were not able to infiltrate into the tumors and into the draining lymph nodes (dLNs) (data not shown). Thus, $CD4^+$ T cells of TCR transgenic OT-II mice were isolated and pre-activated with either IA^b restricted $OVA_{323-339}$ peptide or CD3/CD28 beads in the presence of IL-2 for 3 days, respectively. To assess the capability of these pre-activated $CD4^+$ T cells to secrete IFNγ upon target cell recognition, an IFNγ ELISpot assay using peptide loaded ($OVA_{323-339}$) 771 B cell lymphoma cells as targets was performed. As shown in Figure 3.39 A, $CD4^+$ T cells pre-activated with peptide or CD3/CD28 beads secreted IFNγ upon co-culture with $OVA_{323-339}$

loaded targets, whereas naïve $CD4^+$ T cells which were freshly isolated from OT-II mice did not. Both pre-activation strategies resulted in highly specific $CD4^+$ T cells only secreting IFNγ in the presence of target cells loaded with IA^b restricted OVA epitope as demonstrated by the included negative controls (T cells only (T cells) and target cells loaded with HBV core antigen control $peptide_{128-140}$ (HBV)). Subsequent analysis of various T cell activation (CD25 and CD44) and adhesion molecules (LFA-1, CD2 and VLA-4) by flow cytometry revealed that at least 96 % of pre-activated $CD4^+$ T cells were positive for all the markers tested (data not shown). All naïve $CD4^+$ T cells (≥ 98.3 %) were stained positive for the adhesion molecules LFA-1, CD2 and VLA-4. In contrast, the percentage of naïve $CD4^+$ T cells expressing CD25 (5.6 %) or CD44 (13 %) was low (data not shown). Analysis of the MFI values revealed a higher expression level of all tested markers on the surface of peptide pre-activated $CD4^+$ T cells compared to CD3/CD28 pre-activated or naïve cells (Figure 3.39 B). For instance, peptide pre-activated $CD4^+$ T cells (MFI: 78522) showed a 35.5 fold higher CD25 (low affinity IL-2 receptor α chain) expression level compared to naïve T cells (MFI: 2213) and a 2.25 fold increase when compared to cells pre-activated with CD3/CD28 beads (MFI: 34802).

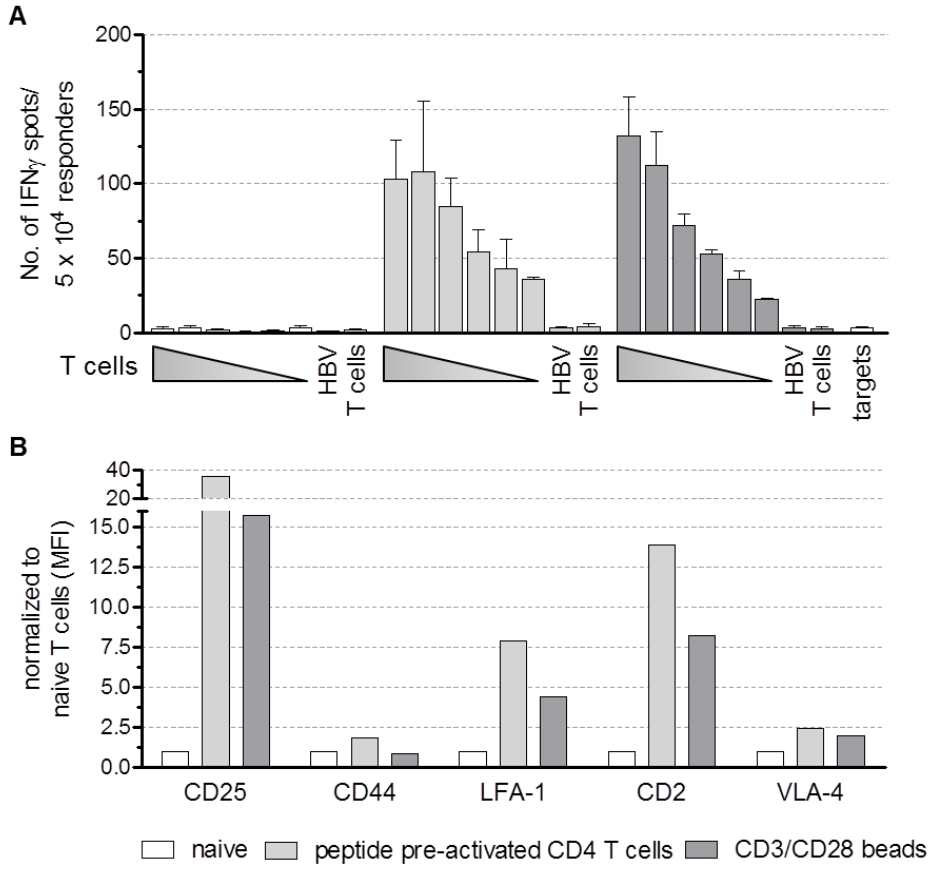

Figure 3.39: Expression of activation markers and specificity of pre-activated OT-II cells.
(A) OT-II splenocytes were isolated and either cultured in the presence of 1 µg/ml IA^b restricted $OVA_{323-339}$ peptide (peptide pre-activated CD4 T cells) or positively selected for $CD4^+$ T cells and incubated with CD3/CD28 beads (CD3/CD28 beads). Three days after incubation, peptide pre-activated $CD4^+$ T cells were purified by positive selection and co-cultured with peptide loaded (1 µg/ml) 771 B cell lymphoma cells (5×10^4) over night. $CD4^+$ T cells pre-activated with CD3/CD28 beads were co-cultured without any further purification. IFNγ secretion was detected by IFNγ ELISpot assay. For comparison, freshly isolated OT-II splenocytes underwent positive CD4 selection and were included in the assay (naive). The highest T cell number used within the assay was 2.5×10^4 followed

by serial 1:2 dilutions. Error bars represent SD of technical triplicates. **(B)** $CD4^+$ T cells were stained with monoclonal antibodies specific for T cell activation markers as well as adhesion molecules and subsequently analyzed by flow cytometry. MFI values of the positive populations were normalized to the corresponding MFI value obtained for naive T cells. Gating strategy: single cells (FSC-A vs. FSC-H) → living cells → $CD3^+$ → $CD4^+CD8^-$ → marker vs. FSC-H.

In a next step, the infiltration of OVA specific $CD4^+$ T cells into B16F10/OVA-F tumors, draining lymph nodes (dLNs) and spleens was analyzed. Therefore, 5×10^6 pre-activated or naïve $CD4^+$ T cells were injected i.v. into B16F10/OVA-F tumor bearing mice ten days after tumor cell injection (Figure 3.40 A). Four days later, tumors, spleens and dLNs were harvested to prepare single cell suspensions for subsequent flow cytometry analysis. The cells were stained using monoclonal antibodies specific for the congenic markers CD45.1 or CD45.2, facilitating differentiation between adoptively transferred ($CD45.2^+$) and endogenous $CD4^+$ T cells ($CD45.1^+$). As shown in the upper panel of Figure 3.40 B, the percentage of adoptively transferred $CD4^+$ T cells ($CD3^+CD4^+CD45.2^+$) in spleens and dLNs was significantly higher when mice received peptide pre-activated T cells compared to CD3/CD28 pre-activated or naïve T cells. Most importantly, the percentage of $CD45.2^+$ T cells within the $CD3^+CD4^+$ cell population in tumors of mice that received peptide pre-activated $CD4^+$ T cells (35.2 %) was 3 fold higher compared to mice that received CD3/CD28 pre-activated cells (12.5 %). Naïve $CD4^+$ T cells only accounted for 3 % of all $CD3^+CD4^+$ cells detected in the tumors. Thus, the capacity of the T cells to infiltrate into the different organs and the tumor correlated with the surface expression level of the tested activation and adhesion molecules (compare to Figure 3.39 B).
The absolute quantification demonstrated that around 1.5×10^6 peptide pre-activated $CD4^+$ T cells reached the spleen, whereas only 6.2×10^4 had the capability to infiltrate into the tumors (Figure 3.40 B, lower panel). However, this absolute number is still higher compared to the number of CD3/CD28 pre-activated (1.4×10^4) or naïve $CD4^+$ T cells (3.2×10^4) that reached the tumor.
In summary, these results demonstrate the importance of upregulating activation and adhesion markers by T cell pre-activation to enable T cell infiltration into tumors. The peptide pre-activated $CD4^+$ T cells showed superior tumor infiltration capacity compared to CD3/CD28 pre-activated or naïve T cells and were used for subsequent experiments.

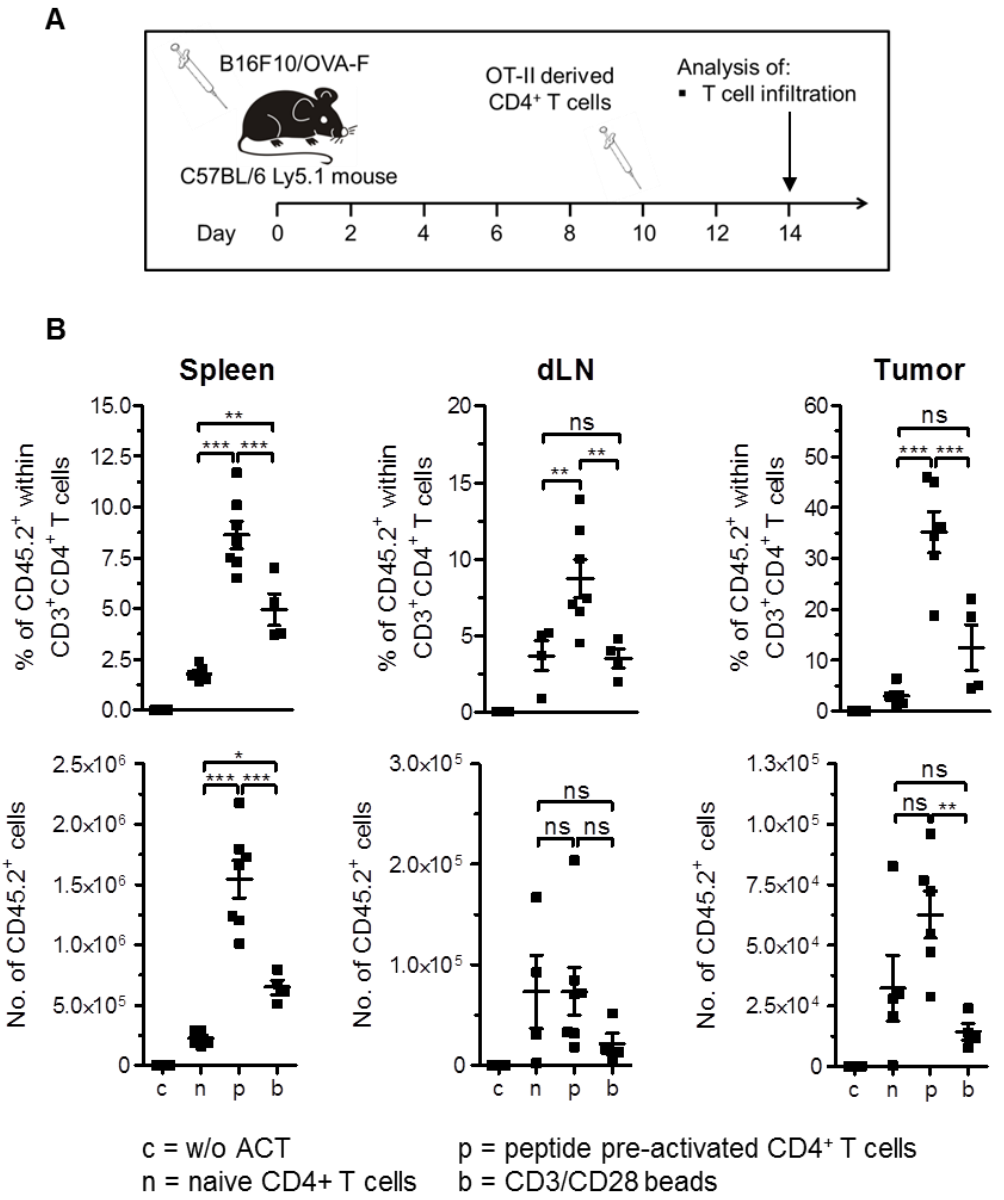

Figure 3.40: Infiltration of adoptively transferred OVA specific CD4$^+$ T cells into spleens, dLNs and tumors of B16F10/OVA-F tumor bearing mice.
(A) Experimental workflow: C57BL/6 Ly5.1 mice (n = 5-7) were injected s.c. with 2 x 10^5 B16F10/OVA-F cells. Ten days after tumor inoculation, mice were injected i.v. with 5 x 10^6 OVA specific CD4$^+$ T cells obtained from OT-II splenocytes. CD4$^+$ T cells were either injected without pre-activation (naïve = n) or after incubation with 1 µg/ml $OVA_{323-339}$ peptide (peptide = p) or CD3/CD28 beads (CD3/CD28 beads = b) for 3 days. Mice that did not receive any T cells served as control groups (w/o ACT = c). Infiltration of CD45.2$^+$CD4$^+$CD8$^-$ cells into spleens, dLNs and tumors was analyzed by flow cytometry four days after adoptive cellular therapy. **(B)** Infiltration of adoptively transferred T cells into spleens, dLNs and tumors presented as percentage of CD45.2$^+$ within CD3$^+$CD4$^+$ cells (upper panel) or as total cell numbers (lower panel). Error bars represent SEM within each animal collective. Significance was determined using One-way ANOVA with post-hoc Tukey test (95% CI, ns: not significant, * p ≤ 0.05, ** p < 0.01, *** p ≤ 0.001). Gating strategy: CD45$^+$ → living cells → single cells (FSC-A vs. FSC-H) → CD3$^+$CD4$^+$ → CD45.1 vs. CD45.2.

3.4.4 Adoptive transfer of specific $CD4^+$ T cells affects TAM phenotype

Within the next experiments the polarization of TAMs in OVA expressing B16F10 tumors upon transfer of OVA specific $CD4^+$ T cells was analyzed. Therefore, C57BL/6 Ly5.1 mice were injected with the IA^b deficient, OVA-F expressing B16F10 clone (M2KO/OVA-F). Ten days post tumor cell injection, peptide pre-activated $CD4^+$ T cells were injected i.v. and T cell infiltration as well as TAM polarization was analyzed four days later (Figure 3.41 A). As shown in Figure 3.41 B, the tumor bearing mice were distributed into two groups with equal mean tumor sizes prior adoptive T cell transfer (Day 10), thereby avoiding differences in TAM polarization between these groups due to different tumor sizes. Mice within the control group (c = w/o adoptive cellular therapy (ACT)) did not receive T cells, whereas mice of the second group were injected with 5×10^6 peptide pre-activated $CD4^+$ T cells (p). Tumor weight measurement of harvested tumors on day 14 revealed a lower mean tumor weight in mice treated with T cells (546 mg) compared to control mice (640 mg). Analysis of TILs ($CD45^+$) from these tumors showed that on average 2.7×10^4 transferred T cells ($CD4^+CD8^-$ $CD45.2^+$) had reached the tumor, thereby representing 19.3 % of the $CD4^+CD8^-$ TIL compartment (Figure 3.41 C). In contrast, no $CD45.2^+$ cells were detected in tumors from control mice. Deeper analysis of the TIL compartment demonstrated equal frequencies of TAMs ($F4/80^+CD11b^+Gr1^-$) in both groups (c = 34.2 % and p = 32.1 %) (Figure 3.41 D, left). However, the frequency of $CD206^+$ TAMs (Figure 3.41 D, middle) as well as the CD206 surface expression intensity (Figure 3.41 D, right) of these cells was significantly decreased in tumors of mice adoptively transferred with peptide pre-activated $CD4^+$ T cells. At the same time, IA^b surface expression was significantly enhanced on TAMs from tumors of treated mice compared to tumors from control mice (Figure 3.41 D, right), although the overall frequency of IA^b positive TAMs was unchanged between both groups of mice (Figure 3.41 D, middle). No correlation between the percentage of transferred $CD4^+$ T cells and the percentage of CD206 ($r^2 = 0.13$) or IA^b ($r^2 = 0.0$) expressing TAMs within the tumors of treated mice was detected. Thus, tumors harboring high numbers of transferred $CD4^+$ T cells are not necessarily showing lower percentages of $CD206^+$ cells or higher percentages of IA^{b+} cells. Nevertheless, these data indicate that adoptive transfer of $CD4^+$ T cells can induce polarization of TAMs towards a M1-like phenotype. As shown in supplementary Figure 6.7, comparable results were obtained when $CD4^+$ T cells were transferred into C57BL/6 Ly5.1 mice bearing an OVA expressing pancreatic tumor (PDAC/OVA-F). However, no changes in TAM polarization upon T cell transfer were detected if the breast cancer model EO771/OVA-F was used (supplementary Figure 6.8).

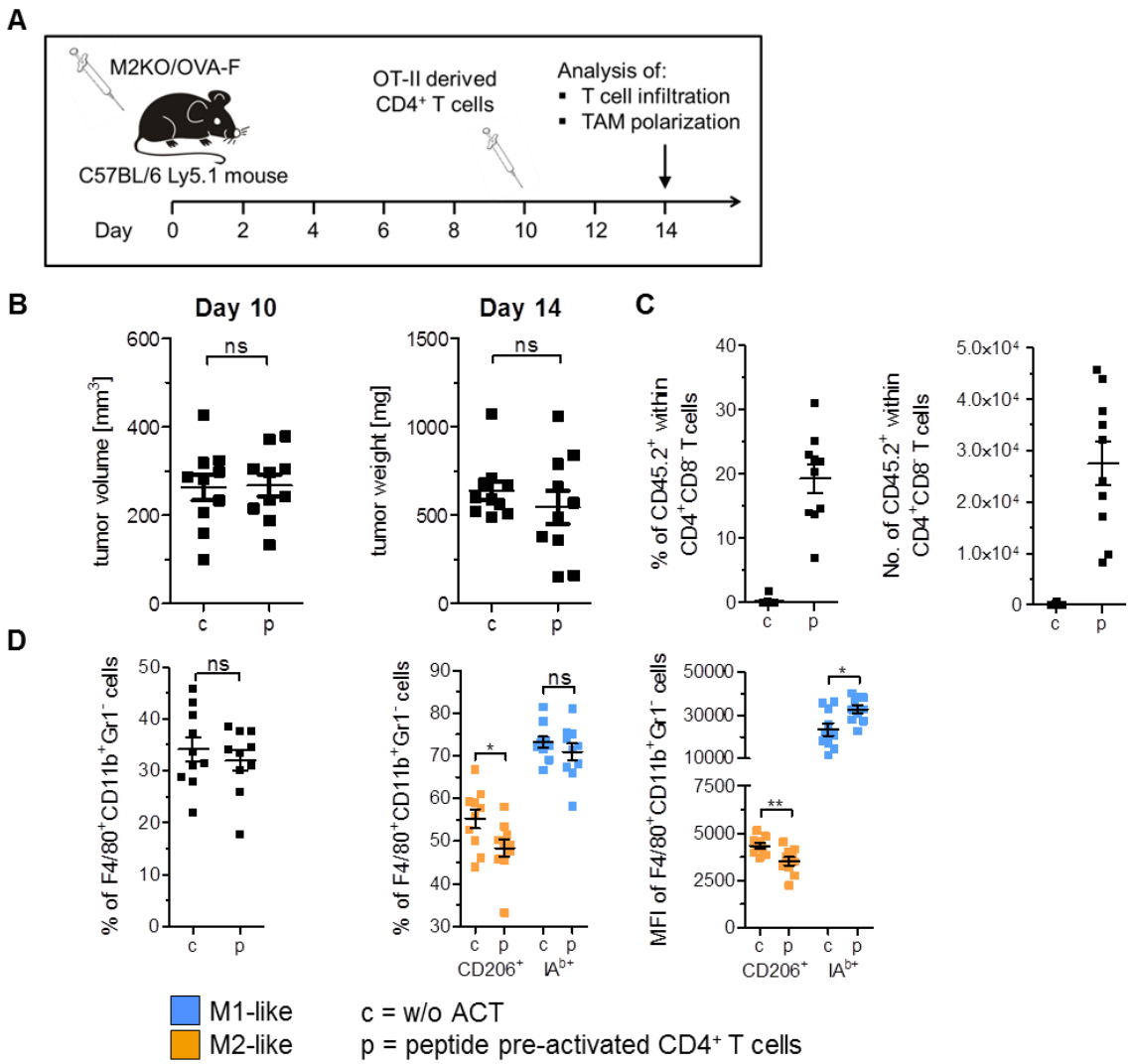

Figure 3.41: Polarization of TAMs in M2KO/OVA-F tumors after adoptive transfer of OVA specific CD4$^+$ T cells.
(A) Experimental workflow: C57BL/6 Ly5.1 mice (n = 10) were injected s.c. with 2 x 10^5 M2KO/OVA-F cells. Ten days post tumor inoculation mice were injected i.v. with 5 x 10^6 peptide pre-activated OVA specific CD4$^+$ T cells. Mice were sacrificed on day 14 and tumors were analyzed by flow cytometry. Control mice (c) did not receive CD4$^+$ T cells. **(B)** Tumor volume and tumor weight 10 and 14 days after tumor cell injection, respectively. **(C)** Infiltration of adoptively transferred T cells into tumors presented as percentage of CD45.2$^+$ within CD4$^+$CD8$^-$ cells or as total numbers within tumors. Error bars represent SEM within each animal collective. Gating strategy: CD45$^+$ → living cells → single cells (FSC-A vs. FSC-H) → CD4$^+$CD8$^-$ → CD45.1 vs. CD45.2. **(D)** Percentages of TAMs (F4/80$^+$CD11b$^+$Gr1$^-$) within CD45$^+$ cells as well as percentages and MFI values of CD206 and IA^b expressing cells within TAMs are shown. Error bars represent SEM within each animal collective. Statistical analysis was done by unpaired Student's *t*-test (95% CI, ns: not significant, * p ≤ 0.05, ** p < 0.01, *** p ≤ 0.001). Gating strategy: CD45$^+$ → living cells → single cells (FSC-A vs. FSC-H) → F4/80$^+$CD11b$^+$Gr1$^-$ → CD206 vs. IA^b.

In a next step, the aforementioned experiment was repeated using the M2KO clone instead of M2KO/OVA-F cells to investigate whether the observed changes in TAM polarization were OVA dependent (Figure 3.42 A). As shown in Figure 3.42 B, the mean tumor volumes of the two groups was almost identical 10 days post tumor cell injection, with 334.8 mm^3 in the control group (c) and 338.6 mm^3 in the treated group (p). Similar to the observation of the first experiment (Figure 3.41 B), M2KO tumor bearing mice treated with CD4$^+$ T cells

(631.8 mg) showed a slightly lower mean tumor weight compared to the control group (754.5 mg) four days post adoptive T cell transfer (Figure 3.42 B, right). As shown in Figure 3.42 C (left) the percentage of infiltrated transferred $CD4^+$ T cells in M2KO tumors (22.1 %) was as high as in M2KO/OVA-F tumors (19.3 %). However, the average absolute number of transferred $CD4^+$ T cells reaching the M2KO tumors (1.5×10^4) was significantly lower compared to M2KO/OVA-F tumors (2.7×10^4) (Figure 3.42 C, right). Most importantly, the differences in TAM polarization observed in M2KO/OVA-F tumors upon adoptive transfer of OVA specific $CD4^+$ T cells were not detectable in TAMs from M2KO tumors lacking OVA expression as demonstrated in Figure 3.42 D.

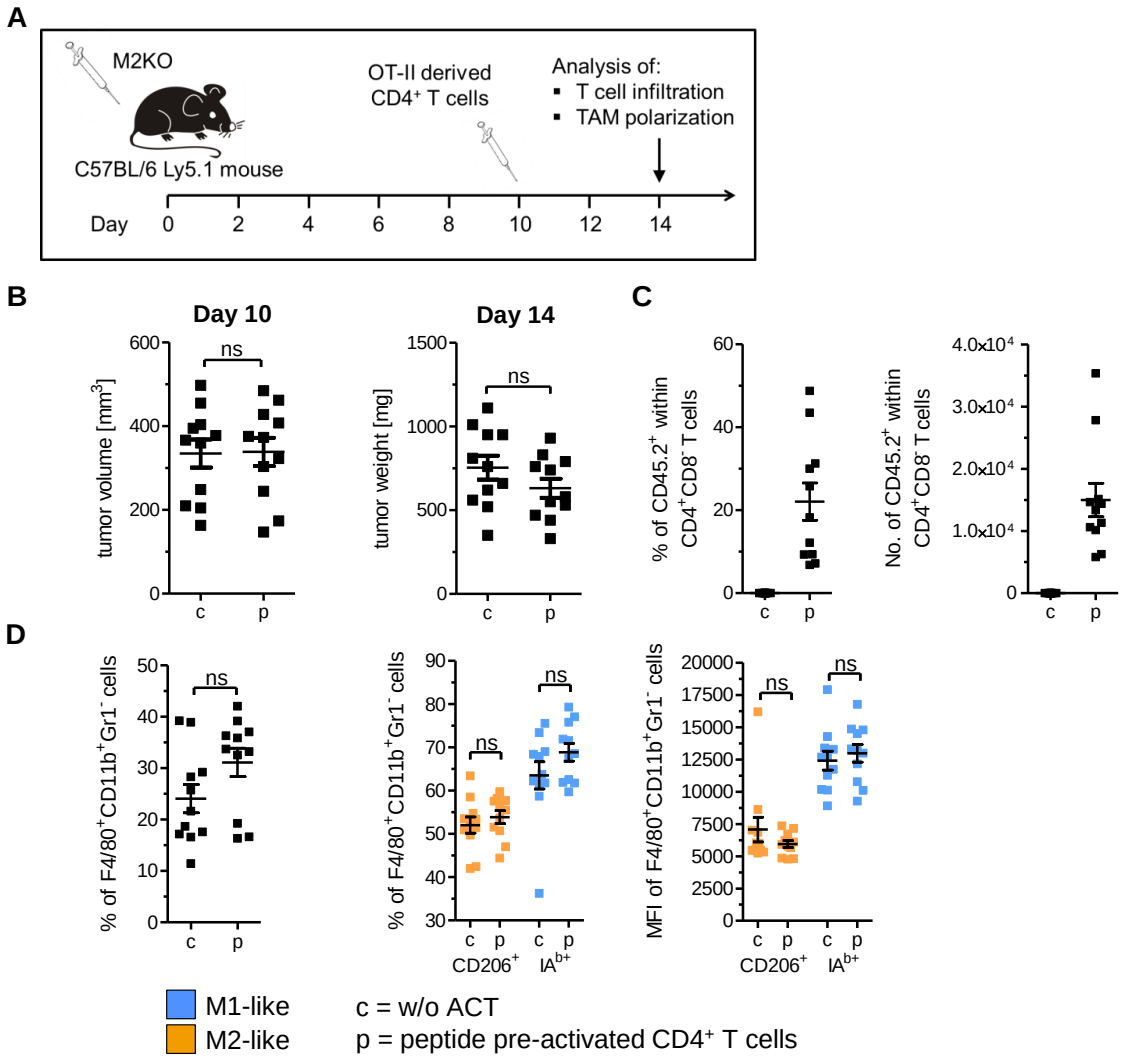

Figure 3.42: Polarization of TAMs in M2KO tumors after adoptive transfer of OVA specific $CD4^+$ T cells.
(A) Experimental workflow: C57BL/6 Ly5.1 mice (n = 11) were injected s.c. with 2×10^5 M2KO cells. Ten days post tumor injection mice were injected i.v. with 5×10^6 peptide pre-activated OVA specific $CD4^+$ T cells. Mice were sacrificed on day 14 and tumors were analyzed by flow cytometry. Control mice (c) did not receive $CD4^+$ T cells. **(B)** Tumor volume and tumor weight 10 and 14 days after tumor cell injection, respectively. **(C)** Infiltration of adoptively transferred T cells into tumors presented as percentage of $CD45.2^+$ within $CD4^+CD8^-$ cells or as total numbers within tumors. Error bars represent SEM within each animal collective. Gating strategy: $CD45^+$ → living cells → single cells (FSC-A vs. FSC-H) → $CD4^+CD8^-$ → CD45.1 vs. CD45.2. **(D)** Percentages of TAMs ($F4/80^+CD11b^+Gr1^-$) within $CD45^+$ cells as well as percentages and MFI values of CD206 and IA^b expressing cells within TAMs are shown. Error bars represent SEM within each animal collective. Statistical analysis was done by

unpaired Student's *t*-test (95% CI, ns: not significant, * $p \leq 0.05$, ** $p < 0.01$, *** $p \leq 0.001$). Gating strategy: $CD45^+$ → living cells → single cells (FSC-A vs. FSC-H) → $F4/80^+CD11b^+Gr1^-$ → CD206 vs. IA^b.

Finally, TAMs of M2KO/OVA-F tumors were sorted four days after adoptive T cell transfer for subsequent RNA isolation and gene expression analysis by qPCR (Figure 3.43 A). The average tumor volume and tumor weight 10 and 14 days after tumor cell injection, respectively, was similar between the two groups (Figure 3.43 B). As shown in Figure 3.43 C (left), treatment of M2KO/OVA-F tumor bearing mice with pre-activated OVA specific $CD4^+$ T cells upregulated expression of M1-associated genes, with *Arg2, Il1b, Cd86, Cxcl10* and *Nos2* expression being significantly increased compared to TAMs of control mice. Expression of the other M1-associated genes *Stat1, Cxcl9* and *Il12* did not change upon $CD4^+$ T cell transfer. In contrast, no significant up- or downregulation was detected for any of the tested M2-associated genes (Figure 3.43 C, right).

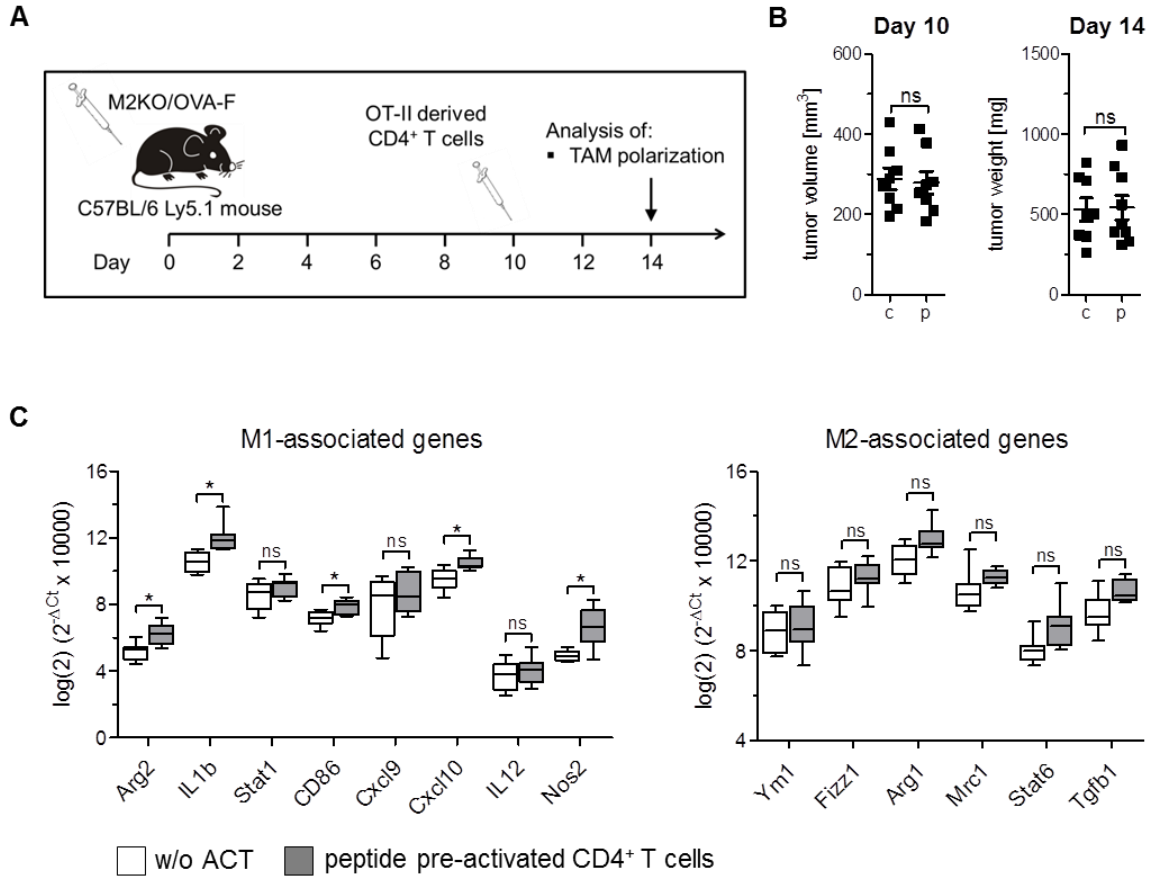

Figure 3.43: Gene expression analysis of TAMs in M2KO/OVA-F tumors after adoptive transfer of OVA specific $CD4^+$ T cells.
(A) Experimental workflow: C57BL/6 Ly5.1 mice (n = 10) were injected s.c. with 2 x 10^5 M2KO/OVA-F cells. Ten days post tumor inoculation mice were injected i.v. with 5 x 10^6 peptide pre-activated OVA specific $CD4^+$ T cells. Mice were sacrificed on day 14 and RNA of sorted TAMs ($F4/80^+CD11b^+Gr1^-$) was isolated to perform qPCR. Control mice (c) did not receive $CD4^+$ T cells. **(B)** Tumor volume and tumor weight 10 and 14 days after tumor cell injection, respectively. **(C)** Gene expression analysis of sorted TAMs. The data were normalized to Rpl19 expression level which served as housekeeping gene. The box and whiskers plots extend from the smallest to the largest values and show the median, the 25th as well as 75th percentiles. Significance was determined using unpaired Student's *t*-test with Bonferroni-Holm p-value correction (95% confidence interval (CI), ns: not significant, * $p \leq 0.05$, ** $p < 0.01$, *** $p \leq 0.001$). Sort strategy: $CD45^+$ → single cells (FSC-A vs. FSC-H) → living cells → $F4/80^+CD11b^+Gr1^-$.

In summary, these results show that the adoptive transfer of $CD4^+$ T cells can repolarize immunosuppressive M2-like macrophages into M1-like macrophages with increased expression levels of M1-associated genes. These effects are dependent on the presence of OVA-F, as changes in macrophage polarization were not observed in the microenvironment of OVA negative tumors. As the tumor cell line is deficient in MHC II expression, a direct activation of adoptively transferred OVA specific $CD4^+$ T cells by $OVA_{323-339}$ presenting B16F10 cells can be excluded. Instead, these results suggest a cognate interaction between APCs which took up OVA-F and presented IA^b restricted OVA epitopes to the transferred $CD4^+$ T cells that in turn became activated and secreted IFNγ, thereby changing macrophage polarization.

4 Discussion

4.1 Generation of IA^b deficient B16F10 cells using the CRISPR/Cas9 system

Parts of the following paragraph have been taken from reference [307] and were originally written by myself. The CRISPR/Cas9 based technology was demonstrated to outperform other genome editing strategies such as zinc finger nucleases (ZFNs) or transcription activator-like effector nucleases (TALENs) in frequency and precision [328]. The Cas9 nuclease in combination with a single guide RNA targeting the gene of interest was already applied in various settings and resulted in high knockout (KO) efficiencies. Transfection of haploid embryonic stem cells with ten-eleven translocation methylcytosine dioxygenase 1 (Tet1) targeting guide RNAs achieved a knockout efficiency of 50 % [329]. Yu and colleagues even demonstrated a 100 % KO efficiency after injecting a guide RNA and *in vitro* transcribed Cas9 mRNA in *Drosophila* embryos [330]. The KO efficiencies of our five IA^b targeting guide RNAs ranged from 13.2 % to 45.6 %, indicating that the on-target mutagenesis is highly dependent on the guide RNA sequence (Figure 3.3). Similar variations in the efficiencies of guide RNAs have been reported in several other studies. Targeting of the β_2 microglobulin (B2M) gene in HEK293T cells was reported to ablate B2M surface expression in 7 % to 48 % of transfected cells depending on the guide RNA [331]. Another study was using two guide RNAs to target the AAVS1 locus in HEK293T cells, human chronic myelogenous leukemia K562 cells and human induced pluripotent stem cells and demonstrated varying target gene KO rates of 10 % to 25 %, 13 % to 38 % and 2 % to 4 %, respectively [332]. The understanding of the relationship between on-target activity and the sequence characteristics of a certain guide RNA still remains limited. However, recent studies demonstrated that the nucleotide composition (e.g. GC content) and the secondary structure of a guide RNA as well as the genomic context of the target site (besides the well-established importance of the protospacer adjacent motif (PAM) sequence) are features which are associated with DNA cleavage efficiency [333, 334].

Our functional *in vitro* analysis clearly showed that our finally selected IA^b KO clone had lost susceptibility to recognition by $CD4^+$ T cells (Figure 3.5). The absence of MHC II did not alter the tumor growth behavior *in vivo* when compared to the parental B16F10 cell line (Figure **3.5**). Even though we did not observe any phenotypical changes of our generated KO clones, we cannot rule out any off-target mutations induced by one of the guide RNAs. Single and double mismatches of guide RNAs have been reported to occur at varying frequencies dependent on their position within the guide RNA/DNA duplex. Of note, studies using human cell-based reporter assays revealed that some off-target sites have comparable mutagenesis frequencies than the once detected at the on-target site [335]. We maximized specificity of our guide RNAs by selecting guide sequences with high on-target scores and at least 3 base pair mismatches to any predicted off-target sequence in the genome. Several strategies to reduce off-target mutagenesis and increase Cas9 specificity have been developed. The use of truncated guide RNAs (<20 nucleotides in length) was shown to result in fewer cleavages at off-target sites without reducing on-target editing efficiencies [336]. Kleinstiver and colleagues developed Cas9 variants harboring amino acid exchanges at DNA contact sites. These so called high fidelity Cas9 nucleases reduced off-target events and retained on-target activities comparable to WT Cas9 [337]. Other authors

generated fusion proteins composed of catalytically inactive Cas9 and FokI nuclease (fCas9). As a consequence, the induction of DNA double-strand breaks requires the association of two fCas9 fusion proteins binding their respective target sites (15 or 25 base pairs apart from each other) [338]. DNA cleavage using this strategy is dependent on simultaneous binding of two guide RNAs to their respective target sites, thereby reducing undesired off-target modifications. A similar approach is implemented by mutating the nuclease domains of Cas9 to create DNA "nickases" which introduce single-strand instead of double-strand breaks [339]. Thus, the use of paired Cas9 nickases, both binding specifically to their respective target site is required for cooperative genome editing and to induce double-strand breaks. Ran and colleagues demonstrated a 50 – 1000 fold reduction of off-target activity in different cell lines when paired Cas9 nickases were used compared to WT Cas9 [339]. In contrast to the aforementioned techniques, Cas9 nickases generate sticky ends instead of blunt ends making them an attractive tool for subsequent gene integration.

Our analysis of CRISPR/Cas9 (guide #4) induced mutations in the finally selected IA^b KO clone revealed the same 11 bp deletion in all tested bacterial colonies (Table 3.1). As the parental cell line B16F10 has been shown to be near tetraploid, we would have expected to identify four different mutations (one mutation on each chromosome 17 on which the H2-Ab1 gene is located). However, fluorescence *in situ* hybridization (FISH) of the IA^b KO clone using mouse chromosome 17 painting probes demonstrated a marked chromosomal instability which resulted in a variety of hybridization patterns (data not shown; FISH analysis was done by CHROM*BIOS*, Nußdorf, Germany). In most of the cells, three intact copies of chromosome 17 and a small translocated segment of chromosome 17 close to the centromere of an unidentified chromosome were observed. In the other cells, additional variations of chromosome 17 were detected which included a fusion of two chromosomes, two copies of the translocated chromosome, an additional abnormal chromosome, only two copies of the chromosome or cells with four copies of the chromosome. These data suggest that our selected IA^b KO clone had only a single chromosome 17 at the time of guide RNA transfection, thus resulting in a single mutation. Subsequent culturing of the clone provided advantageous conditions for chromosome duplications and translocations as observed in the FISH analysis. Even though the interpretation of the mutation analyses has not yet been clarified, the CRISPR/Cas9 system has proven to be an efficient and straight forward strategy to generate murine MHC II KO cell clones which represent an ideal tool to investigate anti-tumor $CD4^+$ T cell responses that function independently of MHC surface expression by the tumor.

4.2 Establishment of OVA and luciferase expressing B16F10 clones

Ovalbumin (OVA) is a non-inhibitory serpin representing the major protein found in egg white [340]. The identification of MHC I [341] and MHC II [342] restricted T cell epitopes and the availability of T cell receptor transgenic mice for both OVA specific $CD4^+$ (OT-II mice) [342, 343] and $CD8^+$ T cells (OT-I mice) [344] have made it an attractive model antigen to analyze antigen-specific immune responses in C57BL/6 mice. The native, full length OVA contains a signal peptide (amino acids 22 – 48) which is not cleaved and facilitates membrane translocation by forming an amphipathic hairpin structure [315, 345]. Most studies investigating antigen-specific immune responses against OVA expressing tumor cells make

use of the secreted, full length OVA protein, thereby neglecting the fact that most tumor-associated antigens are not secreted under physiological conditions. Within this study we were aiming for the clarification of whether anti-tumor $CD4^+$ T cell responses are dependent on secreted antigen or not. Therefore, we generated B16F10 clones expressing either the full length, secreted OVA (OVA-F) or a truncated version of OVA (OVA-T) lacking the signal peptide (not secreted). The different clones generated from transduced B16F10 cells expressed OVA-F and OVA-T in variable quantities as demonstrated by qPCR analysis (Figure 3.6). Moreover, the presence of full length OVA in whole cell protein samples as well as in culture supernatants was confirmed by Western blot analysis (Figure 3.10). However, OVA-T was only detected after blocking proteasomal degradation, indicating a rapid turnover of the truncated protein due to the lacking signal peptide (Figure 3.10). Indeed, several studies reported similar results and even determined the half-life of OVA-T and OVA-F. In whole cell protein samples of HEK293T cells and DCs transduced with OVA encoding lentiviral vectors, Western blot analysis revealed a strong signal of OVA-F at the expected protein size [346]. In contrast, the truncated version of OVA, lacking the first 48 amino acids, was almost not detected. Shen and colleagues generated stable fibroblast transfectants expressing either OVA-F or OVA-T and performed pulse-chase experiments after ^{35}S metabolic labeling [347]. They found that the full length OVA protein had a half-life of around 280 min. In contrast, OVA-T had a half-life of only 40 min, suggesting a rapid degradation as observed in our experiments. All OVA transduced clones gave rise to tumors after s.c. injection into C57BL/6 mice in our study. However, the tumor growth was significantly delayed compared to the parental B16F10 cell line (except for B16F10/OVA-T) (Figure 3.11). The expression of the xenogenic antigen OVA by murine tumor cells was shown to be associated with delayed tumor growth in several studies [348, 349]. Moreover, Gilfillan and colleagues demonstrated a rejection of MC-38/OVA tumors in an antigen dependent manner mediated by endogenous $CD8^+$ T cells [350].

In a next step, the OVA expressing B16F10 clones were transduced with luciferase encoding retroviral particles which allows subsequent tumor growth monitoring by *in vivo* bioluminescence imaging. After injecting the different luciferase expressing clones into C57BL/6 mice we observed remarkable differences in tumor growth (Figure 3.13). Reduced tumor growth was accompanied by higher luciferase expression levels (Figure 3.12). In addition, 4 out of 5 luciferase expressing EO771 clones were completely rejected after s.c. injection into C57BL/6 mice, whereas the parental cell line showed a continuous tumor growth (data not shown). The growing EO771/OVA clone had a significantly lower luciferase expression than the rejected clones (data not shown). Similar result were already reported [351] and indicate an immune mediated rejection of luciferase expressing tumors in immunocompetent mice. The identification of luciferase specific CD8 T cell epitopes and the presence of luciferase specific $CD8^+$ T cells in C57BL/6 mice support this assumption [352].

4.3 Generation of an OVA specific $CD4^+$ T cell line

The generation of murine antigen specific T cell lines usually involves the immunization of mice with the respective antigen in combination with an adjuvant. In this study we immunized C57BL/6 mice s.c. with the IA^b restricted OVA epitope$_{323-339}$ in combination with complete Freund's Adjuvant. The culture of splenocytes from immunized mice in the presence of

synthetic IA^b restricted OVA peptide resulted in IFNγ release by activated OVA specific $CD4^+$ T cells, indicating successful *in vivo* T cell priming (Figure 3.14). In contrast, no OVA specific $CD4^+$ T cells were detected *ex vivo* among splenocytes of mice immunized with the IA^b restricted OVA epitope core sequence (aa 329 – 337 [316]), suggesting that application of the core sequence was not sufficient to induce T cell priming *in vivo*. The splenocytes of mice immunized with the epitope core sequence died after several days of culturing in the presence of the respective peptide and IL-2. In contrast, immunization with OVA $epitope_{323-339}$ and subsequent culturing for several weeks allowed the generation of a polyclonal, OVA specific $CD4^+$ T cell line. Moreover, we generated two additional OVA specific $CD4^+$ T cell lines by culturing splenocytes from TCR transgenic OT-II mice in the presence of IA^b restricted OVA $epitope_{323-339}$ or CD3/CD28 Dynabeads. The T cell cultures were restimulated every 4 weeks by adding irradiated syngeneic feeder cells together with antigenic peptide. As all $CD4^+$ T cells in OT-II mice express the same OVA specific TCR recognizing IA^b restricted OVA $epitope_{323-339}$, an OVA specific $CD4^+$ T cell line can be generated without the need of *in vivo* immunization. The three $CD4^+$ T cell lines showed a high degree of specificity for the IA^b restricted OVA epitope and equal numbers of activated T cells (i.e. secreting IFNγ) upon co-culture with peptide loaded 771 B cell lymphoma cells, demonstrating that the different strategies to generate a $CD4^+$ T cell line worked equally well (Figure 3.15). However, staining with monoclonal antibodies specific for CD3, CD4 and CD8 revealed high frequencies of double negative ($CD4^-CD8^-$) $CD3^+$ T cells in both T cell lines generated from OT-II splenocytes (Figure 3.15). In contrast, 99.9 % of $CD3^+$ T cells of the T cell line generated through peptide immunization of C57BL/6 mice were $CD4^+CD8^-$. Of note, double negative $CD3^+$ T cells were already observed in freshly isolated splenocytes of OT-II mice (data not shown), a phenomenon which was to my knowledge not explicitly reported yet. However, flow cytometry stainings of OT-II splenocytes using CD4 and CD8 specific antibodies were shown in different studies and at least indicate the presence of double negative T cells (as the authors do not comment on their gating strategy it is difficult to interpret the data) [353, 354]. Moreover, high frequencies of abnormal T cell populations, such as double negative T cells have been detected in the periphery and secondary lymphoid tissues of T cell receptor transgenic mice [355]. Boehmer and colleagues described a double negative T cell lineage in HY-transgenic mice which was thymus dependent but did not require positive selection for emigration from the thymus [356]. Even though the origin of this T cell lineage is still not completely understood, these results suggest that the expression of a TCR transgene influences thymocyte development and probably affect the different selection processes involved in T cell differentiation.

4.4 Phenotypic and functional analysis of *in vitro* polarized PECs

Macrophages are a subset of myeloid cells that show phenotypic and functional plasticity. Depending on the environmental signals they can differentiate in M1-like and M2-like macrophages which are involved in a variety of processes such as tumor growth inhibition and promotion, respectively. Even though the concept of classically (M1) and alternatively (M2) macrophages is generally accepted, the two polarization states should only be considered as two extremes within a spectrum of phenotypes. In this study, the two phenotypes of polarized macrophages were comprehensively analyzed by gene and protein expression analysis as well as functional assays. As a source of macrophages we used

thioglycolate elicited peritoneal exudate cells (PECs) which were already used in a variety of studies investigating macrophage polarization [357]. Flow cytometry analysis of PECs revealed surface expression of CD11b and F4/80 on more than 99 % of the cells, making these cells suitable for subsequent analysis of macrophage polarization (Figure 3.16).

Our gene expression analysis confirmed successful polarization of PECs upon treatment with LPS/IFNγ or IL-4 (Figure 3.17). Treatment of PECs with IL-4 decreased the expression of M1-associated genes and induced expression of M2-associated genes within 4 h of stimulation. On the other hand, LPS/IFNγ treatment upregulated expression of the entire M1-associated gene panel within 4 h of stimulation. A similar expression pattern has been described already for LPS treated murine PECs [358]. As expected, no M2-associated marker expression was observed upon stimulation with LPS/IFNγ, except for *Il10* and *Arg1* whose expression was transiently upregulated after 4 h or 24 h, respectively. Even though expression of arginase 1 is typically associated with alternative macrophage polarization, several studies reported that both macrophage phenotypes express the enzyme, albeit in different amounts. IL-4 or IL-13 mediated arginase 1 expression in alternatively activated macrophages requires binding of STAT6 to an enhancer element of the arginase 1 gene [359]. In contrast, intracellular bacteria have been shown to promote arginase 1 expression in chronically infected M1-like macrophages through STAT6 independent TLR pathways [360]. Sonoki and colleagues demonstrated that the expression of arginase 1 in rat peritoneal macrophages was induced in a CCAAT/enhancer-binding protein beta (C/EBPβ) dependent manner upon treatment with LPS [361]. In accordance with our results, arginase 1 expression was shown to be induced more slowly than *Nos2* expression and reached a maximum 12 h post LPS treatment. Interestingly, comparable results have been reported for LPS treated murine PECs in which arginase activity increased even up to 4 days [362]. In summary, these data suggest that arginase 1 expression is induced in classically activated macrophages to decrease arginine availability for *Nos2*, thereby avoiding overproduction of nitric oxide which is toxic to host tissues.

Due to its immunosuppressive properties, IL-10 is mainly associated with M2-like macrophages. However, IL-10 expression is controlled by various signaling pathways and was reported to be present also in M1-like macrophages, albeit in lower levels compared to M2-like macrophages. Similar to the data we obtained, LPS treatment of murine PECs was shown to induce *Il10* expression after 6 h of culturing [363], but was significantly downregulated compared to untreated PECs upon stimulation for 48 h [357]. Indeed, MyD88 and TRIF dependent TLR signaling, including LPS induced TLR4 signaling were reported to induce IL-10 production in bone marrow-derived macrophages (BMMs) [364]. Following TLR stimulation, activation of extracellular signal-regulated kinase (ERK) and p38 is required for inducing *Il10* expression in macrophages [365]. IL-10 can act in a negative feedback loop to regulate its own production by inducing dual specificity protein phosphatase 1 (DUSP1) expression. DUSP1 inactivates the kinase p38 by dephosphorylation, thereby limiting IL-10 production [366]. In addition, IFNγ signaling was shown to inhibit ERK and p38 dependent IL-10 production in macrophages [367]. Taken together, the described signaling events taking place in macrophages upon stimulation with LPS and IFNγ explain the transient upregulation of *Il10* within the first 24 h of stimulation. Further, the observation that IFNγ can inhibit IL-10 production and that IL-10 acts in a negative feedback loop to reduce its own expression might explain *Il10* downregulation after extended stimulation periods.

4.5 Repolarization of M2-like macrophages by CD4$^+$ T cells

4.5.1 Reprogramming of M2-like PECs by CD4$^+$ T cells *in vitro*

Having observed that external addition of cytokines polarizes PECs *in vitro*, we next assessed whether cognate interaction with CD4$^+$ T cells would induce IFNγ secretion by T cells and instruct PECs to acquire a M1-like phenotype. Repolarization of M2-like macrophages by CD4$^+$ T cells was already demonstrated in principle with peptide loaded macrophages *in vitro* [368]. In a study from Heusinkveld and colleagues, the authors polarized human peripheral blood derived macrophages towards a M2-like phenotype by culturing them with culture supernatant of cervical cancer cell lines. Afterwards, they co-cultured peptide-pulsed M2-like macrophages with different HPV specific CD4$^+$ T cell clones which resulted in T cell activation accompanied by secretion of IFNγ. The co-cultured macrophages expressed high levels of M1-like associated genes (*Cd86, Cd83* and *Il12*) and secreted only low amounts of IL-10, indicating a polarization towards the M1-like phenotype. However, our analyses of macrophages upon cognate interaction with CD4$^+$ T cells was more comprehensive and included detailed gene and protein expression analyses as well as functional assays.

In a first step we showed that peptide loaded IL-4 induced M2-like PECs are susceptible to the recognition by OVA specific CD4$^+$ T cells (Figure 3.22). Our data demonstrated that M2-like PECs were significantly less susceptible to CD4$^+$ T cell recognition compared to M1-like macrophages, which is at first glance in line with the low MHC II surface expression observed on M2-like PECs. However, M2-like PECs were also less susceptible to CD4$^+$ T cell recognition than untreated macrophages, even though they had a slightly higher IA^b surface expression. These results indicate that besides the amount of MHC II surface expression, further parameters impact on the T cell susceptibility of macrophages. Indeed, M2-like macrophages are known to impair T cell activity by a variety of mechanisms such as the release of immunosuppressive cytokines (e.g. IL-10 and TGF-β). Moreover, M2 polarized macrophages overexpress the tryptophan degrading enzyme IDO1, thereby depriving T cells of tryptophan and suppressing their activation and proliferation [185]. The expression of arginase 1 by M2-like macrophages further inhibits antigen-specific T cell responses by depriving the cells of the semi-essential amino acid L-arginine [188]. We could demonstrate that M2-like PECs efficiently induced IFNγ secretion by CD4$^+$ T cells, despite their immunosuppressive phenotype. Next, we showed that M2-like macrophages can be instructed to acquire a M1-like phenotype upon cognate interaction with CD4$^+$ T cells (section 3.3.3.2). Peptide-pulsed M2-like PECs co-cultured with CD4$^+$ T cells in the presence of OVA peptide showed a strong upregulation of M1-associated markers when compared to M2-like PECs loaded with control peptide or to PECs cultured without T cells (Figure 3.23). In contrast, most of the M2-associated genes were downregulated (with the exception of *Arg1* and *Il10*) when compared to M2-like PECs cultured with irrelevant peptide. As discussed above (section 4.4), the upregulation of the two immunosuppressive molecules IL-10 and arginase 1 can be explained at least in part by the signaling events taking place during macrophage repolarization. The IFNγ concentration in the supernatants of cultures that had included the OVA specific T cell epitope was increased 210 fold compared to supernatants from co-cultures with irrelevant epitope (HBV), suggesting that IFNγ release by activated T cells represents the key mediator for macrophage repolarization. Besides

detecting successful repolarization of M2-like PECs by comprehensive gene and protein expression analyses, we could also observe a switch towards M1-like functionality. M2-like PECs co-cultured with $CD4^+$ T cells in the presence of relevant peptide showed a lower phagocytic capacity than PECs from the two control groups (Figure 3.24). Taken together, these results clearly show that cognate interaction with $CD4^+$ T cells can instruct M2-like PECs to acquire M1-like phenotype and function.

4.5.2 Characterization of TAMs in Ova expressing B16F10 tumors

We showed that OVA expressing B16F10 tumors in a later stage of development contain higher proportions of $CD206^+$ (i.e. M2-like) TAMs with significantly reduced IA^b expression levels compared to tumors in an earlier stage of development (Figure 3.37). These results are in accordance with the assumption that macrophages infiltrating into the tumor microenvironment are exposed to a variety of cytokines released by tumor cells or stroma cells, inducing their polarization into an immunosuppressive M2-like phenotype [180, 181]. In a next set of experiments, we wanted to show that TAMs from OVA expressing tumors took up the secreted OVA and present IA^b restricted epitopes to $CD4^+$ T cells. This was already demonstrated in principle in a myeloma tumor model secreting immunoglobulin L chain V region (detailed explanation of these studies are given in section 4.5.3) [210, 211]. However, in our tumor model TAMs isolated from OVA expressing tumors could not activate OVA specific $CD4^+$ T cells to a higher extend than TAMs isolated from OVA negative parental tumors (Figure 3.38). This was not due to a lack of MHC II surface expression, as we could demonstrate that peptide pulsed TAMs isolated from B16F10 tumors have the capability to stimulate OVA specific $CD4^+$ T cells, showing that IA^b expression on TAMs was sufficient to facilitate interaction with CD4 TCRs (Figure 3.38). However, our results do not necessarily mean that the secreted OVA was not taken up and processed by TAMs. As isolation of TAMs from B16F10 tumors by MACS separation yielded insufficient purity, we were dependent on performing fluorescence activated cell sorting. Therefore, the tumors were enzymatically digested for 1 h at 37 °C using collagenase D, DNAse I and TLCK which might affect peptide/MHC complex stability. Subsequently, the cell suspensions were stained with monoclonal antibodies and resuspended in FACS buffer. As the TIL infiltration in B16F10 tumors is low, each tumor sample was sorted for at least 1 h to obtain a sufficient number of TAMs. Thus, the sorted macrophages were not in contact with dying or OVA secreting tumor cells within the last hours before performing the co-culture experiment, suggesting that already dissociated peptide or internalized peptide/MHC complexes cannot be replaced by new OVA epitope binding IA^b molecules during that time. It has been reported that the dissociation half-life of peptide/MHC II complexes can vary between 30 min and several days [369]. The predicted IC_{50} value of the IA^b restricted OVA peptide (aa 323-339; ISQAVHAAHAEINEAGR) using the NetMHCII algorithm is 339.4 nM, showing that 339.4 nM of this peptide are sufficient to inhibit 50 % of a reference peptide binding [370]. Peptides with binding affinities below 50 nM are usually considered as strong binders [371], as it is more likely that these peptides remain bound to the respective MHC II molecule. Thus, the IA^b restricted OVA epitope can be considered as a weak binder, which is probably associated with a shorter half-live of the peptide/MHC complex. Therefore, the assumed short half-life of OVA epitope MHC II complexes and the absence of OVA before the co-culture assay might explain our observations.

4.5.3 Reprogramming of M2-like TAMs by adoptive CD4$^+$ T cell transfer

Finally, we investigated whether TAA specific CD4$^+$ T cells would mediate a repolarization of TAMs in IA^b deficient B16F10 tumors. This was already demonstrated in principle using s.c. injected, Matrigel embedded MOPC315 myeloma cells in an Id-specific T cell receptor transgenic immunodeficient mouse model. The severe combined immunodeficiency (SCID) mice, in which the CD4$^+$ T cells recognize a MHC II restricted tumor-specific peptide (Id) derived from the secreted immunoglobulin L chain of MOPC315 myeloma cells, have been shown to reject s.c. injected MOPC315 cells. As MOPC315 cells lack the expression of MHC II they are not a direct target of Id-specific CD4$^+$ T cells. Nevertheless, the anti-tumor effects have been reported to be CD4$^+$ T cell mediated, as the tumor rejection was not dependent on the presence of B cells or CTLs [372]. Ten years after the generation of the TCR transgenic SCID mouse system, Corthay and colleagues demonstrated that Id-specific CD4$^+$ T cells become activated upon co-culture with MOPC315 derived TAMs *in vitro*, thus showing that the macrophages took up the secreted TAA and presented TAA derived peptides [210]. Further, the authors detected IFNγ secretion by Id-specific CD4$^+$ T cells upon interaction with TAMs *in vivo* and subsequent upregulation of MHC II surface expression on TAMs. Finally, the authors could show that MOPC315 tumor rejection was mediated by a collaboration of macrophages and TAA specific CD4$^+$ T cells. This study nicely demonstrated that TAMs can activate IFNγ secretion by endogenous Id-specific CD4$^+$ T cells *in vivo* but did not further investigate changes in macrophage polarization. However, in a follow-up study a few years later, the authors used the same transgenic mouse model and observed CD4$^+$ T cell mediated polarization of TAMs towards a tumoricidal M1 phenotype secreting proinflammatory cytokines (IL-6, IL-1β, CXCL9 and CXCL10) [211]. Even though *in vitro* cultured MOPC315 cells lack the expression of MHC II, they might induce surface expression under certain *in vivo* conditions which would facilitate direct tumor cell killing by CD4$^+$ T cells. By repeating some of the above mentioned experiments using MHC II deficient MOPC315 cells, Tveita and colleagues demonstrated that tumor rejection was not dependent on MHC II expression on tumor cells, thereby further supporting the indirect CD4$^+$ T cell mediated tumor cell killing [373]. In another study, the authors injected a mixture of TAA positive and TAA negative MOPC315 cells into the TCR transgenic mice to investigate whether the indirect tumor cell killing mediated by CD4$^+$ T cells would also result in bystander killing of TAA negative MOPC315 cells [374]. The authors frequently observed an outgrowth of TAA negative tumor cells, even in the presence of large excess of TAA positive cells. They further demonstrated that the CD4$^+$ T cell/Macrophage mediated tumor cell killing is restricted to areas of TAA positive MOPC315 cells, thus allowing the escape of TAA negative tumor cells. Moreover, it was reported that some TAA positive MOPC315 tumor cells persist in a dormant state and eventually grow out to form tumors [375]. The authors demonstrated that these tumor cells could escape by impairing indirect TAA antigen presentation by macrophages through modulating the quaternary structure of the TAA.

Taken together, these studies demonstrated that endogenous TAA specific CD4$^+$ T cells can indirectly mediate tumor rejection by polarizing macrophages in an “artificial” tumor microenvironment (Matrigel containing cytokines such as CCL2, CXCL9, IL-15, IL-18, LIF, VEGF, TGFβ) using TCR transgenic immunodeficient mice. In contrast, we are the first who comprehensively investigate TAM polarization in a “natural” TME upon adoptive transfer of OVA specific CD4$^+$ T cells into tumor bearing immunocompetent mice.

The absolute quantification of tumor infiltrated lymphocytes upon adoptive T cell transfer revealed that only a very small number of transferred $CD4^+$ T cells reached the tumor (Figure 3.40). Indeed, it is well known that tumor cells exert a variety of mechanisms to exclude T cells from the TME. Tumor cells can secrete the proangiogenic factor VEGF, which is at least in part responsible for the establishment of an abnormal tumor vasculature, thereby impairing T cell trafficking into the TME [376, 377]. Blocking the VEGF/VEGFR axis by anti-VEGF antibodies was reported to normalize the tumor vasculature and increase the infiltration of adoptively transferred T cells into B16 tumors [378]. Further, Klug and colleagues showed that neoadjuvant local low-dose gamma irradiation stimulated iNOS expression in TAMs which induced vascular normalization and facilitated enhanced T cell recruitment [212]. Besides modulating the vasculature, tumor cells can build up physical (e.g. collagen deposits) as well as metabolic (anaerobic glucose poor environment) barriers which inhibit T cell migration and T cell functionality, respectively [379]. Genetically engineered T cells, expressing tumor-specific chemokine receptors might overcome these barriers. Indeed, transduction of CAR T cells with the chemokine receptor CCR2b was demonstrated to result in significantly higher T cell infiltration into the TME of CCL2 secreting tumor cells [380].

Even though only a low number of transferred T cells reached the M2KO/OVA tumors in our experiments, we could demonstrate that the adoptive transfer of $CD4^+$ T cells mediated a repolarization of immunosuppressive M2-like TAMs into M1-like macrophages with decreased CD206 surface expression and increased expression levels of M1-associated genes (*Arg2, Il1b, Cd86, Cxcl10* and *Nos2*) (Figure 3.41 and Figure 3.43). Moreover, we showed that these effects are dependent on the presence of OVA, as changes in macrophage polarization were not observed in the microenvironment of OVA negative tumors (Figure 3.42). A direct activation of adoptively transferred OVA specific $CD4^+$ T cells by $OVA_{323-339}$ presenting B16F10 cells can be excluded as we were using our established IA^b deficient tumor cell line. Instead, our results suggest a cognate interaction between APCs which took up OVA and presented IA^b restricted OVA epitopes to the transferred $CD4^+$ T cells that in turn became activated and secreted IFNγ, thereby changing macrophage polarization. As macrophages are present within the TME of M2KO/OVA tumors in high frequencies (Figure 3.41) and typically have a high phagocytic capacity (especially M2-like macrophages as demonstrated in Figure 3.21), we assume that these cells could be particularly important in presenting OVA epitopes (as illustrated in Figure 4.1).

However, so far we cannot rule out that also other APCs, such as B cells and DCs take up OVA and present IA^b restricted epitopes to transferred $CD4^+$ T cells. The role of DCs in presenting TAAs is well known and several studies reported that DCs can take up TAAs and present MHC I and MHC II restricted TAAs derived epitopes to $CD8^+$ and $CD4^+$ T cells, respectively [381-383]. In contrast, it is still unclear whether B cells are physiologically relevant APCs in the TME. Peptide-pulsed (SIINFEKL) B cells injected in syngeneic C57BL/6 mice have been reported to induce OVA specific T cell tolerance [384]. Another study demonstrated that the presence of B cells blocked an anti-tumor response *in vivo* after vaccination with irradiated tumor cells [385]. However, as soon as resting B cells become activated by $CD4^+$ T cells through CD40-CD40L interaction, they upregulate the surface expression of co-stimulatory molecules and MHC molecules. These B cells have an enhanced capacity to present antigenic peptides and to activate T cells and might play a role

in presenting TAAs in the TME [386, 387]. Thus, more comprehensive analyses are required to investigate the individual contribution of the different APCs in mediating TAM repolarization.

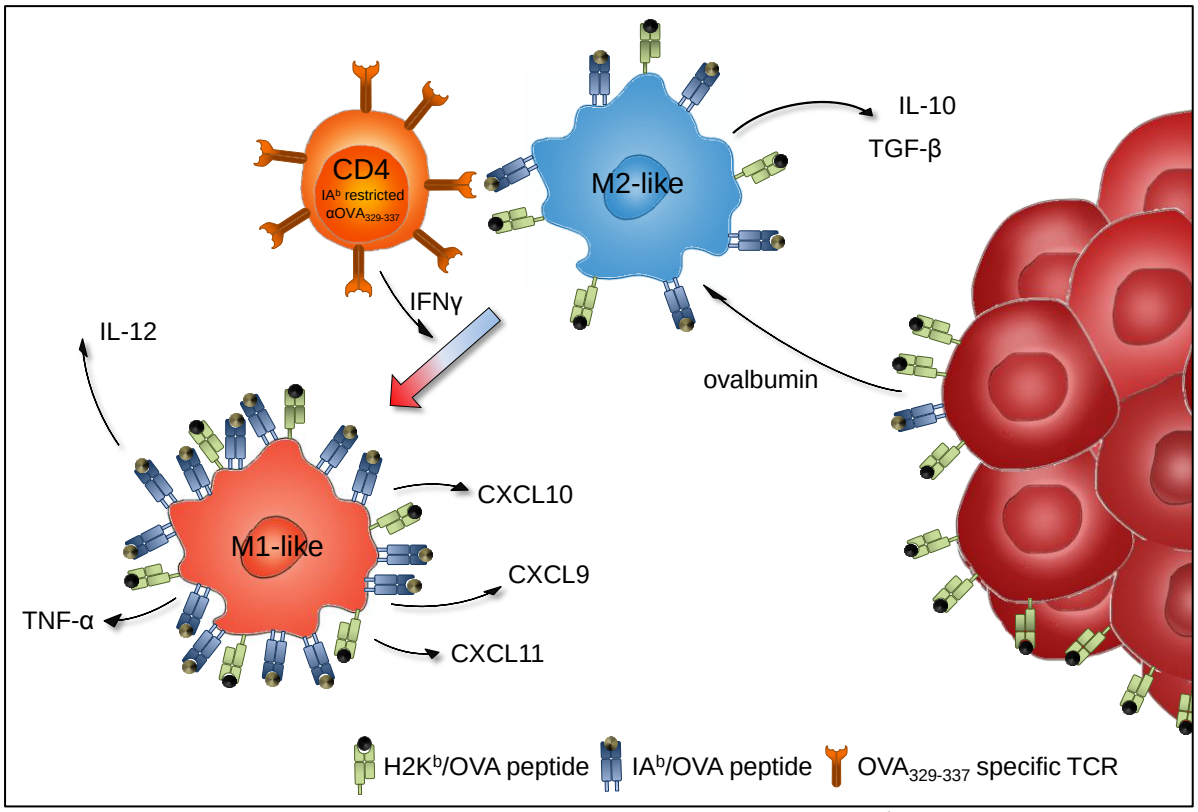

Figure 4.1: Proposed model of TAM repolarization upon adoptive CD4$^+$ T cell transfer. B16F10 cells (dark red) are injected subcutaneously into C57BL/6J mice to induce tumor growth. Tumor infiltrating M2-like macrophages (blue) engulf ovalbumin released by tumor cells and present MHC class II (IA^b) restricted OVA epitopes to adoptively transferred OVA specific CD4$^+$ T helper cells (orange). The activated CD4$^+$ T helper cells secrete IFNγ which induces macrophages to polarize to proinflammatory M1 (light red).

4.6 Modulation of macrophage polarization by transcription factor knock down

Extensive research has led to a better understanding of the signaling pathways that underlie macrophage polarization. However, the exact TF mediated control is still not fully elucidated. In this study, our collaboration partners combined TF binding information with RNA expression profiles and identified five TFs required to retain the M2-like phenotype. The expression of the five identified TFs CTCF, E2F1, MYC, PPARγ and STAT6 was significantly downregulated in LPS/IFNγ treated PECs compared to untreated cells (Figure 3.27 A). In contrast, the expression level in M2-like PECs was either upregulated (*Ctcf, Myc* and *Pparg*) or downregulated (*E2f1* and *Stat6*) compared to M0, but consistently higher as in M1-like macrophages. Moreover, all five *in silico* predicted TFs demonstrated a high activity in M2-like PECs and a low activity in M1-like PECs (Figure 3.27 B), supporting the detected differences in gene expression levels and emphasizing their importance in maintaining the M2-like phenotype. Transfection of *Ctcf, E2f1, Myc, Pparg* and *Stat6* targeting siRNAs into M2 polarized PECs resulted in strong upregulation of M1-associated genes and in

downregulated expression of M2-associated genes compared to M2-like PECs treated with negative control siRNA. Further, the secretion of proinflammatory cytokines, such as IL-6, TNFα, IL-1α and IFNβ was significantly increased upon TF knockdown. Almost the same expression profiles were detected when the experiment was repeated excluding *Ctcf* targeting siRNAs, suggesting that knockdown of CTCF was not required for the observed effects. Taken together, our data provide strong evidence for the importance of these TFs in maintaining a M2-like phenotype in IL-4 stimulated PECs.

The next paragraphs will give an overview of the known functions of the five identified TFs in the process of macrophage polarization. Moreover, published results in accordance with as well as disparate from our data will be discussed.

STAT6 (Signal transducer and activator of transcription 6)

The important role of STATs in regulating macrophage polarization has been well-established. While STAT1 is a pivotal TF to induce IFNγ mediated M1 polarization, STAT6 is required to drive alternative activation of macrophages in the presence of IL4 and/or IL-13. Expression of many M2-associated genes, such as *Fizz1, Arg1, Mrc1* and *Ym1* is regulated by STAT6 and accompanied by modifications of the chromatin structure and epigenetic changes [388]. siRNA mediated knockdown of STAT6 in murine PECs inhibited the induction of M2-associated genes upon treatment with IL-4 [215]. In accordance with these data, the overexpression of STAT6 in RAW264.7 cells significantly decreased the percentage of CD86 positive cells, whereas M2 marker expression was increased [389]. Moreover, IL-4 induced inhibition of proinflammatory gene expression is largely mediated by STAT6 [388, 390]. STAT6 was reported to directly and/or indirectly suppress IFNγ mediated STAT1 expression [390-392], and STAT6 knockout mice lose IL-4 induced inhibition of the IFNγ/STAT1 signaling pathway [393]. Further, siRNA knockdown of STAT6 in M1-like RAW264.7 cells abrogated IL-4 induced inhibition of *Nos2* gene expression [394]. In addition, STAT6 is known to modulate expression of other TFs involved in macrophage polarization. For instance, expression of Krüppel-like factor (KLF4), an essential factor for IL-4 induced M2-like polarization was shown to be dependent on STAT6 in RAW264.7 cells [395]. Both TFs were found to cooperate to induce M2 marker gene expression. Taken together, the importance of STAT6 in inducing and maintaining a M2-like phenotype in murine macrophages was demonstrated in various experimental settings. Therefore, the identification of STAT6 in our study as one of the five key TFs involved in M2 polarization using the mixed-integer-linear programming approach is in accordance with present knowledge.

PPARγ (Peroxisome proliferator-activated receptor gamma)

The human genome encodes for three PPAR subtypes, PPARα, -γ and –δ which are expressed in various cell types and tissues [396]. PPARs control virtually all processes of fatty acid metabolism, including fatty acid synthesis, storage, transport and their oxidation. PPARγ was found to be expressed mainly in adrenal glands, spleens and adipose tissue and has major functions in regulating lipid metabolism in macrophages and adipocyte differentiation. In macrophages, PPARγ is constitutively expressed and can be induced upon stimulation with IL-4 and/or IL-13. Already 20 years ago, Ricote and colleagues demonstrated that activated PPARγ inhibits the expression of TFs (STAT, AP-1 and NK-κB)

involved in classical macrophage activation [397]. Consistent with these findings, macrophages with *Pparg* deletion were shown to have an impaired capacity to acquire a M2 phenotype [398]. Further, it was demonstrated that treatment of primary human monocytes with PPARγ agonists enhanced the activation of M2-associated gene expression [138]. Treatment of murine PECs with different PPARγ agonists significantly increased CD206 surface expression and enhanced the phagocytic activity of macrophages, both of which are typical features for alternative macrophage activation [399]. Moreover, the authors demonstrated that the treatment of macrophages with a PPARγ antagonist prevents IL-13 induced M2-like polarization. Interestingly, STAT6 has been shown to interact with PPARγ, thereby enhancing PPARγ target gene expression [400]. Thus, crosstalk between IL-4 induced STAT6 and PPARγ is probably required for optimal M2 polarization.
As mentioned earlier (see section 1.2.3), M2 macrophages predominantly use fatty acid oxidation as it is best suited for permanent energy supply required for processes like tissue repair or remodeling [173]. Several studies demonstrated that transcriptional regulation of PPARγ and its coactivator PGC-1β are indispensable for the uptake and oxidation of fatty acids [398, 401]. Macrophages isolated from mice with macrophage specific PPARγ deletion showed a significantly reduced fatty acid oxidation compared to macrophages from WT mice, demonstrating that oxidative metabolism in M2 macrophages is dependent on PPARγ [398]. Our results further emphasize the importance of PPARγ in inducing and maintaining M2-like polarization and are in line with the current state of knowledge.

CTCF (CCCTC-binding factor)

CTCF is a highly conserved DNA binding zinc finger nuclease and plays an important role in the regulation of several cellular processes such as transcriptional activation/repression and imprinting [402]. In contrast to the well-established role of STAT6 and PPARγ in regulating macrophage polarization, very little is known about the expression and function of CTCF in macrophages. In a study from Nikolic and colleagues, the authors crossed LysM-Cre mice with mice carrying a *Ctcf* floxed allele to generate a mouse model with myeloid cell specific *Ctcf* deletion [403]. The absence of *Ctcf* had no significant effects on macrophage frequencies in the peritoneum and the spleens. However, macrophage differentiation from bone marrow derived LysM-Cre $Ctcf^{f/f}$ precursors was significantly reduced *in vitro*. Even though CTCF was previously reported to be involved in the regulation of MHC II molecule expression [404], the authors could not observe any changes in MHC II surface expression on macrophages. *Ctcf* deletion in bone marrow derived macrophages had no significant impact on surface expression of CD86, CD206 and CD16/32. Further, *Ctcf* deficient macrophages had similar phagocytic capacity than macrophages from WT mice. Interestingly, secretion of the M2-associated cytokine IL-10 and the M1-associated cytokine TNF was significantly decreased in bone marrow derived macrophages isolated from LysM-Cre $Ctcf^{f/f}$ mice compared to macrophages from WT mice upon treatment with TLR ligands. Whole RNA sequencing comparing gene expression of *Ctcf* deficient macrophages with WT macrophages revealed 617 differentially expressed genes. Genes which were significantly downregulated in *Ctcf* deficient macrophages included both, M1-associated (*Nos2, Cxcl10*) and M2-associated genes (*Vegfa*). Taken together, these data demonstrate that CTCF is involved in the regulation of macrophage differentiation and modulates expression of a vast amount of genes. However, the role of CTCF in macrophage polarization is still ambiguous

as *Ctcf* deficiency was associated with reduced levels of M1-like and M2-like associated genes.

In contrast, the results shown in this thesis present a clear association between *Ctcf* expression and alternative macrophage activation. *Ctcf* expression in IL-4 treated PECs was upregulated compared to untreated PECs, but significantly downregulated upon treatment with LPS/IFNγ. Further, CTCF activity in M1-like PECs was significantly reduced compared to untreated and M2-like macrophages. However, our results demonstrated that macrophage repolarization upon knockdown of only four TFs (excluding CTCF) was as efficient as knock down of all five TFs. These results indicate that in our experimental setting CTCF was not required to maintain a M2-like phenotype. However, to make sure that CTCF is indeed dispensable for maintaining a M2-like phenotype we would need to perform single knockdown experiments, in which only CTCF expression is reduced without knocking down any other TFs. It might well be that CTCF is dependent on one of the four TFs and can only fulfill its functions if their expression is not reduced by siRNA pools. Nevertheless, our results provide a good basis for deeper analysis of CTCF expression and its importance in macrophage polarization.

E2F1 (E2F transcription factor 1)

E2F1 target genes are involved in cell cycle progression, differentiation, DNA replication and repair. Thus, E2F1 is a key transcription factor regulating cellular proliferation and its activity in tumor cells is often altered [405]. Whereas the role of E2F1 in controlling the cell cycle was investigated comprehensively throughout the last 30 years, almost nothing is known about its function in macrophages. E2F1 binding motifs were found to be overrepresented in genomic loci that are bound by the NF-κB subunit RELA, suggesting a cooperative regulatory function of these two TFs [406]. Moreover, E2F1 together with RELA were shown to be rapidly recruited to the promoter regions of proinflammatory cytokine encoding genes (e.g. TNFα and IL-1β) upon treatment of THP-1 cells with LPS. siRNA mediated knockdown of E2F1 impaired the expression of these LPS induced genes indicating that E2F1 is required to fully activate NF-κB target genes. Similar to these observations, inhibition of E2F1 in J77A4.1 macrophages and subsequent stimulation with LPS resulted in reduced IL-6 and TNFα production [407]. In accordance with these findings, stimulation of bone marrow derived macrophages from *E2f1* knockout mice with different TLR ligands resulted in reduced expression of proinflammatory cytokines (IL-1β, IL-6, IL-12, TNF-α) compared to macrophages from control mice [408]. These results further emphasize the role of E2F1 in regulating the inflammatory response to TLR ligands in macrophages.

In contrast to the results described above, our analyses of macrophage polarization upon siRNA mediated knockdown of E2F1, MYC, CTCF, STAT6 and PPARγ revealed a significant upregulation of proinflammatory genes (*Cxcl9, Cxcl10, Il1b* and *Il12b*), suggesting that E2F1 is involved in repressing rather than activating their transcription. The discrepancy between our observations and previously published data might be explained by the different experimental approaches applied. While the published results are mainly based on data obtained from macrophages treated with LPS after siRNA mediated E2F1 knockdown, our results were generated by knocking down E2F1 in M2 polarized cells. Hence, the published data investigated the impact of E2F1 deficiency on TLR signaling, whereas we investigated the impact of reduced E2F1 expression in IL-4 induced M2 macrophages. It must be

assumed that the regulatory function of E2F1 on its target genes is in great part dependent on the activated signaling pathway (TLR4 signaling induced by LPS vs. JAK/STAT signaling induced by IL-4), which could explain the observed discrepancies between our results and published data.

Myc

Myc is a proto-oncogene involved in a variety of cellular processes (e.g. cell growth and apoptosis) and has been shown to be frequently mutated and/or deregulated in cancer cells [409]. MYC was reported to be required for alternative macrophage polarization. The transcription factor expression and its translocation into the nucleus is induced upon stimulation of macrophages with IL-4 [214]. Expression of *Myc* in BMMs stimulated with IL-4 was shown to be increased 3-fold compared to untreated cells, whereas it was decreased 9-fold in M1-like macrophages [410]. Many M2-associated genes are directly or indirectly controlled by MYC. Of note, treatment of IL-4 stimulated macrophages with MYC inhibitor abrogated *Pparg* and *Stat6* expression, showing that both TFs are regulated by MYC and emphasizing the essential role of MYC in M2 polarization [214].
IL-4 induced M2-like macrophages typically have an enhanced migratory capacity, which is in accordance with their important function in wound healing. Hao and colleagues demonstrated that siRNA mediated MYC knockdown impairs cell migration in IL-4 treated RAW264.7 cells, thereby further supporting the role of MYC in maintaining M2-associated functionality [411]. Moreover, overexpression of a truncated MYC version (MYC-nick) in BMMs was accompanied by upregulation of M2-associated genes and increased phagocytosis [412]. Taken together, these results highlight the significance of MYC in inducing and maintaining alternative macrophage activation, being involved in controlling M2-associated gene expression and functionality. Our data further support the importance of MYC, as we could demonstrate that siRNA mediated knockdown of MYC in M2-like PECs was associated with increased expression of M1-associated genes and proinflammatory cytokine expression.

4.7 Modulation of macrophage polarization through miRNA transfection

This part of the study focused on the identification of key miRNAs inducing classical activation of macrophages. We identified 56 significantly differentially expressed miRNAs in PECs upon treatment with LPS/IFNγ or IL-4 or $CD4^+$ T cell mediated repolarization (Figure **3.34**). In the two groups M1-like vs. untreated and M1-like vs. M2.like, we detected 18 and 19 differentially expressed miRNAs, respectively. After incorporating the RNA sequencing data of polarized PECs in the bioinformatics analysis, significantly enriched miRNAs were identified. Combining the results obtained from both groups revealed a total of 22 miRNAs enriched in M1-like PECs compared to either untreated PECs or M2-like PECs or both. These significantly enriched miRNAs can be arranged into three distinct clusters (Figure **3.35**). One cluster contained miRNAs downregulated in M1-like PECs as well as in PECs co-cultured with OVA specific T cells. The other two clusters encompassed miRNAs either upregulated in M1-like PECs only or upregulated in M1-like PECs and PECs co-cultured with OVA specific T cells. Finally, six miRNAs (miR-210-3p, miR-674-5p, miR-222-3p, let-7i-5p, miR-146a-5p and miR-28a-3p) which were upregulated in both, M1-like (LPS/IFNγ) macrophages and M2-like PECs upon co-culture with OVA specific $CD4^+$ T cells were

selected for subsequent validation as these are the miRNAs supposed to be important for inducing a M1-like phenotype. Transfection of all six miRNAs in untreated or M2-like PECs resulted in strong induction of M1-associated gene expression and downregulation of M2-associated genes (Figure 3.36). Unexpectedly, expression of *Mrc1* (*Cd206*) and *Arg1*, both representing typical M2-associated genes, was upregulated in some of the tested conditions.

Several studies investigated the expression profiles of miRNAs in polarized macrophages. Zhang and colleagues performed miRNA microarray analysis with LPS/IFNγ or IL-4 treated BMMs and identified a total of 109 differentially expressed miRNAs [413]. Of note, 104 of these miRNAs were upregulated in M1-like macrophages compared to M2, whereas only five were downregulated. Of the six miRNAs we have selected, miR-146a was the only one upregulated in M1-like macrophages in their data set, whereas the other five miRNAs were not differentially expressed. In another study, Lu and colleagues performed small RNA sequencing with *in vitro* polarized BMMs [414]. They identified a total of 31 differentially expressed miRNAs, with 24 being upregulated in M1-like macrophages. Three of our six finally selected miRNAs were detected in their data set as well (miR-146a, miR-210 and miR-222) and were shown to be upregulated in M1-like BMMs. Qi and colleagues used thioglycolate elicited PECs treated with LPS and subsequently identified differentially expressed miRNAs by microRNA arrays [415]. They reported a LPS induced upregulation of miR-146 and miR-210, which is in accordance with our data. Unfortunately, the authors did not further comment on their microRNA array results but immediately selected miR-210 for further analyses.

Taken together, three of our differentially expressed and significantly enriched miRNAs, namely miR-210, miR-222 and miR-146a have been reported to be upregulated in M1-like macrophages in at least one of the studies. However, differential expression of miR-674, Let-7i and miR-28a was not detected. In line with our results, the studies identified more upregulated than downregulated miRNAs in M1-like macrophages compared to M2-like. In the following, known functions of our six finally selected miRNAs are described.

miR-210-3p

Several studies identified a strong upregulation of miR-210-3p expression in LPS treated BMMs [416] and PECs [415], suggesting an important role of miR-210-3p in M1-like macrophages. However, the expression of proinflammatory cytokines in macrophages transfected with miR-210 mimics was shown to be significantly reduced after LPS treatment [415]. In accordance with this observation, transfection of macrophages with miR-210 inhibitor and subsequent LPS stimulation resulted in significant upregulation of these cytokines. Our target prediction analysis revealed putative binding sites of miR-210-3p in the 3'UTR of NFKB1 (subunit of NF-κB). Indeed, Qi and colleagues demonstrated that NF-κB is a direct target of miR-210, explaining the induced negative regulation of proinflammatory cytokine secretion in LPS treated cells [415]. Taken together, miR-210 expression is induced in LPS treated macrophages and acts in a negative feedback loop by targeting TLR signaling, thereby inhibiting proinflammatory cytokine secretion.

miR-146a-5p

The substantial effects of miR-146-5p on macrophage polarization have been reported in several studies. In accordance with our results, treatment of macrophages with LPS has been shown to result in a strong NF-κB dependent upregulation of miR-146a [162]. Of note, miR-146a has been demonstrated to target TRAF6 and IRAK1 mRNA, both of which are adapter molecules downstream of cytokine and TLR signaling pathways. Thus, miR-146a expression is induced in classically activated macrophages to control cytokine and TLR signaling in a negative feedback loop and reduce the release of proinflammatory cytokines similar to miR-210-3p as described above [162]. In accordance with these results, inhibition of miR-146a in polarized PECs promoted the expression of M1-associated genes (*Il6* and *Il1b*) and decreased expression of M2-associated genes (*Pdgf* and *Arg1*). Furthermore, miR-146a transfected RAW264.7 cells mixed with 4T1 cells and injected subcutaneously (s.c.) into BALB/c mice significantly promoted tumor growth [163].

miR-674-5p

The targets and functions of miR-674-5p are largely unknown, which is supported by the fact that only five publications including the term “miR-674-5p” can be found when using the PubMed search engine (https://www.ncbi.nlm.nih.gov/pubmed/; accessed: 19.08.18). None of these publications is dealing with miR-674-5p expression in the context of macrophages in general or macrophage polarization in particular. Thus, miR-647-5p is described in this thesis for the first time as miRNA differentially expressed in polarized macrophages. Our target prediction analysis revealed 1038 target genes (predicted by at least two prediction tools) with putative binding sites for miR-647-5p. The predicted targets include genes involved in fatty acid metabolism (*Abcd1*) and purin biosynthesis (*Gart*), both representing processes known to be enhanced in M2-like macrophages [417]. Thus, miR-674-5p expression in M1-like macrophages might be required to downregulate these processes. Our experimental validation indicates that this miRNA plays a role in repolarizing M2-like macrophages. However, more comprehensive analyses as briefly described in section 5 are required to make a final statement.

miR-222-3p

In LNCaP prostate carcinoma cells, stimulation of the NF-κB pathway by TNFα was shown to enhance miR-222 expression [418]. Inhibiting the NF-κB pathway in PC3 prostate carcinoma cells and U87 glioblastoma cells resulted in decreased expression levels of miR-222. These results demonstrate that miR-222 expression is dependent on NF-κB signaling, which is in accordance with our data showing a significant upregulation of miR-222 in LPS/IFNγ treated macrophages. After co-transfecting miR-222-3p in combination with the other five identified miRNAs into M2-like PECs we could detect a repolarization towards the M1-like phenotype with several proinflammatory cytokines being upregulated. In contrast to our results, a study from Ying and colleagues demonstrated polarization of human U937 cells into M2-like macrophages upon transfecting miR-222-3p mimics [419]. However, it can be assumed that the function of miRNAs between different species (and even different cell lines of the same species as observed by Theresa Kordaß) can differ substantially even though their sequences are often highly conserved. A study investigating the function of miR-222-3p in murine macrophages has not been published yet.

let-7i-5p

Ten different mature let-7 miRNAs have been identified until today in both, human and mice [420]. Whereas the whole mature sequence of let-7a is identical across animal species, other members of this family share only the seed sequences. The role of let-7 miRNAs in macrophage polarization was already described for let-7c and let-7b. Let-7c was demonstrated to be significantly higher expressed in M2-like BMMs compared to M1-like BMMs [421]. Further, LPS induced repolarization of M2-like macrophages decreased the expression of let-7c. Transfection with let-7c mimics induced polarization towards a M2-like phenotype with reduced expression of proinflammatory cytokines compared to control transfections. These results demonstrated that let-7c suppresses M1-like polarization and can promote M2-like polarization. The same holds true for let-7b, which was shown to be expressed to significantly higher extent in IL-4 induced human peripheral blood derived macrophages compared to LPS/IFNγ treated or untreated macrophages [422].

The expression and function of let-7i in macrophages has not been described so far. However, it was reported that let-7i targets and downregulates expression of TLR4 in human biliary epithelia cells (cholangiocytes) [423]. At the same time, activation of TLR4 signaling by LPS treatment resulted in decreased let-7i expression levels. Similar regulatory effects of let-7i on TLR4 expression were observed in the human monocytic cell line THP-1 [424]. In contrast to the LPS induced downregulation of let-7i expression observed in cholangiocytes, our miRNA expression data showed a significant upregulation of this miRNA in PECs treated with LPS/IFNγ. Moreover, none of the nine miRNA target prediction tools predicted a TLR4 binding site for let-7i, indicating that regulatory functions of let-7i differ between mice and humans. Indeed, the let-7i binding site in the human TLR4 3'UTR sequence is absent in mice [425].

miR-28a-3p

Not a single publication including the term "miR-28a-3p" can be found by the PubMed search engine and only three publications including the term "miR-28a" are listed in the underlying databases (https://www.ncbi.nlm.nih.gov/pubmed/; accessed: 20.08.18). None of these publications were dealing with the role of miR-28a in macrophage polarization. Therefore, this thesis describes for the first time differential expression of miRNA-28a-3p in polarized macrophages.

Taken together, two of our six finally selected miRNAs have well-known functions in macrophage polarization (miR-210-3p and miR-146a-5p). The role of the remaining four miRNAs is either largely (miR-222-3p) or completely (miR-674-5p, let-7i-5p and miR-28a-3p) unknown. miR-210-3p and miR-146a-5p have been reported to act in a negative feedback loop to inhibit proinflammatory cytokine secretion by macrophages. Therefore, it seems contradictory to use these miRNAs in an attempt to repolarize M2-like macrophages into a M1-like phenotype. However, our enrichment analysis (see section 3.3.5.2) not only guarantees that the selected miRNAs are upregulated after LPS/IFNγ treatment, but also ensures that the predicted targets of these miRNAs are significantly downregulated in M1-like PECs. Thus, these two miRNAs might have a dual role in macrophage polarization. On the one hand they are responsible for fine tuning of NF-κB expression in LPS induced macrophages to prevent excessive release of proinflammatory cytokines and on the other

hand they might facilitate maintenance of the M1-like phenotype by downregulating M2-associated genes. Even though our results indicate that the remaining four miRNA candidates are important in inducing and maintaining a M1-like phenotype, more comprehensive analyses are required to rule out similar negative feedback loops.

In addition to the analysis of differentially miRNA expression in PECs polarized with cytokines, we also included samples of M2-like PECs repolarized by cognate interaction with OVA specific $CD4^+$ T cells. Our *in vitro* data clearly demonstrate T cell mediated reprogramming of these macrophages into an immunostimulatory M1-like phenotype (section 3.3.3). Our gene and protein expression analyses revealed that the repolarized macrophages very much resemble the classically activated macrophages (LPS/IFNγ). Thus, we would have expected very similar miRNA expression profiles between these two groups. However, 29 miRNAs were significantly differentially expressed in the group M1-like vs. M2-like after co-culture with T cells + OVA peptide, clearly demonstrating that M1-like PECs polarized by external cytokine addition (LPS/IFNγ) are different from M2-like PECs which were repolarized into M1-like by $CD4^+$ T cells (section 3.3.5.1). Of note, the difference in the miRNA expression profiles between these two groups was higher than between IL-4 induced M2-like and LPS/IFNγ induced M1-like PECs. These differences are most likely attributed to the fact that a repolarization by cognate T cell interaction incorporates other signaling pathways than the polarization by external cytokine addition. Stimulation of macrophages with LPS/IFNγ activates TLR4 and JAK/STAT signaling pathways, eventually leading to the activation of TFs such as STAT1, STAT2, IRF-1, NF-κB, AP-1, IRF-7 and IRF-3 [144-146]. In contrast, cognate interaction of M2-like macrophages with $CD4^+$ T cells might activate signaling pathways associated with engagement of CD86 and CD80 by CD28 and CTLA-4. Moreover, due to the release of IFNγ by activated $CD4^+$ T cells JAK/STAT signaling pathways become activated. Eventually, the activation of distinct TFs as well as the crosstalk between the activated signaling pathways will determine miRNA expression and probably explain the observed differences between LPS/IFNγ induced PECs and M2-like PECs repolarized through cognate $CD4^+$ T cell interaction.

5 Summary and outlook

This thesis demonstrates reprogramming of immunosuppressive M2-like macrophages upon MHC II restricted interaction with $CD4^+$ T cells, transcription factor knockdown and miRNA transfection.

In the first part of the project we demonstrated that cognate interaction between M2-like PECs and $CD4^+$ T cells was accompanied by IFNγ release of activated $CD4^+$ T cells, thereby instructing macrophage repolarization towards a M1 phenotype. Upon adoptive transfer of OVA specific $CD4^+$ T cells into C57BL/6 mice bearing IA^b deficient OVA expressing tumors, partial repolarization of TAMs freshly isolated from explanted tumors was observed, suggesting that interaction between OVA specific $CD4^+$ T cells and TAMs can shift the M1/M2 balance towards M1 also *in vivo*. However, to make sure that the observed macrophage repolarization is exclusively mediated by cognate interaction between $CD4^+$ T cells and macrophages, we would need to repeat our experiments in transgenic mice with IA^b deficient macrophages [426]. In such a mouse model, the absence of TAM repolarization upon adoptive transfer of $CD4^+$ T cells would proof that the cognate interaction between macrophages and transferred $CD4^+$ T cells is required. Moreover, it would be interesting to repeat the adoptive T cell transfer experiments with our B16F10 transfectant clone expressing a truncated version of OVA (not secreted). These results could clarify whether the $CD4^+$ T cell mediated changes in TAM polarization are dependent on the secretion of tumor associated antigens or not. In the second part of the thesis we identified five TFs (CTCF, E2F1, MYC, PPARγ and STAT6) associated with the induction and maintenance of the M2 phenotype. siRNA mediated TF knockdown induced the expression of proinflammatory cytokines in M2-like PECs. Further, M2-like macrophages expressed elevated levels of M1-associated genes and lower levels of M2-associated genes. As we knocked down all five TF simultaneously, it is difficult to determine to what extend each individual TF contributes to the observed repolarization. However, the on-going analysis of RNA sequencing data from M2-like PECs transfected with each TF targeting siRNA individually will finally clarify the exact functions of each TF in the process of macrophage polarization. Nevertheless, the data we have obtained so far reveal already new insights into the transcriptional reprogramming of macrophages and might be useful for the identification of therapeutic targets to reprogram M2 macrophages into the proinflammatory M1-like macrophages. Finally, small RNA sequencing of *in vitro* polarized PECs revealed 19 miRNAs differentially expressed between M1-like and M2-like PECs. Six miRNAs highly expressed in M1-like PECs were selected for further validation. Transfection of these miRNAs into M2-like or untreated PECs resulted in significant upregulation of M1-associated genes, whereas M2-associated genes were downregulated. Our data indicate that repolarizing M2-like macrophages by a pool of miRNAs is in principle possible. However, future experiments should include individual transfections of each miRNA into M2-like PECs, thus allowing for better interpretation of the function of the different miRNAs. In addition, more comprehensive analyses (cytokine secretion, phagocytosis assays, protein expression) and proper negative controls (pool of negative control miRNAs) are required to draw final conclusions.

6 Appendix

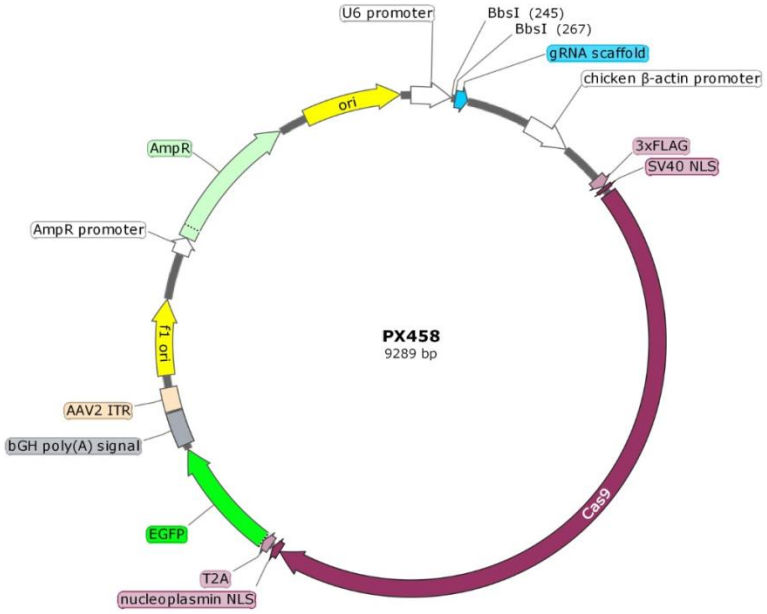

Figure 6.1: Vector chart of PX458.

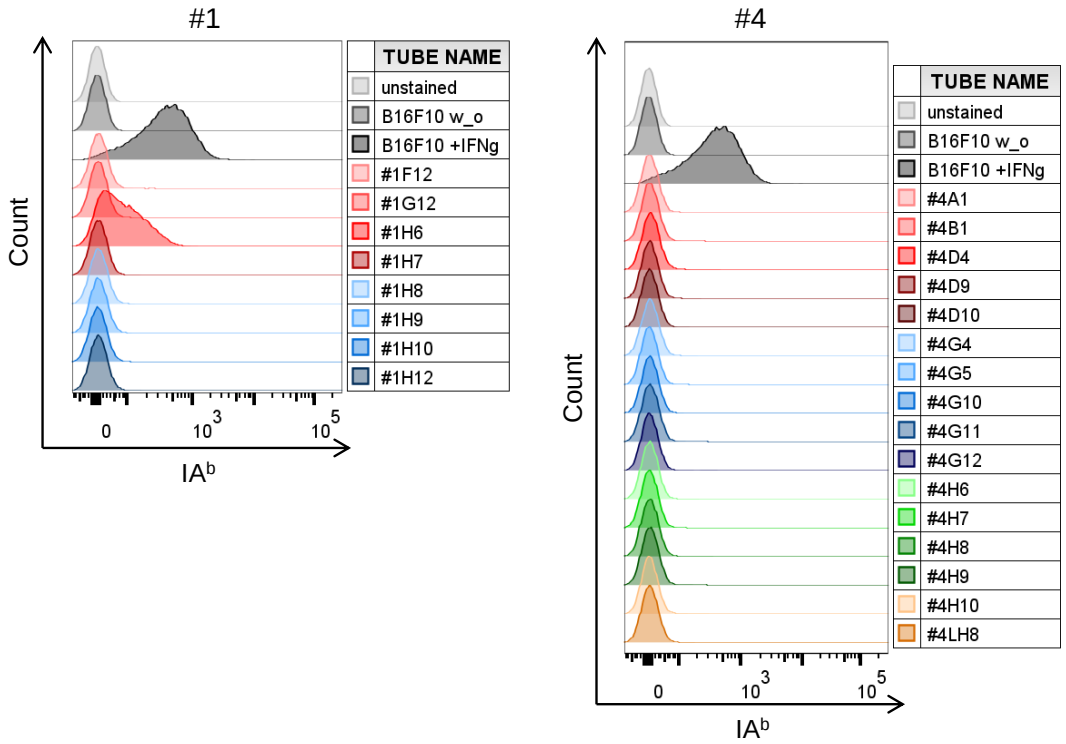

Figure 6.2: Analysis of IA^b surface expression on B16F10 derived transfectant clones.
IA^b surface expression of individual B16F10 derived clones transfected either with guide #1 or guide #4 encoding vector and of parental B16F10 cells after treatment with IFNγ and subsequent staining with IA^b specific monoclonal antibody. Untreated (B16F10 w_o) and unstained B16F10 cells served as background controls, whereas parental B16F10 cells treated with IFNγ (B16F10 + IFNg) served as positive control. Designations of clones are depicted in the column at the right. This figure legend was taken from reference [307] and was originally written by myself.

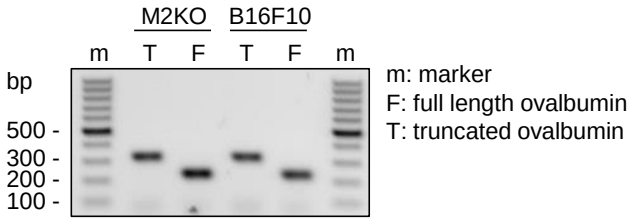

Figure 6.3: Transduced cell lines stably integrated the OVA encoding sequence.
B16F10 or M2KO cells were transduced using lentiviral particles encoding for OVA. Both bulk cultures stably integrated OVA in their genome as confirmed by PCR and subsequent agarose gel electrophoresis. Expected product size for full length OVA is 229 bp and for truncated OVA 323 bp.

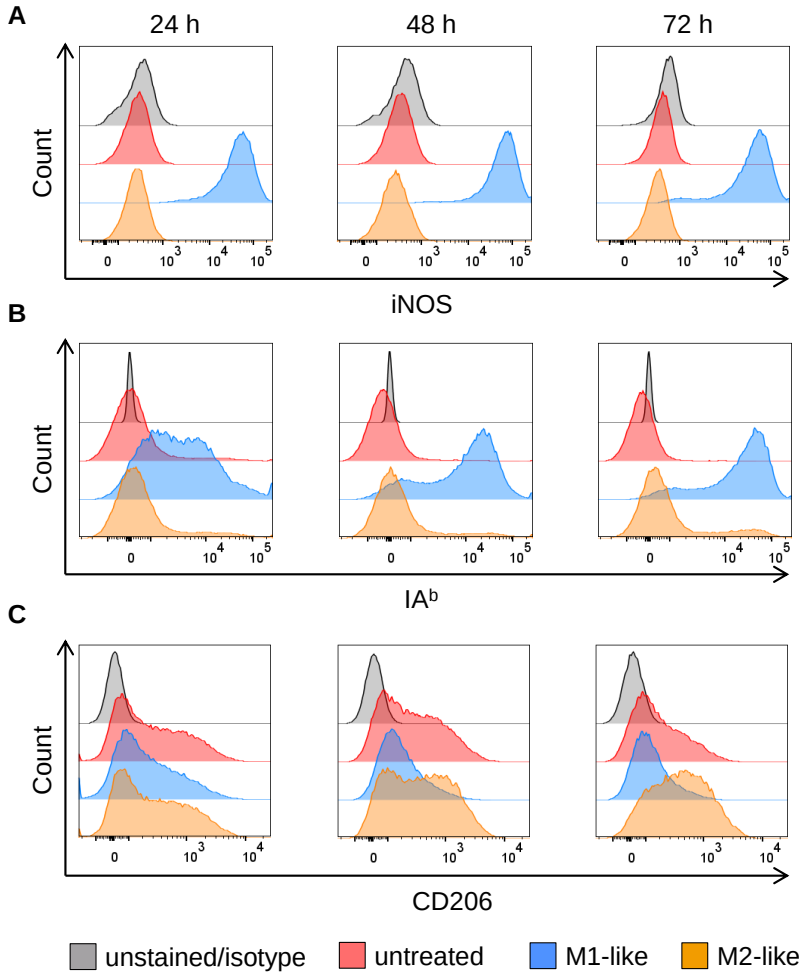

Figure 6.4: Surface protein expression analysis of polarized PECs.
PECs were isolated, purified and polarized either into M1-like (LPS + IFNγ) or M2-like (IL-4) macrophages 4 days after thioglycolate injection. After 24, 48 and 72 h of polarization, the cells were harvested, stained with **(A)** iNOS, **(B)** IA^b or **(C)** CD206 specific monoclonal antibodies and analyzed by flow cytometry. Gating strategy: living cells → single cells (FSC-A vs. FSC-H) → F4/80$^+$CD11b$^+$ → CD206/Egr2 vs. FSC-H

Table 6.1: Transfection of PECs with GFP encoding plasmid.

Detailed depiction of all tested transfection approaches of PECs using 10 different transfection reagents. The corresponding results are illustrated in Figure 3.28.

Reagent	Approach	Cell number	TR [µl]	DNA [µg]	living cells [%]	GFP+ cells [%]
Lipofectamine LTX	untreated	1 x 10^6	0	0	87	0
	mock 1	1 x 10^6	6	0	69.2	0.6
	mock 2	1 x 10^6	15	0	71.4	1
	1	1 x 10^6	6	2.5	4.4	3.6
	2	1 x 10^6	9	2.5	0.6	3.2
	3	1 x 10^6	12	2.5	0.2	14.3
	4	1 x 10^6	15	2.5	0.2	0
	untreated	1 x 10^6	0	0	87	0
	mock 1	2 x 10^6	6	0	89.8	0.1
	mock 2	2 x 10^6	15	0	88.8	0.5
	1	2 x 10^6	6	2.5	22.1	3.6
	2	2 x 10^6	9	2.5	3.5	0.8
	3	2 x 10^6	12	2.5	0.7	1.2
	4	2 x 10^6	15	2.5	0.3	2.5
Lipofectamine 3000	untreated	1 x 10^6	0	0	87	0
	mock 1	1 x 10^6	3.75	0	88.9	0.1
	mock 2	1 x 10^6	7.5	0	89	0.3
	1	1 x 10^6	3.75	2.5	5.4	1.4
	2	1 x 10^6	7.5	2.5	0.4	2.3
	untreated	1 x 10^6	0	0	87	0
	mock 1	2 x 10^6	3.75	0	92.9	0.1
	mock 2	2 x 10^6	7.5	0	93.1	0.1
	1	2 x 10^6	3.75	2.5	29.3	1.2
	2	2 x 10^6	7.5	2.5	1.4	5.3
PromoFectin	untreated	1 x 10^6	0	0	87	0
	mock 1	1 x 10^6	1.5	0	86.3	0.4
	mock 2	1 x 10^6	6	0	84.9	1
	1	1 x 10^6	3	1.5	74.3	0.9
	2	1 x 10^6	1.5	1.5	81.5	0.2
	3	1 x 10^6	4.5	1.5	69.7	1.3
	4	1 x 10^6	6	1.5	63.6	2.1
	untreated	1 x 10^6	0	0	87	0
	mock 1	2 x 10^6	1.5	0	91.3	0.1
	mock 2	2 x 10^6	6	0	91	0.2
	1	2 x 10^6	3	1.5	83.5	0.2
	2	2 x 10^6	1.5	1.5	84.6	0.1
	3	2 x 10^6	4.5	1.5	81	0.5
	4	2 x 10^6	6	1.5	78.2	0.8
TransIT-X2	untreated	1 x 10^6	0	0	87	0
	mock 1	1 x 10^6	7.5	0	88.2	1.5
	mock 2	1 x 10^6	15	0	70.4	0.5
	1	1 x 10^6	7.5	2.5	0.8	2.5
	2	1 x 10^6	15	2.5	0.1	0
	untreated	1 x 10^6	0	0	87	0
	mock 1	2 x 10^6	7.5	0	92	0.4
	mock 2	2 x 10^6	15	0	80.7	0.1
	1	2 x 10^6	7.5	2.5	3.7	2.5
	2	2 x 10^6	15	2.5	0.3	0

Reagent	Approach	Cell number	TR [µl]	DNA [µg]	living cells [%]	GFP+ cells [%]
TransIT-2020	untreated	1 x 10^6	0	0	87	0
	mock 1	1 x 10^6	2.5	0	89.4	0.5
	mock 2	1 x 10^6	7.5	0	90.5	0.8
	1	1 x 10^6	7.5	2.5	45.8	10.7
	2	1 x 10^6	2.5	2.5	50.5	11.1
	untreated	1 x 10^6	0	0	87	0
	mock 1	2 x 10^6	2.5	0	92	0.2
	mock 2	2 x 10^6	7.5	0	92.7	0.3
	1	2 x 10^6	7.5	2.5	72.2	4.6
	2	2 x 10^6	2.5	2.5	71.2	3.3
TurboFect	untreated	1 x 10^6	0	0	87	0
	mock 1	1 x 10^6	4	0	84.6	0.3
	mock 2	1 x 10^6	8	0	81.7	0.4
	1	1 x 10^6	6	4	78	0.6
	2	1 x 10^6	4	4	76.7	0.3
	3	1 x 10^6	8	4	73.9	0.6
	untreated	1 x 10^6	0	0	87	0
	mock 1	2 x 10^6	4	0	92.6	0.1
	mock 2	2 x 10^6	8	0	88.7	0.2
	1	2 x 10^6	6	4	83.4	0.1
	2	2 x 10^6	4	4	81.8	0
	3	2 x 10^6	8	4	82.4	0.1
Viromer Red	untreated	1 x 10^6	0	0	87	0
	mock	1 x 10^6	200	0	82.6	0.5
	1	1 x 10^6	40	0.4	81.9	0.4
	2	1 x 10^6	100	1	74.4	0.7
	3	1 x 10^6	200	2	55.9	2.7
	4	1 x 10^6	300	3	44.8	6.9
	5	1 x 10^6	400	4	39.4	15.1
	untreated	1 x 10^6	0	0	87	0
	mock 1	2 x 10^6	40	0	90.8	0.1
	mock 2	2 x 10^6	400	0	90.3	0.1
	1	2 x 10^6	40	0.4	85.7	0.1
	2	2 x 10^6	100	1	82	0.2
	3	2 x 10^6	200	2	72.8	1.2
	4	2 x 10^6	300	3	62.5	4.1
	5	2 x 10^6	400	4	60.7	7.6
	DNA	2 x 10^6	pos. Ctrl.	-	80.6	0.4
	RNA	2 x 10^6	pos. Ctrl.	-	89.1	17.4

Reagent	Approach	Cell number	TR [µl]	DNA [µg]	living cells [%]	GFP+ cells [%]
Effectene	untreated	2×10^6	0	0	89.4	0
	mock 1	2×10^6	2	0	90.7	0
	mock 2	2×10^6	40	0	85.1	0.2
	1	2×10^6	10	0.4	89.9	0
	2	2×10^6	20	0.4	85.7	0.1
	3	2×10^6	4	0.4	90.7	0
	4	2×10^6	5	0.2	88.5	0
	5	2×10^6	10	0.2	88.8	0
	6	2×10^6	2	0.2	82.8	0
	7	2×10^6	15	0.6	79.2	0.1
	8	2×10^6	30	0.6	80.5	0.3
	9	2×10^6	6	0.6	89.2	0.1
	10	2×10^6	40	0.8	77.5	0.9
	11	2×10^6	8	0.8	87.5	0
	12	2×10^6	20	0.8	75.9	0.5
Dharmafect Duo	untreated	2×10^6	0	0	89.4	0
	mock 1	2×10^6	1	0	92.4	0
	mock 2	2×10^6	12	0	85.4	0
	1	2×10^6	4	2	18.7	0.2
	2	2×10^6	2	2	48.2	0.1
	3	2×10^6	6	2	6.1	0.4
	4	2×10^6	2	1	45.6	0.1
	5	2×10^6	1	1	62.3	0
	6	2×10^6	3	1	25.4	0.2
	7	2×10^6	8	4	1.9	0.8
	8	2×10^6	4	4	11.9	0.2
	9	2×10^6	10	4	0.5	1.6
Metafectene Pro	untreated	2×10^6	0	0	89.4	0
	mock 1	2×10^6	2	0	76.1	0
	mock 2	2×10^6	25	0	32.2	0.9
	1	2×10^6	2	1	84.5	0
	2	2×10^6	5	1	77.7	0
	3	2×10^6	7	1	76.3	0.1
	4	2×10^6	4	2	64	0.3
	5	2×10^6	10	2	55.8	0.8
	6	2×10^6	14	2	77.1	0.1
	7	2×10^6	8	4	37.3	6.6
	8	2×10^6	20	4	48	1.9
	9	2×10^6	28	4	67.7	2.3

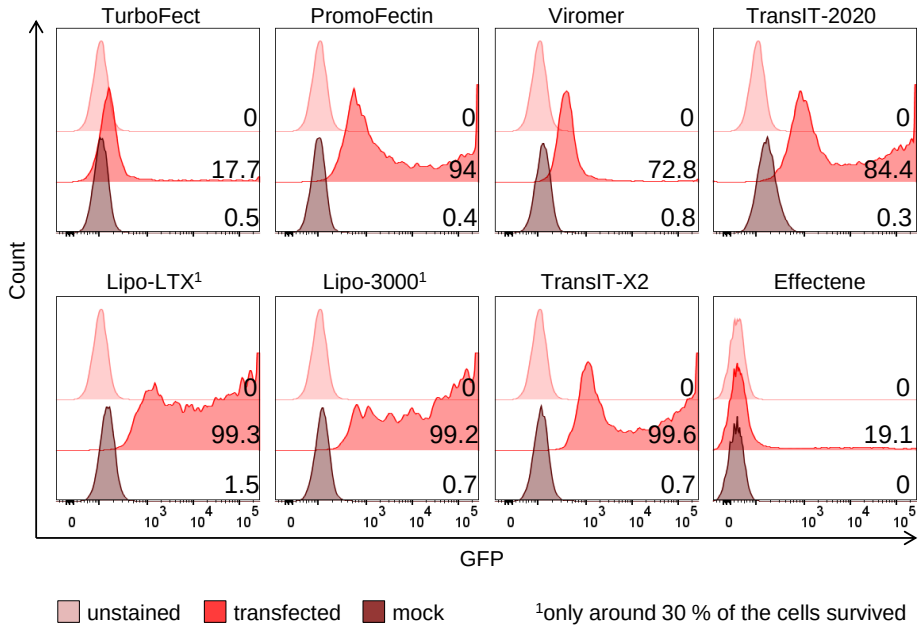

Figure 6.5: Control transfections of B16F10 cells using a GFP encoding plasmid.
B16F10 cells (2 x 10^5) were seeded into a 6-Well plate and transfected with a GFP encoding plasmid using the standard protocol provided by the manufacturer. The cells were harvested and analyzed by flow cytometry 48 h after transfection. The numbers given within the graphs represent the percentages of GFP positive cells. Gating strategy: living cells → single cells (FSC-A vs. FSC-H) → GFP vs. FSC-H.

Table 6.2: In search of an appropriate housekeeping gene for qPCR analysis of polarized PECs after miRNA transfection.
The BaseMean serve as a measure of the expression level of a certain miRNA across all tested samples. The subsequent columns show whether the housekeeping genes are regulated by one of the miRNAs. The numbers show how many of the following tools predict an interaction between miRNA and housekeeping gene: MiRTarBase (validated miRNA targets), Microcosm, miRanda, miRNAMap2, miRMap, miRDB, PITA, Pictar and TargetScan (miRNA-target prediction tools). The log(2) fold change values present the fold change expression between M1-like and M2-like PECs.

Gene	baseMean	let-7e-5p	miR-99b-3p	miR-99b-5p	let-7i-5p	miR-28a-3p	miR-222-3p	miR-221-5p	miR-674-5p	miR-146a-5p	miR-210-3p	miR-1198-5p	miR-27b-3p	miR-744-5p	miR-30e-3p	Sum	log(2) fold change
Hprt	2361	2	0	0	0	1	0	0	1	0	0	0	0	1	0	5	0.28*
Actb	48061	0	0	0	0	0	0	1	0	0	0	0	0	0	0	1	0.38*
Tbp	559	1	1	0	1	1	1	1	2	1	1	1	3	1	1	16	0.24*
Ppia	2894	0	0	0	0	0	1	0	1	0	0	0	0	0	1	3	0.06
Rpl13a	4281	0	1	0	0	0	0	0	1	0	0	0	0	0	0	2	-0.08
Gusb	15590	1	0	1	2	0	0	0	1	1	0	0	2	0	1	9	-1.27*
B2m	125058	0	0	0	0	0	0	0	0	1	0	1	0	0	0	2	1.96
Hmbs	409	1	0	0	1	0	0	0	0	1	0	0	0	1	0	4	-0.89*
Rn18s	n.a.	n.a.	n.a.	n.a.	n.a.	n.a.	n.a.	n.a.	n.a.	n.a.	n.a.	n.a.	n.a.	n.a.	n.a.	n.a.	n.a.
Gapdh	2239	2	0	0	0	0	0	0	0	0	0	0	0	1	0	3	2.44*
Ubc	28430	0	0	0	0	0	0	0	0	1	0	0	0	0	0	1	1.25*
Rpl19	1777	0	0	0	0	0	1	0	0	0	0	0	1	1	0	3	-0.08

n.a. = not available; * p ≤ 0.05

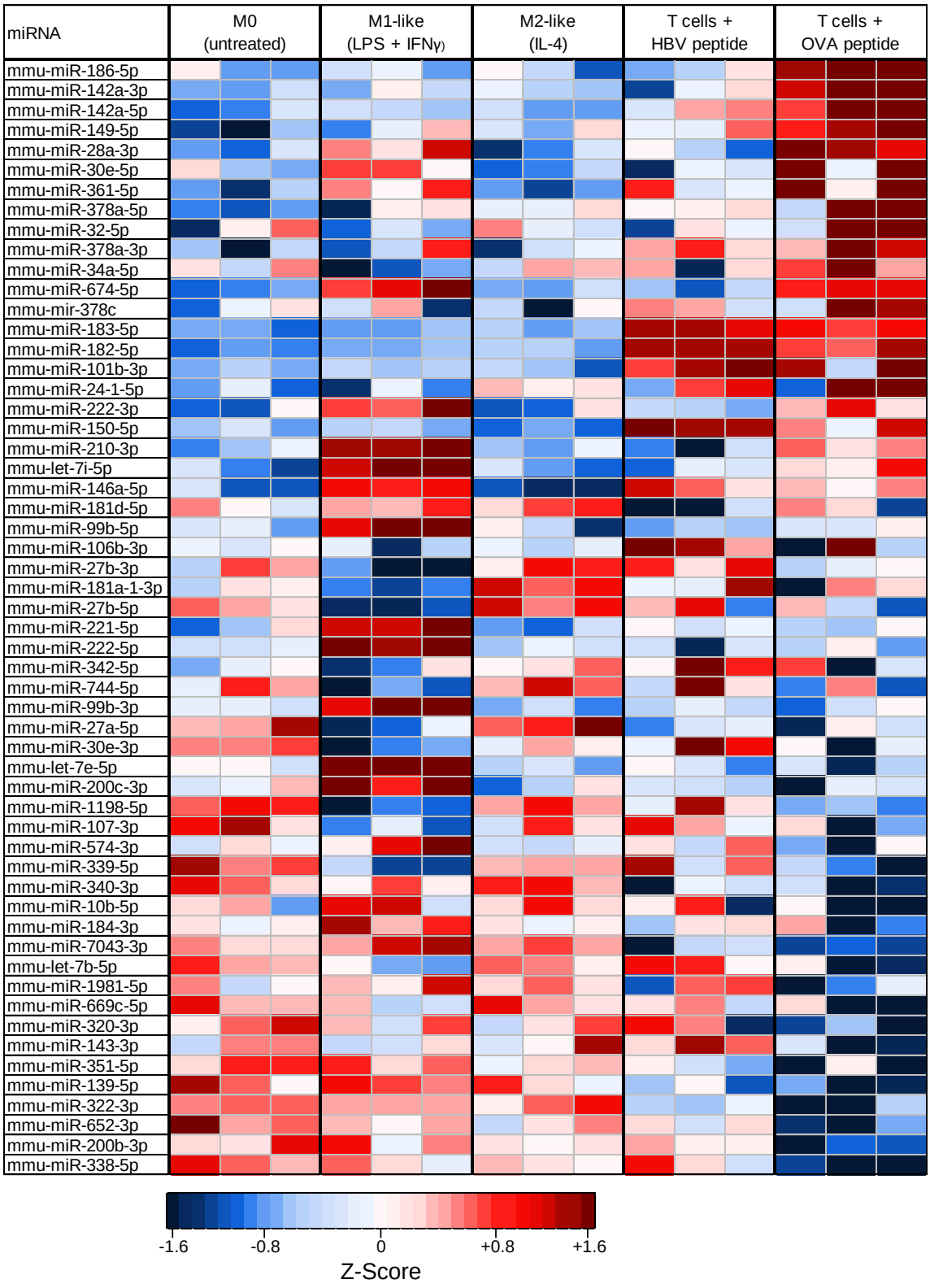

Figure 6.6: Z-scores of differentially expressed miRNAs in polarized PECs.

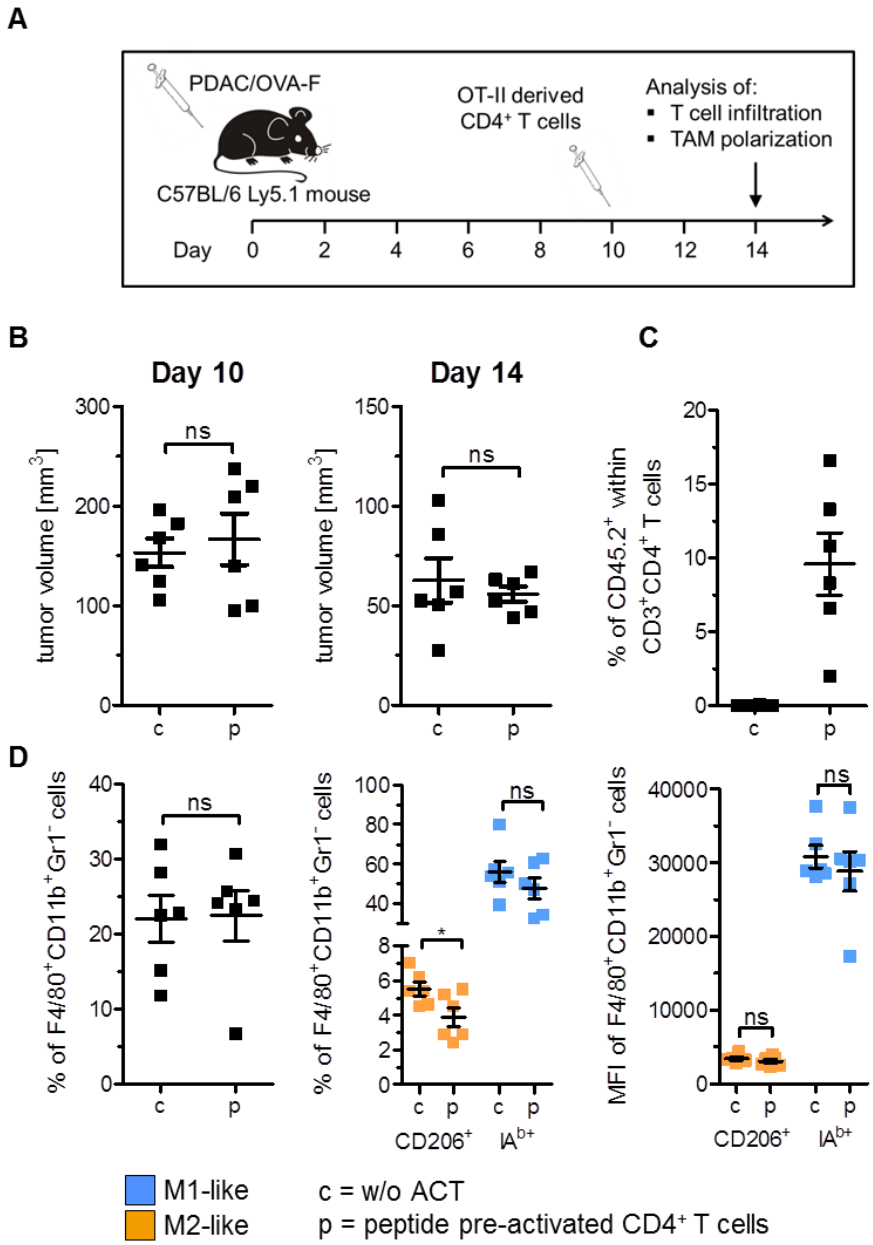

Figure 6.7: Infiltration of adoptively transferred OVA specific CD4$^+$ T cells and polarization of TAMs in PDAC/OVA-F tumor bearing mice.
(A) Experimental workflow: C57BL/6 Ly5.1 mice (n = 6) were injected s.c. with 2 x 10^6 PDAC/OVA-F cells. Ten days after tumor inoculation, mice were injected i.v. with 5 x 10^6 peptide pre-activated OVA specific CD4$^+$ T cells (p). Mice were sacrificed four days later and tumors were analyzed by flow cytometry. Control mice (c) did not receive CD4$^+$ T cells. **(B)** Tumor volume 10 and 14 days after tumor cell injection. **(C)** Infiltration of adoptively transferred T cells into tumors presented as percentage of CD45.2$^+$ within CD3$^+$CD4$^+$ cells. Gating strategy: CD45$^+$ → living cells → single cells (FSC-A vs. FSC-H) → CD3$^+$CD4$^+$ → CD45.1 vs. CD45.2. **(D)** Percentages of TAMs (F4/80$^+$CD11b$^+$Gr1$^-$) within CD45$^+$ cells as well as percentages and MFI values of CD206 and IA^b expressing TAMs. Error bars represent SEM within each animal collective. Statistical analysis was done by unpaired Student's *t*-test (95% CI, ns: not significant, * p ≤ 0.05, ** p < 0.01, *** p ≤ 0.001). Gating strategy: CD45$^+$ → living cells → single cells (FSC-A vs. FSC-H) → F4/80$^+$CD11b$^+$Gr1$^-$ → CD206 vs. IA^b.

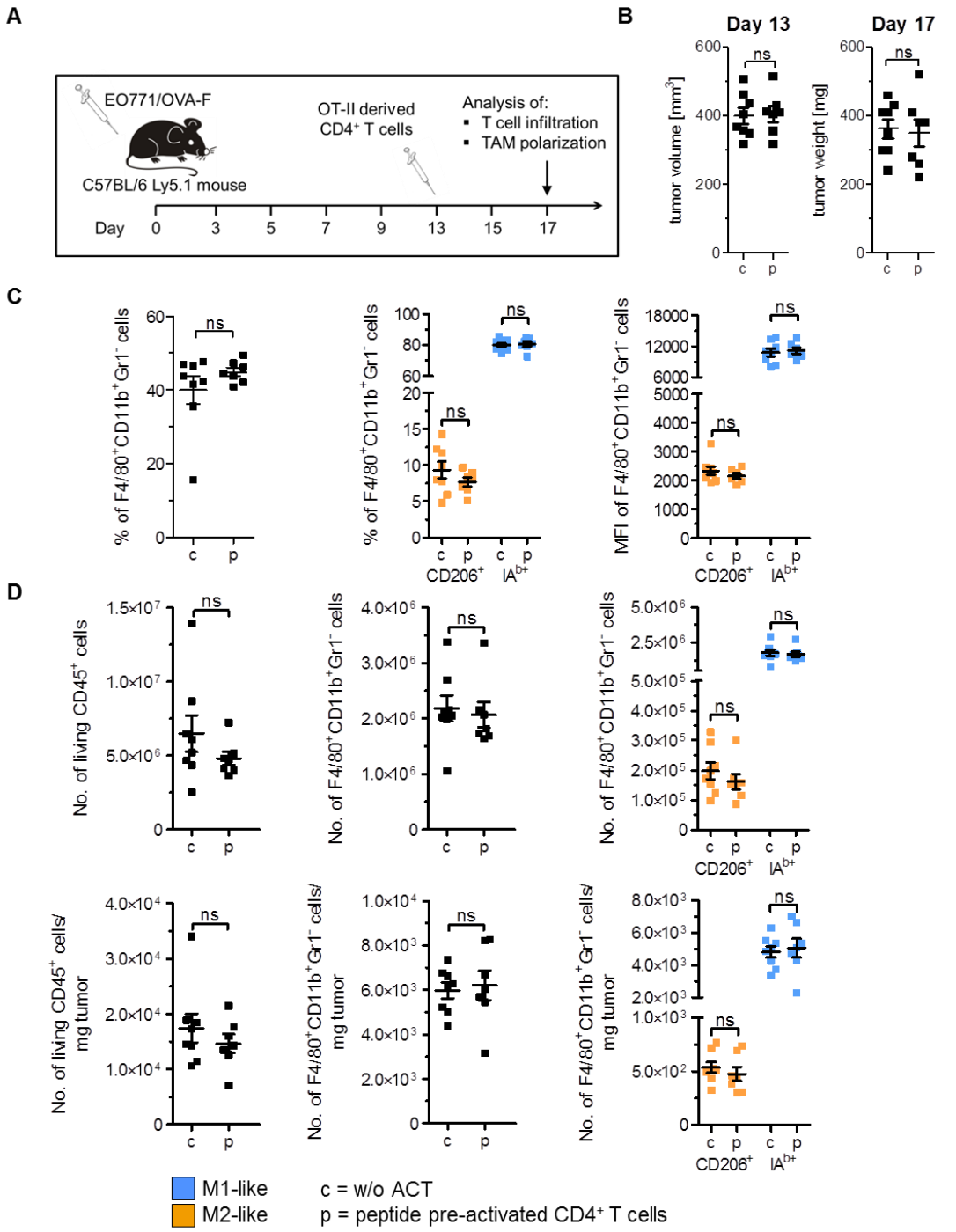

Figure 6.8: Polarization of TAMs in EO771/OVA-F tumors upon ACT with CD4$^+$ T cells.
(A) Experimental workflow: C57BL/6 Ly5.1 mice (n = 7-8) were injected s.c. with 2 x 10^6 EO771/OVA-F cells. Thirteen days post tumor inoculation, mice were injected i.v. with 5 x 10^6 peptide pre-activated OVA-specific CD4$^+$ T cells. Mice were sacrificed on day 17 and tumors were analyzed by flow cytometry. Control mice (c) did not receive CD4$^+$ T cells. **(B)** Tumor volume and tumor weight 13 and 17 days post tumor cell injection, respectively. **(C)** Four days post i.v. injection tumors were analyzed by flow cytometry. Percentages of TAMs (F4/80$^+$CD11b$^+$Gr1$^-$) within CD45$^+$ cells as well as percentages and MFI values of CD206 and IA^b expressing cells within TAMs are shown. **(D)** Total numbers of CD45$^+$ cells, TAMs, CD206 as well as IA^b expressing TAMs (upper panel) within EO771/OVA-F tumors after ACT. Corresponding tumor weight normalizations are depicted in the lower panel. Error bars represent SEM within each animal collective. Statistical analysis was done by unpaired Student's *t*-test (95% CI, ns: not significant, * p ≤ 0.05, ** p < 0.01, *** p ≤ 0.001). Gating strategy: CD45$^+$ → living cells → single cells (FSC-A vs. FSC-H) → F4/80$^+$CD11b$^+$Gr1$^-$ → CD206 vs. IA^b.

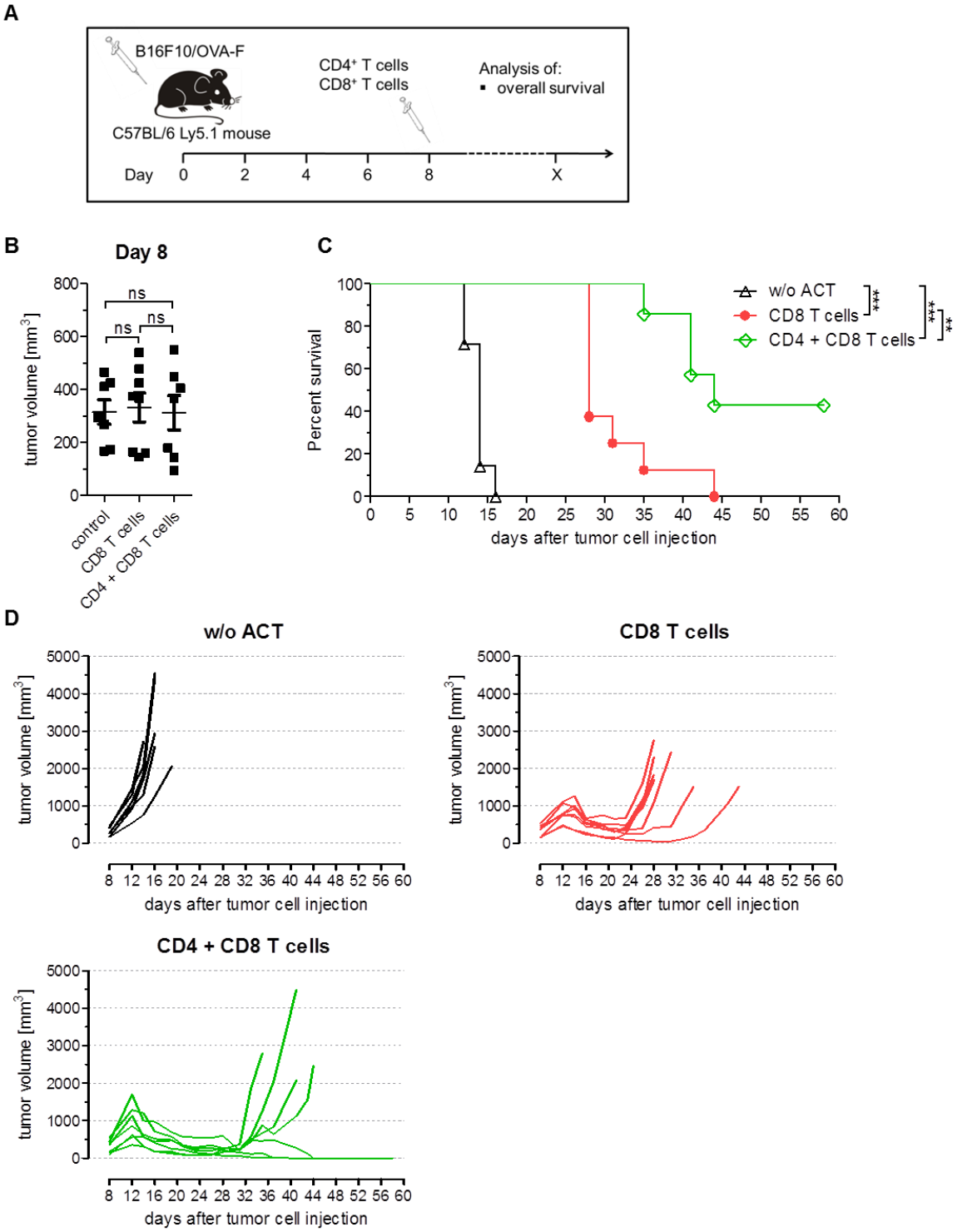

Figure 6.9: Survival of B16F10/OVA-F tumor bearing mice after adoptive T cell transfer with OVA specific CD4$^+$ and CD8$^+$ T cells.
(A) Experimental workflow: C57BL/6 Ly5.1 mice (n = 7 - 8) were injected s.c. with 2 x 10^5 B16F10/OVA-F cells. Eight days after tumor inoculation, mice were injected i.v. either with 5 x 10^6 peptide pre-activated OVA specific CD8$^+$ T cells or a combination of OVA specific CD4$^+$ and CD8$^+$ T cells (5 x 10^6 each). Mice not receiving any T cells served as control group (control). **(B)** Tumor volume of the different treatment groups eight days after tumor cell injection. **(C)** Kaplan-Meier survival curves of mice treated either with CD8$^+$ T cells alone or a combination of CD4$^+$ and CD8$^+$ T cells. Significance was determined using log-rank test. **(D)** Tumor growth of individual tumors within each group. Error bars represent SEM within each animal collective.

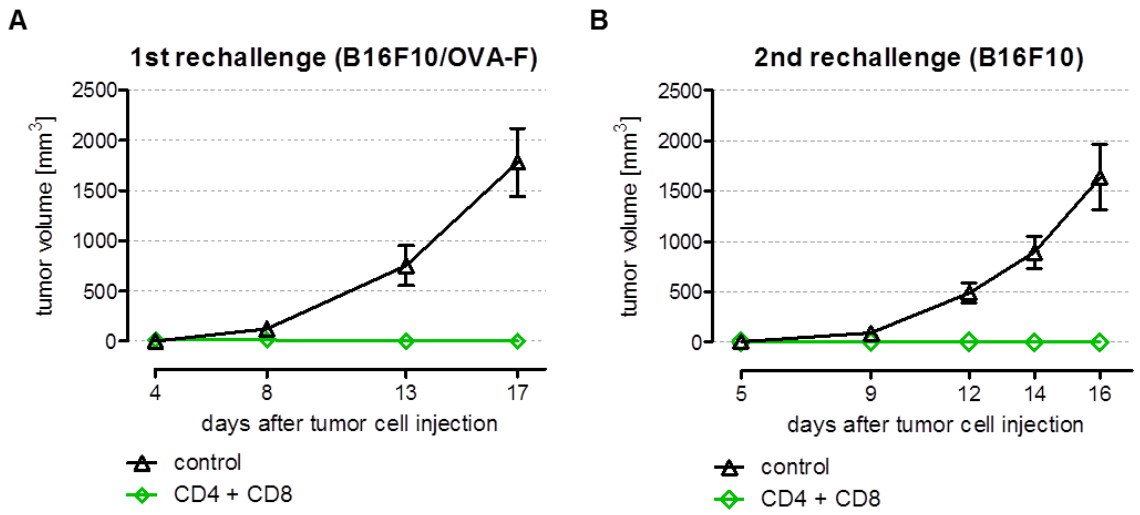

Figure 6.10: Tumor rechallenge of mice after adoptive transfer
C57BL/6 Ly5.1 mice that rejected the B16F10/OVA-F tumor completely (n = 3) as well as a control group of mice (n = 6) were injected s.c. with either 2 x 10^5 B16F10/OVA-F cells 11 weeks post T cell transfer (A) or 2 x 10^5 B16F10 cells 21 weeks post T cell transfer (B). Error bars represent SEM within each animal collective.

Bibliography

1. Moravej, H., et al., *Antimicrobial Peptides: Features, Action, and Their Resistance Mechanisms in Bacteria.* Microb Drug Resist, 2018. **24**(6): p. 747-767.
2. Curtsinger, J.M., et al., *Inflammatory cytokines provide a third signal for activation of naive CD4+ and CD8+ T cells.* J Immunol, 1999. **162**(6): p. 3256-62.
3. Curtsinger, J.M., et al., *Type I IFNs provide a third signal to CD8 T cells to stimulate clonal expansion and differentiation.* J Immunol, 2005. **174**(8): p. 4465-9.
4. Zhou, L., M.M.W. Chong, and D.R. Littman, *Plasticity of CD4+ T Cell Lineage Differentiation.* Immunity, 2009. **30**(5): p. 646-655.
5. Seder, R.A. and W.E. Paul, *Acquisition of lymphokine-producing phenotype by CD4+ T cells.* Annu Rev Immunol, 1994. **12**: p. 635-73.
6. Martinez-A, C. and A. Coutinho, *B-cell activation by helper cells is a two-step process.* Nature, 1981. **290**: p. 60.
7. Old, L.J. and E.A. Boyse, *Immunology of Experimental Tumors.* Annu Rev Med, 1964. **15**: p. 167-86.
8. Burnet, M., *Cancer; a biological approach. I. The processes of control.* Br Med J, 1957. **1**(5022): p. 779-86.
9. Thomas, L. and H. Lawrence, *Cellular and humoral aspects of the hypersensitive states.* New York: Hoeber-Harper, 1959: p. 529-532.
10. Stutman, O., *Tumor development after 3-methylcholanthrene in immunologically deficient athymic-nude mice.* Science, 1974. **183**(4124): p. 534-6.
11. Kaplan, D.H., et al., *Demonstration of an interferon gamma-dependent tumor surveillance system in immunocompetent mice.* Proc Natl Acad Sci U S A, 1998. **95**(13): p. 7556-61.
12. Shankaran, V., et al., *IFNgamma and lymphocytes prevent primary tumour development and shape tumour immunogenicity.* Nature, 2001. **410**(6832): p. 1107-11.
13. Dunn, G.P., et al., *Cancer immunoediting: from immunosurveillance to tumor escape.* Nat Immunol, 2002. **3**(11): p. 991-8.
14. Koebel, C.M., et al., *Adaptive immunity maintains occult cancer in an equilibrium state.* Nature, 2007. **450**(7171): p. 903-7.
15. Jager, E., et al., *Immunoselection in vivo: independent loss of MHC class I and melanocyte differentiation antigen expression in metastatic melanoma.* Int J Cancer, 1997. **71**(2): p. 142-7.
16. Zheng, P., et al., *Two mechanisms for tumor evasion of preexisting cytotoxic T-cell responses: lessons from recurrent tumors.* Cancer Res, 1999. **59**(14): p. 3461-7.
17. Restifo, N.P., et al., *Identification of human cancers deficient in antigen processing.* J Exp Med, 1993. **177**(2): p. 265-72.
18. Korkolopoulou, P., et al., *Loss of antigen-presenting molecules (MHC class I and TAP-1) in lung cancer.* Br J Cancer, 1996. **73**(2): p. 148-53.
19. Schreiber, R.D., L.J. Old, and M.J. Smyth, *Cancer immunoediting: integrating immunity's roles in cancer suppression and promotion.* Science, 2011. **331**(6024): p. 1565-70.
20. Gabrilovich, D.I., et al., *Production of vascular endothelial growth factor by human tumors inhibits the functional maturation of dendritic cells.* Nat Med, 1996. **2**(10): p. 1096-103.
21. Uyttenhove, C., et al., *Evidence for a tumoral immune resistance mechanism based on tryptophan degradation by indoleamine 2,3-dioxygenase.* Nat Med, 2003. **9**(10): p. 1269-74.
22. Vesely, M.D., et al., *Natural innate and adaptive immunity to cancer.* Annu Rev Immunol, 2011. **29**: p. 235-71.

23. Balkwill, F. and A. Mantovani, *Inflammation and cancer: back to Virchow?* Lancet, 2001. **357**(9255): p. 539-45.
24. Moore, O.S., Jr. and F.W. Foote, Jr., *The relatively favorable prognosis of medullary carcinoma of the breast.* Cancer, 1949. **2**(4): p. 635-42.
25. Clark, W.H., Jr., et al., *The histogenesis and biologic behavior of primary human malignant melanomas of the skin.* Cancer Res, 1969. **29**(3): p. 705-27.
26. Tuthill, R.J., et al., *Risk assessment in localized primary cutaneous melanoma: a Southwest Oncology Group study evaluating nine factors and a test of the Clark logistic regression prediction model.* Am J Clin Pathol, 2002. **118**(4): p. 504-11.
27. Day, C.L., Jr., et al., *A prognostic model for clinical stage I melanoma of the upper extremity. The importance of anatomic subsites in predicting recurrent disease.* Ann Surg, 1981. **193**(4): p. 436-40.
28. Clemente, C.G., et al., *Prognostic value of tumor infiltrating lymphocytes in the vertical growth phase of primary cutaneous melanoma.* Cancer, 1996. **77**(7): p. 1303-10.
29. Cohen, P.J., et al., *The immunopathology of sequential tumor biopsies in patients treated with interleukin-2. Correlation of response with T-cell infiltration and HLA-DR expression.* Am J Pathol, 1987. **129**(2): p. 208-16.
30. Rosenberg, S.A., et al., *Use of tumor-infiltrating lymphocytes and interleukin-2 in the immunotherapy of patients with metastatic melanoma. A preliminary report.* N Engl J Med, 1988. **319**(25): p. 1676-80.
31. Belldegrun, A., L.M. Muul, and S.A. Rosenberg, *Interleukin 2 expanded tumor-infiltrating lymphocytes in human renal cell cancer: isolation, characterization, and antitumor activity.* Cancer Res, 1988. **48**(1): p. 206-14.
32. Harlin, H., et al., *Tumor progression despite massive influx of activated CD8(+) T cells in a patient with malignant melanoma ascites.* Cancer Immunol Immunother, 2006. **55**(10): p. 1185-97.
33. Boon, T., et al., *Human T cell responses against melanoma.* Annu Rev Immunol, 2006. **24**: p. 175-208.
34. Taylor, R.C., et al., *Tumor-infiltrating lymphocytes predict sentinel lymph node positivity in patients with cutaneous melanoma.* J Clin Oncol, 2007. **25**(7): p. 869-75.
35. Roszkowski, J.J., et al., *Simultaneous generation of CD8+ and CD4+ melanoma-reactive T cells by retroviral-mediated transfer of a single T-cell receptor.* Cancer Res, 2005. **65**(4): p. 1570-6.
36. Chiou, S.H., et al., *Current concepts of tumor-infiltrating lymphocytes in human malignancies.* J Reprod Immunol, 2005. **67**(1-2): p. 35-50.
37. Hunder, N.N., et al., *Treatment of metastatic melanoma with autologous CD4+ T cells against NY-ESO-1.* N Engl J Med, 2008. **358**(25): p. 2698-703.
38. Conrad, C.T., et al., *Differential expression of transforming growth factor beta 1 and interleukin 10 in progressing and regressing areas of primary melanoma.* J Exp Clin Cancer Res, 1999. **18**(2): p. 225-32.
39. Lowes, M.A., et al., *T helper 1 cytokine mRNA is increased in spontaneously regressing primary melanomas.* J Invest Dermatol, 1997. **108**(6): p. 914-9.
40. Miracco, C., et al., *Utility of tumour-infiltrating CD25+FOXP3+ regulatory T cell evaluation in predicting local recurrence in vertical growth phase cutaneous melanoma.* Oncol Rep, 2007. **18**(5): p. 1115-22.
41. Cox, A.L., et al., *Identification of a peptide recognized by five melanoma-specific human cytotoxic T cell lines.* Science, 1994. **264**(5159): p. 716-9.
42. Falk, K., et al., *Allele-specific motifs revealed by sequencing of self-peptides eluted from MHC molecules.* Nature, 1991. **351**: p. 290.
43. De Plaen, E., et al., *Identification of genes coding for tumor antigens recognized by cytolytic T lymphocytes.* Methods, 1997. **12**(2): p. 125-42.
44. Coulie, P.G., et al., *A new gene coding for a differentiation antigen recognized by autologous cytolytic T lymphocytes on HLA-A2 melanomas.* J Exp Med, 1994. **180**(1): p. 35-42.

45. Linard, B., et al., *A ras-mutated peptide targeted by CTL infiltrating a human melanoma lesion.* J Immunol, 2002. **168**(9): p. 4802-8.
46. Wolfel, T., et al., *A p16INK4a-insensitive CDK4 mutant targeted by cytolytic T lymphocytes in a human melanoma.* Science, 1995. **269**(5228): p. 1281-4.
47. Sharkey, M.S., et al., *CD4(+) T-cell recognition of mutated B-RAF in melanoma patients harboring the V599E mutation.* Cancer Res, 2004. **64**(5): p. 1595-9.
48. Yotnda, P., et al., *Cytotoxic T cell response against the chimeric p210 BCR-ABL protein in patients with chronic myelogenous leukemia.* J Clin Invest, 1998. **101**(10): p. 2290-6.
49. Kenter, G.G., et al., *Vaccination against HPV-16 oncoproteins for vulvar intraepithelial neoplasia.* N Engl J Med, 2009. **361**(19): p. 1838-47.
50. Jungbluth, A.A., et al., *Expression of cancer-testis (CT) antigens in placenta.* Cancer Immun, 2007. **7**: p. 15.
51. De Smet, C., et al., *DNA methylation is the primary silencing mechanism for a set of germ line- and tumor-specific genes with a CpG-rich promoter.* Mol Cell Biol, 1999. **19**(11): p. 7327-35.
52. De Smet, C., et al., *The activation of human gene MAGE-1 in tumor cells is correlated with genome-wide demethylation.* Proc Natl Acad Sci U S A, 1996. **93**(14): p. 7149-53.
53. Chen, Y.T., et al., *A testicular antigen aberrantly expressed in human cancers detected by autologous antibody screening.* Proc Natl Acad Sci U S A, 1997. **94**(5): p. 1914-8.
54. Chomez, P., et al., *An overview of the MAGE gene family with the identification of all human members of the family.* Cancer Res, 2001. **61**(14): p. 5544-51.
55. Anichini, A., et al., *Melanoma cells and normal melanocytes share antigens recognized by HLA-A2-restricted cytotoxic T cell clones from melanoma patients.* J Exp Med, 1993. **177**(4): p. 989-98.
56. Vigneron, N., et al., *Database of T cell-defined human tumor antigens: the 2013 update.* Cancer Immun, 2013. **13**: p. 15.
57. Kim, N.W., et al., *Specific association of human telomerase activity with immortal cells and cancer.* Science, 1994. **266**(5193): p. 2011-5.
58. Vonderheide, R.H., *Telomerase as a universal tumor-associated antigen for cancer immunotherapy.* Oncogene, 2002. **21**(4): p. 674-9.
59. Klemm, F. and J.A. Joyce, *Microenvironmental regulation of therapeutic response in cancer.* Trends Cell Biol, 2015. **25**(4): p. 198-213.
60. Tomasek, J.J., et al., *Myofibroblasts and mechano-regulation of connective tissue remodelling.* Nat Rev Mol Cell Biol, 2002. **3**(5): p. 349-63.
61. Kalluri, R. and M. Zeisberg, *Fibroblasts in cancer.* Nat Rev Cancer, 2006. **6**(5): p. 392-401.
62. Orimo, A., et al., *Stromal fibroblasts present in invasive human breast carcinomas promote tumor growth and angiogenesis through elevated SDF-1/CXCL12 secretion.* Cell, 2005. **121**(3): p. 335-48.
63. Boire, A., et al., *PAR1 is a matrix metalloprotease-1 receptor that promotes invasion and tumorigenesis of breast cancer cells.* Cell, 2005. **120**(3): p. 303-13.
64. Lochter, A., et al., *Matrix metalloproteinase stromelysin-1 triggers a cascade of molecular alterations that leads to stable epithelial-to-mesenchymal conversion and a premalignant phenotype in mammary epithelial cells.* J Cell Biol, 1997. **139**(7): p. 1861-72.
65. Pinchuk, I.V., et al., *PD-1 ligand expression by human colonic myofibroblasts/fibroblasts regulates CD4+ T-cell activity.* Gastroenterology, 2008. **135**(4): p. 1228-1237, 1237 e1-2.
66. Jin, H.T., et al., *Cooperation of Tim-3 and PD-1 in CD8 T-cell exhaustion during chronic viral infection.* Proc Natl Acad Sci U S A, 2010. **107**(33): p. 14733-8.

67. Fourcade, J., et al., *CD8(+) T cells specific for tumor antigens can be rendered dysfunctional by the tumor microenvironment through upregulation of the inhibitory receptors BTLA and PD-1.* Cancer Res, 2012. **72**(4): p. 887-96.
68. Wherry, E.J., et al., *Viral persistence alters CD8 T-cell immunodominance and tissue distribution and results in distinct stages of functional impairment.* J Virol, 2003. **77**(8): p. 4911-27.
69. Wherry, E.J., *T cell exhaustion.* Nat Immunol, 2011. **12**(6): p. 492-9.
70. Hori, S., T. Nomura, and S. Sakaguchi, *Control of regulatory T cell development by the transcription factor Foxp3.* Science, 2003. **299**(5609): p. 1057-61.
71. Fontenot, J.D., M.A. Gavin, and A.Y. Rudensky, *Foxp3 programs the development and function of CD4+CD25+ regulatory T cells.* Nat Immunol, 2003. **4**(4): p. 330-6.
72. Chaudhary, B. and E. Elkord, *Regulatory T Cells in the Tumor Microenvironment and Cancer Progression: Role and Therapeutic Targeting.* Vaccines (Basel), 2016. **4**(3).
73. Strauss, L., et al., *A unique subset of CD4+CD25highFoxp3+ T cells secreting interleukin-10 and transforming growth factor-beta1 mediates suppression in the tumor microenvironment.* Clin Cancer Res, 2007. **13**(15 Pt 1): p. 4345-54.
74. Woo, E.Y., et al., *Regulatory CD4(+)CD25(+) T cells in tumors from patients with early-stage non-small cell lung cancer and late-stage ovarian cancer.* Cancer Res, 2001. **61**(12): p. 4766-72.
75. Deaglio, S., et al., *Adenosine generation catalyzed by CD39 and CD73 expressed on regulatory T cells mediates immune suppression.* J Exp Med, 2007. **204**(6): p. 1257-65.
76. Pandiyan, P., et al., *CD4+CD25+Foxp3+ regulatory T cells induce cytokine deprivation-mediated apoptosis of effector CD4+ T cells.* Nat Immunol, 2007. **8**(12): p. 1353-62.
77. Takahashi, T., et al., *Immunologic self-tolerance maintained by CD25(+)CD4(+) regulatory T cells constitutively expressing cytotoxic T lymphocyte-associated antigen 4.* J Exp Med, 2000. **192**(2): p. 303-10.
78. Kiessling, R., E. Klein, and H. Wigzell, *"Natural" killer cells in the mouse. I. Cytotoxic cells with specificity for mouse Moloney leukemia cells. Specificity and distribution according to genotype.* Eur J Immunol, 1975. **5**(2): p. 112-7.
79. Guerra, N., et al., *NKG2D-deficient mice are defective in tumor surveillance in models of spontaneous malignancy.* Immunity, 2008. **28**(4): p. 571-80.
80. Kim, S., et al., *In vivo natural killer cell activities revealed by natural killer cell-deficient mice.* Proc Natl Acad Sci U S A, 2000. **97**(6): p. 2731-6.
81. Villegas, F.R., et al., *Prognostic significance of tumor infiltrating natural killer cells subset CD57 in patients with squamous cell lung cancer.* Lung Cancer, 2002. **35**(1): p. 23-8.
82. Coca, S., et al., *The prognostic significance of intratumoral natural killer cells in patients with colorectal carcinoma.* Cancer, 1997. **79**(12): p. 2320-8.
83. Ishigami, S., et al., *Prognostic value of intratumoral natural killer cells in gastric carcinoma.* Cancer, 2000. **88**(3): p. 577-83.
84. Nielsen, J.S., et al., *CD20+ tumor-infiltrating lymphocytes have an atypical CD27- memory phenotype and together with CD8+ T cells promote favorable prognosis in ovarian cancer.* Clin Cancer Res, 2012. **18**(12): p. 3281-92.
85. Gunderson, A.J. and L.M. Coussens, *B cells and their Mediators as Targets for Therapy in Solid Tumors.* Experimental cell research, 2013. **319**(11): p. 1644-1649.
86. Jensen, T.O., et al., *Intratumoral neutrophils and plasmacytoid dendritic cells indicate poor prognosis and are associated with pSTAT3 expression in AJCC stage I/II melanoma.* Cancer, 2012. **118**(9): p. 2476-85.
87. Rao, H.L., et al., *Increased intratumoral neutrophil in colorectal carcinomas correlates closely with malignant phenotype and predicts patients' adverse prognosis.* PLoS One, 2012. **7**(1): p. e30806.

88. Jensen, H.K., et al., *Presence of intratumoral neutrophils is an independent prognostic factor in localized renal cell carcinoma.* J Clin Oncol, 2009. **27**(28): p. 4709-17.
89. Fridlender, Z.G., et al., *Polarization of tumor-associated neutrophil phenotype by TGF-beta: "N1" versus "N2" TAN.* Cancer Cell, 2009. **16**(3): p. 183-94.
90. Shen, M., et al., *Tumor-associated neutrophils as a new prognostic factor in cancer: a systematic review and meta-analysis.* PLoS One, 2014. **9**(6): p. e98259.
91. Halazun, K.J., et al., *Elevated preoperative neutrophil to lymphocyte ratio predicts survival following hepatic resection for colorectal liver metastases.* Eur J Surg Oncol, 2008. **34**(1): p. 55-60.
92. Halazun, K.J., et al., *Negative impact of neutrophil-lymphocyte ratio on outcome after liver transplantation for hepatocellular carcinoma.* Ann Surg, 2009. **250**(1): p. 141-51.
93. Coussens, L.M., et al., *MMP-9 supplied by bone marrow-derived cells contributes to skin carcinogenesis.* Cell, 2000. **103**(3): p. 481-90.
94. Gungor, N., et al., *Genotoxic effects of neutrophils and hypochlorous acid.* Mutagenesis, 2010. **25**(2): p. 149-54.
95. Queen, M.M., et al., *Breast cancer cells stimulate neutrophils to produce oncostatin M: potential implications for tumor progression.* Cancer Res, 2005. **65**(19): p. 8896-904.
96. Feng, Y., S. Renshaw, and P. Martin, *Live imaging of tumor initiation in zebrafish larvae reveals a trophic role for leukocyte-derived PGE(2).* Curr Biol, 2012. **22**(13): p. 1253-9.
97. Rigoni, A., M.P. Colombo, and C. Pucillo, *Mast cells, basophils and eosinophils: From allergy to cancer.* Semin Immunol, 2018. **35**: p. 29-34.
98. Gulubova, M. and T. Vlaykova, *Prognostic significance of mast cell number and microvascular density for the survival of patients with primary colorectal cancer.* J Gastroenterol Hepatol, 2009. **24**(7): p. 1265-75.
99. Ribatti, D., et al., *Tumor vascularity and tryptase-positive mast cells correlate with a poor prognosis in melanoma.* Eur J Clin Invest, 2003. **33**(5): p. 420-5.
100. Strouch, M.J., et al., *Crosstalk between mast cells and pancreatic cancer cells contributes to pancreatic tumor progression.* Clin Cancer Res, 2010. **16**(8): p. 2257-65.
101. Rajput, A.B., et al., *Stromal mast cells in invasive breast cancer are a marker of favourable prognosis: a study of 4,444 cases.* Breast Cancer Res Treat, 2008. **107**(2): p. 249-57.
102. Chen, L., et al., *Viral and host inflammation-related factors that can predict the prognosis of hepatocellular carcinoma.* Eur J Cancer, 2012. **48**(13): p. 1977-87.
103. Rigoni, A., M.P. Colombo, and C. Pucillo, *The Role of Mast Cells in Molding the Tumor Microenvironment.* Cancer Microenviron, 2015. **8**(3): p. 167-76.
104. Jutel, M., et al., *Histamine regulates T-cell and antibody responses by differential expression of H1 and H2 receptors.* Nature, 2001. **413**(6854): p. 420-5.
105. Elenkov, I.J., et al., *Histamine potently suppresses human IL-12 and stimulates IL-10 production via H2 receptors.* J Immunol, 1998. **161**(5): p. 2586-93.
106. Morgan, R.K., et al., *Histamine 4 receptor activation induces recruitment of FoxP3+ T cells and inhibits allergic asthma in a murine model.* J Immunol, 2007. **178**(12): p. 8081-9.
107. Fernandez-Acenero, M.J., et al., *Prognostic influence of tumor-associated eosinophilic infiltrate in colorectal carcinoma.* Cancer, 2000. **88**(7): p. 1544-8.
108. Luna-More, S., et al., *Neutral and acid mucins and eosinophil and argyrophil crystalloids in carcinoma and atypical adenomatous hyperplasia of the prostate.* Pathol Res Pract, 1997. **193**(4): p. 291-8.
109. Davis, B.P. and M.E. Rothenberg, *Eosinophils and cancer.* Cancer Immunol Res, 2014. **2**(1): p. 1-8.
110. Kubo, H., et al., *Cytotoxic properties of eosinophil granule major basic protein for tumor cells.* Int Arch Allergy Immunol, 1999. **118**(2-4): p. 426-8.

111. Legrand, F., et al., *Human eosinophils exert TNF-alpha and granzyme A-mediated tumoricidal activity toward colon carcinoma cells.* J Immunol, 2010. **185**(12): p. 7443-51.
112. Reichman, H., D. Karo-Atar, and A. Munitz, *Emerging Roles for Eosinophils in the Tumor Microenvironment.* Trends Cancer, 2016. **2**(11): p. 664-675.
113. Carretero, R., et al., *Eosinophils orchestrate cancer rejection by normalizing tumor vessels and enhancing infiltration of CD8(+) T cells.* Nat Immunol, 2015. **16**(6): p. 609-17.
114. Veglia, F., M. Perego, and D. Gabrilovich, *Myeloid-derived suppressor cells coming of age.* Nat Immunol, 2018. **19**(2): p. 108-119.
115. Marvel, D. and D.I. Gabrilovich, *Myeloid-derived suppressor cells in the tumor microenvironment: expect the unexpected.* J Clin Invest, 2015. **125**(9): p. 3356-64.
116. Umansky, V., et al., *The Role of Myeloid-Derived Suppressor Cells (MDSC) in Cancer Progression.* Vaccines (Basel), 2016. **4**(4).
117. Hu, C.E., et al., *Up-regulated myeloid-derived suppressor cell contributes to hepatocellular carcinoma development by impairing dendritic cell function.* Scand J Gastroenterol, 2011. **46**(2): p. 156-64.
118. Li, H., et al., *Cancer-expanded myeloid-derived suppressor cells induce anergy of NK cells through membrane-bound TGF-beta 1.* J Immunol, 2009. **182**(1): p. 240-9.
119. Movahedi, K., et al., *Identification of discrete tumor-induced myeloid-derived suppressor cell subpopulations with distinct T cell-suppressive activity.* Blood, 2008. **111**(8): p. 4233-44.
120. Tartour, E., et al., *Angiogenesis and immunity: a bidirectional link potentially relevant for the monitoring of antiangiogenic therapy and the development of novel therapeutic combination with immunotherapy.* Cancer Metastasis Rev, 2011. **30**(1): p. 83-95.
121. Shojaei, F., et al., *G-CSF-initiated myeloid cell mobilization and angiogenesis mediate tumor refractoriness to anti-VEGF therapy in mouse models.* Proc Natl Acad Sci U S A, 2009. **106**(16): p. 6742-7.
122. Zhang, S., et al., *The Role of Myeloid-Derived Suppressor Cells in Patients with Solid Tumors: A Meta-Analysis.* PLoS One, 2016. **11**(10): p. e0164514.
123. Zhang, B., et al., *Circulating and tumor-infiltrating myeloid-derived suppressor cells in patients with colorectal carcinoma.* PLoS One, 2013. **8**(2): p. e57114.
124. Huang, A., et al., *Increased CD14(+)HLA-DR (-/low) myeloid-derived suppressor cells correlate with extrathoracic metastasis and poor response to chemotherapy in non-small cell lung cancer patients.* Cancer Immunol Immunother, 2013. **62**(9): p. 1439-51.
125. Yang, G., et al., *Accumulation of myeloid-derived suppressor cells (MDSCs) induced by low levels of IL-6 correlates with poor prognosis in bladder cancer.* Oncotarget, 2017. **8**(24): p. 38378-38388.
126. Diaz-Montero, C.M., et al., *Increased circulating myeloid-derived suppressor cells correlate with clinical cancer stage, metastatic tumor burden, and doxorubicin-cyclophosphamide chemotherapy.* Cancer Immunol Immunother, 2009. **58**(1): p. 49-59.
127. Jordan, K.R., et al., *Myeloid-derived suppressor cells are associated with disease progression and decreased overall survival in advanced-stage melanoma patients.* Cancer Immunol Immunother, 2013. **62**(11): p. 1711-22.
128. Biswas, S.K., P. Allavena, and A. Mantovani, *Tumor-associated macrophages: functional diversity, clinical significance, and open questions.* Semin Immunopathol, 2013. **35**(5): p. 585-600.
129. Stein, M., et al., *Interleukin 4 potently enhances murine macrophage mannose receptor activity: a marker of alternative immunologic macrophage activation.* J Exp Med, 1992. **176**(1): p. 287-92.
130. Mills, C.D., et al., *M-1/M-2 macrophages and the Th1/Th2 paradigm.* J Immunol, 2000. **164**(12): p. 6166-73.

131. Mantovani, A., et al., *Macrophage polarization: tumor-associated macrophages as a paradigm for polarized M2 mononuclear phagocytes.* Trends Immunol, 2002. **23**(11): p. 549-55.
132. Squadrito, M.L., et al., *MicroRNA-mediated control of macrophages and its implications for cancer.* Trends Immunol, 2013. **34**(7): p. 350-9.
133. Junttila, I.S., et al., *Tuning sensitivity to IL-4 and IL-13: differential expression of IL-4Ralpha, IL-13Ralpha1, and gammac regulates relative cytokine sensitivity.* J Exp Med, 2008. **205**(11): p. 2595-608.
134. Rawlings, J.S., K.M. Rosler, and D.A. Harrison, *The JAK/STAT signaling pathway.* J Cell Sci, 2004. **117**(Pt 8): p. 1281-3.
135. Welch, J.S., et al., *TH2 cytokines and allergic challenge induce Ym1 expression in macrophages by a STAT6-dependent mechanism.* J Biol Chem, 2002. **277**(45): p. 42821-9.
136. Ishii, M., et al., *Epigenetic regulation of the alternatively activated macrophage phenotype.* Blood, 2009. **114**(15): p. 3244-54.
137. Satoh, T., et al., *The Jmjd3-Irf4 axis regulates M2 macrophage polarization and host responses against helminth infection.* Nat Immunol, 2010. **11**(10): p. 936-44.
138. Bouhlel, M.A., et al., *PPARgamma activation primes human monocytes into alternative M2 macrophages with anti-inflammatory properties.* Cell Metab, 2007. **6**(2): p. 137-43.
139. Qin, H., et al., *SOCS3 deficiency promotes M1 macrophage polarization and inflammation.* J Immunol, 2012. **189**(7): p. 3439-48.
140. Schmitz, J., et al., *IL-33, an interleukin-1-like cytokine that signals via the IL-1 receptor-related protein ST2 and induces T helper type 2-associated cytokines.* Immunity, 2005. **23**(5): p. 479-90.
141. Kurowska-Stolarska, M., et al., *IL-33 amplifies the polarization of alternatively activated macrophages that contribute to airway inflammation.* J Immunol, 2009. **183**(10): p. 6469-77.
142. Wang, L., et al., *Indirect inhibition of Toll-like receptor and type I interferon responses by ITAM-coupled receptors and integrins.* Immunity, 2010. **32**(4): p. 518-30.
143. Zhang, Y., et al., *Immune complex/Ig negatively regulate TLR4-triggered inflammatory response in macrophages through Fc gamma RIIb-dependent PGE2 production.* J Immunol, 2009. **182**(1): p. 554-62.
144. Takeuchi, O. and S. Akira, *Pattern recognition receptors and inflammation.* Cell, 2010. **140**(6): p. 805-20.
145. Fitzgerald, K.A., et al., *LPS-TLR4 signaling to IRF-3/7 and NF-kappaB involves the toll adapters TRAM and TRIF.* J Exp Med, 2003. **198**(7): p. 1043-55.
146. Lehtonen, A., S. Matikainen, and I. Julkunen, *Interferons up-regulate STAT1, STAT2, and IRF family transcription factor gene expression in human peripheral blood mononuclear cells and macrophages.* J Immunol, 1997. **159**(2): p. 794-803.
147. Biswas, S.K. and A. Mantovani, *Macrophage plasticity and interaction with lymphocyte subsets: cancer as a paradigm.* Nat Immunol, 2010. **11**(10): p. 889-96.
148. Eichmuller, S.B., et al., *Immune Modulatory microRNAs Involved in Tumor Attack and Tumor Immune Escape.* J Natl Cancer Inst, 2017. **109**(10).
149. Graff, J.W., et al., *Identifying functional microRNAs in macrophages with polarized phenotypes.* J Biol Chem, 2012. **287**(26): p. 21816-25.
150. Tili, E., et al., *Modulation of miR-155 and miR-125b levels following lipopolysaccharide/TNF-alpha stimulation and their possible roles in regulating the response to endotoxin shock.* J Immunol, 2007. **179**(8): p. 5082-9.
151. Kim, S.W., et al., *MicroRNAs miR-125a and miR-125b constitutively activate the NF-kappaB pathway by targeting the tumor necrosis factor alpha-induced protein 3 (TNFAIP3, A20).* Proc Natl Acad Sci U S A, 2012. **109**(20): p. 7865-70.
152. Chaudhuri, A.A., et al., *MicroRNA-125b potentiates macrophage activation.* J Immunol, 2011. **187**(10): p. 5062-8.

153. O'Connell, R.M., et al., *MicroRNA-155 is induced during the macrophage inflammatory response.* Proc Natl Acad Sci U S A, 2007. **104**(5): p. 1604-9.
154. Wang, P., et al., *Inducible microRNA-155 feedback promotes type I IFN signaling in antiviral innate immunity by targeting suppressor of cytokine signaling 1.* J Immunol, 2010. **185**(10): p. 6226-33.
155. Nazari-Jahantigh, M., et al., *MicroRNA-155 promotes atherosclerosis by repressing Bcl6 in macrophages.* J Clin Invest, 2012. **122**(11): p. 4190-202.
156. Martinez-Nunez, R.T., F. Louafi, and T. Sanchez-Elsner, *The interleukin 13 (IL-13) pathway in human macrophages is modulated by microRNA-155 via direct targeting of interleukin 13 receptor alpha1 (IL13Ralpha1).* J Biol Chem, 2011. **286**(3): p. 1786-94.
157. Cai, X., et al., *Re-polarization of tumor-associated macrophages to pro-inflammatory M1 macrophages by microRNA-155.* J Mol Cell Biol, 2012. **4**(5): p. 341-3.
158. O'Connell, R.M., et al., *Inositol phosphatase SHIP1 is a primary target of miR-155.* Proc Natl Acad Sci U S A, 2009. **106**(17): p. 7113-8.
159. Yanaihara, N., et al., *Unique microRNA molecular profiles in lung cancer diagnosis and prognosis.* Cancer Cell, 2006. **9**(3): p. 189-98.
160. Chen, J., B.C. Wang, and J.H. Tang, *Clinical significance of microRNA-155 expression in human breast cancer.* J Surg Oncol, 2012. **106**(3): p. 260-6.
161. Volinia, S., et al., *A microRNA expression signature of human solid tumors defines cancer gene targets.* Proc Natl Acad Sci U S A, 2006. **103**(7): p. 2257-61.
162. Taganov, K.D., et al., *NF-kappaB-dependent induction of microRNA miR-146, an inhibitor targeted to signaling proteins of innate immune responses.* Proc Natl Acad Sci U S A, 2006. **103**(33): p. 12481-6.
163. Li, Y., et al., *Functions of miR-146a and miR-222 in Tumor-associated Macrophages in Breast Cancer.* Sci Rep, 2015. **5**: p. 18648.
164. Liu, G., et al., *miR-147, a microRNA that is induced upon Toll-like receptor stimulation, regulates murine macrophage inflammatory responses.* Proc Natl Acad Sci U S A, 2009. **106**(37): p. 15819-24.
165. Asangani, I.A., et al., *MicroRNA-21 (miR-21) post-transcriptionally downregulates tumor suppressor Pdcd4 and stimulates invasion, intravasation and metastasis in colorectal cancer.* Oncogene, 2008. **27**(15): p. 2128-36.
166. Bazzoni, F., et al., *Induction and regulatory function of miR-9 in human monocytes and neutrophils exposed to proinflammatory signals.* Proc Natl Acad Sci U S A, 2009. **106**(13): p. 5282-7.
167. Rossato, M., et al., *IL-10-induced microRNA-187 negatively regulates TNF-alpha, IL-6, and IL-12p40 production in TLR4-stimulated monocytes.* Proc Natl Acad Sci U S A, 2012. **109**(45): p. E3101-10.
168. Veremeyko, T., et al., *IL-4/IL-13-dependent and independent expression of miR-124 and its contribution to M2 phenotype of monocytic cells in normal conditions and during allergic inflammation.* PLoS One, 2013. **8**(12): p. e81774.
169. Ruckerl, D., et al., *Induction of IL-4Ralpha-dependent microRNAs identifies PI3K/Akt signaling as essential for IL-4-driven murine macrophage proliferation in vivo.* Blood, 2012. **120**(11): p. 2307-16.
170. Zhou, Y., et al., *Mannose receptor modulates macrophage polarization and allergic inflammation through miR-511-3p.* J Allergy Clin Immunol, 2018. **141**(1): p. 350-364 e8.
171. Squadrito, M.L., et al., *miR-511-3p modulates genetic programs of tumor-associated macrophages.* Cell Rep, 2012. **1**(2): p. 141-54.
172. Rodriguez-Prados, J.C., et al., *Substrate fate in activated macrophages: a comparison between innate, classic, and alternative activation.* J Immunol, 2010. **185**(1): p. 605-14.
173. Odegaard, J.I. and A. Chawla, *Alternative macrophage activation and metabolism.* Annu Rev Pathol, 2011. **6**: p. 275-97.

174. Biswas, S.K. and A. Mantovani, *Orchestration of metabolism by macrophages.* Cell Metab, 2012. **15**(4): p. 432-7.
175. Nairz, M., et al., *The co-ordinated regulation of iron homeostasis in murine macrophages limits the availability of iron for intracellular Salmonella typhimurium.* Cell Microbiol, 2007. **9**(9): p. 2126-40.
176. Alam, J., et al., *Nrf2, a Cap'n'Collar transcription factor, regulates induction of the heme oxygenase-1 gene.* J Biol Chem, 1999. **274**(37): p. 26071-8.
177. Cairo, G., et al., *Iron trafficking and metabolism in macrophages: contribution to the polarized phenotype.* Trends Immunol, 2011. **32**(6): p. 241-7.
178. Otterbein, L.E., et al., *Carbon monoxide has anti-inflammatory effects involving the mitogen-activated protein kinase pathway.* Nat Med, 2000. **6**(4): p. 422-8.
179. Qian, B.Z., et al., *CCL2 recruits inflammatory monocytes to facilitate breast-tumour metastasis.* Nature, 2011. **475**(7355): p. 222-5.
180. Zaynagetdinov, R., et al., *A critical role for macrophages in promotion of urethane-induced lung carcinogenesis.* J Immunol, 2011. **187**(11): p. 5703-11.
181. Movahedi, K., et al., *Different tumor microenvironments contain functionally distinct subsets of macrophages derived from Ly6C(high) monocytes.* Cancer Res, 2010. **70**(14): p. 5728-39.
182. Sica, A., et al., *Macrophage polarization in tumour progression.* Semin Cancer Biol, 2008. **18**(5): p. 349-55.
183. Kuang, D.M., et al., *Activated monocytes in peritumoral stroma of hepatocellular carcinoma foster immune privilege and disease progression through PD-L1.* J Exp Med, 2009. **206**(6): p. 1327-37.
184. Curiel, T.J., et al., *Specific recruitment of regulatory T cells in ovarian carcinoma fosters immune privilege and predicts reduced survival.* Nat Med, 2004. **10**(9): p. 942-9.
185. Munn, D.H., et al., *Inhibition of T cell proliferation by macrophage tryptophan catabolism.* J Exp Med, 1999. **189**(9): p. 1363-72.
186. Kryczek, I., et al., *B7-H4 expression identifies a novel suppressive macrophage population in human ovarian carcinoma.* J Exp Med, 2006. **203**(4): p. 871-81.
187. Smith, J.B., C. Stashwick, and D.J. Powell, *B7-H4 as a potential target for immunotherapy for gynecologic cancers: a closer look.* Gynecol Oncol, 2014. **134**(1): p. 181-189.
188. Rodriguez, P.C., et al., *Arginase I production in the tumor microenvironment by mature myeloid cells inhibits T-cell receptor expression and antigen-specific T-cell responses.* Cancer Res, 2004. **64**(16): p. 5839-49.
189. Lin, E.Y., et al., *Macrophages regulate the angiogenic switch in a mouse model of breast cancer.* Cancer Res, 2006. **66**(23): p. 11238-46.
190. DeNardo, D.G., et al., *CD4(+) T cells regulate pulmonary metastasis of mammary carcinomas by enhancing protumor properties of macrophages.* Cancer Cell, 2009. **16**(2): p. 91-102.
191. Giraudo, E., M. Inoue, and D. Hanahan, *An amino-bisphosphonate targets MMP-9-expressing macrophages and angiogenesis to impair cervical carcinogenesis.* J Clin Invest, 2004. **114**(5): p. 623-33.
192. Leek, R.D., et al., *Association of macrophage infiltration with angiogenesis and prognosis in invasive breast carcinoma.* Cancer Res, 1996. **56**(20): p. 4625-9.
193. Hanada, T., et al., *Prognostic value of tumor-associated macrophage count in human bladder cancer.* Int J Urol, 2000. **7**(7): p. 263-9.
194. Lissbrant, I.F., et al., *Tumor associated macrophages in human prostate cancer: relation to clinicopathological variables and survival.* Int J Oncol, 2000. **17**(3): p. 445-51.
195. Goswami, S., et al., *Macrophages promote the invasion of breast carcinoma cells via a colony-stimulating factor-1/epidermal growth factor paracrine loop.* Cancer Res, 2005. **65**(12): p. 5278-83.

196. Zhang, Q.W., et al., *Prognostic significance of tumor-associated macrophages in solid tumor: a meta-analysis of the literature.* PLoS One, 2012. **7**(12): p. e50946.
197. Medrek, C., et al., *The presence of tumor associated macrophages in tumor stroma as a prognostic marker for breast cancer patients.* BMC Cancer, 2012. **12**: p. 306.
198. Jensen, T.O., et al., *Macrophage markers in serum and tumor have prognostic impact in American Joint Committee on Cancer stage I/II melanoma.* J Clin Oncol, 2009. **27**(20): p. 3330-7.
199. Ma, J., et al., *The M1 form of tumor-associated macrophages in non-small cell lung cancer is positively associated with survival time.* BMC Cancer, 2010. **10**: p. 112.
200. Soria, G. and A. Ben-Baruch, *The inflammatory chemokines CCL2 and CCL5 in breast cancer.* Cancer Lett, 2008. **267**(2): p. 271-85.
201. Zhang, J., Y. Lu, and K.J. Pienta, *Multiple roles of chemokine (C-C motif) ligand 2 in promoting prostate cancer growth.* J Natl Cancer Inst, 2010. **102**(8): p. 522-8.
202. Gazzaniga, S., et al., *Targeting tumor-associated macrophages and inhibition of MCP-1 reduce angiogenesis and tumor growth in a human melanoma xenograft.* J Invest Dermatol, 2007. **127**(8): p. 2031-41.
203. D'Incalci, M. and C.M. Galmarini, *A review of trabectedin (ET-743): a unique mechanism of action.* Mol Cancer Ther, 2010. **9**(8): p. 2157-63.
204. Allavena, P., et al., *Anti-inflammatory properties of the novel antitumor agent yondelis (trabectedin): inhibition of macrophage differentiation and cytokine production.* Cancer Res, 2005. **65**(7): p. 2964-71.
205. Luo, Y., et al., *Targeting tumor-associated macrophages as a novel strategy against breast cancer.* J Clin Invest, 2006. **116**(8): p. 2132-2141.
206. Guiducci, C., et al., *Redirecting in vivo elicited tumor infiltrating macrophages and dendritic cells towards tumor rejection.* Cancer Res, 2005. **65**(8): p. 3437-46.
207. Banerjee, S., et al., *The combination of a novel immunomodulator with a regulatory T cell suppressing antibody (DTA-1) regress advanced stage B16F10 solid tumor by repolarizing tumor associated macrophages in situ.* Oncoimmunology, 2015. **4**(3): p. e995559.
208. Buhtoiarov, I.N., et al., *Anti-tumour synergy of cytotoxic chemotherapy and anti-CD40 plus CpG-ODN immunotherapy through repolarization of tumour-associated macrophages.* Immunology, 2011. **132**(2): p. 226-39.
209. Rolny, C., et al., *HRG inhibits tumor growth and metastasis by inducing macrophage polarization and vessel normalization through downregulation of PlGF.* Cancer Cell, 2011. **19**(1): p. 31-44.
210. Corthay, A., et al., *Primary antitumor immune response mediated by CD4+ T cells.* Immunity, 2005. **22**(3): p. 371-83.
211. Haabeth, O.A., et al., *Inflammation driven by tumour-specific Th1 cells protects against B-cell cancer.* Nat Commun, 2011. **2**: p. 240.
212. Klug, F., et al., *Low-dose irradiation programs macrophage differentiation to an iNOS(+)/M1 phenotype that orchestrates effective T cell immunotherapy.* Cancer Cell, 2013. **24**(5): p. 589-602.
213. Yan, H., et al., *IL-32γ Induces M2 Macrophage Polarization with Enhanced Ability of Macrophage-Mediated Drug Resistance in Myeloma Cells through STAT3 and NF-κB Activation.* Blood, 2017. **130**(Suppl 1): p. 1781-1781.
214. Pello, O.M., et al., *Role of c-MYC in alternative activation of human macrophages and tumor-associated macrophage biology.* Blood, 2012. **119**(2): p. 411-21.
215. Kapoor, N., et al., *Transcription factors STAT6 and KLF4 implement macrophage polarization via the dual catalytic powers of MCPIP.* J Immunol, 2015. **194**(12): p. 6011-23.
216. Tang, X., et al., *Anti-tumour strategies aiming to target tumour-associated macrophages.* Immunology, 2013. **138**(2): p. 93-104.
217. Rosenberg, S.A. and N.P. Restifo, *Adoptive cell transfer as personalized immunotherapy for human cancer.* Science, 2015. **348**(6230): p. 62-8.

218. Muul, L.M., et al., *Identification of specific cytolytic immune responses against autologous tumor in humans bearing malignant melanoma.* J Immunol, 1987. **138**(3): p. 989-95.
219. Pilon-Thomas, S., et al., *Efficacy of adoptive cell transfer of tumor-infiltrating lymphocytes after lymphopenia induction for metastatic melanoma.* J Immunother, 2012. **35**(8): p. 615-20.
220. Radvanyi, L.G., et al., *Specific lymphocyte subsets predict response to adoptive cell therapy using expanded autologous tumor-infiltrating lymphocytes in metastatic melanoma patients.* Clin Cancer Res, 2012. **18**(24): p. 6758-70.
221. Besser, M.J., et al., *Adoptive transfer of tumor-infiltrating lymphocytes in patients with metastatic melanoma: intent-to-treat analysis and efficacy after failure to prior immunotherapies.* Clin Cancer Res, 2013. **19**(17): p. 4792-800.
222. Rosenberg, S.A., et al., *Durable complete responses in heavily pretreated patients with metastatic melanoma using T-cell transfer immunotherapy.* Clin Cancer Res, 2011. **17**(13): p. 4550-7.
223. Morgan, R.A., et al., *Cancer regression in patients after transfer of genetically engineered lymphocytes.* Science, 2006. **314**(5796): p. 126-9.
224. Rapoport, A.P., et al., *NY-ESO-1-specific TCR-engineered T cells mediate sustained antigen-specific antitumor effects in myeloma.* Nat Med, 2015. **21**(8): p. 914-921.
225. Yip, A. and R.M. Webster, *The market for chimeric antigen receptor T cell therapies.* Nat Rev Drug Discov, 2018. **17**(3): p. 161-162.
226. Kumai, T., et al., *Peptide vaccines in cancer-old concept revisited.* Curr Opin Immunol, 2017. **45**: p. 1-7.
227. Slingluff, C.L., Jr., et al., *Helper T-cell responses and clinical activity of a melanoma vaccine with multiple peptides from MAGE and melanocytic differentiation antigens.* J Clin Oncol, 2008. **26**(30): p. 4973-80.
228. Slingluff, C.L., Jr., et al., *Immunologic and clinical outcomes of a randomized phase II trial of two multipeptide vaccines for melanoma in the adjuvant setting.* Clin Cancer Res, 2007. **13**(21): p. 6386-95.
229. Janssen, E.M., et al., *CD4+ T-cell help controls CD8+ T-cell memory via TRAIL-mediated activation-induced cell death.* Nature, 2005. **434**(7029): p. 88-93.
230. Zwaveling, S., et al., *Established human papillomavirus type 16-expressing tumors are effectively eradicated following vaccination with long peptides.* J Immunol, 2002. **169**(1): p. 350-8.
231. Fotin-Mleczek, M., et al., *Highly potent mRNA based cancer vaccines represent an attractive platform for combination therapies supporting an improved therapeutic effect.* J Gene Med, 2012. **14**(6): p. 428-39.
232. Kübler, H., et al., *Final analysis of a phase I/IIa study with CV9103, an intradermally administered prostate cancer immunotherapy based on self-adjuvanted mRNA.* Journal of Clinical Oncology, 2011. **29**(15_suppl): p. 4535-4535.
233. Hess, P.R., et al., *Vaccination with mRNAs encoding tumor-associated antigens and granulocyte-macrophage colony-stimulating factor efficiently primes CTL responses, but is insufficient to overcome tolerance to a model tumor/self antigen.* Cancer Immunol Immunother, 2006. **55**(6): p. 672-83.
234. Kranz, L.M., et al., *Systemic RNA delivery to dendritic cells exploits antiviral defence for cancer immunotherapy.* Nature, 2016. **534**(7607): p. 396-401.
235. Hsueh, E.C., et al., *Prolonged survival after complete resection of disseminated melanoma and active immunotherapy with a therapeutic cancer vaccine.* J Clin Oncol, 2002. **20**(23): p. 4549-54.
236. *CancerVax Announces Results of Phase 3 Clinical Trials of Canvaxin™ in Patients With Stage III and Stage IV Melanoma*. 2006 [cited 09.08.2018; Available from: http://www.marketwired.com/press-release/cancervax-announces-results-phase-3-clinical-trials-canvaxin-patients-with-stage-iii-nasdaq-cnvx-675445.htm.

237. Ward, J.E. and D.G. McNeel, *GVAX: an allogeneic, whole-cell, GM-CSF-secreting cellular immunotherapy for the treatment of prostate cancer.* Expert Opin Biol Ther, 2007. **7**(12): p. 1893-902.
238. Arlen, P.M., et al., *Promising novel immunotherapies and combinations for prostate cancer.* Future Oncol, 2009. **5**(2): p. 187-96.
239. Shak, S., *Overview of the trastuzumab (Herceptin) anti-HER2 monoclonal antibody clinical program in HER2-overexpressing metastatic breast cancer. Herceptin Multinational Investigator Study Group.* Semin Oncol, 1999. **26**(4 Suppl 12): p. 71-7.
240. Saltz, L.B., et al., *Phase II trial of cetuximab in patients with refractory colorectal cancer that expresses the epidermal growth factor receptor.* J Clin Oncol, 2004. **22**(7): p. 1201-8.
241. Gibson, T.B., A. Ranganathan, and A. Grothey, *Randomized phase III trial results of panitumumab, a fully human anti-epidermal growth factor receptor monoclonal antibody, in metastatic colorectal cancer.* Clin Colorectal Cancer, 2006. **6**(1): p. 29-31.
242. Davis, T.A., et al., *Rituximab anti-CD20 monoclonal antibody therapy in non-Hodgkin's lymphoma: safety and efficacy of re-treatment.* J Clin Oncol, 2000. **18**(17): p. 3135-43.
243. Scott, A.M., J.D. Wolchok, and L.J. Old, *Antibody therapy of cancer.* Nat Rev Cancer, 2012. **12**(4): p. 278-87.
244. Beatty, G.L., et al., *CD40 agonists alter tumor stroma and show efficacy against pancreatic carcinoma in mice and humans.* Science, 2011. **331**(6024): p. 1612-6.
245. Lawler, S.E., et al., *Oncolytic Viruses in Cancer Treatment: A Review.* JAMA Oncol, 2017. **3**(6): p. 841-849.
246. Liu, B.L., et al., *ICP34.5 deleted herpes simplex virus with enhanced oncolytic, immune stimulating, and anti-tumour properties.* Gene Ther, 2003. **10**(4): p. 292-303.
247. Aghi, M., et al., *Oncolytic herpes virus with defective ICP6 specifically replicates in quiescent cells with homozygous genetic mutations in p16.* Oncogene, 2008. **27**(30): p. 4249-54.
248. Singh, P., et al., *Development of PROSTVAC immunotherapy in prostate cancer.* Future Oncol, 2015. **11**(15): p. 2137-48.
249. Ahn, K., et al., *Molecular mechanism and species specificity of TAP inhibition by herpes simplex virus ICP47.* EMBO J, 1996. **15**(13): p. 3247-55.
250. Andtbacka, R.H., et al., *Talimogene Laherparepvec Improves Durable Response Rate in Patients With Advanced Melanoma.* J Clin Oncol, 2015. **33**(25): p. 2780-8.
251. Pol, J., et al., *Trial Watch:: Oncolytic viruses for cancer therapy.* Oncoimmunology, 2014. **3**: p. e28694.
252. Ohno, S., et al., *Phase I trial of Wilms' Tumor 1 (WT1) peptide vaccine with GM-CSF or CpG in patients with solid malignancy.* Anticancer Res, 2012. **32**(6): p. 2263-9.
253. Ratliff, T.L., *Bacillus Calmette-Guerin (BCG): mechanism of action in superficial bladder cancer.* Urology, 1991. **37**(5 Suppl): p. 8-11.
254. Centers for Disease, C. and Prevention, *FDA licensure of bivalent human papillomavirus vaccine (HPV2, Cervarix) for use in females and updated HPV vaccination recommendations from the Advisory Committee on Immunization Practices (ACIP).* MMWR Morb Mortal Wkly Rep, 2010. **59**(20): p. 626-9.
255. Vacchelli, E., et al., *Trial Watch: Toll-like receptor agonists for cancer therapy.* Oncoimmunology, 2013. **2**(8): p. e25238.
256. *Skin Cancer Treatment (PDQ(R)): Health Professional Version*. PDQ Cancer Information Summaries 2018 [cited 23.07.2018; Available from: https://www.cancer.gov/types/skin/hp/skin-treatment-pdq.
257. *Melanoma Treatment (PDQ®)–Health Professional Version*. PDQ Cancer Information Summaries 2018 [cited 23.07.2018; Available from: https://www.cancer.gov/types/skin/hp/melanoma-treatment-pdq.
258. Miller, A.J. and M.C. Mihm, Jr., *Melanoma.* N Engl J Med, 2006. **355**(1): p. 51-65.

259. Liu, Y. and M.S. Sheikh, *Melanoma: Molecular Pathogenesis and Therapeutic Management.* Mol Cell Pharmacol, 2014. **6**(3): p. 228.
260. Ferlay, J., et al., *Cancer incidence and mortality worldwide: sources, methods and major patterns in GLOBOCAN 2012.* Int J Cancer, 2015. **136**(5): p. E359-86.
261. Shain, A.H. and B.C. Bastian, *From melanocytes to melanomas.* Nat Rev Cancer, 2016. **16**(6): p. 345-58.
262. Lawrence, M.S., et al., *Mutational heterogeneity in cancer and the search for new cancer-associated genes.* Nature, 2013. **499**(7457): p. 214-218.
263. Hodis, E., et al., *A landscape of driver mutations in melanoma.* Cell, 2012. **150**(2): p. 251-63.
264. Rozeman, E.A., et al., *Advanced Melanoma: Current Treatment Options, Biomarkers, and Future Perspectives.* Am J Clin Dermatol, 2018. **19**(3): p. 303-317.
265. Huang, F.W., et al., *Highly recurrent TERT promoter mutations in human melanoma.* Science, 2013. **339**(6122): p. 957-9.
266. Krauthammer, M., et al., *Exome sequencing identifies recurrent somatic RAC1 mutations in melanoma.* Nat Genet, 2012. **44**(9): p. 1006-14.
267. Lawrence, D. and K. Rubin, *Melanoma.* Harrison's manual of oncology. New York: McGraw Hill, 2008: p. 537-48.
268. *Melanoma Staging: A Review of the Revised American Joint Committee on Cancer Guidelines*. Vol. 2. 2010. 260-261.
269. Gershenwald, J.E., et al., *Melanoma staging: Evidence-based changes in the American Joint Committee on Cancer eighth edition cancer staging manual.* CA Cancer J Clin, 2017. **67**(6): p. 472-492.
270. Marchesi, F., et al., *Triazene compounds: mechanism of action and related DNA repair systems.* Pharmacol Res, 2007. **56**(4): p. 275-87.
271. Middleton, M.R., et al., *Randomized phase III study of temozolomide versus dacarbazine in the treatment of patients with advanced metastatic malignant melanoma.* J Clin Oncol, 2000. **18**(1): p. 158-66.
272. Lee, S.M., D.C. Betticher, and N. Thatcher, *Melanoma: chemotherapy.* Br Med Bull, 1995. **51**(3): p. 609-30.
273. Davies, H., et al., *Mutations of the BRAF gene in human cancer.* Nature, 2002. **417**(6892): p. 949-54.
274. Robert, C., et al., *Improved overall survival in melanoma with combined dabrafenib and trametinib.* N Engl J Med, 2015. **372**(1): p. 30-9.
275. Larkin, J., et al., *Combined vemurafenib and cobimetinib in BRAF-mutated melanoma.* N Engl J Med, 2014. **371**(20): p. 1867-76.
276. Robert, C., et al., *Three-year estimate of overall survival in COMBI-v, a randomized phase 3 study evaluating first-line dabrafenib (D) + trametinib (T) in patients (pts) with unresectable or metastatic BRAF V600E/K–mutant cutaneous melanoma.* Annals of Oncology, 2016. **27**(suppl_6): p. LBA40-LBA40.
277. Long, G.V., et al., *Dabrafenib and trametinib versus dabrafenib and placebo for Val600 BRAF-mutant melanoma: a multicentre, double-blind, phase 3 randomised controlled trial.* Lancet, 2015. **386**(9992): p. 444-51.
278. Long, G.V., et al., *Dabrafenib plus trametinib versus dabrafenib monotherapy in patients with metastatic BRAF V600E/K-mutant melanoma: long-term survival and safety analysis of a phase 3 study.* Ann Oncol, 2017. **28**(7): p. 1631-1639.
279. Ascierto, P.A., et al., *Cobimetinib combined with vemurafenib in advanced BRAF(V600)-mutant melanoma (coBRIM): updated efficacy results from a randomised, double-blind, phase 3 trial.* Lancet Oncol, 2016. **17**(9): p. 1248-60.
280. Daud, A., et al., *Indirect treatment comparison of dabrafenib plus trametinib versus vemurafenib plus cobimetinib in previously untreated metastatic melanoma patients.* J Hematol Oncol, 2017. **10**(1): p. 3.
281. Schumacher, T.N. and R.D. Schreiber, *Neoantigens in cancer immunotherapy.* Science, 2015. **348**(6230): p. 69-74.

282. Chow, P., P. Angulo, and K.K. Adkins, *Current Therapy for Advanced Melanoma and a Look at Future Signaling Pathways to Target.* 2018, 2018. **2**(4): p. 12.
283. Ahmed, F., et al., *Mutations in Human Interferon alpha2b Gene and Potential as Risk Factor Associated with Female Breast Cancer.* Cancer Biother Radiopharm, 2016. **31**(6): p. 199-208.
284. Thomas, H., G. Foster, and D. Platis, *Mechanisms of action of interferon and nucleoside analogues.* J Hepatol, 2003. **39 Suppl 1**: p. S93-8.
285. Fox, M.C., et al., *Management options for metastatic melanoma in the era of novel therapies: a primer for the practicing dermatologist: part I: Management of stage III disease.* J Am Acad Dermatol, 2013. **68**(1): p. 1 e1-9; quiz 10-12.
286. Miyazaki, T., et al., *Three distinct IL-2 signaling pathways mediated by bcl-2, c-myc, and lck cooperate in hematopoietic cell proliferation.* Cell, 1995. **81**(2): p. 223-31.
287. Blackman, M.A., et al., *A model system for peptide hormone action in differentiation: interleukin 2 induces a B lymphoma to transcribe the J chain gene.* Cell, 1986. **47**(4): p. 609-17.
288. Gaffen, S.L. and K.D. Liu, *Overview of interleukin-2 function, production and clinical applications.* Cytokine, 2004. **28**(3): p. 109-23.
289. Khatri, V.P., et al., *Ultra low dose interleukin-2 therapy promotes a type 1 cytokine profile in vivo in patients with AIDS and AIDS-associated malignancies.* J Clin Invest, 1998. **101**(6): p. 1373-8.
290. Fox, M.C., et al., *Management options for metastatic melanoma in the era of novel therapies: a primer for the practicing dermatologist: part II: Management of stage IV disease.* J Am Acad Dermatol, 2013. **68**(1): p. 13 e1-13; quiz 26-8.
291. Garbe, C., et al., *Systematic review of medical treatment in melanoma: current status and future prospects.* Oncologist, 2011. **16**(1): p. 5-24.
292. Simpson, T.R., et al., *Fc-dependent depletion of tumor-infiltrating regulatory T cells co-defines the efficacy of anti-CTLA-4 therapy against melanoma.* J Exp Med, 2013. **210**(9): p. 1695-710.
293. Hodi, F.S., et al., *Improved survival with ipilimumab in patients with metastatic melanoma.* N Engl J Med, 2010. **363**(8): p. 711-23.
294. Larkin, J., et al., *Combined Nivolumab and Ipilimumab or Monotherapy in Untreated Melanoma.* N Engl J Med, 2015. **373**(1): p. 23-34.
295. Robert, C., et al., *Pembrolizumab versus Ipilimumab in Advanced Melanoma.* N Engl J Med, 2015. **372**(26): p. 2521-32.
296. Schachter, J., et al., *Pembrolizumab versus ipilimumab for advanced melanoma: final overall survival results of a multicentre, randomised, open-label phase 3 study (KEYNOTE-006).* Lancet, 2017. **390**(10105): p. 1853-1862.
297. Wolchok, J.D., et al., *Overall Survival with Combined Nivolumab and Ipilimumab in Advanced Melanoma.* N Engl J Med, 2017. **377**(14): p. 1345-1356.
298. Weber, J., *Ipilimumab: controversies in its development, utility and autoimmune adverse events.* Cancer Immunol Immunother, 2009. **58**(5): p. 823-30.
299. Robert, C., et al., *Nivolumab in previously untreated melanoma without BRAF mutation.* N Engl J Med, 2015. **372**(4): p. 320-30.
300. Robert, C., et al., *Long-term outcomes in patients (pts) with ipilimumab (ipi)-naive advanced melanoma in the phase 3 KEYNOTE-006 study who completed pembrolizumab (pembro) treatment.* Journal of Clinical Oncology, 2017. **35**(15_suppl): p. 9504-9504.
301. Robert, C., et al., *Ipilimumab plus dacarbazine for previously untreated metastatic melanoma.* N Engl J Med, 2011. **364**(26): p. 2517-26.
302. Hodi, F.S., et al., *Combined nivolumab and ipilimumab versus ipilimumab alone in patients with advanced melanoma: 2-year overall survival outcomes in a multicentre, randomised, controlled, phase 2 trial.* Lancet Oncol, 2016. **17**(11): p. 1558-1568.
303. Tatano, Y., T. Shimizu, and H. Tomioka, *Unique macrophages different from M1/M2 macrophages inhibit T cell mitogenesis while upregulating Th17 polarization.* Sci Rep, 2014. **4**: p. 4146.

304. Zhu, L., et al., *TSC1 controls macrophage polarization to prevent inflammatory disease.* Nat Commun, 2014. **5**: p. 4696.
305. Davis, M.J., et al., *Macrophage M1/M2 polarization dynamically adapts to changes in cytokine microenvironments in Cryptococcus neoformans infection.* MBio, 2013. **4**(3): p. e00264-13.
306. Shaul, M.E., et al., *Dynamic, M2-like remodeling phenotypes of CD11c+ adipose tissue macrophages during high-fat diet--induced obesity in mice.* Diabetes, 2010. **59**(5): p. 1171-81.
307. Das, K., et al., *Generation of murine tumor cell lines deficient in MHC molecule surface expression using the CRISPR/Cas9 system.* PLoS One, 2017. **12**(3): p. e0174077.
308. Cong, L., et al., *Multiplex genome engineering using CRISPR/Cas systems.* Science, 2013. **339**(6121): p. 819-23.
309. Pacheco, P., D. White, and T. Sulchek, *Effects of microparticle size and Fc density on macrophage phagocytosis.* PLoS One, 2013. **8**(4): p. e60989.
310. Seyrantepe, V., et al., *Regulation of phagocytosis in macrophages by neuraminidase 1.* J Biol Chem, 2010. **285**(1): p. 206-15.
311. Kim, D., et al., *TopHat2: accurate alignment of transcriptomes in the presence of insertions, deletions and gene fusions.* Genome Biol, 2013. **14**(4): p. R36.
312. Liao, Y., G.K. Smyth, and W. Shi, *The Subread aligner: fast, accurate and scalable read mapping by seed-and-vote.* Nucleic Acids Res, 2013. **41**(10): p. e108.
313. Liao, Y., G.K. Smyth, and W. Shi, *featureCounts: an efficient general purpose program for assigning sequence reads to genomic features.* Bioinformatics, 2014. **30**(7): p. 923-30.
314. Love, M.I., W. Huber, and S. Anders, *Moderated estimation of fold change and dispersion for RNA-seq data with DESeq2.* Genome Biol, 2014. **15**(12): p. 550.
315. Robinson, A., C. Meredith, and B.M. Austen, *Isolation and properties of the signal region from ovalbumin.* FEBS Lett, 1986. **203**(2): p. 243-6.
316. Robertson, J.M., P.E. Jensen, and B.D. Evavold, *DO11.10 and OT-II T cells recognize a C-terminal ovalbumin 323-339 epitope.* J Immunol, 2000. **164**(9): p. 4706-12.
317. Li, L., et al., *The effect of the size of fluorescent dextran on its endocytic pathway.* Cell Biology International, 2015. **39**(5): p. 531-539.
318. Commisso, C., R.J. Flinn, and D. Bar-Sagi, *Determining the macropinocytic index of cancer cells through a quantitative image-based assay.* Nature protocols, 2014. **9**(1): p. 182-192.
319. Poos, A.M., et al., *Mixed Integer Linear Programming based machine learning approach identifies regulators of telomerase in yeast.* Nucleic Acids Res, 2016. **44**(10): p. e93.
320. Schacht, T., et al., *Estimating the activity of transcription factors by the effect on their target genes.* Bioinformatics, 2014. **30**(17): p. i401-7.
321. Schnyder, J., et al., *Secretion of Lysosomal Enzymes by Macrophages*, in *Mononuclear Phagocytes: Functional Aspects*, R. van Furth, Editor. 1980, Springer Netherlands: Dordrecht. p. 1369-1384.
322. Consortium, E.P., *An integrated encyclopedia of DNA elements in the human genome.* Nature, 2012. **489**(7414): p. 57-74.
323. Essaghir, A. and J.B. Demoulin, *A minimal connected network of transcription factors regulated in human tumors and its application to the quest for universal cancer biomarkers.* PLoS One, 2012. **7**(6): p. e39666.
324. Essaghir, A., et al., *Transcription factor regulation can be accurately predicted from the presence of target gene signatures in microarray gene expression data.* Nucleic Acids Res, 2010. **38**(11): p. e120.
325. Lachmann, A., et al., *ChEA: transcription factor regulation inferred from integrating genome-wide ChIP-X experiments.* Bioinformatics, 2010. **26**(19): p. 2438-44.

326. Loots, G. and I. Ovcharenko, *ECRbase: database of evolutionary conserved regions, promoters, and transcription factor binding sites in vertebrate genomes.* Bioinformatics, 2007. **23**(1): p. 122-4.
327. Sloan, C.A., et al., *ENCODE data at the ENCODE portal.* Nucleic Acids Res, 2016. **44**(D1): p. D726-32.
328. Sander, J.D. and J.K. Joung, *CRISPR-Cas systems for editing, regulating and targeting genomes.* Nat Biotechnol, 2014. **32**(4): p. 347-55.
329. Horii, T., et al., *Genome engineering of mammalian haploid embryonic stem cells using the Cas9/RNA system.* PeerJ, 2013. **1**: p. e230.
330. Yu, Z., et al., *Highly efficient genome modifications mediated by CRISPR/Cas9 in Drosophila.* Genetics, 2013. **195**(1): p. 289-91.
331. Mandal, P.K., et al., *Efficient ablation of genes in human hematopoietic stem and effector cells using CRISPR/Cas9.* Cell Stem Cell, 2014. **15**(5): p. 643-52.
332. Mali, P., et al., *RNA-guided human genome engineering via Cas9.* Science, 2013. **339**(6121): p. 823-6.
333. Liu, X., et al., *Sequence features associated with the cleavage efficiency of CRISPR/Cas9 system.* Sci Rep, 2016. **6**: p. 19675.
334. Wong, N., W. Liu, and X. Wang, *WU-CRISPR: characteristics of functional guide RNAs for the CRISPR/Cas9 system.* Genome Biol, 2015. **16**: p. 218.
335. Fu, Y., et al., *High-frequency off-target mutagenesis induced by CRISPR-Cas nucleases in human cells.* Nat Biotechnol, 2013. **31**(9): p. 822-6.
336. Fu, Y., et al., *Improving CRISPR-Cas nuclease specificity using truncated guide RNAs.* Nat Biotechnol, 2014. **32**(3): p. 279-284.
337. Kleinstiver, B.P., et al., *High-fidelity CRISPR-Cas9 nucleases with no detectable genome-wide off-target effects.* Nature, 2016. **529**(7587): p. 490-5.
338. Guilinger, J.P., D.B. Thompson, and D.R. Liu, *Fusion of catalytically inactive Cas9 to FokI nuclease improves the specificity of genome modification.* Nat Biotechnol, 2014. **32**(6): p. 577-582.
339. Ran, F.A., et al., *Double nicking by RNA-guided CRISPR Cas9 for enhanced genome editing specificity.* Cell, 2013. **154**(6): p. 1380-9.
340. Hu, H.Y. and H.N. Du, *Alpha-to-beta structural transformation of ovalbumin: heat and pH effects.* J Protein Chem, 2000. **19**(3): p. 177-83.
341. Rotzschke, O., et al., *Exact prediction of a natural T cell epitope.* Eur J Immunol, 1991. **21**(11): p. 2891-4.
342. Murphy, K.M., A.B. Heimberger, and D.Y. Loh, *Induction by antigen of intrathymic apoptosis of CD4+CD8+TCRlo thymocytes in vivo.* Science, 1990. **250**(4988): p. 1720-3.
343. Barnden, M.J., et al., *Defective TCR expression in transgenic mice constructed using cDNA-based alpha- and beta-chain genes under the control of heterologous regulatory elements.* Immunol Cell Biol, 1998. **76**(1): p. 34-40.
344. Hogquist, K.A., et al., *T cell receptor antagonist peptides induce positive selection.* Cell, 1994. **76**(1): p. 17-27.
345. Meek, R.L., K.A. Walsh, and R.D. Palmiter, *The signal sequence of ovalbumin is located near the NH2 terminus.* J Biol Chem, 1982. **257**(20): p. 12245-51.
346. Rowe, H.M., et al., *Immunization with a lentiviral vector stimulates both CD4 and CD8 T cell responses to an ovalbumin transgene.* Mol Ther, 2006. **13**(2): p. 310-9.
347. Shen, L. and K.L. Rock, *Cellular protein is the source of cross-priming antigen in vivo.* Proc Natl Acad Sci U S A, 2004. **101**(9): p. 3035-40.
348. Ramsbottom, K.M., et al., *Lethal giant larvae-1 deficiency enhances the CD8(+) effector T-cell response to antigen challenge in vivo.* Immunol Cell Biol, 2016. **94**(3): p. 306-11.
349. Gottschalk, S., et al., *A vaccine that co-targets tumor cells and cancer associated fibroblasts results in enhanced antitumor activity by inducing antigen spreading.* PLoS One, 2013. **8**(12): p. e82658.

350. Gilfillan, S., et al., *DNAM-1 promotes activation of cytotoxic lymphocytes by nonprofessional antigen-presenting cells and tumors.* J Exp Med, 2008. **205**(13): p. 2965-73.
351. Baklaushev, V.P., et al., *Luciferase Expression Allows Bioluminescence Imaging But Imposes Limitations on the Orthotopic Mouse (4T1) Model of Breast Cancer.* Sci Rep, 2017. **7**(1): p. 7715.
352. Limberis, M.P., C.L. Bell, and J.M. Wilson, *Identification of the murine firefly luciferase-specific CD8 T-cell epitopes.* Gene Ther, 2009. **16**(3): p. 441-7.
353. Chen, Z., C. Benoist, and D. Mathis, *How defects in central tolerance impinge on a deficiency in regulatory T cells.* Proceedings of the National Academy of Sciences of the United States of America, 2005. **102**(41): p. 14735-14740.
354. Zou, Q., et al., *T cell development involves TRAF3IP3-mediated ERK signaling in the Golgi.* The Journal of Experimental Medicine, 2015. **212**(8): p. 1323-1336.
355. Egawa, T., et al., *Lineage Diversion of T Cell Receptor Transgenic Thymocytes Revealed by Lineage Fate Mapping.* PLOS ONE, 2008. **3**(1): p. e1512.
356. von Boehmer, H., J. Kirberg, and B. Rocha, *An unusual lineage of alpha/beta T cells that contains autoreactive cells.* The Journal of Experimental Medicine, 1991. **174**(5): p. 1001-1008.
357. Oishi, S., et al., *M2 polarization of murine peritoneal macrophages induces regulatory cytokine production and suppresses T-cell proliferation.* Immunology, 2016. **149**(3): p. 320-328.
358. Rodriguez, D., et al., *Tumor microenvironment profoundly modifies functional status of macrophages: peritoneal and tumor-associated macrophages are two very different subpopulations.* Cell Immunol, 2013. **283**(1-2): p. 51-60.
359. Gray, M.J., et al., *Induction of arginase I transcription by IL-4 requires a composite DNA response element for STAT6 and C/EBPbeta.* Gene, 2005. **353**(1): p. 98-106.
360. El Kasmi, K.C., et al., *Toll-like receptor-induced arginase 1 in macrophages thwarts effective immunity against intracellular pathogens.* Nat Immunol, 2008. **9**(12): p. 1399-406.
361. Sonoki, T., et al., *Coinduction of nitric-oxide synthase and arginase I in cultured rat peritoneal macrophages and rat tissues in vivo by lipopolysaccharide.* J Biol Chem, 1997. **272**(6): p. 3689-93.
362. Ryan, J.L., W.B. Yohe, and D.C. Morrison, *Stimulation of peritoneal cell arginase by bacterial lipopolysaccharides.* Am J Pathol, 1980. **99**(2): p. 451-62.
363. Watanabe, N., et al., *Sepsis induces incomplete M2 phenotype polarization in peritoneal exudate cells in mice.* J Intensive Care, 2016. **4**: p. 6.
364. Boonstra, A., et al., *Macrophages and myeloid dendritic cells, but not plasmacytoid dendritic cells, produce IL-10 in response to MyD88- and TRIF-dependent TLR signals, and TLR-independent signals.* J Immunol, 2006. **177**(11): p. 7551-8.
365. Saraiva, M. and A. O'Garra, *The regulation of IL-10 production by immune cells.* Nat Rev Immunol, 2010. **10**(3): p. 170-81.
366. Hammer, M., et al., *Control of dual-specificity phosphatase-1 expression in activated macrophages by IL-10.* Eur J Immunol, 2005. **35**(10): p. 2991-3001.
367. Hu, X., et al., *IFN-gamma suppresses IL-10 production and synergizes with TLR2 by regulating GSK3 and CREB/AP-1 proteins.* Immunity, 2006. **24**(5): p. 563-74.
368. Heusinkveld, M., et al., *M2 Macrophages Induced by Prostaglandin E2 and IL-6 from Cervical Carcinoma Are Switched to Activated M1 Macrophages by CD4+ Th1 Cells.* The Journal of Immunology, 2011. **187**(3): p. 1157-1165.
369. Belmares, M.P., et al., *Structural factors contributing to DM susceptibility of MHC class II/peptide complexes.* J Immunol, 2002. **169**(9): p. 5109-17.
370. Nielsen, M. and O. Lund, *NN-align. An artificial neural network-based alignment algorithm for MHC class II peptide binding prediction.* BMC Bioinformatics, 2009. **10**: p. 296.
371. Nielsen, M., et al., *Reliable prediction of T-cell epitopes using neural networks with novel sequence representations.* Protein Sci, 2003. **12**(5): p. 1007-17.

372. Bogen, B., et al., *Naive CD4+ T cells confer idiotype-specific tumor resistance in the absence of antibodies.* Eur J Immunol, 1995. **25**(11): p. 3079-86.
373. Tveita, A., et al., *Tumor-specific CD4+ T cells eradicate myeloma cells genetically deficient in MHC class II display.* Oncotarget, 2016. **7**(41): p. 67175-67182.
374. Tveita, A.A., et al., *Indirect CD4+ T-cell-mediated elimination of MHC II(NEG) tumor cells is spatially restricted and fails to prevent escape of antigen-negative cells.* Eur J Immunol, 2014. **44**(9): p. 2625-37.
375. Tveita, A.A., et al., *Tumors Escape CD4+ T-cell-Mediated Immunosurveillance by Impairing the Ability of Infiltrating Macrophages to Indirectly Present Tumor Antigens.* Cancer Res, 2015. **75**(16): p. 3268-78.
376. Huang, Y., et al., *Vascular normalization as an emerging strategy to enhance cancer immunotherapy.* Cancer Res, 2013. **73**(10): p. 2943-8.
377. Nagy, J.A., et al., *Why are tumour blood vessels abnormal and why is it important to know?* Br J Cancer, 2009. **100**(6): p. 865-9.
378. Shrimali, R.K., et al., *Antiangiogenic agents can increase lymphocyte infiltration into tumor and enhance the effectiveness of adoptive immunotherapy of cancer.* Cancer Res, 2010. **70**(15): p. 6171-80.
379. Baruch, E.N., et al., *Adoptive T cell therapy: An overview of obstacles and opportunities.* Cancer, 2017. **123**(S11): p. 2154-2162.
380. Moon, E.K., et al., *Expression of a functional CCR2 receptor enhances tumor localization and tumor eradication by retargeted human T cells expressing a mesothelin-specific chimeric antibody receptor.* Clin Cancer Res, 2011. **17**(14): p. 4719-30.
381. Russo, V., et al., *Dendritic cells acquire the MAGE-3 human tumor antigen from apoptotic cells and induce a class I-restricted T cell response.* Proc Natl Acad Sci U S A, 2000. **97**(5): p. 2185-90.
382. Berard, F., et al., *Cross-priming of naive CD8 T cells against melanoma antigens using dendritic cells loaded with killed allogeneic melanoma cells.* J Exp Med, 2000. **192**(11): p. 1535-44.
383. Nouri-Shirazi, M., et al., *Dendritic cells capture killed tumor cells and present their antigens to elicit tumor-specific immune responses.* J Immunol, 2000. **165**(7): p. 3797-803.
384. Bennett, S.R., et al., *B cells directly tolerize CD8(+) T cells.* J Exp Med, 1998. **188**(11): p. 1977-83.
385. Qin, Z., et al., *B cells inhibit induction of T cell-dependent tumor immunity.* Nat Med, 1998. **4**(5): p. 627-30.
386. Clatza, A., et al., *CD40-induced aggregation of MHC class II and CD80 on the cell surface leads to an early enhancement in antigen presentation.* J Immunol, 2003. **171**(12): p. 6478-87.
387. Buhlmann, J.E., et al., *In the absence of a CD40 signal, B cells are tolerogenic.* Immunity, 1995. **2**(6): p. 645-53.
388. Czimmerer, Z., et al., *The Transcription Factor STAT6 Mediates Direct Repression of Inflammatory Enhancers and Limits Activation of Alternatively Polarized Macrophages.* Immunity, 2018. **48**(1): p. 75-90 e6.
389. Gong, M., X. Zhuo, and A. Ma, *STAT6 Upregulation Promotes M2 Macrophage Polarization to Suppress Atherosclerosis.* Med Sci Monit Basic Res, 2017. **23**: p. 240-249.
390. Ohmori, Y. and T.A. Hamilton, *STAT6 is required for the anti-inflammatory activity of interleukin-4 in mouse peritoneal macrophages.* J Biol Chem, 1998. **273**(44): p. 29202-9.
391. Nguyen, V.T. and E.N. Benveniste, *IL-4-activated STAT-6 inhibits IFN-gamma-induced CD40 gene expression in macrophages/microglia.* J Immunol, 2000. **165**(11): p. 6235-43.

392. Ohmori, Y. and T.A. Hamilton, *Interleukin-4/STAT6 represses STAT1 and NF-kappa B-dependent transcription through distinct mechanisms.* J Biol Chem, 2000. **275**(48): p. 38095-103.
393. Takeda, K., et al., *Essential role of Stat6 in IL-4 signalling.* Nature, 1996. **380**(6575): p. 627-30.
394. Hiroi, M., et al., *Anti-inflammatory cytokine interleukin-4 inhibits inducible nitric oxide synthase gene expression in the mouse macrophage cell line RAW264.7 through the repression of octamer-dependent transcription.* Mediators Inflamm, 2013. **2013**: p. 369693.
395. Liao, X., et al., *Kruppel-like factor 4 regulates macrophage polarization.* J Clin Invest, 2011. **121**(7): p. 2736-49.
396. Chawla, A., *Control of macrophage activation and function by PPARs.* Circ Res, 2010. **106**(10): p. 1559-69.
397. Ricote, M., et al., *The peroxisome proliferator-activated receptor-gamma is a negative regulator of macrophage activation.* Nature, 1998. **391**(6662): p. 79-82.
398. Odegaard, J.I., et al., *Macrophage-specific PPARgamma controls alternative activation and improves insulin resistance.* Nature, 2007. **447**(7148): p. 1116-20.
399. Coste, A., et al., *PPARgamma promotes mannose receptor gene expression in murine macrophages and contributes to the induction of this receptor by IL-13.* Immunity, 2003. **19**(3): p. 329-39.
400. Szanto, A., et al., *STAT6 transcription factor is a facilitator of the nuclear receptor PPARgamma-regulated gene expression in macrophages and dendritic cells.* Immunity, 2010. **33**(5): p. 699-712.
401. Vats, D., et al., *Oxidative metabolism and PGC-1beta attenuate macrophage-mediated inflammation.* Cell Metab, 2006. **4**(1): p. 13-24.
402. Phillips, J.E. and V.G. Corces, *CTCF: master weaver of the genome.* Cell, 2009. **137**(7): p. 1194-211.
403. Nikolic, T., et al., *The DNA-binding factor Ctcf critically controls gene expression in macrophages.* Cell Mol Immunol, 2014. **11**(1): p. 58-70.
404. Majumder, P., J.A. Gomez, and J.M. Boss, *The human major histocompatibility complex class II HLA-DRB1 and HLA-DQA1 genes are separated by a CTCF-binding enhancer-blocking element.* J Biol Chem, 2006. **281**(27): p. 18435-43.
405. Iglesias-Ara, A. and A.M. Zubiaga, *The stress of coping with E2F loss.* Mol Cell Oncol, 2016. **3**(1): p. e1038423.
406. Lim, C.A., et al., *Genome-wide mapping of RELA(p65) binding identifies E2F1 as a transcriptional activator recruited by NF-kappaB upon TLR4 activation.* Mol Cell, 2007. **27**(4): p. 622-35.
407. Yang, I.V., et al., *Novel regulators of the systemic response to lipopolysaccharide.* Am J Respir Cell Mol Biol, 2011. **45**(2): p. 393-402.
408. Ivana V. Yang, L.A.W., Steve D. Groshong, David A. Schwartz *The role of the E2F1 transcription factor in innate immunity in mice*. 2010; Available from: https://doi.org/10.1164/ajrccm-conference.2010.181.1_MeetingAbstracts.A5739
409. Meyer, N. and L.Z. Penn, *Reflecting on 25 years with MYC.* Nat Rev Cancer, 2008. **8**(12): p. 976-90.
410. Jablonski, K.A., et al., *Novel Markers to Delineate Murine M1 and M2 Macrophages.* PLoS One, 2015. **10**(12): p. e0145342.
411. Hao, J., et al., *Involvement of JNK signaling in IL4-induced M2 macrophage polarization.* Exp Cell Res, 2017. **357**(2): p. 155-162.
412. Zhong, X., et al., *Myc-nick promotes efferocytosis through M2 macrophage polarization during resolution of inflammation.* FASEB J, 2018: p. fj201800223R.
413. Zhang, Y., et al., *Expression profiles of miRNAs in polarized macrophages.* Int J Mol Med, 2013. **31**(4): p. 797-802.
414. Lu, L., et al., *Time Series miRNA-mRNA integrated analysis reveals critical miRNAs and targets in macrophage polarization.* Sci Rep, 2016. **6**: p. 37446.

415. Qi, J., et al., *microRNA-210 negatively regulates LPS-induced production of proinflammatory cytokines by targeting NF-kappaB1 in murine macrophages.* FEBS Lett, 2012. **586**(8): p. 1201-7.
416. Dueck, A., et al., *A miR-155-dependent microRNA hierarchy in dendritic cell maturation and macrophage activation.* FEBS Lett, 2014. **588**(4): p. 632-40.
417. Jha, A.K., et al., *Network integration of parallel metabolic and transcriptional data reveals metabolic modules that regulate macrophage polarization.* Immunity, 2015. **42**(3): p. 419-30.
418. Galardi, S., et al., *NF-kB and c-Jun induce the expression of the oncogenic miR-221 and miR-222 in prostate carcinoma and glioblastoma cells.* Nucleic Acids Res, 2011. **39**(9): p. 3892-902.
419. Ying, X., et al., *Epithelial ovarian cancer-secreted exosomal miR-222-3p induces polarization of tumor-associated macrophages.* Oncotarget, 2016. **7**(28): p. 43076-43087.
420. Bussing, I., F.J. Slack, and H. Grosshans, *let-7 microRNAs in development, stem cells and cancer.* Trends Mol Med, 2008. **14**(9): p. 400-9.
421. Banerjee, S., et al., *MicroRNA let-7c regulates macrophage polarization.* J Immunol, 2013. **190**(12): p. 6542-9.
422. Wang, Z., et al., *miRNA let-7b modulates macrophage polarization and enhances tumor-associated macrophages to promote angiogenesis and mobility in prostate cancer.* Sci Rep, 2016. **6**: p. 25602.
423. Chen, X.M., et al., *A cellular micro-RNA, let-7i, regulates Toll-like receptor 4 expression and contributes to cholangiocyte immune responses against Cryptosporidium parvum infection.* J Biol Chem, 2007. **282**(39): p. 28929-38.
424. Satoh, M., et al., *Expression of let-7i is associated with Toll-like receptor 4 signal in coronary artery disease: effect of statins on let-7i and Toll-like receptor 4 signal.* Immunobiology, 2012. **217**(5): p. 533-9.
425. Wei, Y. and A. Schober, *MicroRNA regulation of macrophages in human pathologies.* Cell Mol Life Sci, 2016. **73**(18): p. 3473-95.
426. Wolf, Y., et al., *Microglial MHC class II is dispensable for experimental autoimmune encephalomyelitis and cuprizone-induced demyelination.* Eur J Immunol, 2018.

Publications and Abstracts

Publications

Laske K, Shebzukhov YV, Grosse-Hovest L, Kuprash DV, Khlgatian SV, Koroleva EP, Sazykin AY, Penkov DN, Belousov PV, Stevanovic S, Vass V, Walter S, Eisel D, Schmid-Horch BD, Nedospasov SA, Rammensee HG, Gouttefangeas C, *Alternative variants of human HYDIN are novel cancer-associated antigens recognized by adaptive immunity*. Cancer Immunol Res, 2013. **1**(3): p. 190-200.

Das K*, Eisel D*, Lenkl C, Goyal A, Diederichs S, Dickes E, Osen W, Eichmüller SB, *Generation of murine tumor cell lines deficient in MHC molecule surface expression using the CRISPR/Cas9 system.* PLoS One, 2017. 12(3): p. e0174077. *contributed equally

Kordaß T, Weber C, Eisel D, Pane A, Osen W, Eichmüller SB, *miR-193b and miR-30c-1* inhibit, whereas miR-576-5p enhances melanoma cell invasion in vitro.*
Oncotarget, 2018. 9:32507-32522.

Das K, Eisel D, Vormehr M, Müller-Decker K, Hommertgen A, Jäger D, Zörnig I, Feuerer M, Kopp-Schneider A, Osen W, Eichmüller SB, *A transplantable tumor model allowing investigation of NY-BR-1-specific T cell responses in HLA-DRB1*0401 transgenic mice.*
Submitted to Cancer Immunology, Immunotherapy, 2018.

Herster F, Bittner Z, Dickhoefer S, Eisel D, Eigenbrod T, Knorpp T, Schneiderhan-Marra N, Loeffler MW, Hartl D, Heiser M, Ghoreschi K, Weber ANR, *Complexes of RNA and the antimicrobial peptide, LL37, trigger TLR-mediated cytokine release from psoriasis neutrophils.*
Submitted to Nature Communications, 2018. (in revision)

Ast V, Kordaß T, Oswald M, Kolte A, Eisel D, Osen W, Eichmüller SB, Berndt A, König R, *Piecewise linear regression identifies miR-192, miR-200c and miR-17 as fibroblast-mediated inhibitors of colorectal cancer invasion.*
Submitted to Oncotarget, 2018. (in revision).

Abstracts

Das K, Eisel D, Nicolaus C, Goyal A, Diederichs S, Dickes E, Osen W, Eichmüller SB.
Generation of MHC class I and class II deficient tumor cell lines using the CRISPR/Cas9 system.
Cancer Immunotherapy Meeting 2016, Mainz, Germany.
(poster presentation)

Eisel D, Das K, Osen W, Eichmüller SB.
Antigen-specific interaction with activated CD4 T cells induces M1 associated gene expression in M2 polarized macrophages.
Tumor Immunology meets Oncology Meeting 2017, Halle, Germany.
(oral presentation)

Eisel D, Das K, Osen W, Eichmüller SB.
Antigen-specific interaction with CD4 T cells induces M1 associated gene expression in M2 polarized macrophages.
ENII Summer School of Immunology 2017, Porto Cervo, Italy.
(poster presentation)

Eisel D, Das K, Osen W, Eichmüller SB.
Antigen-specific interaction with activated CD4 T cells induces M1 associated gene expression in M2 polarized macrophages.
CRI-CIMT-EATI-AACR International Cancer Immunotherapy Conference 2017, Mainz, Germany.
(poster presentation)

Hoerhold F, Oswald M, Eisel D, Kolte A, Eichmüller SB, and König R.
Modeling the metabolic reprogramming of macrophage activation.
Weimar Sepsis Update 2017, Weimar, Germany.

Hoerhold F, Oswald M, Eisel D, Kolte A, Eichmüller SB, and König R.
Modeling the metabolic reprogramming of macrophage activation.
Systems Biology of Microbial Infection 2017, Jena, Germany.

Eisel D, Das K, Osen W, Hoerhold F, König R, Eichmüller SB.
Antigen-specific interaction with CD4 T cells induces M1 associated gene expression in M2 polarized macrophages.
Hallmarks of Skin Cancer Conference 2017, Heidelberg, Germany.
(poster presentation)

Kordaß T, Weber C, Eisel D, Osen W, and Eichmüller SB.
miRNAs with opposing effects on melanoma cell invasion.
Hallmarks of Skin Cancer Conference 2017, Heidelberg, Germany.

Eisel D, Das K, Osen W, Hoerhold F, König R, Eichmüller SB.
Cognate interaction with $CD4^+$ T cells instructs M2-like macrophages to acquire M1-like phenotype.
EFIS-EJI Tatra Immunology Conference 2018, Štrbské Pleso, Slovakia.
(poster presentation)

Acknowledgements

Mein besonderer Dank gilt:

Prof. Dr. Stefan Eichmüller,
für die Möglichkeit in seinem Team an diesem Projekt zu arbeiten. Danke für die vielen wissenschaftlichen Diskussionen und die jederzeit gewährleistete Unterstützung.

Dr. Wolfram Osen,
für die konstante Betreuung und seinen wissenschaftlichen Input, nicht nur während meiner Zeit im Labor, sondern auch während des Schreibens dieser Arbeit.

Prof. Dr. Viktor Umansky und Dr. Cécile Gouttefangeas,
die als Mitglieder meines TAC-Komitees stetiges Interesse an meinem Projekt hatten und konstruktive wissenschaftliche Beiträge geleistet haben.

Des Weiteren möchte ich mich bedanken bei:

Prof. Dr. Suat Özbek und Prof. Dr. Martin Müller, dass sie sich als Mitglieder meiner Prüfungskommission dazu bereit erklärt haben, mich bei dem letzten Schritt zur Erlangung der Doktorwürde zu unterstützen.

Elke Dickes, für die unzähligen Stunden die du mit mir im Maushaus verbracht hast!!! Ohne dich wären viele große Experimente nicht möglich gewesen, bzw. ich würde heute noch am FACS sitzen und qPCR Platten pipettieren.

Meinen lieben Leidensgenossen Krishna, Laura, Theresa und Toni, für die wunderbare Arbeitsatmosphäre, die vielen lustigen Abende, die unzähligen wissenschaftlichen Diskussionen und eure jederzeit gewährte Unterstützung.

Adriane, die mir insbesondere in der Anfangszeit meiner Doktorarbeit sehr viel gezeigt und beigebracht hast.

Mario, für die schnelle und zuverlässige Synthese meiner Peptide und den wunderbaren Geruch im Labor, den ich so sehr vermissen werde.

Miriam und Nardine, für eure wertvolle Unterstützung meiner Projekte. Ich bin mir sicher, dass sich die vielen Überstunden die ihr geleistet habt irgendwann auszahlen werden.

Allen anderen Mitarbeitern der Arbeitsgruppe (Claudia, Edurne, Julia und Rainer) für ihre Hilfsbereitschaft.

Der FACS Core facility, Rainer Will und den Tierpflegern, ohne die der reibungslose Ablauf von vielen Experimenten nicht funktioniert hätte.

Unseren Kooperationspartnern Prof. Dr. Rainer König, Franziska Hörhold und Daniela Röll für die gute und konstruktive Zusammenarbeit.

Christine, für deine konstante Unterstützung während meines gesamten Studiums und der letzten 3 ½ Jahre.

Anna, die mich in den schwierigen Phasen dieser Arbeit immer wieder ermutigt hat.